

FINAL REPORT  
CONTRACT NAS8-20717

APPENDICES

OPTICAL GUIDANCE SYSTEM (OGS)  
FOR RENDEZVOUS AND DOCKING



N70-15815

FACILITY FORM 602

(ACCESSION NUMBER)	(THRU)
233	
(PAGES)	(CODE)
108-102387	21
(NASA CR OR TMA OR AD NUMBER)	(CATEGORY)

SUBMITTED TO

NASA

GEORGE C. MARSHALL SPACE FLIGHT CENTER

JULY 31, 1969

Prepared by:

L. Cardone	D. McEntyre
D. Coombes	L. Rosenberg
R. Deters	H. Sarrafian
T. Flom	T. Trilling
G. Horn	B. Yancey
B. Kusnick	



FINAL REPORT  
CONTRACT NAS8-20717

OPTICAL GUIDANCE SYSTEM (OGS)  
for  
Rendezvous & Docking

APPENDICES

Submitted to:

NASA

George C. Marshall Space Flight Center

July 1969

Prepared by:

L. Cardone	D. McEntyre
D. Coombes	L. Rosenberg
R. Deters	H. Sarrafian
T. Flom	T. Trilling
G. Horn	B. Yancey
B. Yancey	

## APPENDIX A

### RANGE AND RANGE RATE PERFORMANCE ANALYSIS

#### 1.0 RANGING ERRORS

##### 1.1 Error Sources

Residual errors in range measurements arise from two sources: 1) quantization error, and 2) errors introduced by noise at the threshold detector. Quantization error refers specifically to those errors which arise due to the finite range bins within which range measurements will yield the same value. The length  $\Delta R$  of these bins is simply:

$$\Delta R = \frac{cT}{2n} = \frac{c\Delta T}{2} \quad (A-1)$$

where  $c$  is the velocity of light,  $T$  is the period between pulses,  $n$  is the number of time increments into which the period  $T$  has been divided through the use of delay line taps, and  $\Delta T$  is the length of the individual time increments. Quantization error can be minimized by assuming that the actual time of detection  $t_d$  occurred when the clock pulse leading edge was in the exact center of the delay line section following the last tap at which the clock pulse was observed. In other words this error will be minimized if it is assumed that:

$$t_d = t_i + \frac{1}{2} \Delta t \quad (A-2)$$

where  $t_i$  denotes the time indicated by the last delay line tap to sense the presence of a clock pulse at the instant at which the echo pulse was detected. Figure A-1 shows a plot of quantization error  $\epsilon_q$  as a function of the actual detection time after the beginning of the interval. Under the above assumption the peak

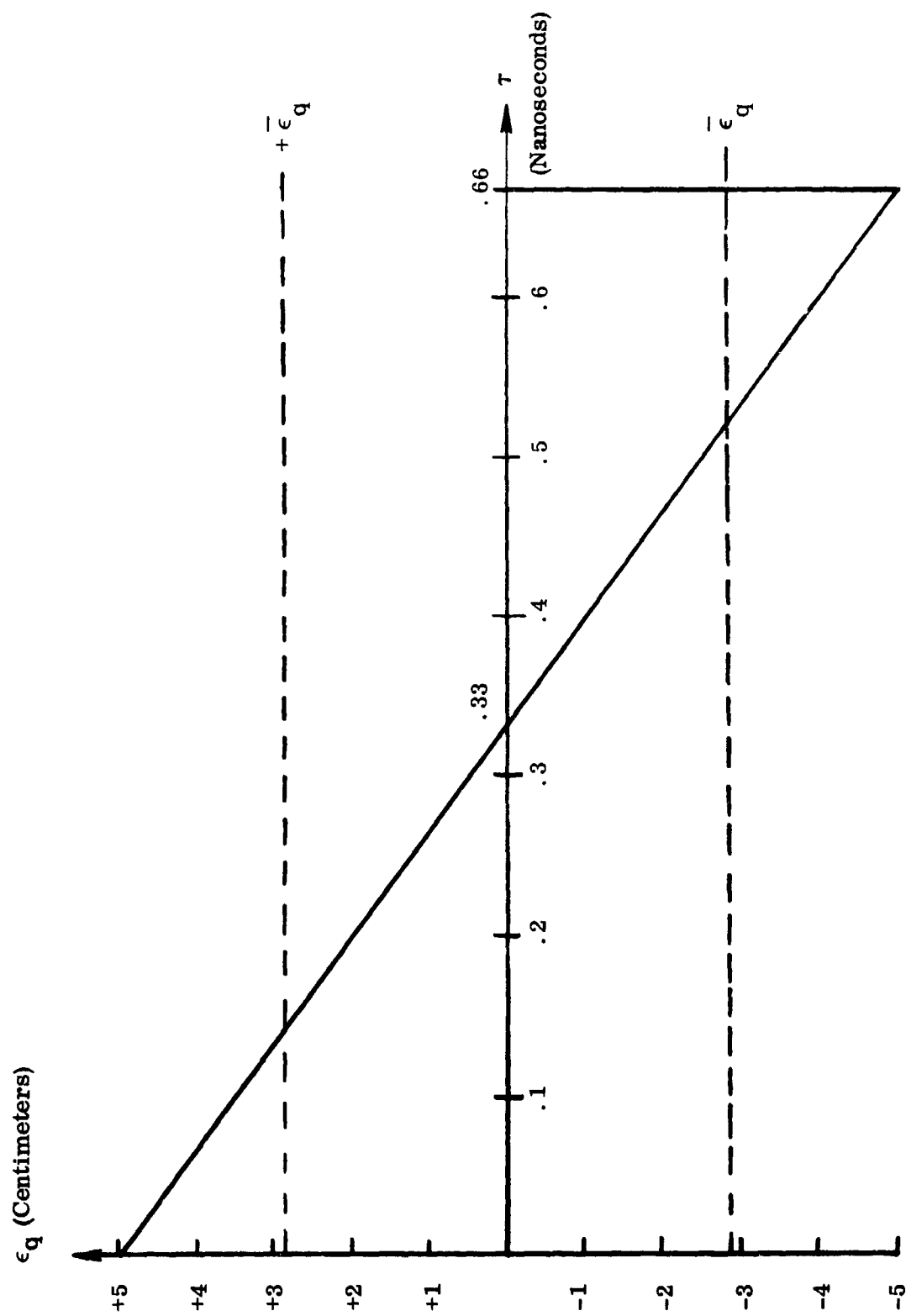


Figure A-1. Quantization Error  $\epsilon_q$  Versus Time  $\tau$  of Actual Detection



quantization error will be  $1/2 \Delta t$  corresponding to an error in range of  $1/2 \Delta R$ , which in the system under consideration is 5 centimeters. The rms quantization error  $\bar{\epsilon}_q$  will be

$$\bar{\epsilon}_q = \lim_{\xi \rightarrow \infty} \left[ \frac{1}{2\xi} \int_{-\xi}^{\xi} \epsilon_q^2(t) dt \right]^{1/2} \quad (A-3)$$

Since  $\epsilon_q(t)$  is repetitive, Equation (A-3) simplifies to

$$\bar{\epsilon}_q = \left[ \frac{1}{\Delta t} \int_{-1/2 \Delta t}^{1/2 \Delta t} \epsilon_q^2(t) dt \right]^{1/2}$$

which gives

$$\epsilon_q = \frac{\sqrt{3 \Delta t}}{6} \quad (A-4)$$

Since  $\Delta t = 0.667$  nanosecond for the proposed system, Equation (A-4) yields

$$\bar{\epsilon}_q = 0.192 \text{ nanoseconds,}$$

Corresponding to a round-trip rms range error of 0.289 centimeters.

Let us now consider the effect of noise upon the accuracy of a range measurement. The presence of noise superposed upon the received pulse will introduce a Gaussian uncertainty as to the time that the threshold detector will sense the leading edge of the pulse. This effect exists due to the finite risetime of the pulse at the input of the detector. If we denote the slope of the leading edge of a

received signal pulse at the threshold level of the detector as  $\frac{di_s}{dt}$  and the one-sigma value of the superposed noise current<sup>1</sup> as  $i_n$ , the one-sigma uncertainty in the detection time of the received pulse will be

$$\sigma_t = \frac{i_n}{\frac{di_s}{dt}} \quad (A-5)$$

Figure A-2 illustrates this transformation of noise into time jitter around the leading edge of the received echo pulse. We now shall proceed to formulate a generalized analysis which takes into consideration the effects of both quantization error and noise-induced error.

## 1.2 The Effect of Noise

In the absence of noise, the leading edge of the received pulse will be detected after an interval of time  $\tau$  following the time  $t_1$  at which the leading edge of the clock pulse passes the last delay line tap which is designated as the  $i$ th tap (see Figure A-2). However, due to the presence of noise, the actual detection may occur either earlier or later, and if the noise is Gaussian, the actual time of detection will obey the standard Gaussian probability density function.

$$p(t) = \frac{1}{\sqrt{2\pi}\sigma_t} e^{-\frac{t^2}{2\sigma_t^2}} \quad (A-6)$$

<sup>1</sup>The rms noise current may be evaluated from the expression

$$i_n = \sqrt{2e(I_t + I_b + I_d)\Delta F}$$

where  $e$  is the charge of the electron,  $\Delta F$  is the video bandwidth and  $I_t$ ,  $I_b$  and  $I_d$  are the signal current required to reach the detector threshold, the DC background current, and the dark current, respectively. This expression is valid only when signal pulses are of low duty cycle, in which cases it may be assumed that the average current level between pulses in an AC-coupled video amplifier is zero.

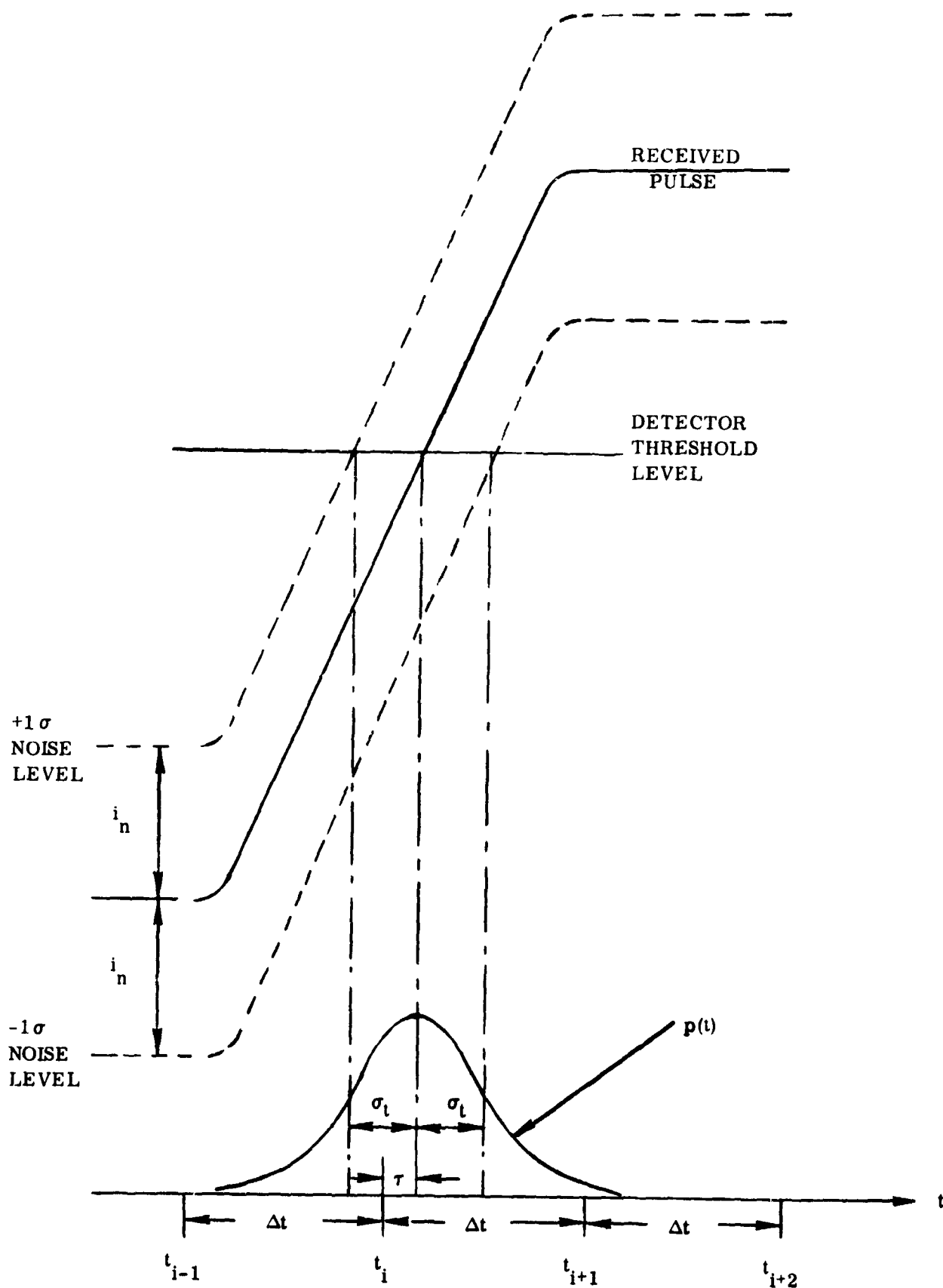


Figure A-2. The Effect of Gaussian Noise Upon Range Measurements

where  $t$  is the time of actual detection before or after  $\tau$ , i.e.  $t = 0$  indicates a detection at a time  $\tau$  after the beginning of an incremental interval as would occur with absolute certainty in the absence of noise. The parameter  $\sigma_t$  is determined by means of Equation A-5.

Since the ranging electronics are unable to determine when an actual threshold crossing occurs within a  $\Delta t$  interval, we will be concerned only with determining whether the crossing will occur somewhere within the proper interval and the probabilities of its occurrence within other intervals. Clearly, a range measurement will be unaffected by noise during a given sample as long as the noise does not place the detection time obtained in that sample outside of the interval in which it would have occurred in the absence of noise. Thus we are concerned only with determining within which interval a detection is observed. The probability  $q(0)$  that the pulse will be detected in the same interval as would have occurred in the absence of noise is

$$q(0) = \int_{-\tau}^{\Delta t - \tau} p(t) dt \quad (A-7)$$

The probability that the detection will be observed during the preceding interval is

$$q(-1) = \int_{-\Delta t - \tau}^{-\tau} p(t) dt$$

and the probability of detection in the subsequent interval is

$$q(+1) = \int_{\Delta t - \tau}^{2\Delta t - \tau} p(t) dt,$$

Or in general the probability that a detection in the  $s$ th interval following the one in which a noise-free detection would occur is

$$q(s) = \int_{s \Delta t - \tau}^{(s+1) \Delta t - \tau} p(t) dt \quad (A-8)$$

It should be noted that intervals preceding the proper interval ( $s = 0$ ) are designated by negative values for  $s$ .

We have evaluated the probability  $q(s)$  of a detection occurring within the  $s$ th interval in terms of a particular value of  $\tau$ . In order to evaluate the total effect of noise upon a range measurement, we must determine a cumulative probability  $Q(s)$  which is composite of all of the values for  $q(s)$  resulting from values for  $\tau$  from 0 to  $\Delta t$ . Let us consider the case in which a particular value for  $\tau$  lies between  $\tau$  and  $\tau + d\tau$ . Since  $\tau$  has a uniform probability of occurrence between 0 and  $\Delta t$ , the probability density for  $\tau$  must be  $\frac{1}{\Delta t}$  over this range in order for the probability density function for  $\tau$  to be normalized. Thus the probability that  $\tau$  lies inside an interval of length  $d\tau$  is simply  $\frac{1}{\Delta t} d\tau$ . When  $\tau$  is within this interval, a certain set of  $q(s)$  values result, as given by Equation (A-8). The contributions  $d [Q(s)]$  which result when  $\tau$  is within the interval  $d$  are simply

$$d [Q(s)] = q(s) \frac{1}{\Delta t} d\tau = \frac{1}{\Delta t} \left[ \int_{s \Delta t - \tau}^{(s+1) \Delta t - \tau} p(t) dt \right] d\tau$$

so that

$$Q(s) = \frac{1}{\Delta t} \int_0^{\tau} \int_{s \Delta t - \tau}^{(s+1) \Delta t - \tau} p(t) dt d\tau \quad (A-9)$$

The function  $Q(s)$  is discontinuous in that it is defined only at those points along the abscissa for which  $s$  is an integer is zero. The function  $Q(s)$  may be transformed into a probability density function  $\eta(s)$  by convolving  $Q(s)$  with the

Dirac delta function:

$$\eta(s) = \int_{-\infty}^{\infty} Q(\varphi) \delta(s - \varphi) d\varphi. \quad (A-10)$$

In order to obtain a probability density function  $u(s)$  which combines the effects of quantization error and noise-induced error, we convolve the noise-error probability function  $\eta(s)$  with the rectangular quantization error probability function  $\gamma(s)$  [where  $\gamma(s) = 1$  for  $-\frac{1}{2} < s < \frac{1}{2}$  and zero elsewhere]:

$$u(s) = \int_{-\infty}^{\infty} \eta(\varphi) \gamma(s - \varphi) d\varphi. \quad (A-11)$$

The rms value of the total error probability function  $u(s)$  is

$$\bar{\epsilon}_t(s) = \left[ \int_{-\infty}^{\infty} s^2 u(s) ds \right]^{1/2} \quad (A-12)$$

Finally the rms error may be expressed in centimeters of range by multiplying Equation (A-12) by  $\Delta R$  which is 10 centimeters in the proposed system.

The implementation of the computations described here requires the use of a computer program and is to be undertaken at ITTA in the immediate future. However, the resultant data may be readily approximated by taking the root-sum-square combinations of quantization error and noise induced Gaussian jitter error for various signal-to-noise ratios and pulse risetimes. The results are plotted in Figure A-3.

## 2.0 RANGE RATE ERRORS

Range rate errors arise from the same sources as range errors since range rate is derived from range by differentiation and smoothing. More specifically, in the proposed system, 32 consecutive range measurements are averaged and the resultant is subtracted from the average of another group of 32 range

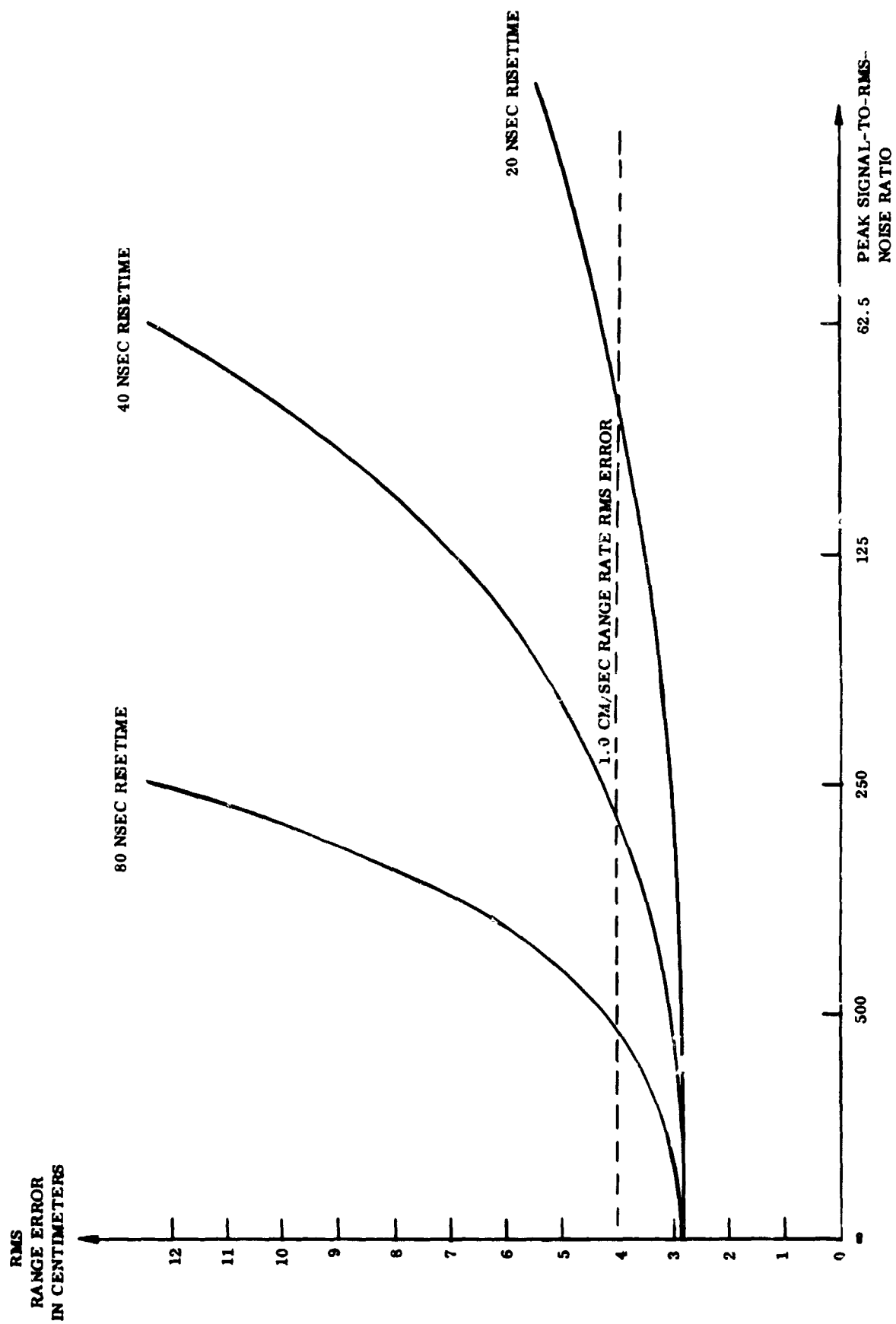


Figure A-3. RMS Range Error Versus Signal-to-Noise Ratio and Risettime

measurements made one second later. This difference is divided by one second to obtain the mean velocity during the one second interval.

The accuracy of these range rate measurements may be evaluated easily if the accuracies of the range measurements are known. The standard deviation  $\sigma_{av}$  of the average of a group of  $n$  measurements is obtained from the standard deviation  $\sigma_i$  of the individual measurements by the relation.

$$\sigma_{av} = \frac{\sigma_i}{\sqrt{n}} \quad (A-13)$$

Two values for  $\sigma_{av}$  are obtained, one for each group of 32 measurements. In practice these two quantities will be equal, since the signal-to-noise ratio will not change measurably over a one second interval. The standard deviation of the difference of these two averaged range measurements will be their root-sum-square which in this case will be simply  $\sqrt{2\sigma_{av}^2}$ .

Since highly accurate range rate measurements are required only at short to intermediate ranges, say less than 5 km, the effects of noise will be small and one may take  $\sigma_i = \epsilon_q$  or 2.89 cm. Equation (A-13) gives for  $n = 32$  a value for  $\sigma_{av}$  of 0.51 cm. The standard deviation of the difference of the two range averages will then be 0.722 cm. Since the two range averages are separated by a one second interval, the standard deviation of range rate measurements will be 0.722 cm/sec. Noise induced ranging errors thus may bring the rms range error as high as 4.0 cm before the 1 cm/second rms velocity error figure is exceeded (see Figure A-3).



### 3.0 MAXIMUM RANGE CAPABILITY

The range capability of the Optical Guidance System may be determined by straightforward optical radar analysis. Initially it is necessary to derive expressions which relate the signal-to-noise ratio observed at the Chaser detector to the range between the Chaser and Target vehicles. The analysis will be performed for both the Chaser laser transmitter and for the Target laser beacon. Range vs. signal-to-noise is then plotted in Figures A-4 and A-5 for each case.

The Chaser laser transmitter emitting  $P_t$  watts, over a full cone angle  $\Theta_t$ , will produce a power flux per unit area ( $\Phi_c$ ) at the target vehicle equal to

$$\Phi_c = \frac{4 P_t}{\pi (R \Theta_t)^2} \quad (A-14)$$

where  $R$  is the range between the Target and the Chaser. It is assumed  $\Theta_t$  is small. A circular corner cube reflector, on the Target, of diameter  $d_c$  will reflect an amount

$$P_{\text{reflected}} = \left( \frac{\pi}{4} d_c^2 \right) \Phi_c = \frac{P_t d_c^2}{R^2 \Theta_t^2} \quad (A-15)$$

directly back to the Chaser receiver. At long ranges, the light returned by the reflector will be distributed over a sizeable area due to the diffraction introduced by the finite dimensions of the corner cube reflector. For simplicity, it shall be assumed here that the corner cube reflector has a circular boundary. Similarly it is assumed that the reflector is diffraction-limited over its full aperture. As it will be shown, this latter condition has a major effect upon the amount of signal returned to the Chaser receiver. The angular distance from

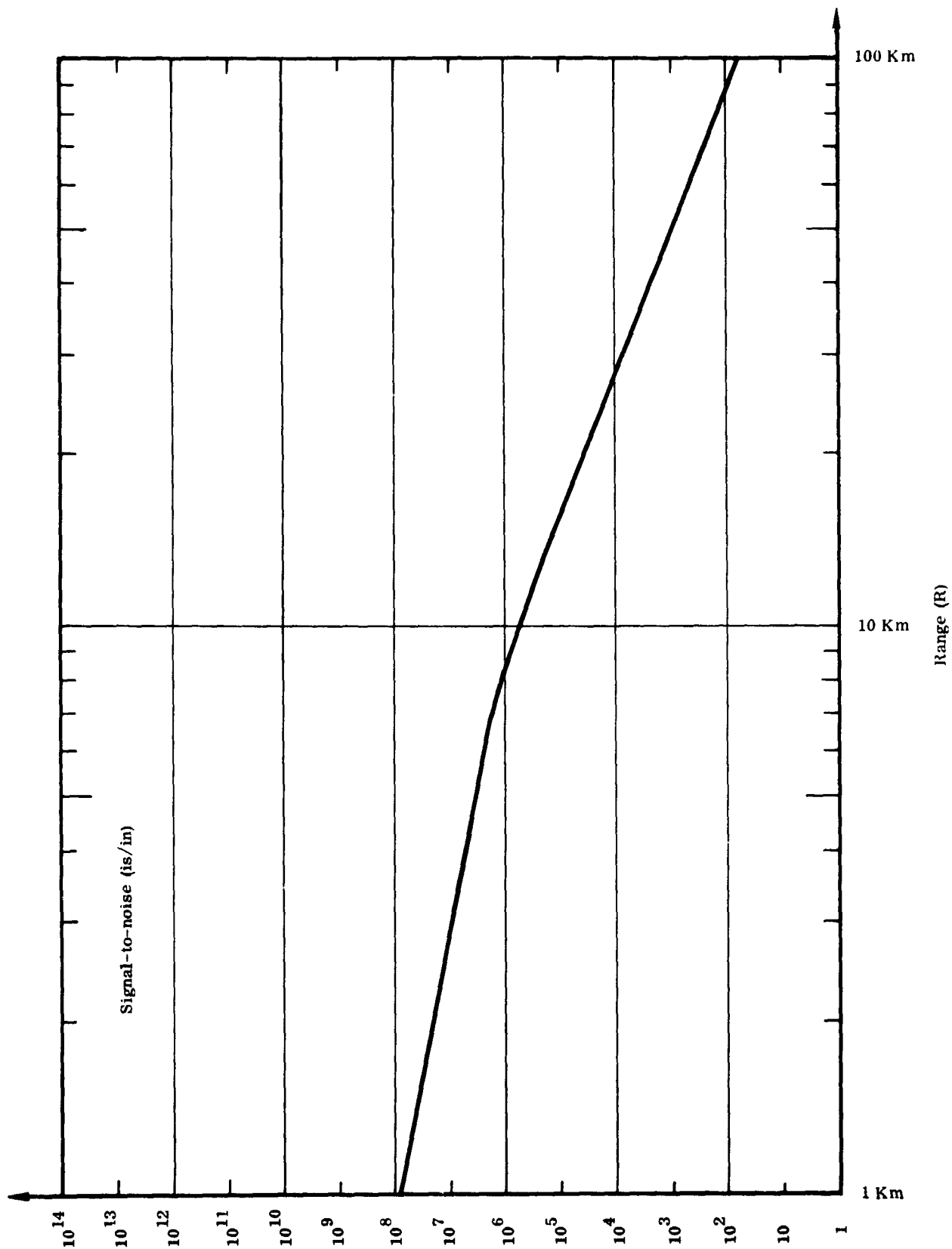


Figure A-4. Optical Guidance System Range Capability, Range vs Signal-to-Noise for Chaser Laser Transmitter

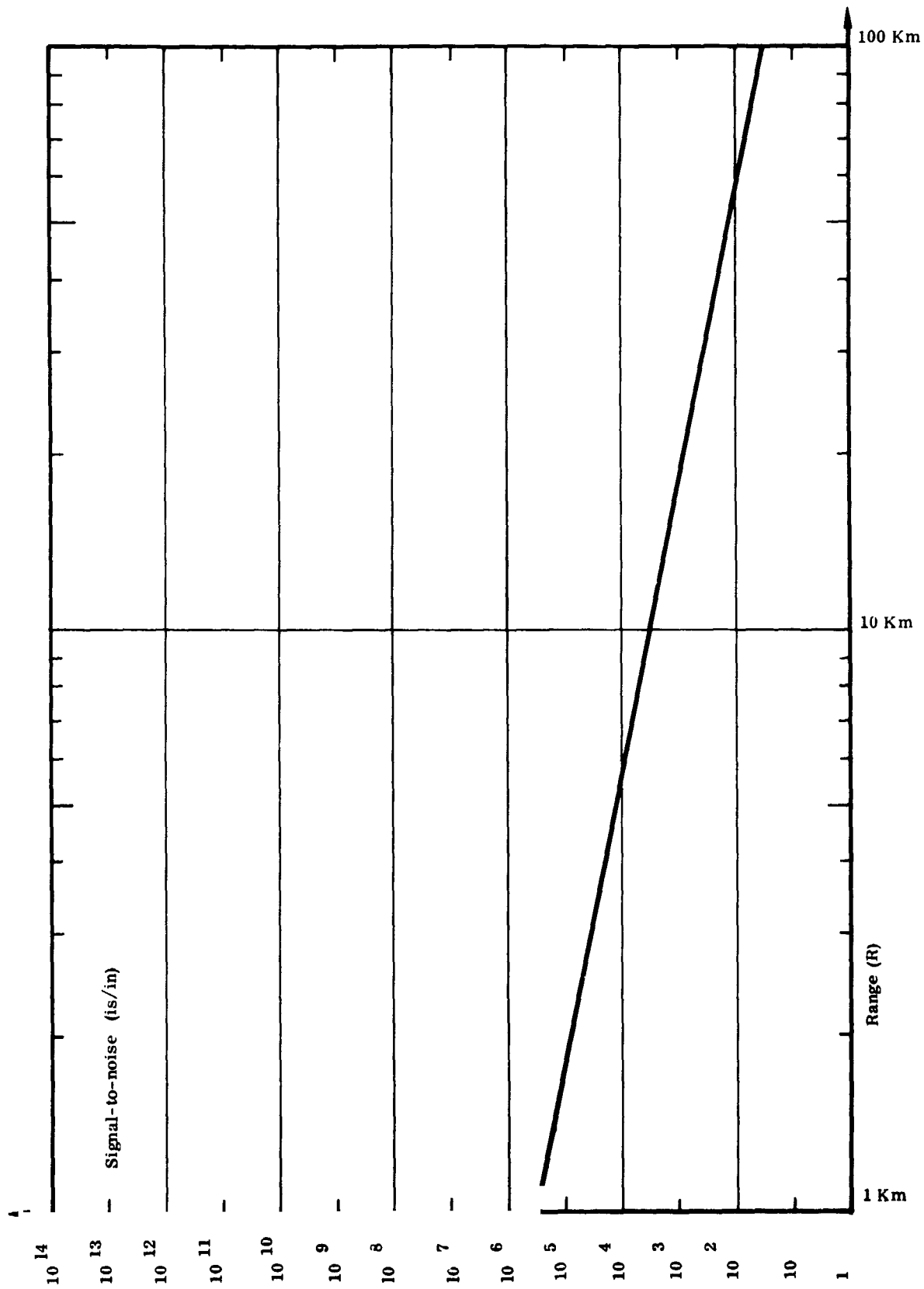


Figure A-5. Optical Guidance System - Range Capability Range vs Signal-to-Noise for Target Laser Beacon

the central maximum to the first null of the diffraction pattern is given by the familiar relation

$$\sin \rho = 1.22 \frac{\lambda}{d_c}$$

or for small angles

$$\rho = 1.22 \frac{\lambda}{d_c}$$

If we make the simplifying assumption that the radiant flux is distributed uniformly within a cone of full apex angle  $\rho$ , the area of the spot at the Chaser receiver will be

$$A_r = \frac{\pi}{4} (R\rho)^2 = \frac{R^2 \lambda^2}{2.7 d_c^2} \quad (A-16)$$

From equations A-15 and A-16, and using the above assumptions, the reflected flux density is

$$\Phi_r = \frac{P_{\text{reflected}}}{A_r} = \frac{2.7 \left( \frac{P_t d_c^2}{R^2 \Theta_t^2} \right)}{\pi \left( \frac{R^2 \lambda^2}{d_c^2} \right)}$$

or

$$\Phi_r = \frac{2.7 P_t d_c^4}{\pi R^4 \Theta_t^2 \lambda^2} \quad (A-17)$$

Thus the Chaser photocathode signal current ( $i_s$ ) is then the amount of reflected flux density ( $\Phi_r$ ) collected by the Chaser receiver aperture of diameter ( $d_r$ ), multiplied by the photocathode sensitivity ( $k$ )

$$i_s = \left( \frac{1}{4} \pi d_r^2 \right) k \Phi_r$$

$$i_s = \frac{P_t d_r^2 d_c^4 k}{1.5 R^4 \Theta_t^2 \lambda^2}$$

(A-18)

Under worst-case conditions, the dominant source of noise will be due to stray illumination upon that portion of the photocathode within the instantaneous field-of-view. In such a case all other sources of noise will be negligible. The DC noise current at the photocathode is given by

$$I_n = \frac{1}{4} \pi d_r^2 \Theta_r^2 \Delta \lambda N_b k. \quad (\text{A-19})$$

where  $N_b$  is the spectral radiance of the background. The noise observed at the Chaser detector between returned pulses will be shot noise due to  $I_n$ . The rms shot noise may be obtained from the familiar expression

$$i_n = \sqrt{2 e I_n \Delta F} \quad (\text{A-20})$$

where  $e$  is the charge of the electron and  $\Delta F$  is the video bandwidth of the Chaser receiver. Substituting A-19 into A-20 we obtain

$$i_n = d_r \Theta_r \sqrt{\frac{1}{2} e \pi \Delta F \Delta \lambda N_b k} \quad (\text{A-21})$$

Equation (8) may be divided into (5) to give the resultant signal-to-noise ratio  $\frac{I_s}{i_n}$ . Figure 10 gives a plot of this ratio for ranges from 1 km to 100 km. For this plot the following parameter values were used:

$d_c$	=	10 cm
$d_r$	=	8.75 cm
$\Theta_t$	=	0.03°
$\Theta_r$	=	0.03°
$\rho_t$	=	5 watts
$\lambda$	=	0.9 $\mu$
$\Delta \lambda$	=	0.01
$\Delta F$	=	10 <sup>7</sup> Hz
$N_b$	=	0.01 watt/cm <sup>2</sup> -steradian-micron (sunlit cloud background)
$k$	=	0.002 ampere/watt (S1 photocathode at 0.9 $\mu$ )

The curve in Figure A-4 deviates from the results described by the above equations for ranges less than about 10 km. This change occurs when the range becomes sufficiently small to permit most or all of the diffraction spot formed by the corner cube reflector to be imaged within the receiver aperture. Under such conditions, the range equation involves  $R^2$  instead of  $R^4$  in the denominator.

In order to evaluate the performance of the Target laser beacon, we may use Equation A-14. It also applies to the power flux density ( $\phi_c$ ) at the Chaser receiver due to the laser beacon on the Target vehicle. Multiplying Equation A-14 by the area of the Chaser receiver lens gives the power on the Chaser photocathode:

$$P = \frac{P_t d_r^2}{R^2 \Theta_t^2} \quad (A-22)$$

where the subscript "t" here refers to the laser beacon. It thus follows that the Chaser photocathode signal current ( $i_s$ ) due to the target beacon is

$$i_s = \frac{k P_t d_r^2}{R^2 \Theta_t^2} \quad (A-23)$$

The signal-to-noise ratio may be determined for a particular range by dividing Equation A-23 by Equation A-21. Figure A-5 gives  $\frac{i_s}{i}$  versus  $R$  for a laser beacon on the Target vehicle for which  $P_t = 2$  kilowatts and  $\Theta_t = 10^\circ$ . All other parameters are the same as were used in the Chaser laser case.

## APPENDIX B

### ANGLE TRACKER ANALYSIS

An evaluation of the capability and accuracy of the digital angle tracker is presented in this Appendix. The angle tracker analysis is divided into three parts: Acquisition Scan, Acquisition to Track Transition, and Track Scan. Parameters and characteristics of the angle tracker that are most pertinent are: (It should be noted that all of the following are functions of target angular velocity and velocity direction.)

- Acquisition time
- Variation of acquisition capability with target motion
- Transient capabilities - i.e., ability of the angle tracker to acquire and build up velocity and position feedback.
- Angle tracking accuracy
- Angle-rate accuracy
- Maximum angle-rate capability.

All three studies have used the following tracker characteristics:

Angle tracker scan rate	1 kHz
Receiver instantaneous aperture	1 mil (.03 degree)
Track steps per aperture	8
Acquisition field-of-view	30° x 30°
Acquisition steps	1000 x 1000
Track step	.00375°

## APPENDIX B.1

### 1.0 INTRODUCTION

The Acquisition Scan Program simulates the tracker's search mode of operation. The two principal factors of interest are target acquisition time, and maximum target velocity that can be acquired. The tracker's capabilities in these two areas are evaluated in the program.

### 2.0 ACQUISITION SCAN PROGRAM

#### 2.1 Description

The acquisition scan consists of moving a 0.03 degree instantaneous aperture in discrete steps over a 30° by 30° field-of-view. This process consists of 1000 steps from left to right starting at the (-15°, +15°) point which is -15° horizontal and +15° vertical from the boresight axis, (see Figure B-1). When the instantaneous aperture has scanned one horizontal line from left to right it is moved down one step (0.03°) and then stepped from right to left. At the end of this scan the aperture is moved down one step and the process is started over.

If the target is not acquired during the first scan, the instantaneous aperture starts a new scan from the final position of the first scan (i. e., -15°, +15°). The second scan has a fast vertical sweep and a slow horizontal sweep (see Figure B-2).



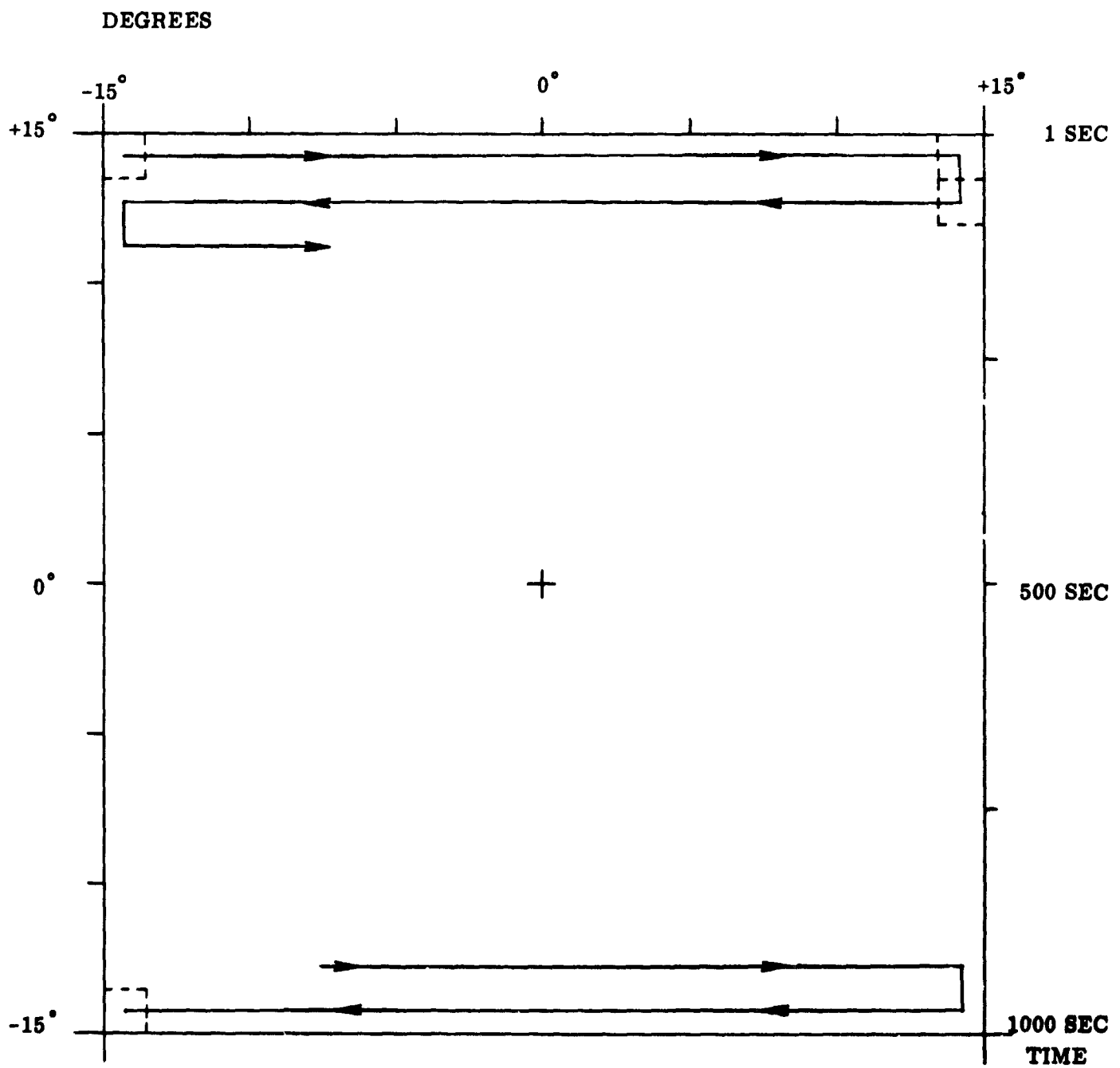


Figure B-1. First Acquisition Scan

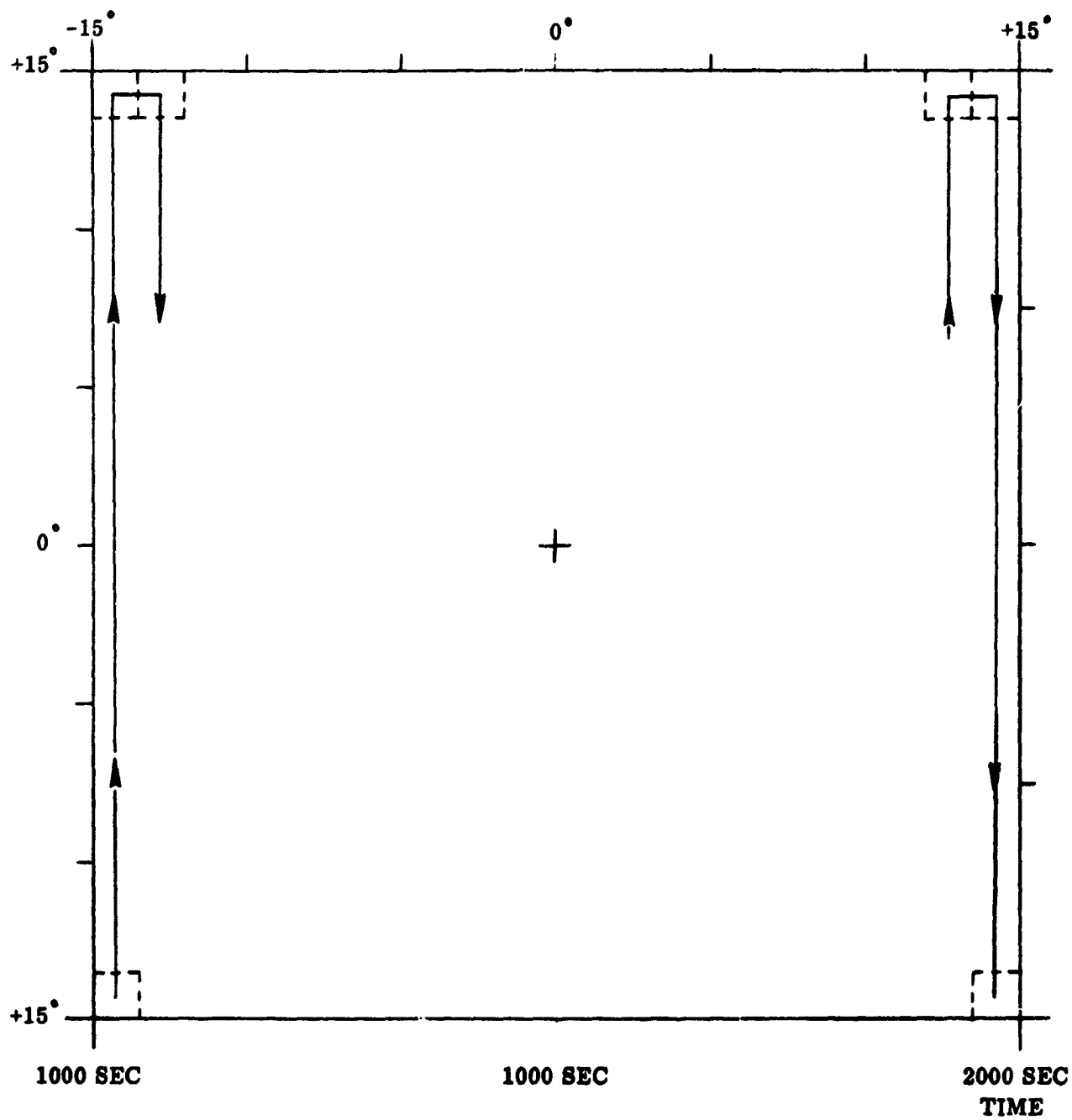


Figure B-2. Second Acquisition Scan

One complete acquisition scan takes 1000 seconds at a prf of 1 kHz. With 1000 steps per line, 1 second is required to scan one line. The times shown in Figure B-3 at the right-hand side indicates the time it takes the acquisition scan to reach the corresponding physical locations adjacent to the time marks.

The simulation of the acquisition scan consists of starting a target at some point in the  $30^\circ \times 30^\circ$  field-of-view, with a specified angular velocity and velocity angle with respect to the angle tracker boresight axis. The aperture then begins its predetermined scan until the target falls within the aperture. By changing the target angular velocity, velocity angle and starting point, an analysis of the tracker acquisition capability is made.

### 3.0 DATA

Three different sample cases are illustrated in Figure B-3: Target acquisition on the first scan; Target acquisition on the second scan; Target left field-of-view and was not acquired in two scans. The approximate time of acquisition can be estimated from the position of the black dot. Acquisition time for a target acquired on the second pass is labeled on each graph - and is always greater than 1000 seconds. The results of the various cases run on a computer are shown graphically in Figures B-4 through B-8.

Table B-1 is a summary of selected cases and gives the percent of targets acquired and missed for each angular velocity. Time to acquisition can vary from a few milliseconds to almost 2000 seconds, depending upon the target angular velocity and starting position.

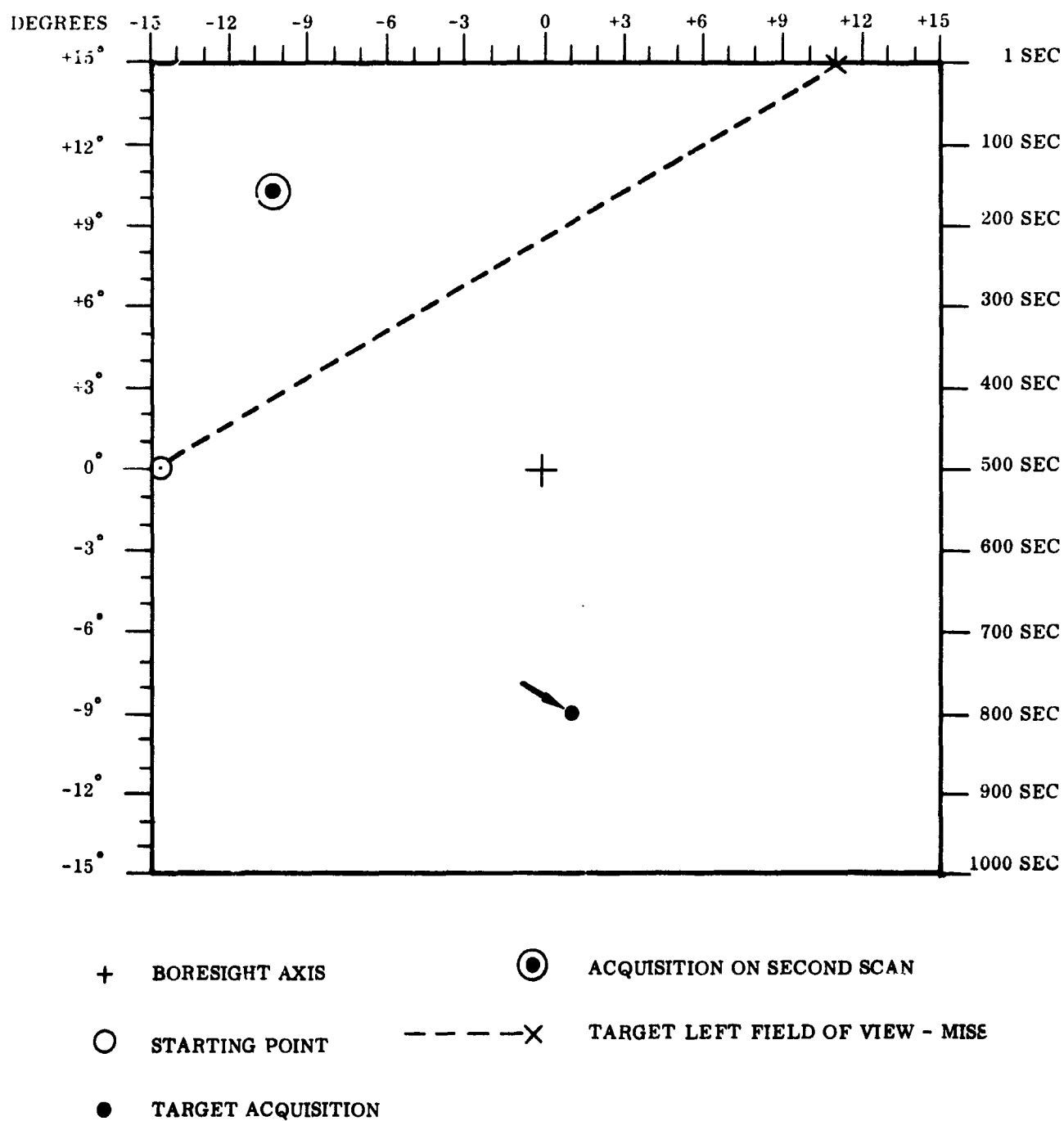


Figure B-3. Acquisition Scan













TABLE B-1.  
ACQUISITION SCAN SUMMARY

VELOCITY DEG./SEC.	% MISSED	% ACQUISITION FIRST PASS	% ACQUISITION SECOND PASS
.01	1	87	12
.02	44	53	3
.03	52	47	1
.04	58.5	41.5	0
.05	57.5	42.5	0

NOTE: These are for 1 kHz scan rate.

Most acquisition times are less than 1000 seconds, i. e. , during the first pass. Very few targets are acquired during the second pass of the acquisition scan because the target usually had time to leave the field-of-view within 1000 seconds.

#### 4.0 CONCLUSION

In specifying the maximum target angular velocity the tracker is able to acquire, it should be remembered that it is a function of the following:

- Direction of target (varied in study)
- Angle tracker scan rate (1 kHz).
- Receiver instantaneous aperture (.03° x .03°)
- Acquisition field-of-view (30° x 30°)
- Acquisition steps (1000 x 1000).

The values in parentheses indicates the values chosen for the selected cases studied here in this report. Note, that if the scan rate is increased by a factor of 10, the target angular velocity can be increased by a factor of 10. If the instantaneous aperture is increased, or if the acquisition field-of-view is reduced the target angular velocity can also be correspondingly increased. Many trade-offs are possible, thus the results of this study are not to be taken as fixed performance parameters of the angle tracker.

## APPENDIX B.2

### TRANSITION FROM ACQUISITION TO TRACK

#### 1.0 INTRODUCTION

The transition program simulates the track scan mode of operation with the purpose of evaluating the tracker's capability to build up velocity and position feedback constants in order to track a target moving at a constant angular velocity. Quantities of interest are the maximum target angular velocity that the tracker can track after acquisition, and the variation of the tracking capability with the direction of target motion and initial target position within the instantaneous aperture.

#### 2.0 DESCRIPTION

In order to analyze the transition characteristics of the tracker, the following conditions were set up. The tracker is assumed to have acquired the target at five different starting points within the instantaneous aperture (see Figure B-9 for acquisition-to-track transition model). The direction of the target motion with respect to the corresponding starting point is varied in increments of  $10^\circ$  through a full  $360^\circ$ . The target is given a constant angular velocity. Three different constant angular velocities ( $0.3^\circ/\text{sec}$ ,  $0.4^\circ/\text{sec}$ ,  $0.5^\circ/\text{sec}$ ) are used to evaluate the tracker's transition capability for each of the five corresponding starting points. Figures B-10, B-11, and B-12 are plots of the results. The plots indicate whether or not the tracker will successfully track the target for given starting point, direction, and velocity. Again, it should be mentioned these results are representative for a scan rate of 1 kHz, an instantaneous aperture of  $.03^\circ$ , and 8 track steps per aperture.

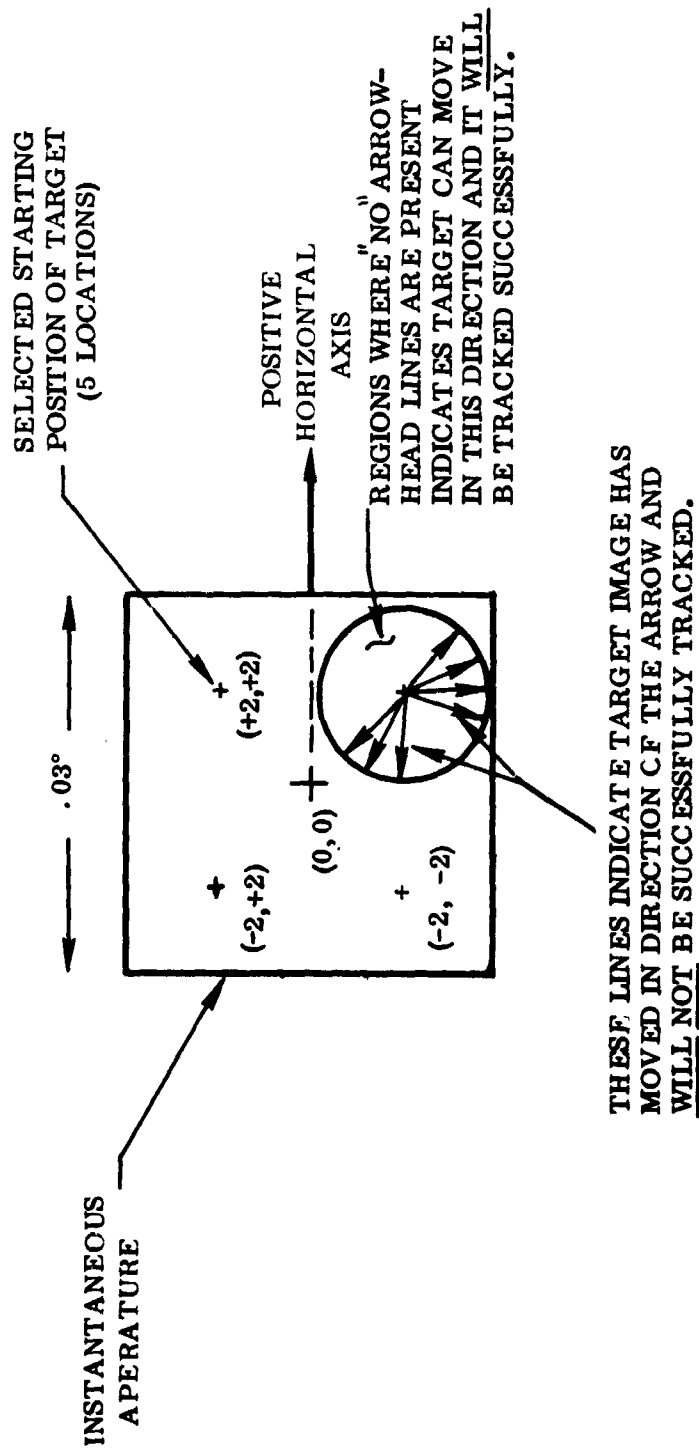


Figure B-9. Acquisition to Track Transition Model

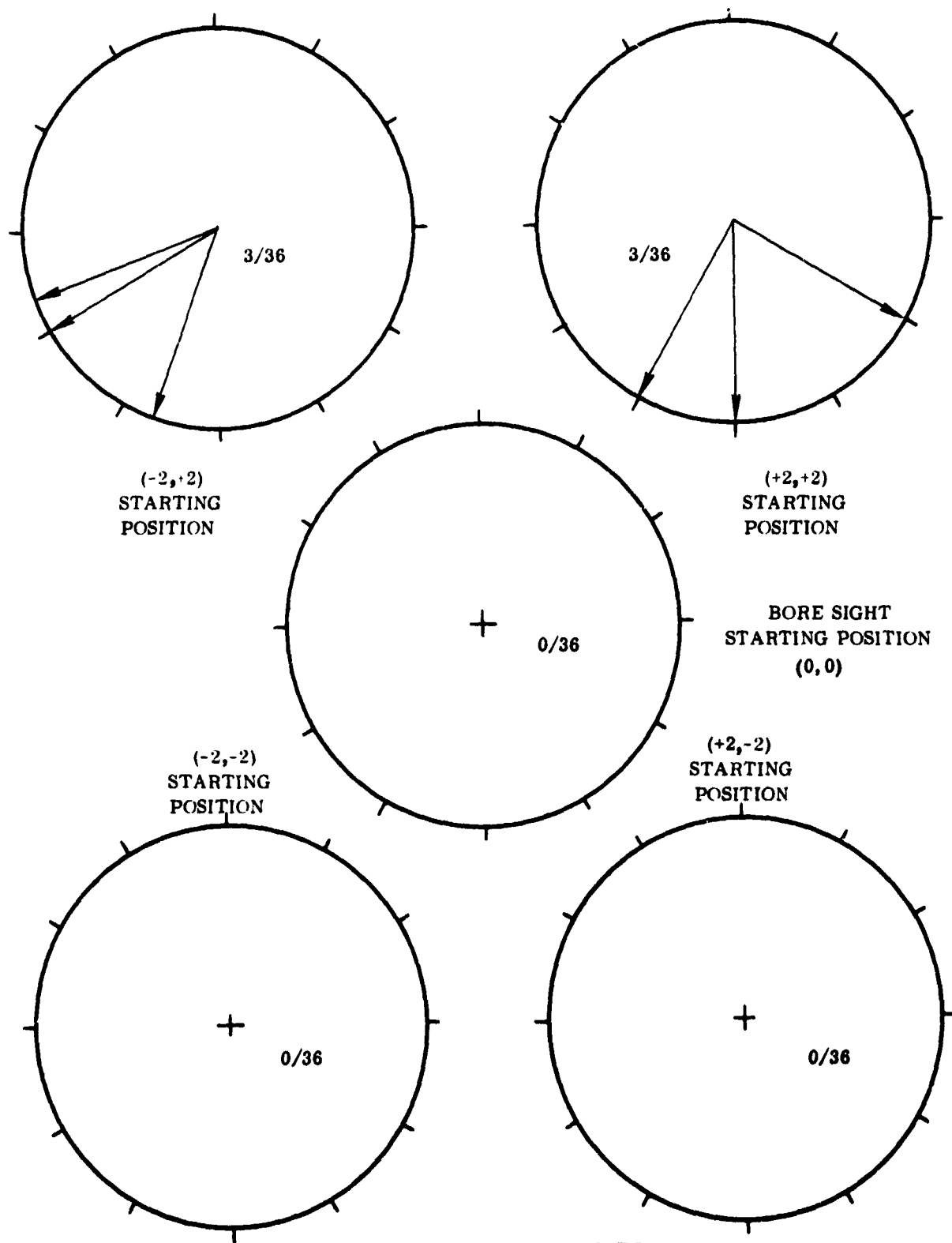
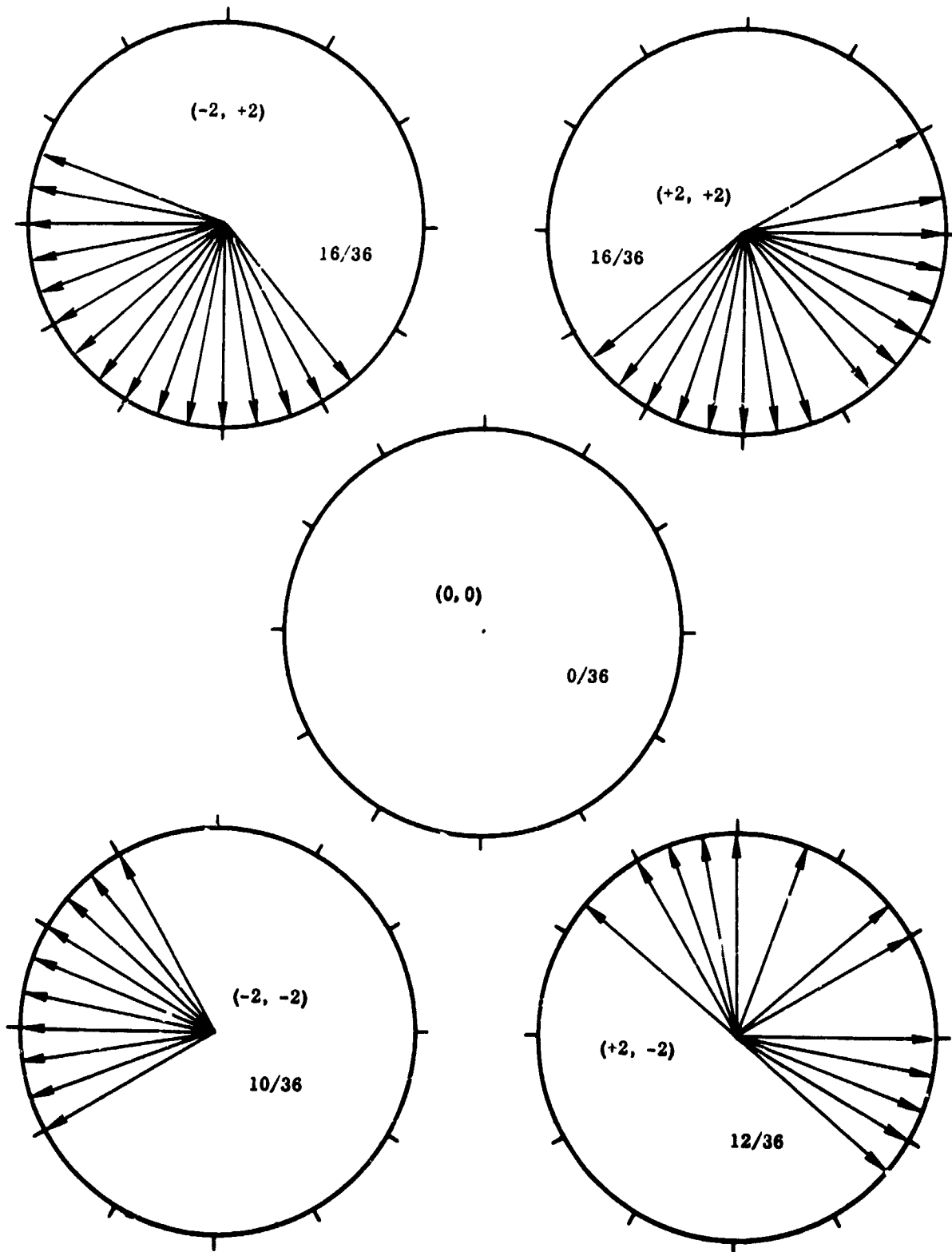


Figure B-10. Loss of Track Diagram



NOTE:

TARGET VELOCITY  $0.4^\circ/\text{s}$

Figure B-11. Loss of Track Diagram

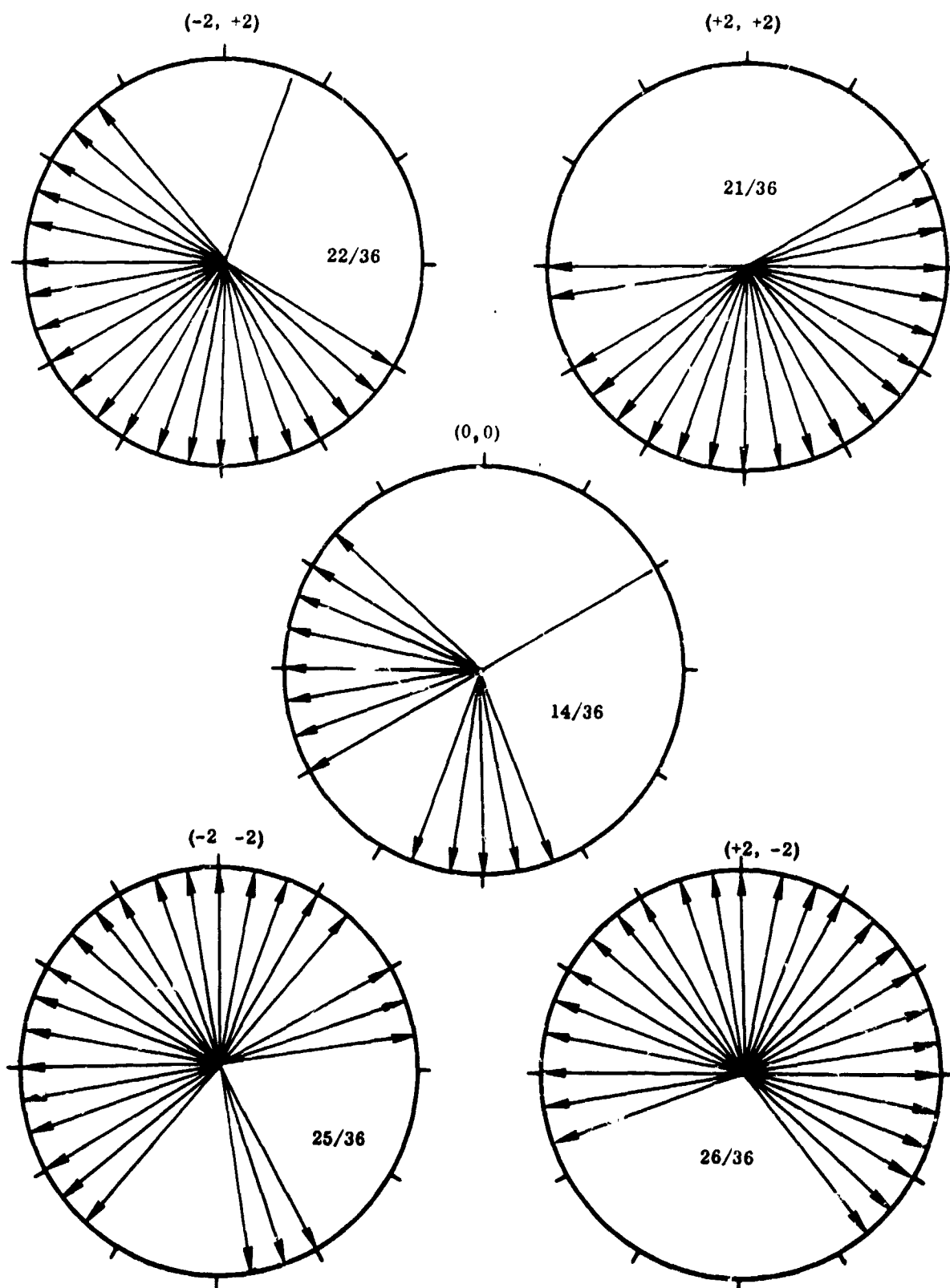


Figure B-12. Loss of Track Diagram

## APPENDIX B.3

### 1.0 INTRODUCTION

The Track Scan Program was designed to simulate the digital angle tracker. This portion of the analysis has, as its main goal, the determination of the tracker's angle and angle-rate tracking accuracies and the maximum angle-rate capability.

### 2.0 TRACK SCAN PROGRAM

#### 2.1 Description

The Track Scan (Figure B-13) is divided into 64 track steps, of which the first 32 are in the vertical direction and the second 32 in horizontal direction. The positive portion of the vertical track scan consists of 8 steps up and 8 steps down. The negative vertical scan is 8 down and 8 up. The dwell time on each stepped position of the track scan is 1 ms, at a repetition rate of 1 KHz, taking 64 ms to complete one track scan. A signal is received from the target only if one half or more of the target image is inside the aperture. At any of the scanned step positions, if the target image is exactly in the center of the track scan pattern, the identical number of returns will be received during the positive vertical scan as during the negative vertical scan, yielding zero net vertical returns. The horizontal scan will similarly yield net horizontal returns. There will be positive net returns if the target image is in the positive vertical scan more times than the negative vertical scan. The net returns represent an angular error which is processed and corrected for in the tracker by changing the



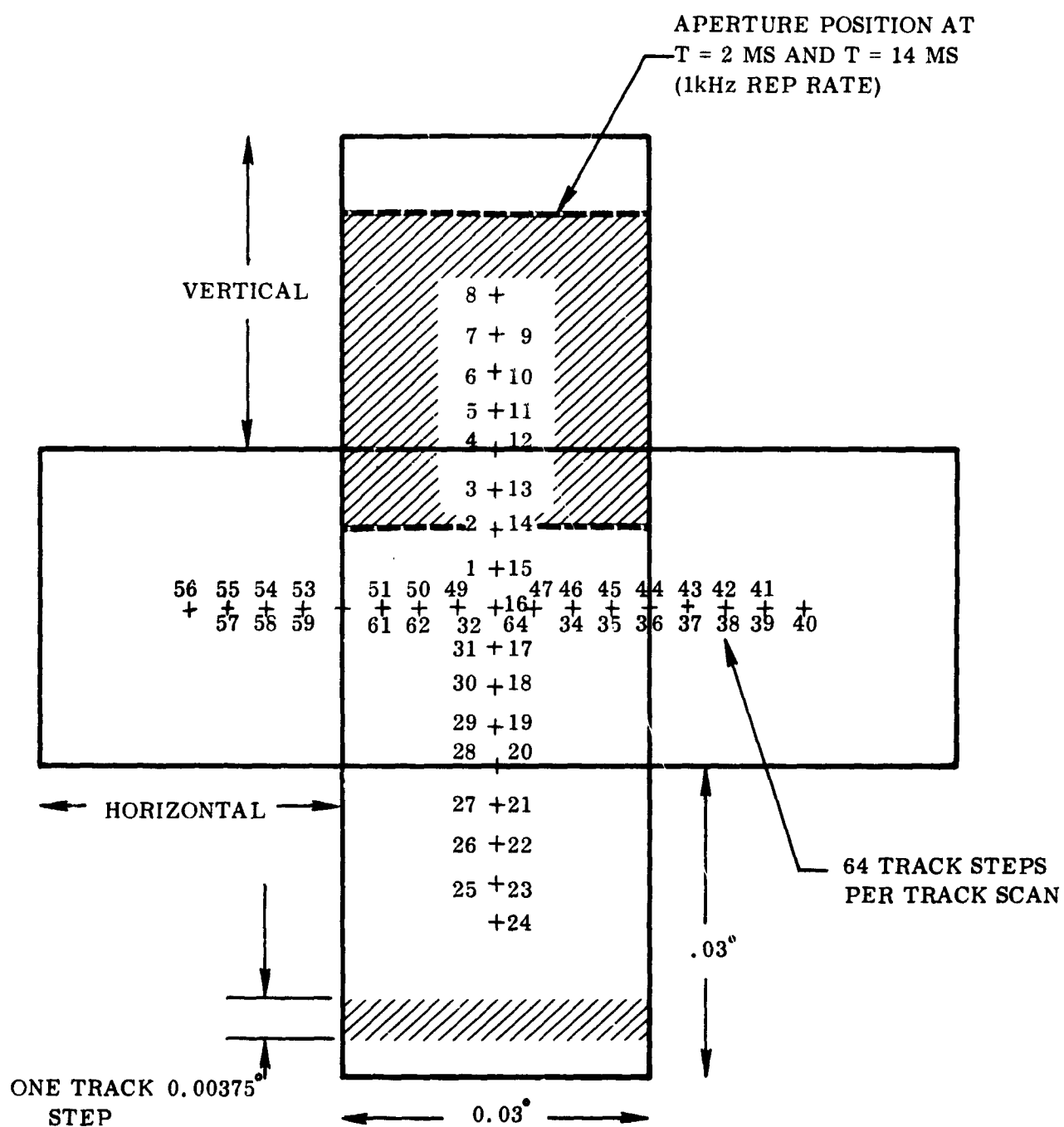


Figure 13. Scan Pattern for Track Mode

current in the deflection coils. This is accomplished by adding the appropriate correction to the aperture position in the computer program (Figure B-14).

By summing the successive position errors angular velocity error is generated. Correcting for velocity error has the effect of overshooting the target position initially, and then damping. Velocity feedback ideally gives the capability of following a constant velocity target with zero velocity error and a very small positional error. The tracker deviates from the ideal due to the digitized method of scanning and the particular type of track cross scan.

The angle tracker acquires the desired target and then builds up tracking constants. The tracker is capable of building up tracking constants for targets whose initial velocity and acceleration are relatively small. Once the target is acquired and the necessary feedback constants are built up, the tracker is capable of following the target, even if the target is moving at a relatively high angular rate.

The track scan computer program was designed with the following assumptions:

- The tracker is following a constant angular velocity target (with maximum angular velocity of 0.937 deg./sec.).
- The target attained this velocity slowly so that the tracker could build up feedback constants.
- In the program, feedback constants corresponding to the target velocity are initially set into the velocity return counters.

The effect of setting up these conditions is to cause an initial transient in tracker errors before the tracker settles down to a steady state condition. This steady state tracking is the normal operating mode of the tracker. Any effect of the transient on the computer data is to be ignored, because it is a result of forced initial conditions. Attention is focused on steady state tracking errors and capability.

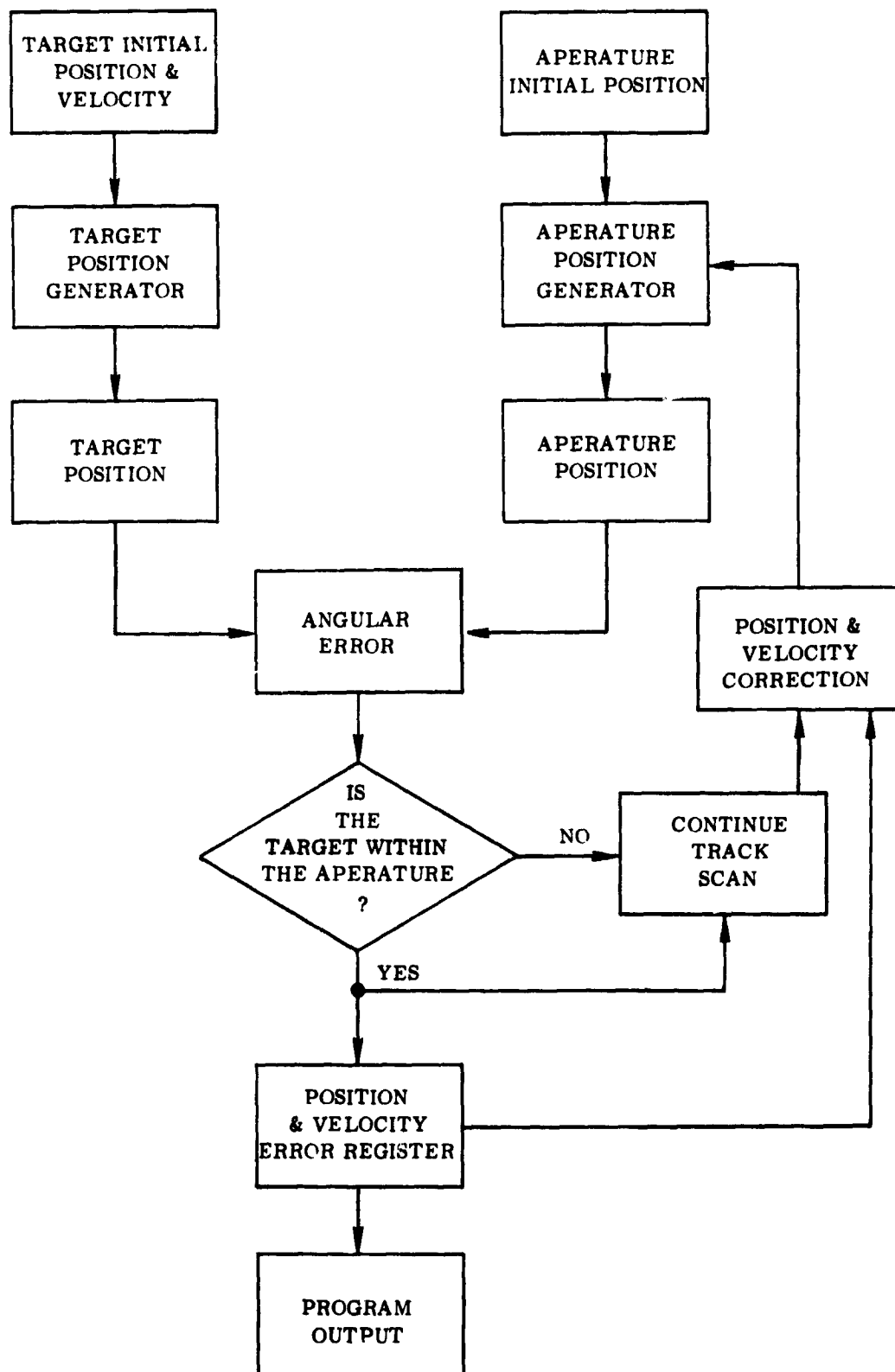


Figure B-14. Functional Block Diagram of Track Scan Program

### 3.0 DATA

The more important results desired from the track program are the tracker's angle and angular velocity tracking accuracies while following a target. Two forms of results are obtained from the program:

The average angular velocity and angle errors (Figures B-15, B-16, B-17, and B-18) of the tracker for a constant velocity target (these errors contain the effects of some transients).

Figures B-15 and B-16 show the average angular error for different velocities as a function of target velocity angle. The velocity angle is the true direction of the target with respect to the boresight axis of the angle tracker. The points denoted as X's on the curves represent target velocities and velocity angles at which the tracker cannot maintain track (i. e. , the target does not appear in the track scan). In most cases, this is a result of an ambiguous velocity or position feedback.

It should be noted that for target angular velocities less than or equal to 0.5 deg./sec. the average absolute angular error is less (usually much less) than one track step (see Figure B-15). The larger average errors show some of the effects of the initial transient, and finally the limitations of the tracker to follow a larger angular velocity (see Figure B-16).

The average angular velocity error for various target angular velocities and as a function of target angular velocity angles is shown in Figure B-17 and B-18. The majority of these errors are a result of the initial transient but it is observed that for a target angular velocity of 0.1 deg./sec. , the average error is only +.003 deg./sec/ to -.001 deg./sec. including transient. For a target angular velocity of 0.5 deg./sec. the error increased to +.008 deg./sec. and -.004 deg./sec. including transient. These errors are very small even with the added error.

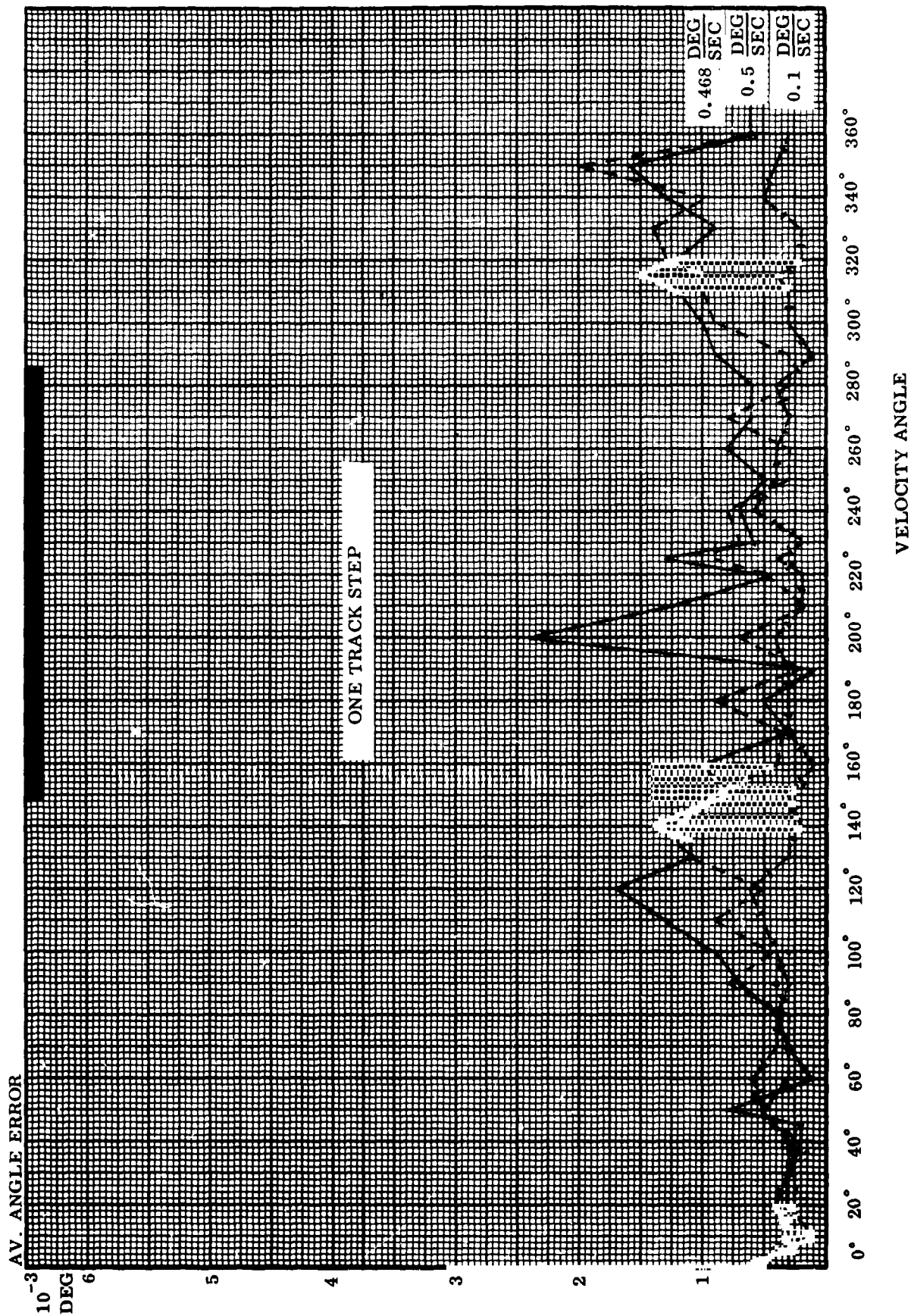


Figure 15. Average Angle Error

$|ZAV|$   
 $10^{-3}$  DEG

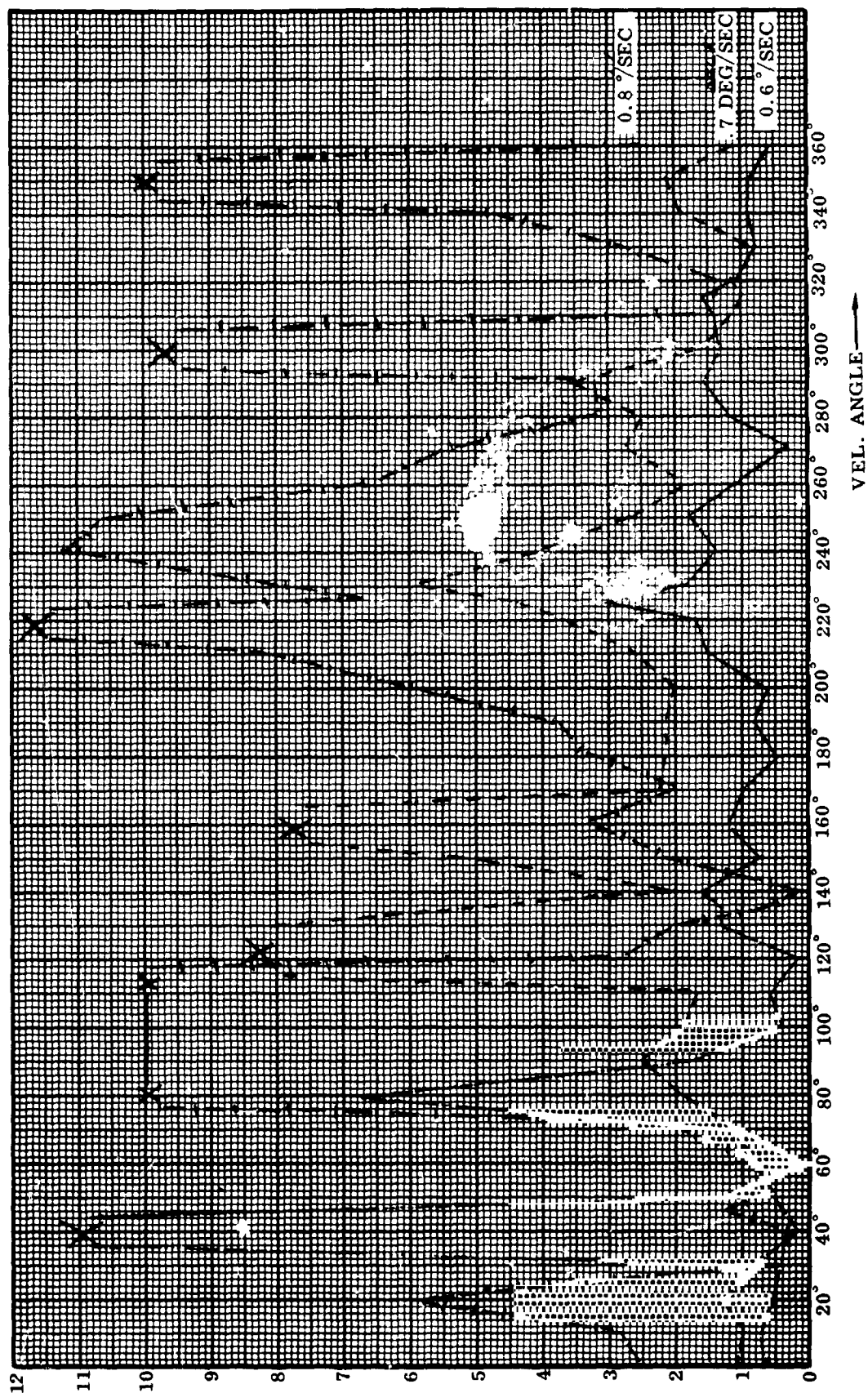


Figure B-16. Average Angle Error

AV. VEL. ERROR  
-3 DEG/SEC

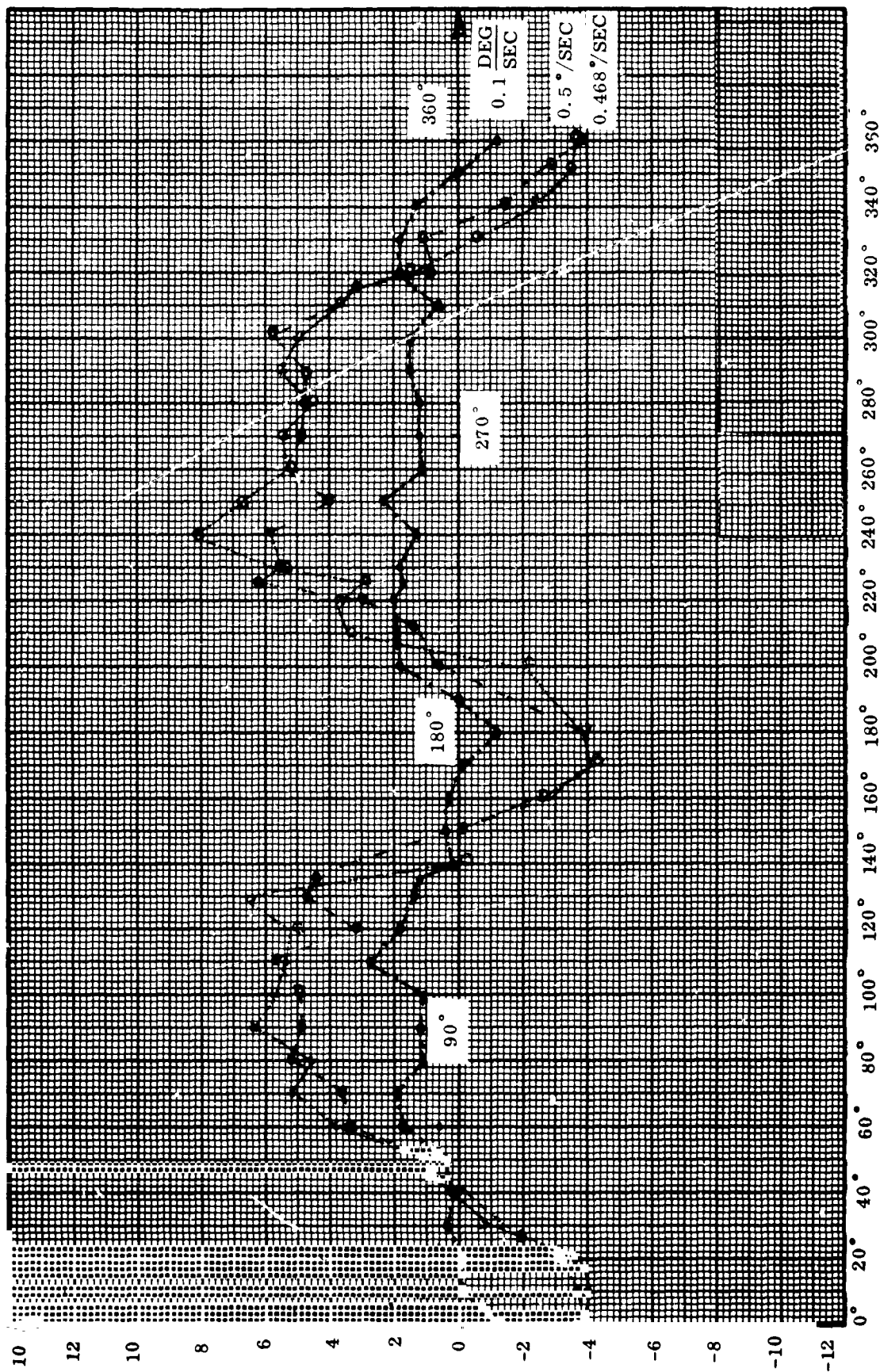


Figure 17. Average Velocity Error

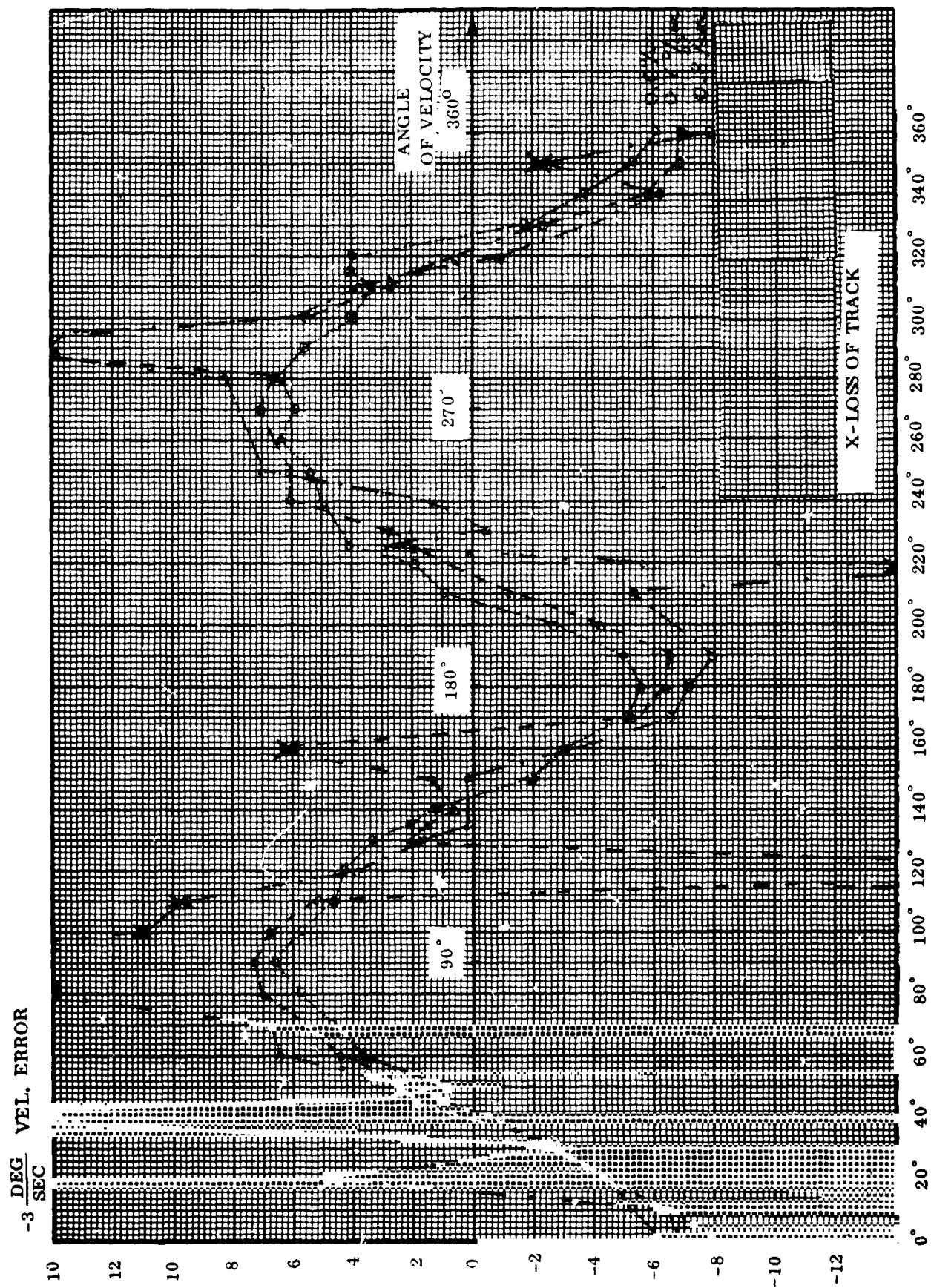


Figure B-18. Average Velocity Error



An example of the point-by-point data output of the program is shown in Figures B-19 and B-20 for a target angular velocity error is .005 deg./sec. The absolute angular error (Figure B-20) is characterized by a large initial variation which damps out to a small variation about some constant angular error (.011 degree).

Obviously the tracker cannot follow a target angular velocity with zero angular velocity error. The example in Figures B-21 and B-22 shows that the velocity error oscillates with a peak of  $\pm .02$  deg./sec. about zero. When the target is moving with an angular velocity of .7 deg./sec. and an angle of 30 degrees, the absolute angle error varies about .0113 degree.

The question might be asked as to why the absolute angular error in both cases oscillates about .011 degree. This question is best answered by looking at a detailed plot of the target and tracker position during steady state. Figure B-23 shows that the tracker is always ahead of the target at the beginning of a scan and behind at the end, (i. e. , at the beginning of the vertical scan the tracker aperture leads the target position in the vertical direction, but lags the target position at the end of the vertical scan). This has the effect of having the target move through the middle of the scan resulting in zero net returns. In this case the tracker will receive enough correction from the velocity return counter to put it ahead of the target at the beginning of the next scan. From this we see that at the beginning of the vertical scan the tracker must lead the target by  $1/2$  of the angle the target will travel during the vertical scan. For a target angular velocity of 0.7 deg./sec. and an angle of  $50^\circ$ , the horizontal and vertical components are .45°/s and 0.535°/s respectively. The horizontal and vertical angles travelled by the target during 16 ms are .0072° and .0085°. The absolute error is then determined to be

$$(.0072^\circ)^2 + (.0085^\circ)^2 - 1/2 = .0112^\circ.$$

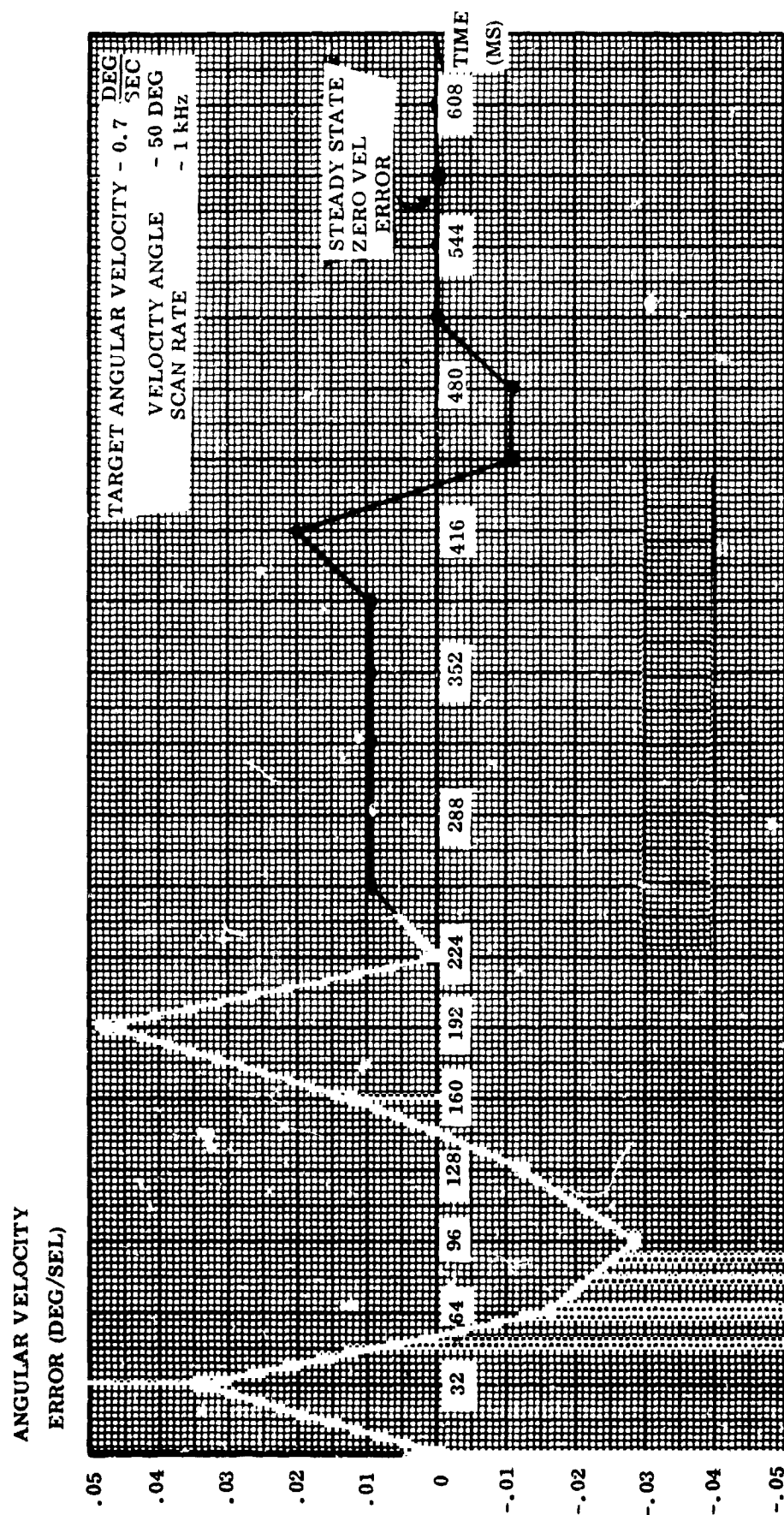


Figure B-19. Example of Velocity Error

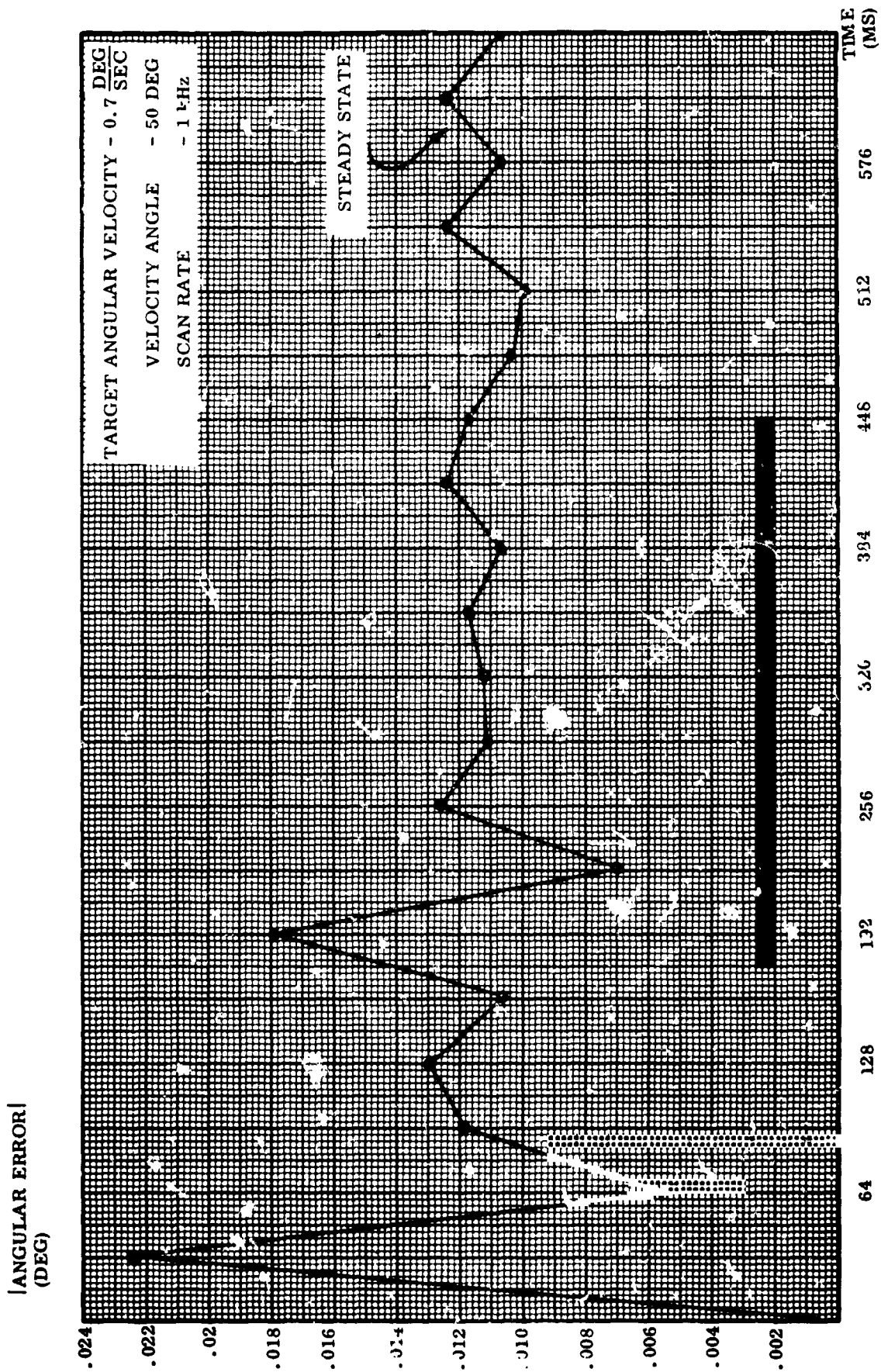
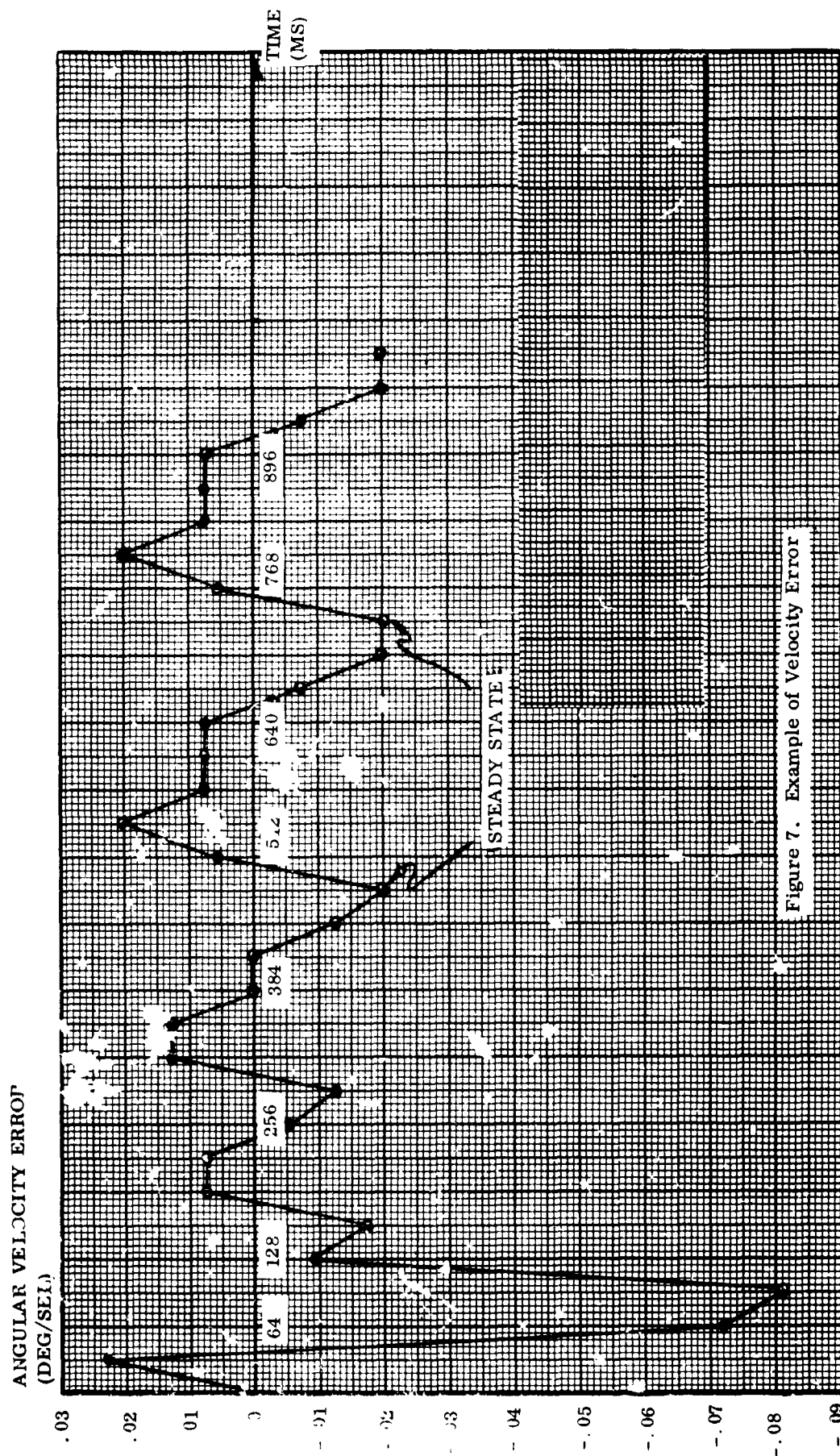


Figure B-20. Example of ABS Angle Error



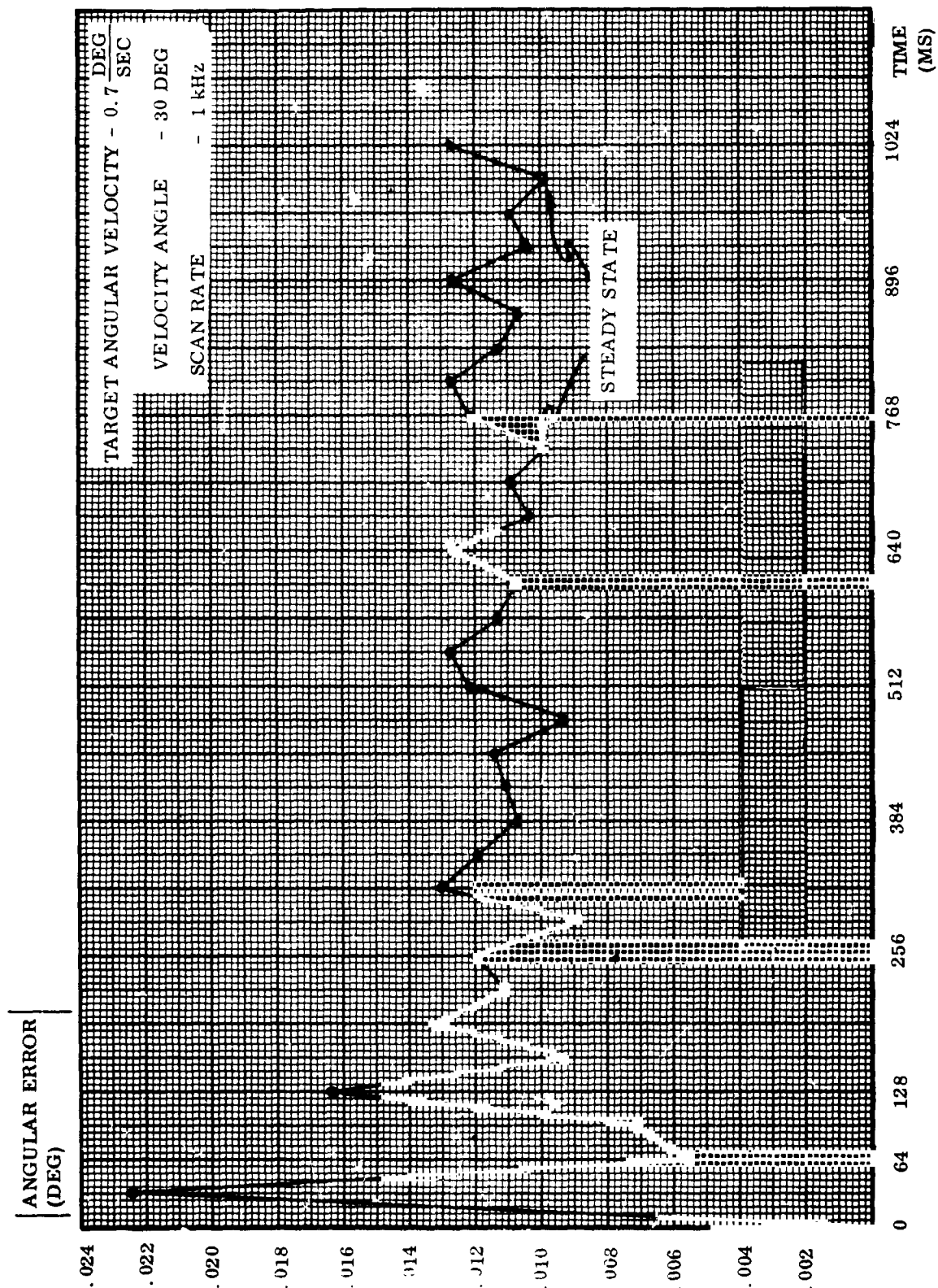


Figure B-22. Example of ABS Angle Error

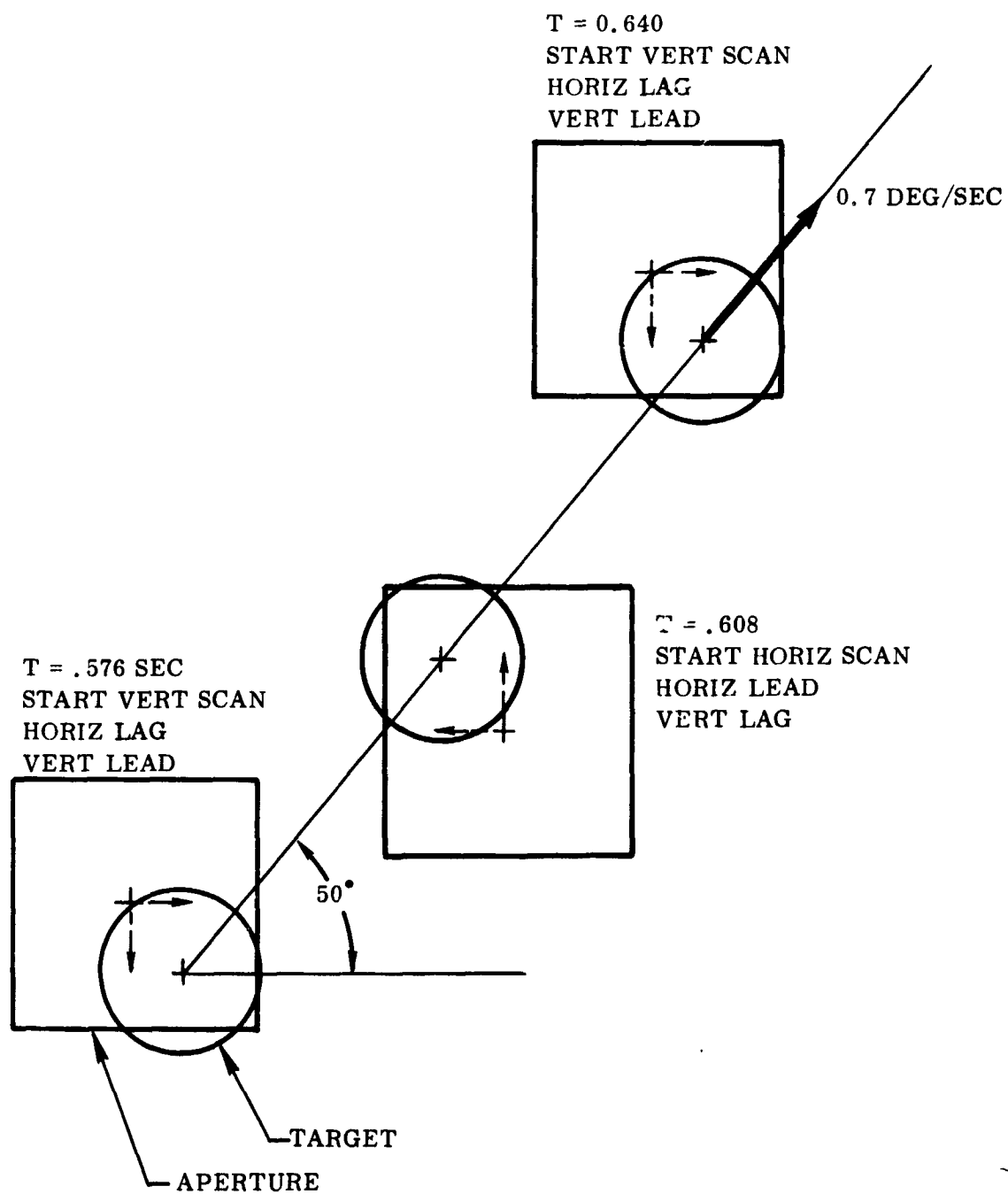


Figure B-23. Steady State Aperture and Target Position (Rep. Rate 1kHz)

The conclusion to be drawn from this, is that under study state conditions the average absolute angular error will be the distance the target will move in 16 ms. This conclusion is subject to the ability of the tracker to pick up the horizontal and vertical components of target angular velocity. This conclusion also gives a simple reason for the increase in absolute angular error with the target angular velocity (Figure B-15).

#### 4.0 CONCLUSION

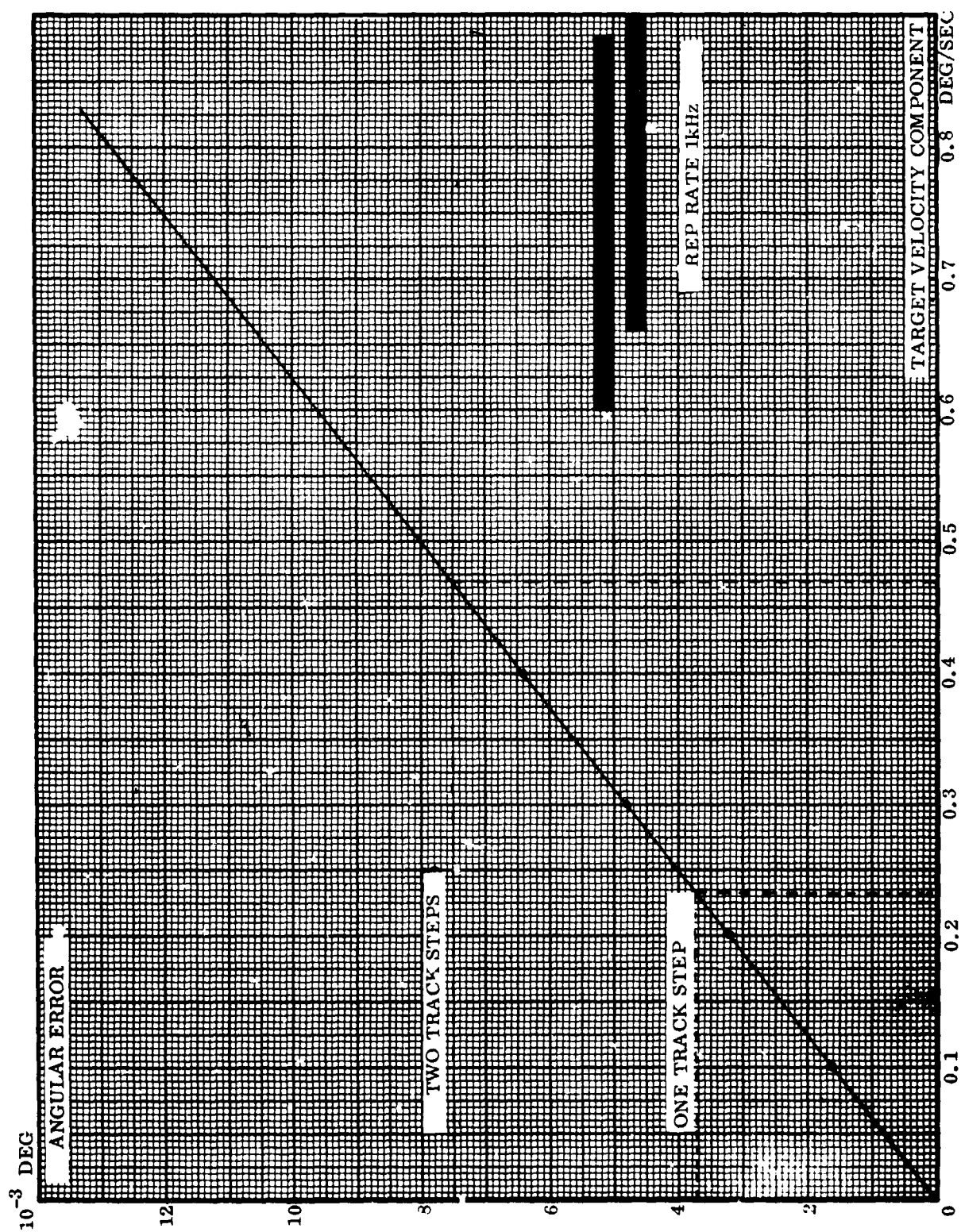
It is seen from Figure B-16 that the digital angular tracker can track a maximum angular velocity of 0.6 deg./sec. using a 1 kHz stepping rate. At .6 deg./sec. the tracker loses the target only at an angle of  $40^{\circ}$ . A target with the same velocity at any other angle can be tracked with average errors much less than one track step.

The angular position accuracy at the beginning of a horizontal or vertical scan is a function of the horizontal or vertical component of target angular velocity. Figure B-24 shows that if a target has a velocity of .1 deg./sec. in a horizontal direction then a reading of the tracker aperture position at the beginning of horizontal scan will give an error in target position of .0016 degree, or approximately one-half a track step. An additional error of  $\pm 1/4$  track step will be superimposed on this error due to the discrete resolution of the tracker.

Values of instantaneous angular velocity are obtained from the velocity return counters. These numbers represent the target angular velocity components in  $1/4$  track step per 64 ms. The limiting resolution in this case is  $1/4$  track step/64 ms or .01465 deg./sec. (no smoothing) for either the horizontal component or the vertical component.

The accuracy of the tracker average angular position and average angular velocity data will depend on the number of samples collected, the accuracy of the samples, and the type of average computed (mean, RMS, etc.). For a





ERROR VS. TARGET VELOCITY

Figure B-24. Instantaneous Angle Error vs. Target Velocity



simple mean of the horizontal and vertical position error sampled every 32 ms, the angular position accuracy is on the order of .001 degree and the angular velocity accuracy on the order of .006 deg./sec.

## APPENDIX C

### SENSOR PACKAGE THERMAL ANALYSIS

#### 1.0 INTRODUCTION

The Sensor Package described in this report as a part of the Optical Guidance System (OGS) is exposed to the same environment as the exterior of the vehicle itself. This fact, plus the possibility of supplanting or backing up an existing guidance system, implies that those parts of the OGS exposed to the environment be capable of thermal control with a minimum of support equipment for cooling and/or heating.

The actual sensor package, as defined in this report, is analyzed with respect to the high and low temperature extremes expected in its space environment. Methods of cooling and/or heating are described, and the predicted and actual results of a thermal-vacuum test of a representative model are discussed.

#### 2.0 THE GUIDELINES ASSUMED FOR THE THERMAL ANALYSIS OF THE OGS SENSOR PACKAGE ARE:

- The Sensor Package is mounted external to the vehicle and inhabits the same environmental extremes as the vehicle itself.
- The Sensor Package is thermally isolated from the vehicle.
- Since cooling of a package is more costly (with respect to size, weight, and power) than heating, the package is to be passively cooled by radiant heat transfer.
- Worst case condition for the package is when the internal electronics are functioning and the Sensor Package exposes its maximum surface to the sun. This occurs when the sun is perpendicular to the boresight of the package.

3.0 DETERMINATION OF UPPER TEMPERATURE LIMIT: THE SENSOR PACKAGE IS DEFINED IN FIGURE C-1. THE TOTAL HEAT INPUT FROM INTERNAL ELECTRONICS IS 20 WATTS (20 JOULES-SEC<sup>-1</sup>). THERMAL COOLING IS TO BE ACCOMPLISHED BY RADIANT HEAT TRANSFER.

The total heat input to the package is a combination of heat caused by the internal electronics (20 watts) plus heat due to solar impingement upon the exterior of the package.

$$Q_{IN} = A_P I_{SC} + I_{INT}$$

$I_{IN}$  = Internal Heat  
 $A_P$  = Projected Area of Package  
 $I_{SC}$  = Solar Constant

$$Q_{IN} = (.191 \text{ m}) (.432 \text{ m}) (1.39 \times 10^3 \text{ Joules-Sec}^{-1} \text{ m}^{-2}) + 20 \text{ Joules-Sec}^{-1}$$

$$Q_{IN} = (114.675 + 20) \text{ Joules-Sec}^{-1} (\text{WATTS}) = 134.675 \text{ watts}$$

If the Sensor Package is considered to have the radiation characteristics of the black body or ideal radiator, then it will absorb all radiation incident on its surface and the quality and intensity of the emitted radiation are determined by its temperature. The total radiative flux throughout a hemisphere from a black body of surface area A is then defined by the Stefan-Boltzmann Law:

$$Q_r = \sigma A T^4 \text{ where:}$$

$\sigma$  =  $5.67 \times 10^{-8} \text{ watts-M}^{-2} \text{ } ^\circ\text{K}^{-4}$   
 $A$  = Area in Meters<sup>2</sup>  
 $Q_r$  = Heat Input in Watts  
 $T$  = Temp <sup>o</sup>K

For the Sensor Package:

$$Q_r = 134.675 \text{ watts}$$

$$\sigma = 5.67 \times 10^{-8} \text{ watts-M}^{-2} \text{ } ^\circ\text{K}^{-4}$$

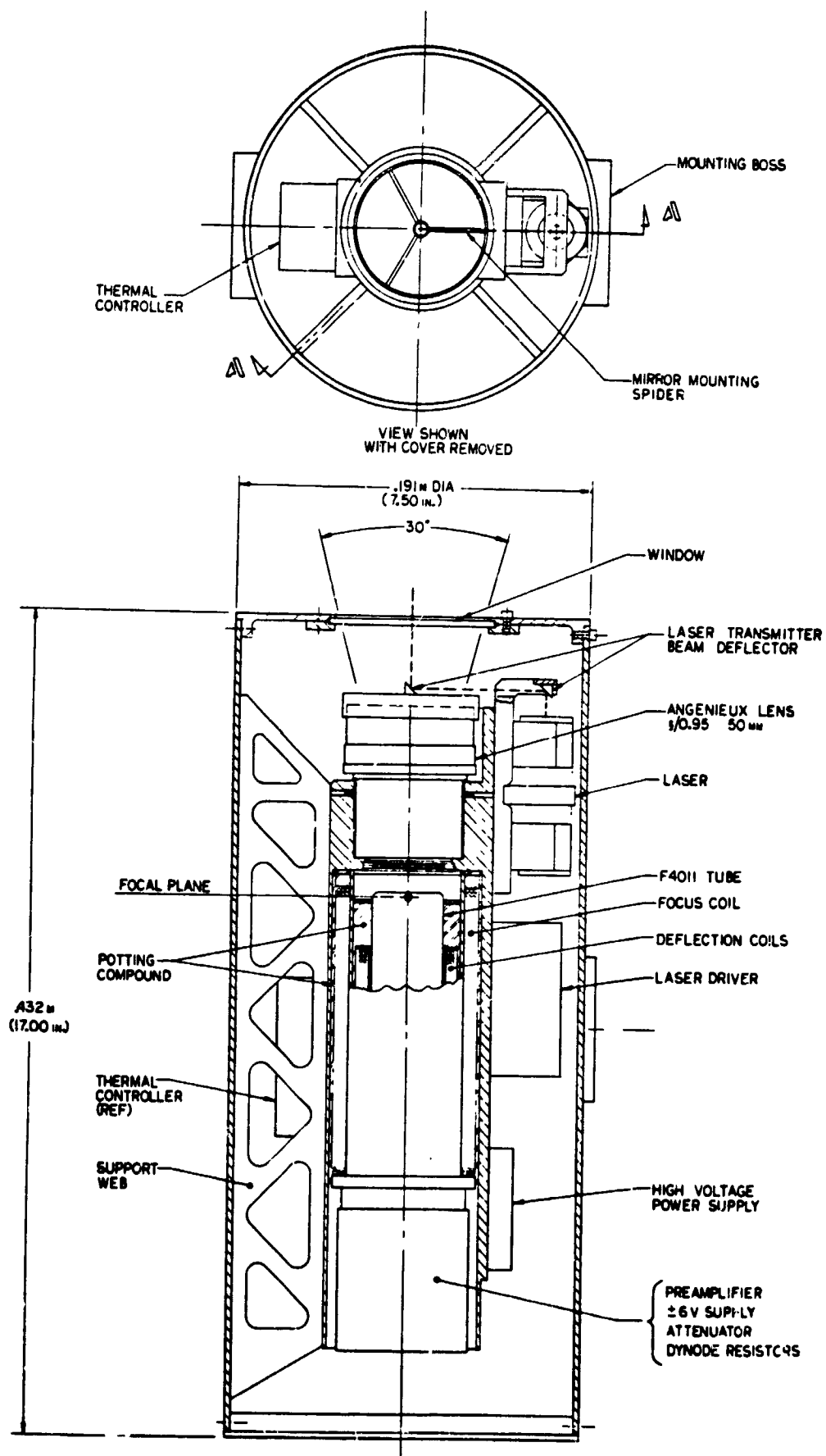


Figure C-1. Transmitter/Receiver Configuration (Sensor Package)  
C-3

$$A = \pi (.191 \text{ m}) (.432 \text{ m}) + \frac{\pi (.191)^2}{4} + \pi \left( \frac{.191^2 - .1^2}{4} \right)$$

$$A = .259 \text{ m}^2 + .028 \text{ m}^2 + .020 \text{ m}^2 = .307 \text{ m}^2$$

then  $T^4 = \frac{Q_r}{\sigma A} = \frac{134.675 \text{ watts}}{(5.67 \times 10^{-8} \text{ w-m}^{-2} \text{ } ^\circ\text{K}^{-4}) (.307 \text{ m}^2)} = .00774 \times 10^{12} \text{ } ^\circ\text{K}$

and  $T = 296.5^\circ\text{K} = 23.5^\circ\text{C} (74.3^\circ\text{F})$ . This steady state temperature is well within the operating range of the laser.

#### 4.0 DETERMINATION OF LOWER TEMPERATURE LIMIT

The temperature of the Sensor package when the electronics are turned off, and when there is no solar impingement on its surface, will drop to the temperature of its surroundings,  $-157^\circ\text{C} (-250^\circ\text{F})$ . If the equipment is required to operate in this environment, the only heat input will be the 20 watts radiated by the internal electronics. This 20 watts will result in a temperature of:

$$T^4 = \frac{Q_r}{\sigma A} = \frac{20 \text{ watt}}{(5.67 \times 10^{-8} \text{ w-m}^{-2} \text{ } ^\circ\text{K}^{-4}) (.307 \text{ m}^2)}$$

$$T^4 = .00115 \times 10^{12} \text{ } ^\circ\text{K}$$

$$T = 184^\circ\text{K} = -89^\circ\text{C} (-128.2^\circ\text{F})$$

#### 5.0 THERMAL MODEL ANALYSIS

To verify the temperature extremes defined in Parts III and IV above, a thermal model of the Sensor Package was fabricated and given a thermal-vacuum test to simulate actual flight conditions. The thermal test model (TTM) is defined in Figure C-2. The dimensions chosen for the diameter and length of the TTM are such that the ratio of projected area to actual surface area of the TTM approximates that of the actual Sensor Package. On the TTM, 15% of the area

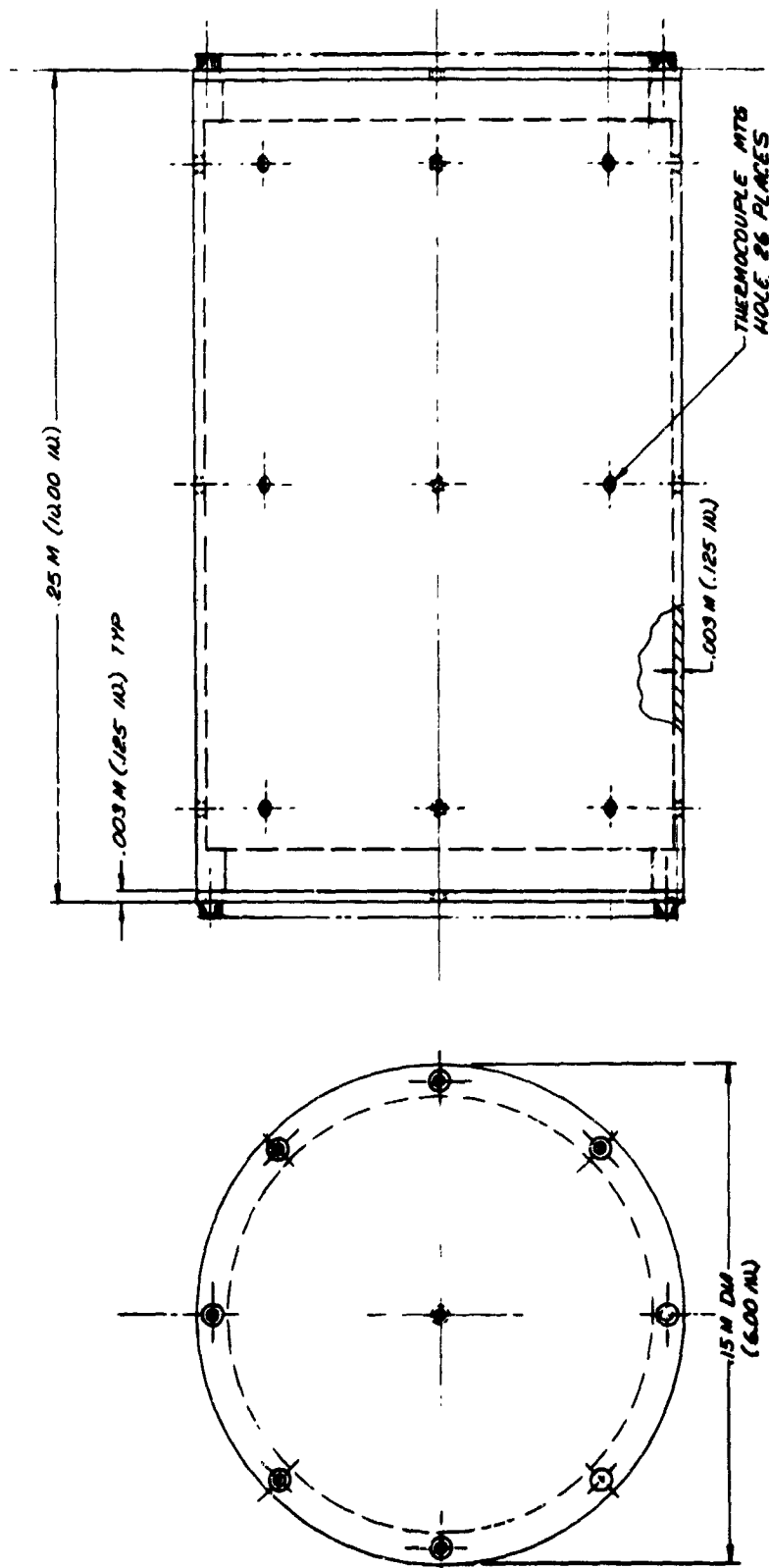


Figure C-2. Thermal Test Method

consisted of reflective stripes (aluminized mylar tape) in an attempt to gain a better heat balance (See Figure C-3). A simulated 20 watt electronics load was fabricated and mounted inside of the cylinder (See Figure C-4, C-5). Fourteen thermocouples were fastened to the TTM per Figure C-6. The TTM was then suspended in the ITT AOD space simulator and connected to the monitor console (See Figures C-7, C-8, C-9). The space simulator was sealed shut, pumped down, and the 20-watt load was turned on at the same time that the cold walls in the simulator were flooded with  $\text{LN}_2$ . Upon stabilizing at a low temperature, the solar simulator was positioned to illuminate the TTM and was turned on. One solar constant was directed at the TTM until the temperature was again stabilized, (See Figure C-10). The solar simulator was then turned off and the TTM was again allowed to stabilize. The 20-watt load was then turned off and the TTM was allowed to "cold-soak" until the temperature reached approximately  $-197^\circ\text{C}$  ( $-150^\circ\text{F}$ ). The 20-watt load was then turned on again and the TTM was again allowed to stabilize. This concluded the test.

## 5.1 TEMPERATURE PREDICTIONS

Utilizing the Stefan-Boltzmann Law to predict the temperatures to be encountered yielded the following results:

### 5.1.1 Temperature due to internal heating (20 watts) and solar impingement.

#### a. Surfaces all radiative

$$Q_{\text{IN}} = A_{\text{P}} I_{\text{SC}} + I_{\text{IN}}$$

$I_{\text{IN}}$  = Internal Heat  
 $A_{\text{P}}$  = Projected Area of Package  
 $I_{\text{SC}}$  = Solar Constant

$$Q_{\text{IN}} = (.152 \text{ m}) (.254) (1.39 \times 10^3 \text{ Joules-Sec}^{-1} \text{ m}^{-2}) + 20 \text{ watts}$$

$$Q_{\text{IN}} = (53.654 + 20) \text{ watts} = 73.654 \text{ watts}$$

NOT REPRODUCIBLE

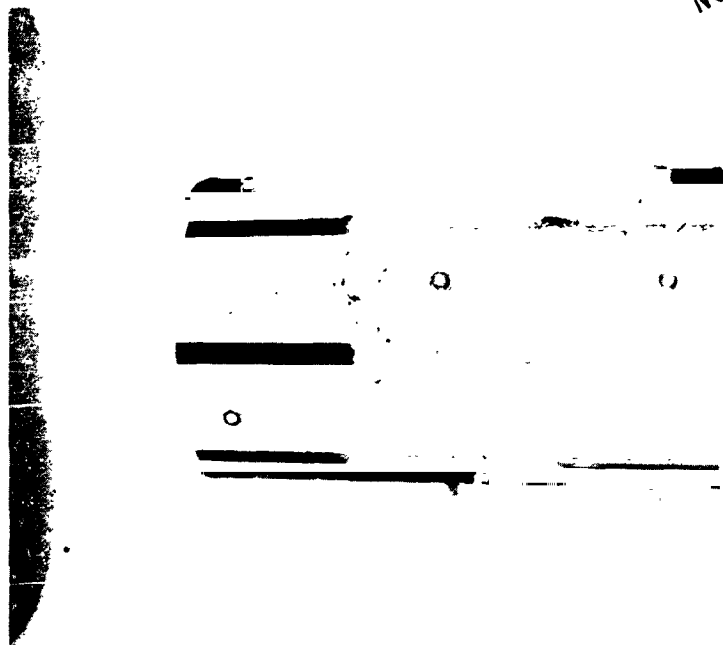


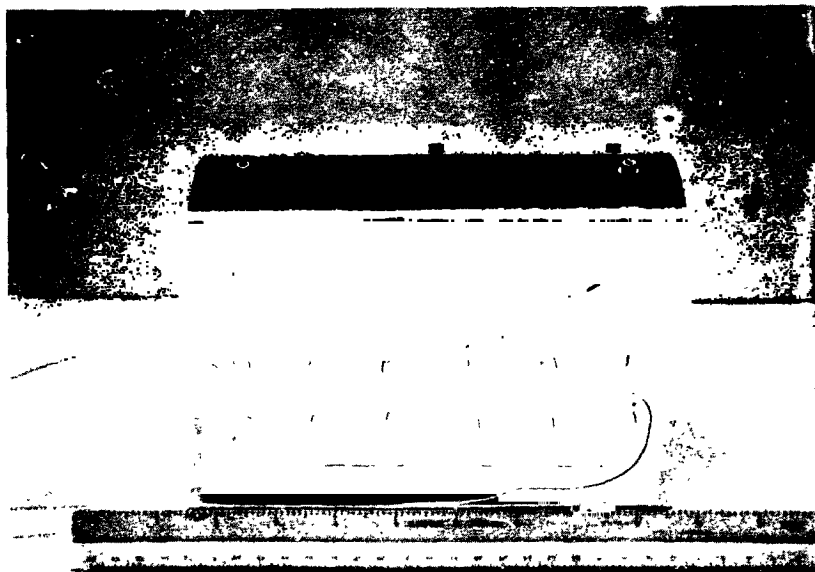
Figure C-3. Thermal Test Model With Reflective Stripes



Figure C-4. Simulated 20 Watt Load

ITT69/0443





ITT69/0443

Figure C-5. Simulated 20 Watt Load

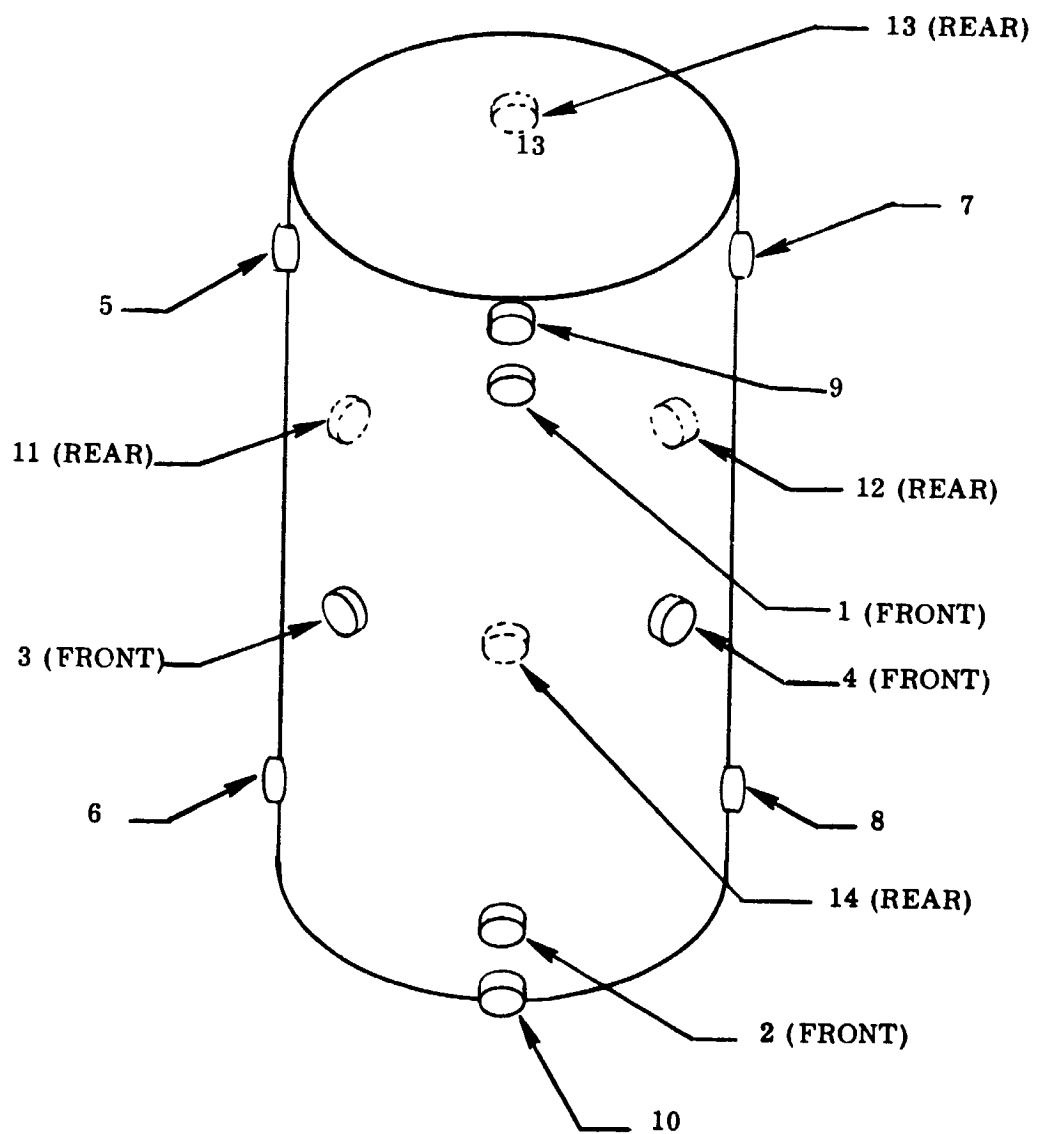


Figure C-6. Thermocouple Locations (1 thru 14) TTM

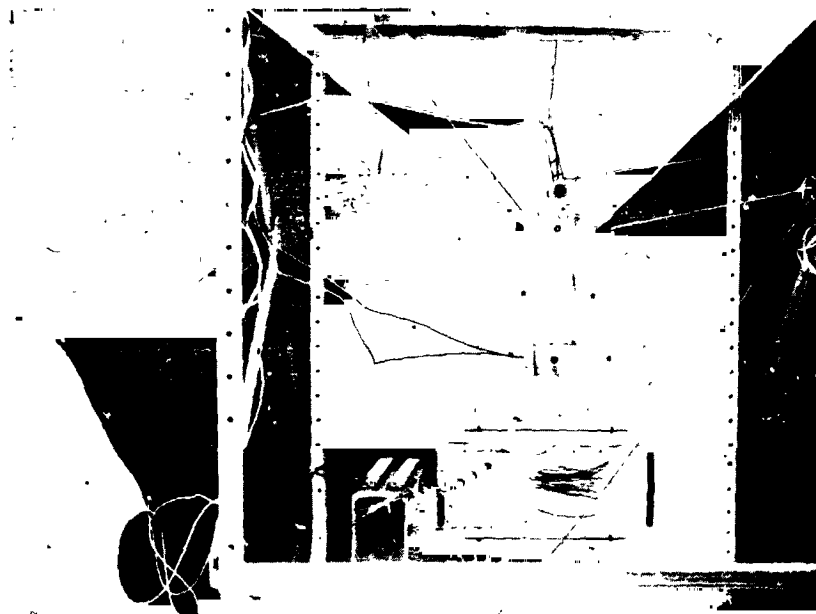


Figure C-7. TTM In ITTA/OD Simulator



Figure C-8. ITTA/OD Space Simulator

ITT69 0413

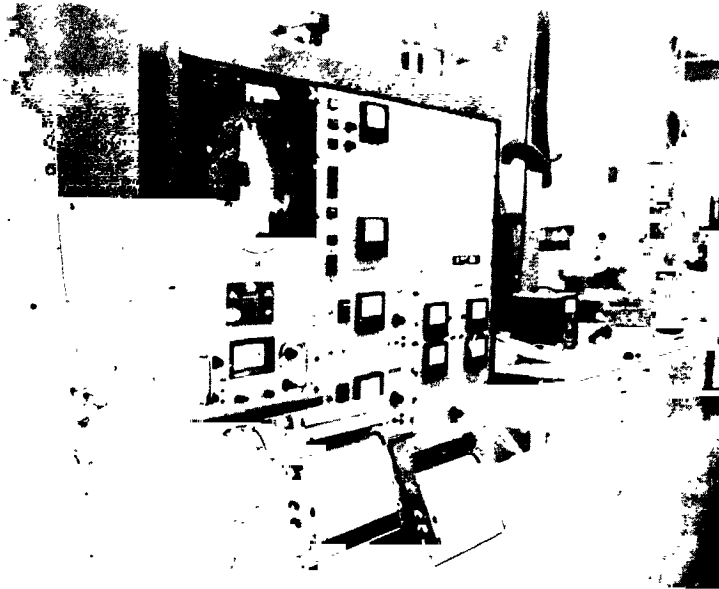


Figure C-9. ITTA/OD Space Simulator Control Console

NOT REPRODUCIBLE



Figure C-10. Solar Constant Applied

11765-9411

then:  $T^4 = \frac{Q_r}{\sigma_A} \quad A = (.152) (.254) + \frac{\pi}{2} (.152)^2 =$   
 $= .121 \text{ m}^2 + .036 \text{ m}^2 = .157 \text{ m}^2$   
 $T^4 = \frac{73.654 \text{ watts}}{(5.67 \times 10^{-8} \text{ w-m}^{-2} \text{ } ^\circ\text{K}^{-4}) (.157 \text{ m}^2)} = .0083 \times 10^{12} \text{ } ^\circ\text{K}$   
 $T = 301.5 \text{ } ^\circ\text{K} = 27.5 \text{ } ^\circ\text{C} (81.5 \text{ } ^\circ\text{F})$

5.1.2 Surfaces 15% reflective

$$T^4 = \frac{Q_r}{A}$$

$$Q_{IN} = 20 \text{ watts} + .85 (53.654) \text{ watts} = 65.594 \text{ watts}$$

$$A = .036 \text{ m}^2 + .85 (.121 \text{ m}^2) + .138 \text{ m}^2$$

$$T^4 = \frac{65.594 \text{ watts}}{(5.67 \times 10^{-8} \text{ w-m}^{-2} \text{ } ^\circ\text{K}^{-4}) (.138 \text{ m}^2)} = .0083 \times 10^{12} \text{ } ^\circ\text{K}$$

$$T = 301.5 \text{ } ^\circ\text{K} = 27.5 \text{ } ^\circ\text{C} (81.5 \text{ } ^\circ\text{F}) \text{ No apparent difference.}$$

<sup>1</sup> To obtain steady state low-end temperatures would have required extensive "soaking" at these two points of the test. It is felt that the critical results required are the high temperature points.

A graph of the average temperature of the TTM vs. Time is shown in Figure C-11.

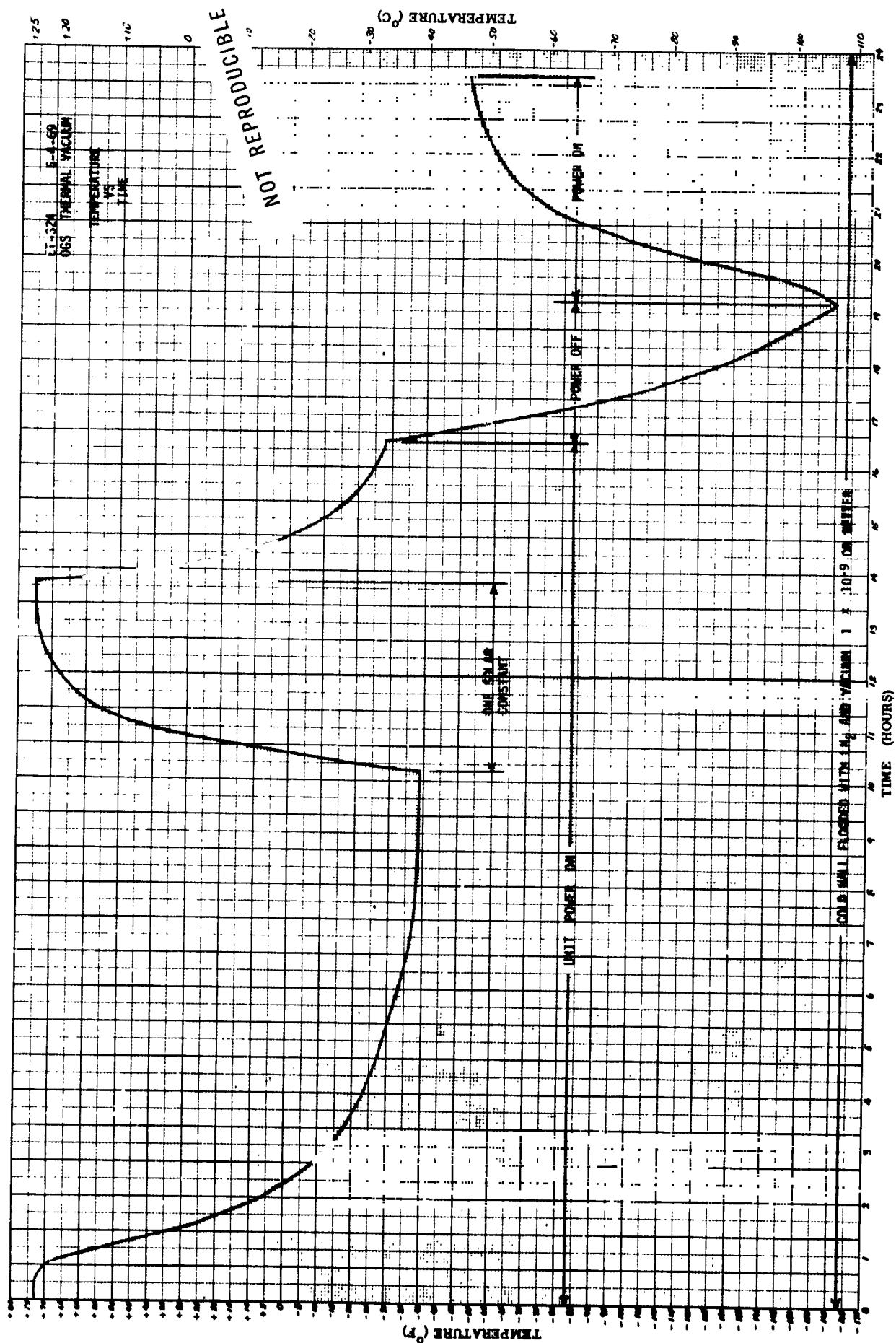


Figure C-11. OGS, Thermal Vacuum, Temperature Time

5.1.3 Temperature due to internal heating only

$$T^4 = \frac{20 \text{ watts}}{(5.67 \times 10^{-8} \text{ w} \cdot \text{m}^{-2} \cdot \text{K}^{-4}) (.157 \text{ m}^2)} = .00225 \times 10^{12} \text{ }^\circ\text{K}$$

$$T = 217.8 \text{ }^\circ\text{K} = -55.2 \text{ }^\circ\text{C} (-67 \text{ }^\circ\text{F})$$

5.1.4 Tabulation of Results Obtained Utilizing Stefan-Boltzmann Law:

(Table C-1)

Versus Experimental Data

<u>SUN</u>	<u>EXPERIMENTAL DATA</u>		<u>TEMPERATURE</u>
	<u>20 WATT LOAD</u>	<u>PREDICTED</u>	<u>ACTUAL</u>
OFF	ON	-55.2 <sup>o</sup> C	-40 <sup>o</sup> C <sup>1</sup>
ON	ON	+27.5 <sup>o</sup> C	+23.9 <sup>o</sup> C
OFF	OFF	-196 <sup>o</sup> C	-107 <sup>o</sup> C <sup>1</sup>

## APPENDIX D

### LASER SAFETY ANALYSIS

The Optical Guidance System uses laser radar to determine the relative position between two spacecraft. Because there is a possibility that an astronaut will be exposed to the laser radiation, ITT has conducted a preliminary laser safety study.

During rendezvous and docking, one spacecraft will illuminate a corner cube reflector on the second spacecraft with a pulsed laser beam. The laser irradiance is greater when the two spacecraft are closer together (predocking and docking). The worst case condition would occur at short range if the entire laser beam was accidentally diverted into a spacecraft window and into the astronaut's eye. See Figure D-1 for the short range example. At longer ranges, part of the laser beam will invariably enter the spacecraft windows in the line-of-sight, however, the irradiance will be reduced greatly because of the beam-spread. See Figure D-2 for the long range example. All cases that could be a potential hazard to the safety of the astronauts are considered.

The eye is the most sensitive part of the human body to laser radiation in the visible and near infrared electromagnetic spectrum. The retina of the eye is particularly vulnerable because of the focusing properties of the ocular system. Figure D-3 shows the basic structure of the eye. A simple model of the irradiance at the retina of an eye due to a laser is shown in Figure D-4. The eye can be represented as a simple optical system that has a receiving lens with an adjustable diameter and focal length, and an optical sensor that reacts differently for various wavelengths of incident radiation.



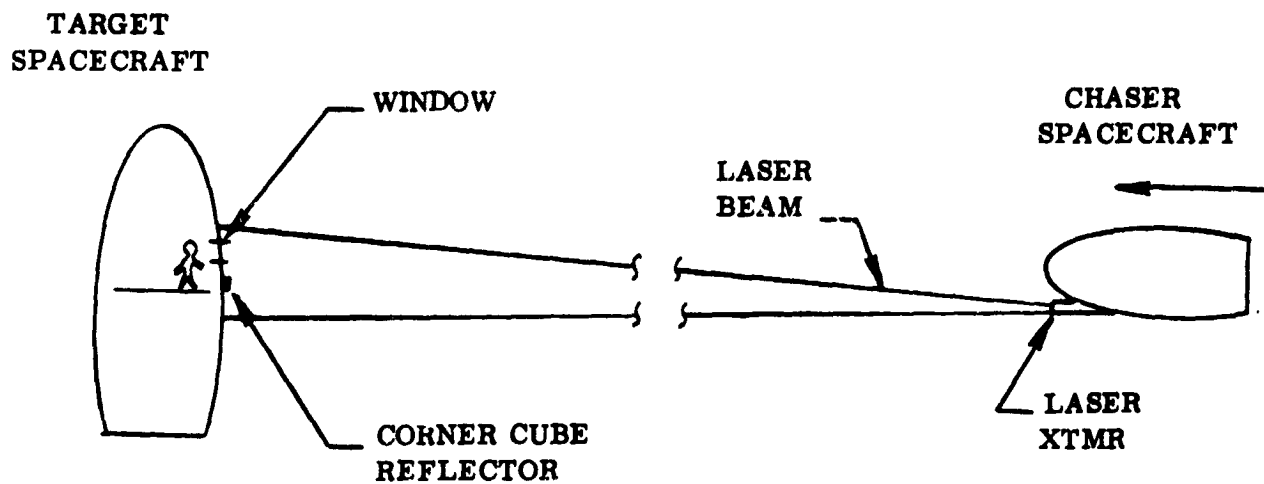


Figure D-1. Long Range Example

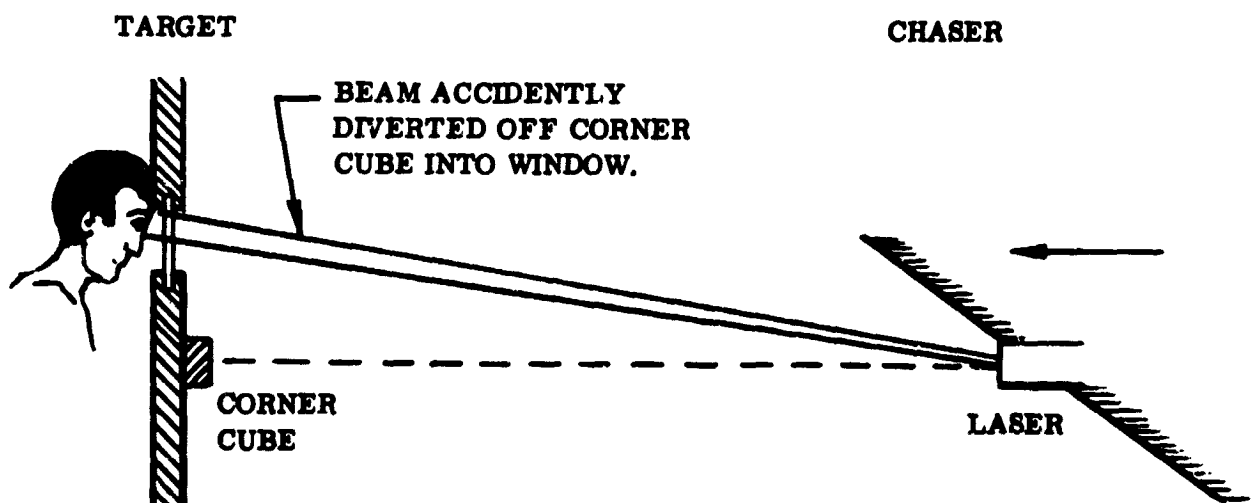


Figure D-2. Short Range Example

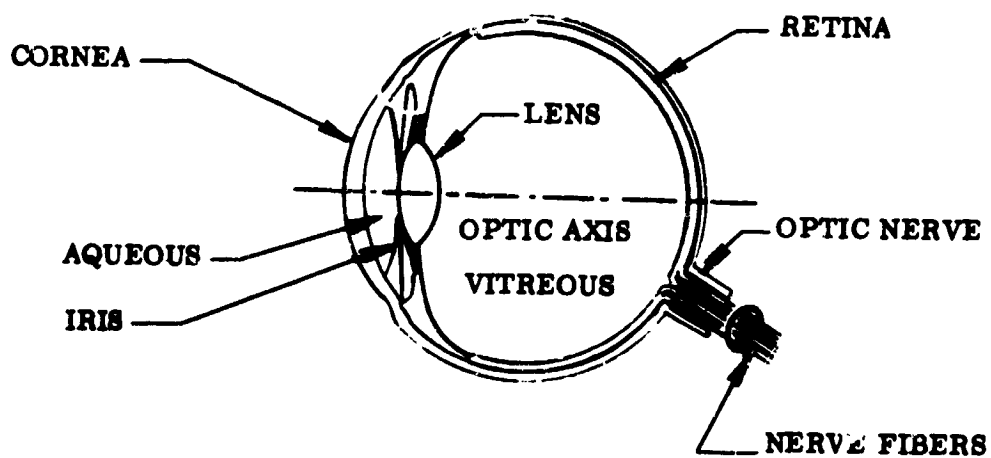


Figure D-3. Structure of Eye

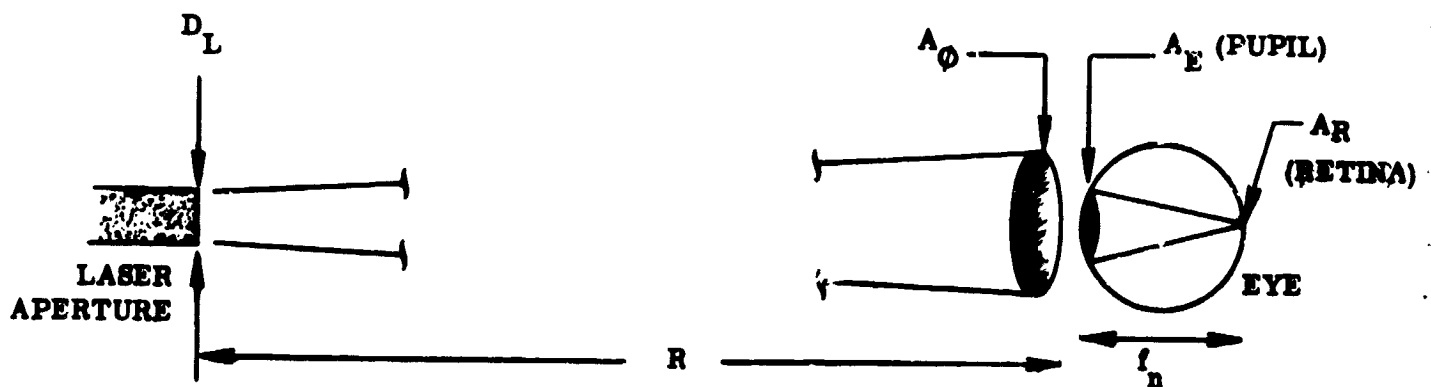


Figure D-4. Irradiance at Retina

In order to simplify the problem, and also to obtain the worst case results, certain assumptions were made in the laser safety calculations presented here. The diameter of the iris (entrance pupil of eye) can vary from 2 mm (light adapted) to 7 mm (dark adapted). The largest diameter is assumed because it can collect more radiation. The eye is also assumed to be unaccommodated (focused at infinity). This means that incoming parallel light rays will be focused to a small spot at the retina determined by Fraunhofer diffraction. To simplify the calculations it is assumed that the radiant emittance is constant at the laser exit aperture, even though it is recognized that hot spots often exist in many lasers.

Employing the above assumptions, expressions are developed so that safe levels of operation can be determined. First, a general expression is developed for the irradiance ( $H_r$ ) at the retina of the eye due to direct exposure from a laser source. Worst cases are then considered. Next, an expression is developed for the minimum safe distance ( $R_s$ ) that an exposed eye can be from the laser source before attenuation filters are needed.

The irradiance ( $H_r$ ) at the retina of the eye (see Figure D-4) can be expressed as:

$$H_r = \frac{P_L p_\lambda \left[ \frac{A_E}{A_\phi} \right]}{A_r} \quad (D-1)$$

where:

- $H_r$  = Retinal irradiance
- $P_L$  = Radiant emittance of laser
- $p_\lambda$  = Spectral trans. of eye at  $\lambda$
- $A_E$  = Area of eye at iris (pupil)
- $A_\phi$  = Area of laser beam at pupil
- $A_r$  = Area of smallest possible laser spot at the retina (eye focused at infinity)

After inserting the proper expressions for the areas  $A_E$ ,  $A_\phi$ , and  $A_r$  (area of central maximum of Fraunhofer diffraction pattern) the expression for retinal irradiance becomes:

$$H_r = \frac{P_L P_\lambda \left[ \frac{\frac{\pi}{4} (D_E)^2}{\frac{\pi}{4} (\phi R + D_L)^2} \right]}{\frac{\pi}{4} \left[ \frac{2.44 f_n \lambda}{D_E} \right]^2} \quad (D-2)$$

where:

$D_E$  = Pupil diameter

$\phi$  = Laser divergence

$R$  = Range from eye to laser

$D_L$  = Laser source diameter (The radiating aperture will be a square, but a circle is assumed to simplify calculations.)

$f_n$  = Focal length of unaccommodated eye

$\lambda$  = Wavelength of laser

The transmitter used in the Optical Guidance System is a GaAs diffraction limited laser. It will be operated in the pulsed mode at a 10 kHz maximum pulse repetition rate. The pulse width will be 100 ns and the peak output power will be approximately 5 watts. Because of the relatively high repetition rate for this laser, both the average retinal irradiance and peak retinal irradiance must be considered. The worst case for both of these occurs when all of the energy from the laser enters the eye and is focused into the smallest retinal spot possible. For this  $A_E/A_\phi = 1$ , and the maximum retinal irradiance expression is:

$$H_{r_{\max}} = \frac{P_L p_\lambda}{\frac{\pi}{4} \left[ \frac{2.44 f_n \lambda}{D_E} \right]^2}$$

The radiant emittance ( $P_L$ ) of the laser is the only parameter in the above expression that is different for the peak and average worst cases. Using the following values the maximum peak and maximum average retinal irradiances are calculated:

$$P_L(\text{Peak}) = P_{pk} \Delta t = (5w) (100ns) = 5 \times 10^{-7} \text{ joules}$$

$$P_L(\text{Avg.}) = \frac{P \Delta t}{T} = \frac{(5w) (100ns)}{.1 \text{ ms}} = 5 \text{ mwatts}$$

$$p_\lambda = .74$$

$$f_n = 1.7 \text{ cm}$$

$$\lambda = .910 \times 10^{-4} \text{ cm}$$

$$D_E = .7 \text{ cm (dark adapted)}$$

$$A_r = \frac{\pi}{4} \left[ \frac{2.44 (1.7 \text{ cm}) (.910 \times 10^{-4} \text{ cm})}{.7 \text{ cm}} \right]^2 = \frac{\pi}{4} \left[ 5.4 \times 10^{-4} \text{ cm} \right]^2$$

$$A_r = 22.6 \times 10^{-8} \text{ cm}^2$$

Thus:

$$H_{r_{\max}}(\text{Peak}) = 1.6 \text{ joules/cm}^2$$

$$H_{r_{\max}}(\text{Avg.}) = 1.6 \times 10^4 \text{ watts/cm}^2$$

The human eye can be directly exposed to laser radiation as long as the retinal irradiance is below a prescribed safe level. There are two basic methods to keep the retinal irradiance below the safe level for given laser parameters. The first method is to establish a minimum safe range ( $R_s$ ) that the exposed eye must be from the laser source. Because the laser beam is diverging, the exposed eye will subtend only a small portion of the projected beam at long ranges ( $A_\phi > A_E$ ).

The minimum safe range ( $R_s$ ) can be determined by setting

$$\frac{1}{K} = \frac{A_E}{A_\phi}$$

or:

$$\frac{1}{K} = \frac{\frac{\pi}{4} (D_E)^2}{\frac{\pi}{4} (R_s + D_L)^2}$$

where  $K$  is the safety factor needed to reduce the maximum irradiance ( $H_{r_{\max}}$ ) down to a safe level ( $H_{r_{\text{safe}}}$ ).

Thus:

$$K = \frac{H_{r_{\max}}}{H_{r_{\text{safe}}}}$$

Solving for  $R_s$  in the equation above will give the following expression for the minimum safe range:

$$R_s = \frac{(K)^{1/2} D_E - D_L}{\phi} \quad (D-3)$$

The second method to keep the retinal irradiance below the safe level is to put an optical blocking filter in front of the exposed eyes. The optical blocking filter will attenuate the laser radiation (9100 Å) down to a safe level, but will not attenuate light in the visible spectrum (4000 Å - 7000 Å). An optical blocking filter placed on each spacecraft window will adequately protect the astronauts even for the worst case where the entire beam spread would be subtended by the eye.

The next question that must be answered is: what are the safe peak and safe average retinal irradiance levels. Numerous reports have been written concerning laser safety the last couple years. Safe levels have not been universally established, however, it is generally agreed that an allowable safe level for peak retinal irradiance (narrow pulses of 5 ns-100 ns) is  $1.0 \times 10^{-3}$  joules/cm<sup>2</sup>. And, an allowable safe level for average retinal irradiance of 0.1 watts/cm<sup>2</sup>. A safety factor of approximately 10 above present experimental threshold damage levels is included in these safe levels. It is expected that additional experimental data within the next year or two will allow universally acceptable safe levels to be established. If it appears that this will not occur, or that the data will not be directly applicable to the GaAs diffraction limited laser, then ITT will recommend that a qualified medical center perform a laser safety experiment using the same laser that will be used in the Optical Guidance System. ITT has already discussed such an experiment with Stanford Research Institute and the University of Cincinnati, both of which have already conducted numerous safety experiments for various laser applications.

Using the above mentioned safe levels, the safety factor (K), the attenuation needed to reduce the maximum retinal irradiance ( $H_{r \max}$ ) down to a safe level, can be calculated for the laser applications discussed in this report.

$$K(\text{Peak}) = \frac{H_{r_{\text{max}}}(\text{Peak})}{H_{r_{\text{safe}}}(\text{Peak})} = \frac{1.6 \text{ joules/cm}^2}{1.0 \times 10^{-3} \text{ joules/cm}^2} = 1.6 \times 10^3$$

$$K(\text{Avg}) = \frac{H_{r_{\text{max}}}(\text{Avg})}{H_{r_{\text{safe}}}(\text{Avg})} = \frac{1.6 \times 10^4 \text{ watts/cm}^2}{0.1 \text{ watts/cm}^2} = 1.6 \times 10^5$$

The first method for keeping the retinal irradiance below the safe level for given laser parameters can now be examined qualitatively. The minimum safe range ( $R_s$ ) that the exposed eye must be from the laser source is then calculated as follows:

$$R_s = \frac{(K)^{1/2} D_E - D_L}{\phi}$$

where:

$$K(\text{Peak}) = 1.6 \times 10^3$$

$$K(\text{Avg}) = 1.6 \times 10^5$$

$$D_E = .7 \text{ cm}$$

$$D_L = .5 \text{ cm}$$

$$\phi = .03^\circ = .51 \times 10^{-3} \text{ radians}$$

Thus:

$$R_s(\text{Peak}) = 540 \text{ meters} \approx 1/3 \text{ mile}$$

$$R_s(\text{Avg}) = 5,600 \text{ meters} \approx 3 \text{ miles}$$



The first method is therefore not practical for rendezvous and docking applications. For a larger laser beamwidth ( $\phi = 3^\circ$ ), the  $R_s(\text{Avg}) = 56$  meters, however, the constraint of making sure the astronaut never gets into the line-of-sight of the laser during pre-docking could be difficult to implement.

The second method of providing the spacecraft windows with optical blocking filters is the most feasible and practical method. Using the worst case safety factor,  $K(\text{Avg})$ , the optical blocking filter would be designed to attenuate the laser radiation ( $9100 \text{ \AA}$ ) by  $1.6 \times 10^5$ . Again, the visual spectrum ( $4000 \text{ \AA} - 7000 \text{ \AA}$ ) will not be attenuated.

The purpose of this preliminary laser safety study was to determine the hazards of using a laser, in the Optical Guidance System, and to recommend precautionary methods that would eliminate or greatly reduce the hazards. Man has always lived in a radiation environment that is potentially harmful to his eyes. Direct exposure to the sun for short periods will damage the retina of the eye. However this rarely occurs, because of a natural tendency to avoid direct viewing of the sun. Lasers can be potentially more dangerous than the sun, but as long as the hazards are recognized, precautionary methods can afford adequate safety (i.e., optical blocking filters in windows).

It is worthwhile to examine the comparison between the retinal irradiance due to the sun and the GaAs laser that will be used by the OGS. The comparison is made for direct exposure of the sun, and for the worst case where all the laser energy enters the eye. Figures D-5 and D-6 pictorially depict these examples. The retinal irradiance ( $H_{R_S}$ ) due to the sun is:

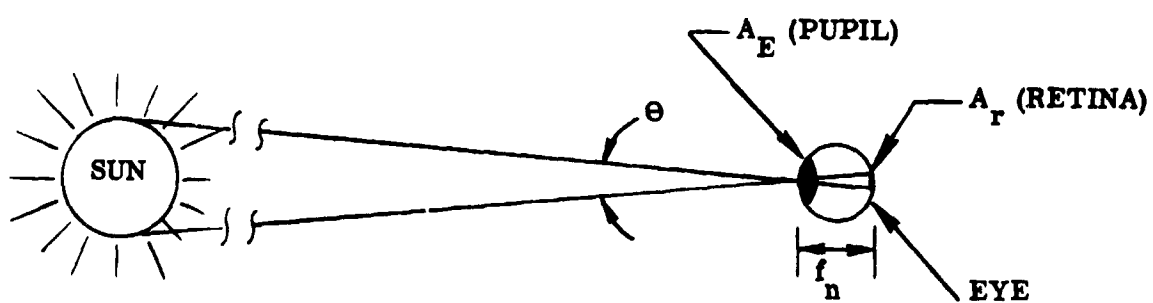


Figure D-5. Retinal Irradiance Due to Sun

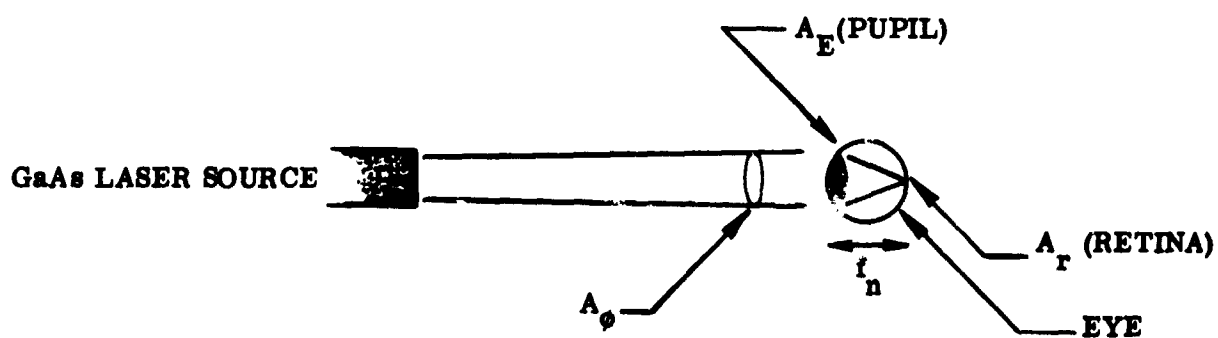


Figure D-6. Retinal Irradiance Due to GaAs Laser  
(Worst Case-Eye Subtends Entire Beam Spread)

$$H_{R_S} = \frac{H_S A_E}{A_R} \quad (D-4)$$

where:

$$H_S = .134 \text{ watts/cm}^2 \text{ (irradiance at eye pupil due to sun)}$$

$$A_E = \frac{\pi}{4} D_E^2 = \frac{\pi}{4} (3 \text{ mm})^2$$

$$A_R = \frac{\pi}{4} d_R^2 \quad d_R = \Theta f_n \approx (.5^\circ) (1.7 \text{ cm}) = .16 \text{ mm}$$

$$A_R = \frac{\pi}{4} (.16 \text{ mm})^2$$

$$H_{R_S} = \frac{(.134 \text{ w/cm}^2) \left[ \frac{\pi}{4} (3 \text{ mm})^2 \right]}{\frac{\pi}{4} (.16 \text{ mm})^2} = 54 \text{ watts/cm}^2$$

The maximum retinal irradiance,  $H_{r_{\max}}$  (Avg), due to the GaAs laser was previously calculated to be  $1.6 \times 10^4 \text{ watts/cm}^2$ . The ratio between these is:

$$C_o = \frac{H_{r_{\max}} \text{ (Avg) [laser]}}{H_{R_S} \text{ [sun]}} = \frac{1.6 \times 10^4 \text{ watts/cm}^2}{54 \text{ watts/cm}^2}$$

$$C_o = 300$$

or in other words, the GaAs laser under worst case conditions is potentially 300 times more dangerous than direct exposure to the sun.

## APPENDIX E

### DETAILED GIMBAL CONSIDERATIONS

#### 1.0 MATERIALS

A detailed analysis of three of the candidate materials for use in the gimbals is contained below. Each material is analyzed to determine deflection, maximum stress, natural frequency, and linear expansion.

The formulas employed are noted below. They are for a beam loaded in the center and fixed at both ends. The load in each case is one half of the total payload multiplied by 50 G's. All values are preliminary and for purposes of comparison.

$$\text{DEFLECTION} = \frac{WL^3}{48EI}$$

where:

W = Load

L = Beam length

E = Modulus of elasticity

I = Moment of inertia

I for a channel taken vertically

$$= \frac{hd^3 - h^3(h-t)}{12}$$

where:

h = channel width

d = channel height outside

b = channel height inside

t = web thickness

Maximum stress for a channel loaded at the center is given by:

$$S = \frac{Wl}{4Z}$$

where:

W = load

l = beam length

$$Z = \text{section modulus} = \frac{bd^3 - h^3(b-t)}{6d}$$

b, d, and t have similar values as noted above.

The natural frequency of the beam employing the Rayleigh method is given by

$$\omega = \frac{\sqrt{48EIG}}{(W + .486 w) l^3}$$

w = beam weight

All other values are the same as noted above.

## 1.1 DEFLECTION

### a. Beryllium

$$D = \frac{10 \times 50 \times 20^3}{48 \times 44 \times 10^6 \times \frac{(.75 \times 4^3) - (3.75)^3 (.75 - .125)}{12}} = .0015 \text{ in.} \quad (.037 \text{ mm})$$

### b. Aluminum (6061 - T6)

Web thickness will be .083 in. (207 min.) based on equal weight with beryllium:

$$D = \frac{10 \times 50 \times 20^3}{48 \times 10^7 \times \frac{(.75 \times 4^3) - (3.834)^3 (.75 - .083)}{12}} = .0092 \text{ in.} \quad (0.23 \text{ mm})$$

c. Titanium 6AL-4V (Aged)

Web thickness will be .052 (1.30 min.) based on equal weight with beryllium:

$$D = \frac{10 \times 50 \times 20^3}{48 \times 15 \times 10^6 \times \frac{(.75 \times 4^3) - (3.896)^3}{12} - (.74 - .052)} = .010 \text{ in.} \quad (0.25 \text{ mm})$$

## 1.2 MAXIMUM STRESS

a. Beryllium

$$S = \frac{10 \times 50 \times 20}{4 \times \frac{(.75 \times 4^3) - (3.75)^3}{16} (.75 - .125)} = 2660 \text{ PSI} \quad (18.34 \text{ Newtons/mm}^2)$$

b. Aluminum (6061 - T6)

$$S = \frac{10 \times 50 \times 20}{4 \times \frac{(.75 \times 4^3) - (.3834)^3}{16} (.75 - .083)} = 4640 \text{ PSI} \quad (31.99 \text{ Newtons/mm}^2)$$

c. Titanium 6AL - 4V (Aged)

$$S = \frac{10 \times 30 \times 20}{4 \times \frac{(.75 \times 4^3) - (3.896)^3}{16} (.75 - .052)} = 5800 \text{ PSI} \quad (39.99 \text{ Newtons/mm}^2)$$

## 1.3 NATURAL FREQUENCY

The natural frequency is calculated on the basis of a 10G load.

a. Beryllium

$$\omega = \frac{\sqrt{48 \times 44 \times 10^6 \times 1.27 \times 386}}{[(20 \times 10) + (.486 \times .88)]20^3} = 684 \text{ Hz}$$

b. Aluminum

$$\omega = \frac{\sqrt{48 \times 10^7 \times .86 \times 386}}{200 + (.41 \times .88) 20^3} = 563 \text{ Hz}$$

c. Titanium

$$= \frac{\sqrt{48 \times 155 \times 10^6 \times .54 \times 386}}{200 + (.486 \times .9) 20^3} = 307 \text{ Hz}$$

#### 1.4 DIMENSIONAL CHANGES DUE TO THERMAL CONDITIONS IN THE SPACE ENVIRONMENT

The range of temperatures (-108°C to 126.6°C) encountered in the space environment can result in large dimensional changes in the gimbals. This can result in orthogonality errors and in increased torque requirements because of increased friction in the bearings.

The problem of orthogonality errors will be minimized by using materials which have the same or closely matched coefficients of linear expansion. It is assumed that all parts of the gimbals will be exposed to uniform temperatures and that the temperature gradients if any will be small.

The change for the outer gimbal is noted below for reference.

a. Beryllium - Coefficient of linear expansion -

$$11.6 \times 10^{-6} \text{ per } ^\circ\text{C}$$

$$\text{Temperature range } (-108^\circ\text{C to } 126.6^\circ\text{C}) = 234.6^\circ\text{C}$$

$$\Delta D = 234.6 \times 11.6 \times 10^{-6} \times 20 = .054 \text{ in. (1.35 mm)}$$

b. Aluminum (6061 - T6)

$$\text{Coefficient of linear expansion } 21.8 \times 10^{-6} \text{ per } ^\circ\text{C}$$

$$\Delta D = 234.6 \times 21.8 \times 10^{-6} \times 20 = .102 \text{ in. (2.54 mm)}$$

PHYSICAL PROPERTIES OF CANDIDATE MATERIALS

Material	Weight <sub>3</sub> Lb/in.	Modulus of Elasticity <sub>6</sub> Psi x 10 <sup>6</sup>	Elongation %	Tensile Strength Lbs/in. <sup>2</sup> x 10 <sup>3</sup>	Coeff. of Thermal Expansion <sub>0</sub> in. in. 0° F x 10 <sup>-6</sup>	Yield Strength lbs./in. <sup>2</sup> x 10 <sup>3</sup>
Beryllium	.067	44 x 10 <sup>6</sup>	1 to 3.5 (70°F) 6 to 15 (392°F)	33 to 51 (70°F)	6.5	27 to 38
Alum-6061-T6	.098	10	12 (70°F) 20% (300°F)	45 (70°F) 34 (300°F)	12.4	40 (70°F) 31 (300°F)
Alum-7075-T6	.101	10.4	11 (70°F) 30 (300°F)	83 (70°F) 25 (300°F)	12.4	73 (70°F) 21 (300°F)
Alum-356-T6	.097	10.5	3.5 (70°F) 6 (300°F)	33 (70°F) 23 (300°F)		24 (70°F) 29 (300°F)
Magnesium ZH62A	.067	6.5	4	35 (70°F)	14.4	22 (70°F)
Magnesium M1A	.064	6.5	7 (70°F) 15 (300°F)	35 (70°F) 25 (300°F)	14.4	26 (70°F) 21 (300°F)
Titanium	.16	15	7 (70°F- 300°F)	170 (70°F)		150 (70°F)
6AL-4V (Aged)				140 (300°F)		125 (300°F)

Table E-1. Source Metals Handbook - 8th Edition - American Society for Metals



c. Titanium (6AL-4V) coefficient of linear expansion

$$= 10.8 \times 10^{-6} \text{ per } ^\circ\text{C}$$

$$\Delta D = 234.6 \times 10.8 \times 10^{-6} \times 20 = .050 \text{ in. (1.25 mm)}$$

## 2.0 DRIVE SYSTEM COMPONENTS

### 2.1 TORQUE MOTOR CHARACTERISTICS

<u>WINDING CONSTANTS</u>	<u>UNITS</u>	<u>SYMBOL</u>	<u>VALUE</u>
DC resistance (25°C)	ohms	$R_M$	20.0
Volts at peak torque (25°C)	volts	$V_P$	25.6
Amps at peak torque	amps	$I_P$	1.3
Torque sensitivity	oz-in/amp	$K_T$	46.8
Back EMF	volts/rad/sec	$K_B$	0.33
Inductance	milli-hys.	$L_M$	19
<u>MOTOR SIZE CONSTANTS</u>	<u>UNITS</u>	<u>SYMBOL</u>	<u>VALUE</u>
Peak torque	oz-in	$T_P$	60
Motor constant	oz-in/ $\sqrt{\text{watt}}$	$K_M$	10.5
Electrical time constant	milli-sec	$\tau_M$	1.0
Mechanical time constant	milli-sec	$\tau_M$	13.2
Power input, stalled, at peak torque (25°C)	watts	$P_P$	32
Viscous damping coefficients:			
Zero impedance source	oz-in/rad/sec	$F_O$	0.81
Infinite impedance source	oz-in/rad/sec	$F_I$	0.04

<u>MOTOR SIZE CONSTANTS</u>	<u>UNITS</u>	<u>SYMBOL</u>	<u>VALUE</u>
Motor friction torque	oz-in	$T_F$	1.5
Ripple torque, average to peak	percent	$T_R$	6
Ripple cycles per revolution	cycles/rev	---	33
Ultimate temperature rise per watt	deg C	TPR	6.8
Max permissible winding temperature	deg C	---	105
Rotor moment of inertia	oz-in-sec <sup>2</sup>	$J_M$	0.011
Max power rate	oz-in/sec <sup>2</sup>	$\dot{P}$	$3.3 \times 10^5$
Max theoretical acceleration	rad/sec <sup>2</sup>	$\alpha_M$	5450
No load speed	rad/sec	$\omega_{NL}$	75
Motor weight	oz	---	13.8
Peak torque	oz-in.	$T_P$	60
Motor constant	oz-in/ $\sqrt{\text{watt}}$	$K_M$	10.5
Electrical time constant	milli-sec	M	1.0
Mechanical time constant	milli-sec	M	13.2
Power input, stalled, at peak torque (25°C)	watts	$P_P$	32
Viscous damping coefficients:			
Zero impedance source	oz-in/rad/sec	$F_O$	0.81
Infinite impedance source	oz-in/rad/sec	$F_I$	0.04

## 2.2 TACHOMETER CHARACTERISTICS

TACHOMETER GENERATOR SIZE CONSTANTS	<u>UNITS</u>	<u>SYMBOL</u>	<u>VALUE</u>
Tach generator friction torque	oz-in	$T_F$	2.8
Ripple voltage, average to peak	percent	$E_R$	5.0
Ripple cycles per revolution	cycles/rev	---	33
Rotor moment of inertia	oz-in-sec <sup>2</sup>	$J_M$	0.011
Tach generator weight	oz	---	14

TACHOMETER GENERATOR WINDING CONSTANTS	<u>UNITS</u>	<u>TOL</u>	<u>SYMBOL</u>	<u>VALUE</u>
DC resistance (25°C)	ohms	+12.5%	$R_T$	710
Voltage sensitivity	volts/rad/sec	+10%	$K_G$	2.20
Inductance	henries	+30%	$L_M$	0.58
Min load resistance	ohms	nom	$R_{L(min)}$	70K
Max operating speed	rad/sec	nom	max	28.1
Volts @ max operating speed	volts	nom	$V_{max}$	62.0

## 3.0 TORQUE REQUIREMENTS

The torque requirements for the inner and outer gimbals is evaluated below under conditions of maximum acceleration and friction.

### 3.1 SYSTEM INERTIA

The inertia of the sensing head is computed by employing the formula for a cylinder rotating on a transverse axis through the center of mass, and is given by:

$$I = M \frac{l^2}{3} + \frac{r^2}{4}$$

where

$$M = \text{Mass} = \frac{20}{386} = .051 \text{ (lb-sec}^2/\text{in.)}$$

$$l = \text{length} = 8.5 \text{ inches (.215 meters)}$$

$$r = \text{radius} = 3.5 \text{ inches (.089 meters)}$$

$$I = .051 \frac{8.5^2}{3} + \frac{(3.5)^2}{4} = 1.38 \text{ lb-in. -sec}^2$$

Tach generator rotor inertia - 0.056 oz. -in. -sec<sup>2</sup>

Torque motor rotor inertia - 0.011 oz. -in. -sec<sup>2</sup>

Sensing head inertia - 22.08 oz. -in. -sec<sup>2</sup>

Total inertia; 22.75 oz. -in. -sec<sup>2</sup>  
(4145 oz. cm-sec<sup>2</sup>)

The torque requirement for the inertial load accelerated to 20°/sec<sup>2</sup> is:

$$T = I \alpha$$

where:

I = Inertia

$\alpha$  = Acceleration

$$T = 22.75 \times \frac{20}{57.3} = 8 \text{ in. oz.} \\ (576 \text{ GR. CM.})$$

The inertial load for the outer gimbal is:

Sensing head -	22.08 oz. in. sec <sup>2</sup>
Torque motor	.011
Tach generator	<u>.056</u>
Total	22.147 oz. in. sec <sup>2</sup>

The inertia of the outer gimbal is approximated by:

$$I = \frac{M}{12} (h^2 + b^2)$$

where:

M = mass

h = gimbal width

b = gimbal length

$$I = \frac{48}{32 \times 12 \times 12} (4^2 + 10^2) = 1.6 \text{ oz. in. sec}^2$$

The inertia of the tach generator and the torque motor:

$$I = 2 \left( \frac{14}{386} \right) \times (5)^2 = 1.80 \text{ oz. in. sec}^2$$

The inertia of the shaft encoder is:

$$I = \frac{10}{386} \times (7.5)^2 = 1.4 \text{ oz. in. sec}^2$$

$$\Sigma I \text{ outer gimbal} = 22.15 + 1.6 + 1.8 + 1.4 = 26.95 \text{ oz. in. sec}^2$$

The torque requirement for the outer gimbal accelerated to 20°/sec<sup>2</sup> is:

$$T = 26.95 \times \frac{20}{57.3} = 9.4 \text{ oz. in. sec}^2$$

### 3.2 FRICTION LOADS

The friction loads for the inner gimbal are:

Tach Generator -	2.8 oz. in. (201.6 GR. CM.)
Torque motor -	1.5 oz. in. (108 GR. CM.)
Bearings (Starting Torque)	.35 oz. in. (25.2 GR. CM.)
Shaft encoder	<u>.10 oz. in.</u> (7.2 GR. CM.)
Total friction torque -	4.75 oz. in. (342 GR. CM.)

The total torque requirement for the inner gimbal is:

Inertial torque	8 in. oz.
Friction torque	<u>4.75 in. oz.</u>
Total	12.75 in. oz. (918 GR. CM.)

The total torque requirement for the outer gimbal friction loads are:

Tach generator	2.8 oz. in.
Torque motor	1.5 oz. in.
Bearings	.35 oz. in.
Shaft encoder	<u>.10 oz. in.</u>
Total friction torque	4.75 oz. in. (342 GR. CM.)

The total torque requirement for the outer gimbal is:

Inertial torque -	9.4 oz. in.
Friction torque -	<u>4.75 oz. in.</u>
Total torque	14.15 oz. in. (1018 GR. CM.)

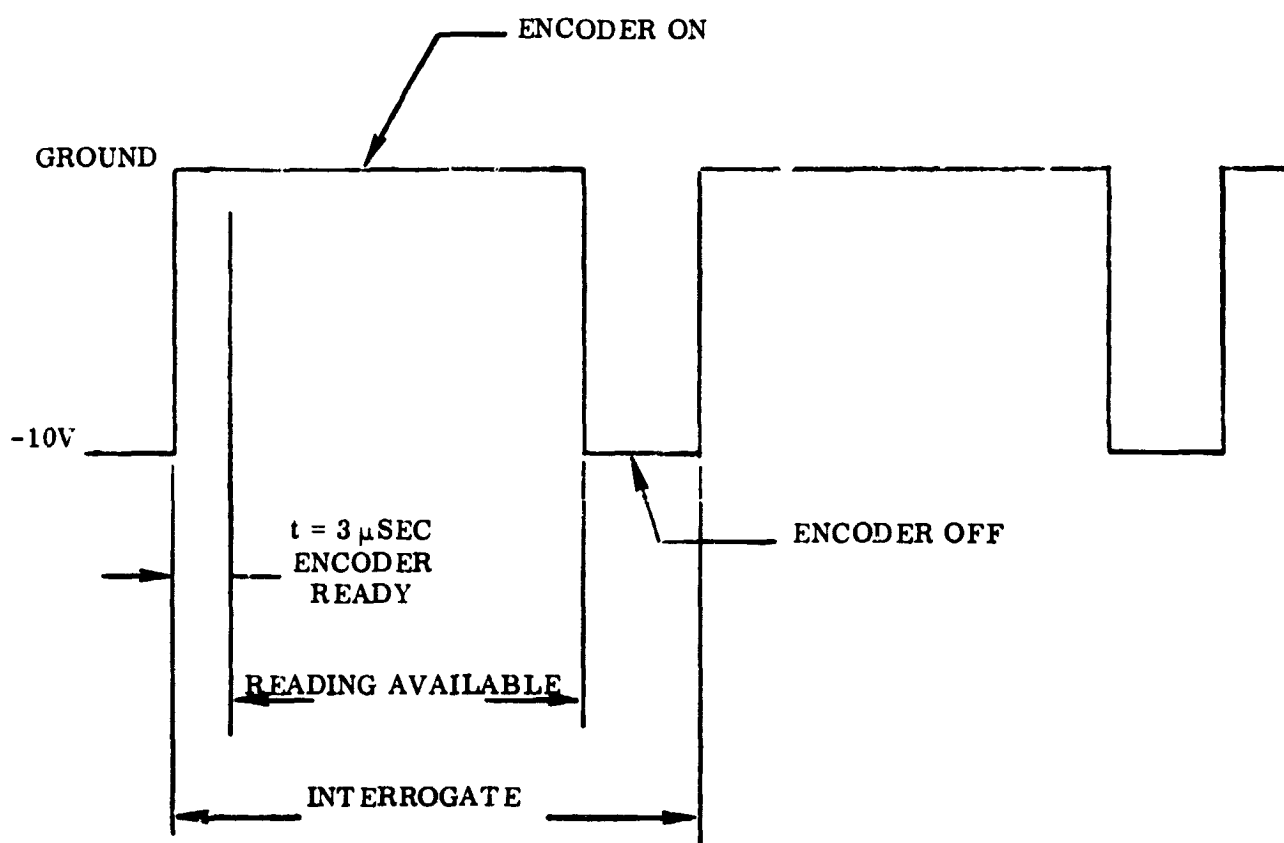
#### 4.0 OPTICAL ENCODER CHARACTERISTICS

##### a. Physical Characteristics:

Overall Dimensions	1.75 O.D. x 4.50 long
Mounting Dimensions	Synchro size 18
Shaft Dimensions	.1874/.1872
Weight	10.0 oz. max.
Code	Binary
Scan	V-scan
Function	Linear
Capacity	16384 total count
Resolution	1/16384
Starting Torque	.10 oz-in. max.
Running Torque	.05 oz-in. max.
Operating Speed	40 RPM
Slew	500 RPM
Termination	Connector: BuWeps 2260041-2
Radial Play	.0005" @ 4.0 oz. rev. ld.
End Play	.0005" @ 8.0 oz. rev. ld.
Direction of Count	Counterclockwise increasing
Light Source	Gallium Arsenide

##### b. Electrical Characteristics:

Input Power	125 ma -28V $\pm 5\%$ max. 25 ma @ +5V $\pm 5\%$ 225 ma @ -5V $\pm 5\%$ 100% duty cycle 85 ma -5V $\pm 5\%$ 25% duty cycle
Logic "0"	Open; See Figure E-1
Logic "1"	0.5V max.
Interrogation	See Figure E-1



**NOTES:**

1. AT THE MAXIMUM INTERROGATION RATE OF 30 K.C., THE ENCODER MUST BE TURNED OFF FOR AT LEAST 1.0 μSEC.

**Figure E-1. Encoder Interrogation**



Input Impedance	5k
Rate	up to 30k Hz
Maximum Read Time	See Figure E-1
Interrogate Activated (Encoder On)	By grounding input select line
Interrogate Inactive (Encoder Off)	When select line is at AT -10V

c. Environment:

Operating Temperature	-108°C to +126.6°C
Humidity	Relative 95%
Vibration	2000 Hz 15g
Shock	50 g for 11 ±1 millisecond

## APPENDIX F

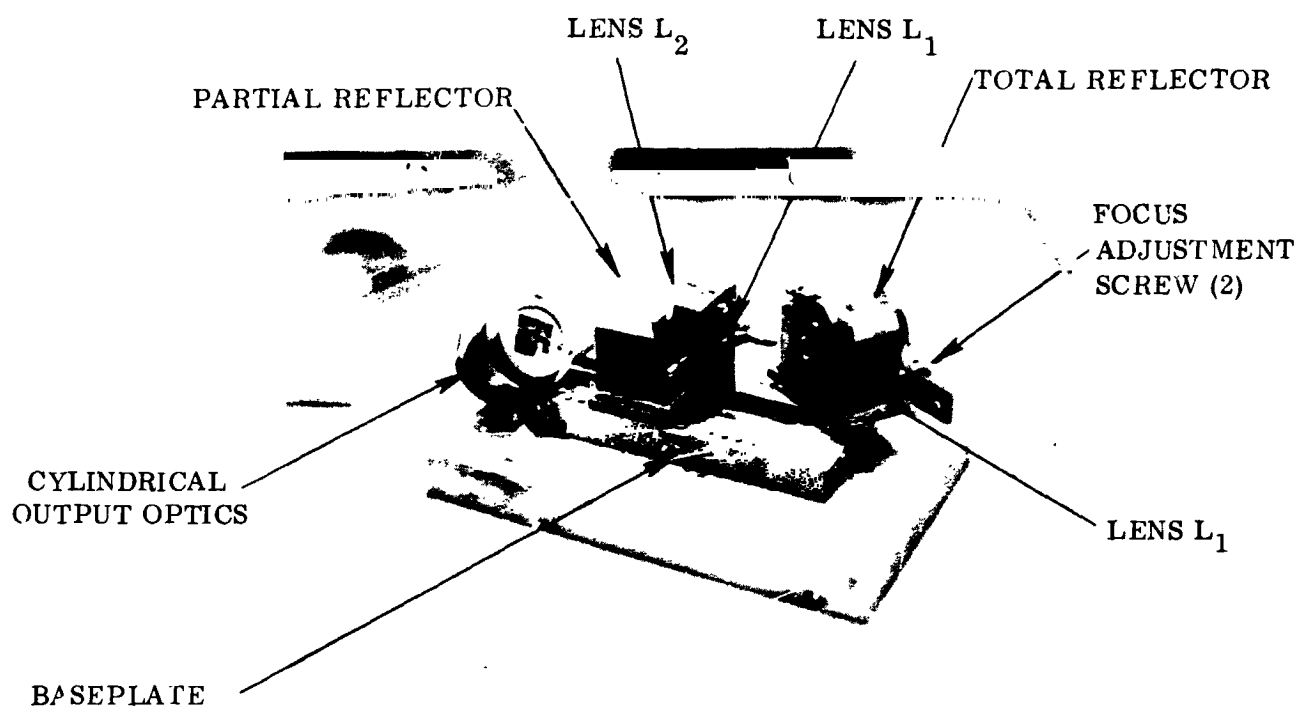
### LASER AND ANGLE TRACKER TESTS

#### 1.0 DIFFRACTION-LIMITED GaAs LASER TESTS

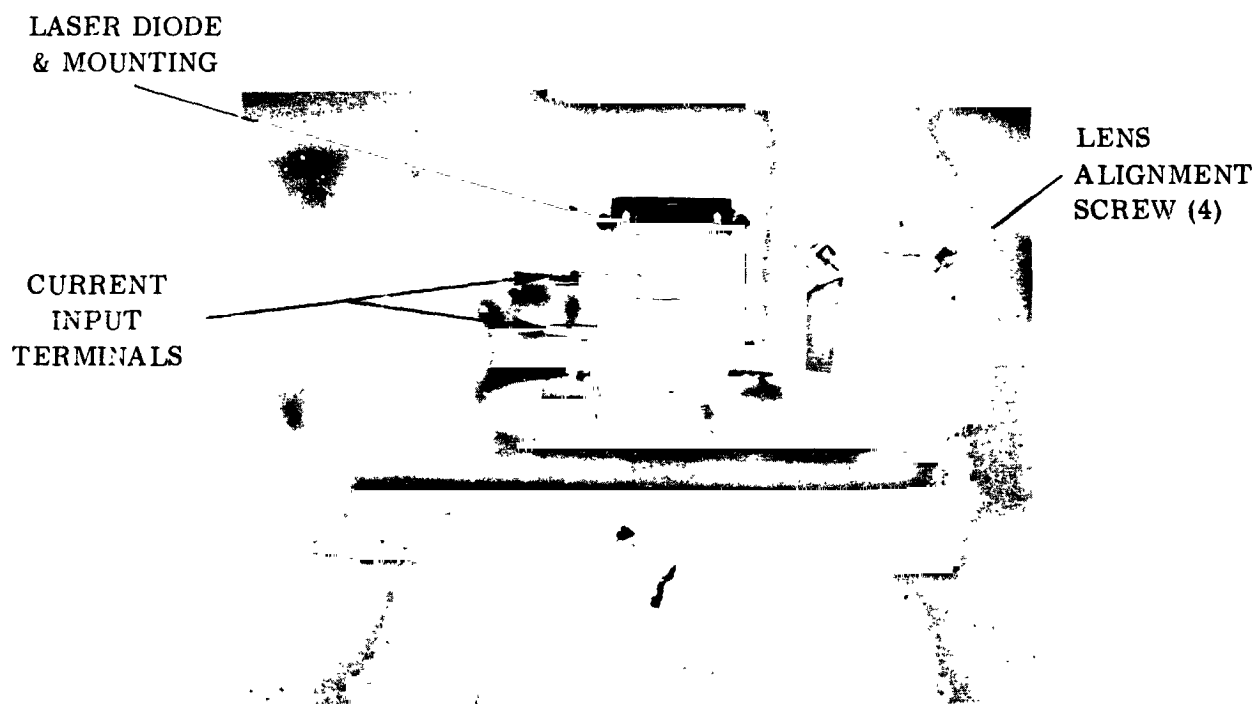
Tests were run on the diffraction-limited GaAs laser (developed by IBM) to determine the basic performance characteristics. The tests reported in Section F. 1. 1 (Current Input Versus Optical Output), Section F. 1. 2 (Far-Field Radiation Pattern), and Section F. 1. 3 (Wavelength Distribution of the Far-Field Radiation) were performed at IBM's Thomas Watson Research Center. All tests reported here were performed with the laser operating at room temperature (300°K). Figure F-1 shows two pictures of the diffraction-limited GaAs laser taken when the laser was partially disassembled. The external dimensions of the laser housing (which holds the reflectors, lenses, laser diode, and heat sink mounting) is approximately 2.5" x 1.3" x 1.2." The entire laser, including the baseplate, weighs approximately 2 pounds.

#### 1.1 CURRENT INPUT VS. OPTICAL OUTPUT

The current input to the diffraction-limited GaAs laser was indirectly obtained by measuring the voltage drop across a sampling resistor ( $R_g$ ) that was placed on the primary side of a 4:1 current transformer. The laser diode was the load on the secondary side of the transformer. Due to the laser cavity configuration, it was not possible to place the sampling resistor on the secondary side with the laser diode. Figure F-2 is a schematic of the test setup used to measure the current input and optical output.



NOTE: LASER WEIGHT INCLUDING BASEPLATE IS 0.89 KG (2.0 LBS)



ITT69/0192  
Figure F-1. Diffraction-Limited Gallium Arsenide Laser

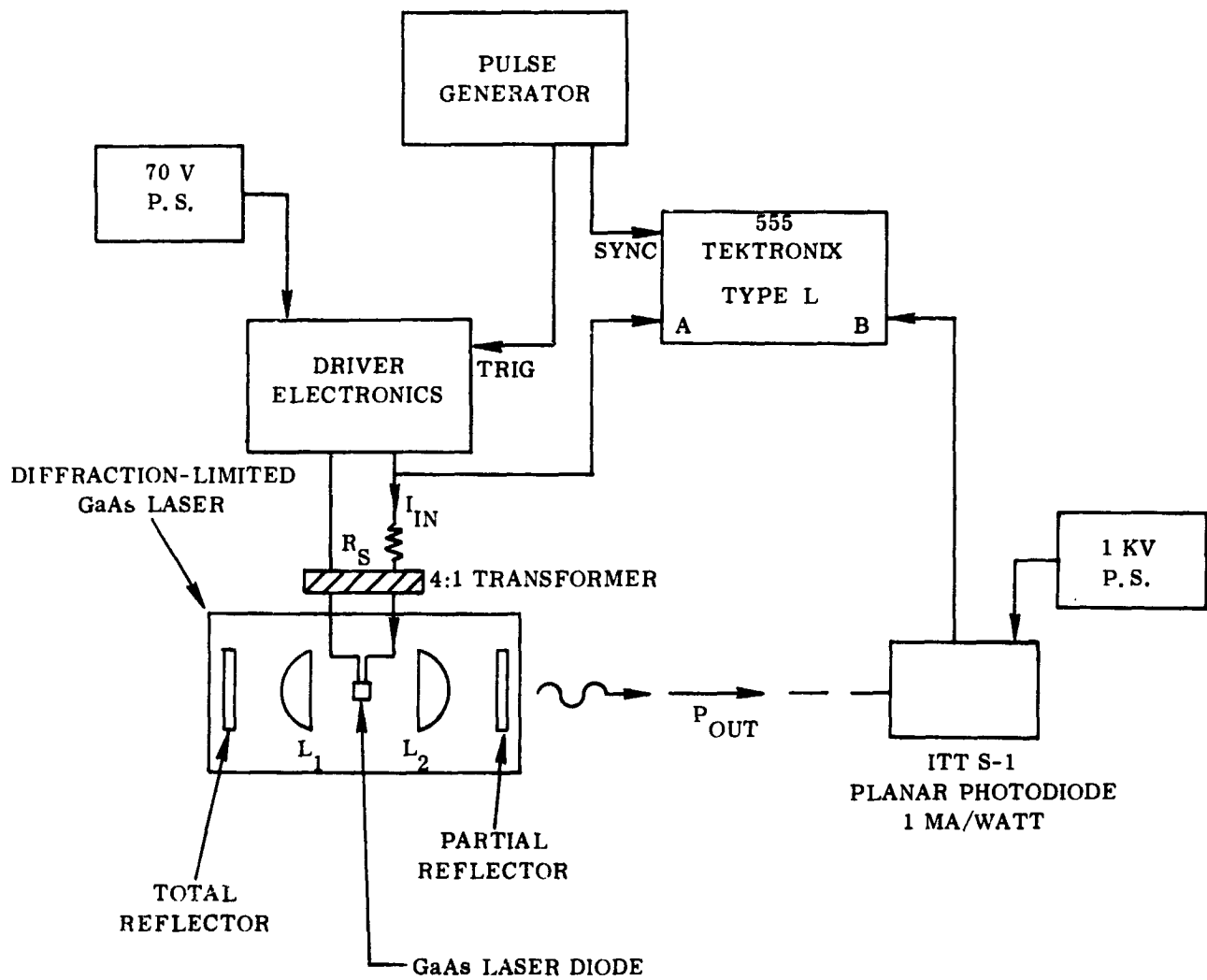


Figure F-2. Test Set-up for Current Input/Optical Output Measurements

A current probe was placed in the primary side to check the current readings obtained by the sampling resistor method. A discrepancy was observed between the two methods. The sampling resistor method indicated the peak current was higher. The rise and fall times were shorter than the direct readings of the current probe. This occurred because the sampling resistor method does not take into account the inductance of the circuit. The current probe was not used permanently because of a difficulty in attaching the probe to short lead lengths. Also, there was some question as to how much inductance the probe itself would introduce to the laser driver circuit. The current probe method is believed to be more accurate. It is recommended future test setups be able to accommodate them. It is also recommended the laser driver be built so it can directly drive the laser diode without a transformer. This will ultimately be necessary in order to reduce pulse widths and rise times on the future diffraction-limited GaAs lasers.

The current threshold level for self-sustaining oscillation in the diffraction-limited GaAs laser was measured to be approximately 46 amperes. The threshold was very sensitive to the optical alignment of the laser cavity. This was the lowest threshold obtained, after many "fine" adjustments were made to the alignment. After the fine alignment had been performed, the stability of the laser appeared reasonably good over an observed period of several hours and could even take a small amount of shock (tapping the cavity housing with knuckles) without going out of alignment. This laser was not designed to pass environmental tests but appears very solid. Future units will have the laser cavity designed to further increase the mode stability and overall ruggedness. There presently appears to be no reason why the diffraction-limited GaAs laser could not pass space qualification tests. All components are solid-state.

The maximum peak radiated power measured from the laser was 2 watts. The corresponding peak current was 100 amperes. Figure F-3 is a graph of the peak current input versus peak radiated output. Figure F-4 shows the oscilloscope waveforms for the current input and optical output versus time for both the threshold case and the maximum case. It should be noted that IBM did not have a laser driver that could provide 100 amperes with pulse widths and rise times shorter than those shown (250 nsec pulse width, 100 nsec rise time). At the maximum peak radiated power (2 watts), and for a current pulse width of 250 nsec and maximum pulse repetition rate of 4 kHz, the maximum duty cycle obtained was .001.

## 1.2 FAR-FIELD RADIATION PATTERN

The far-field radiation pattern (spatial intensity distribution) was experimentally measured using a 10 micron slit aperture, S-1 photomultiplier, sliding carriage, and an xy recorder. The test setup is shown in Figure F-5. The radiation pattern in both the xz and yz planes (see Figure 5-3 of technical report for coordinate reference) was measured with the laser operating at 2-watts output. The graphs in Figures F-6 and F-7 show the far-field radiation patterns plotted for the xz and yz planes respectively. The full angle laser output beamwidth can be calculated to be approximately 0.3 degrees in both planes by measuring the spatial beamspread at the one-half power points from the respective plots. The far-field radiation patterns in Figures F-6 and F-7 have a near Gaussian spatial intensity distribution. These measured far-field patterns are typical for radiation in the lowest order transverse mode (the diffraction-limited mode).

Two cylindrical lenses ( $L_3$  and  $L_4$ ) were placed at the optical output of the laser resonator in order to obtain a symmetrical (square) output beam. The beam waist was experimentally measured at the output of the cylindrical optics ( $L_4$ ) to be approximately 1.5 mm x 1.5 mm. Using the approximation  $\theta = \lambda/d$  for the diffraction-limited beamwidth, one should obtain an output beamwidth of

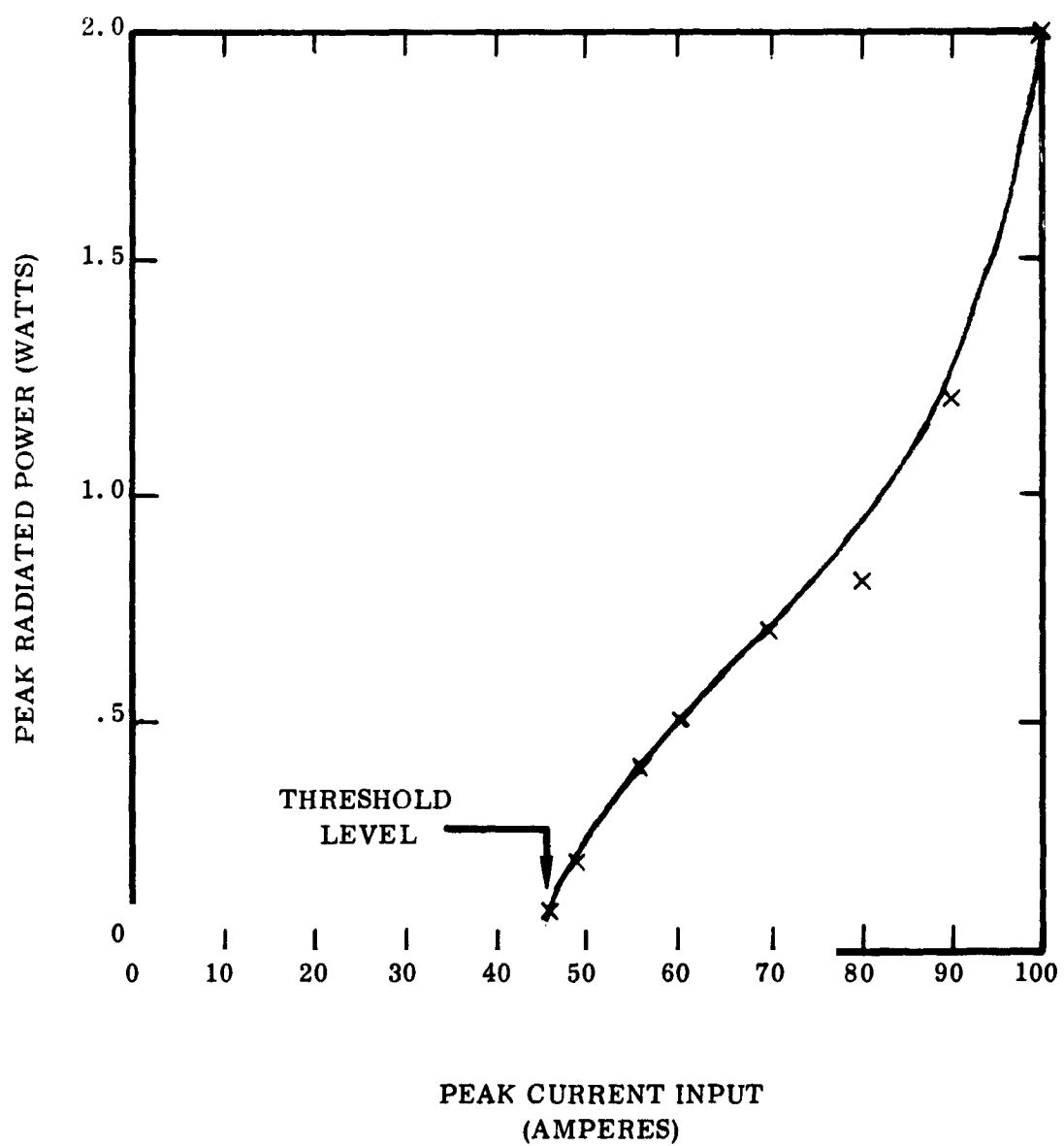


Figure F-3. Peak Current Input Vs Peak Radiated Output

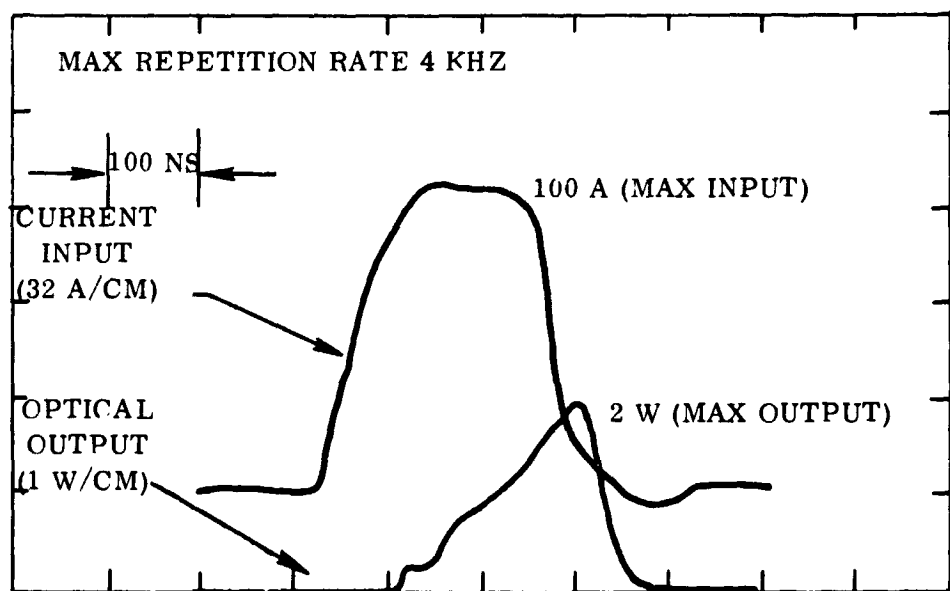
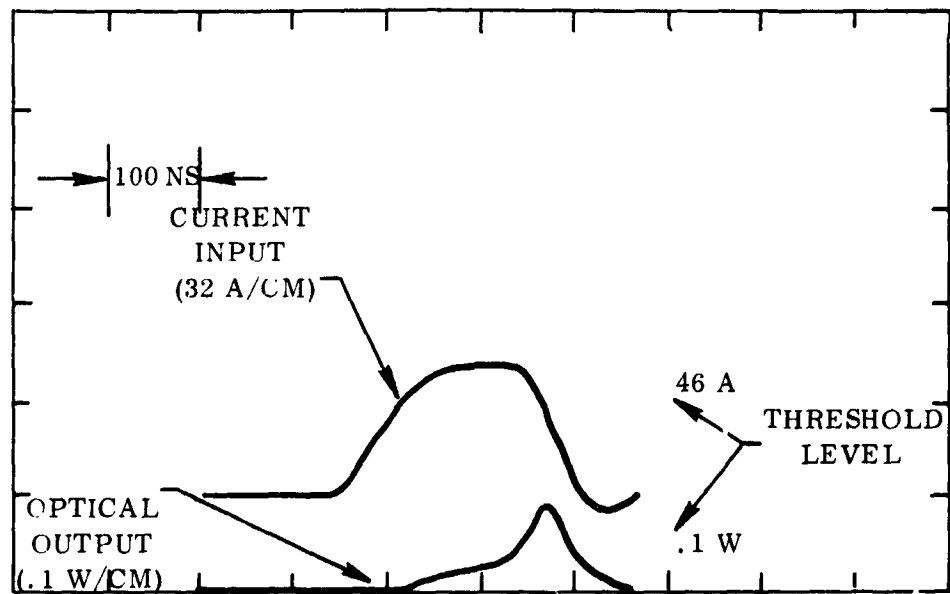


Figure F-4. Current Input & Optical Output Vs Time



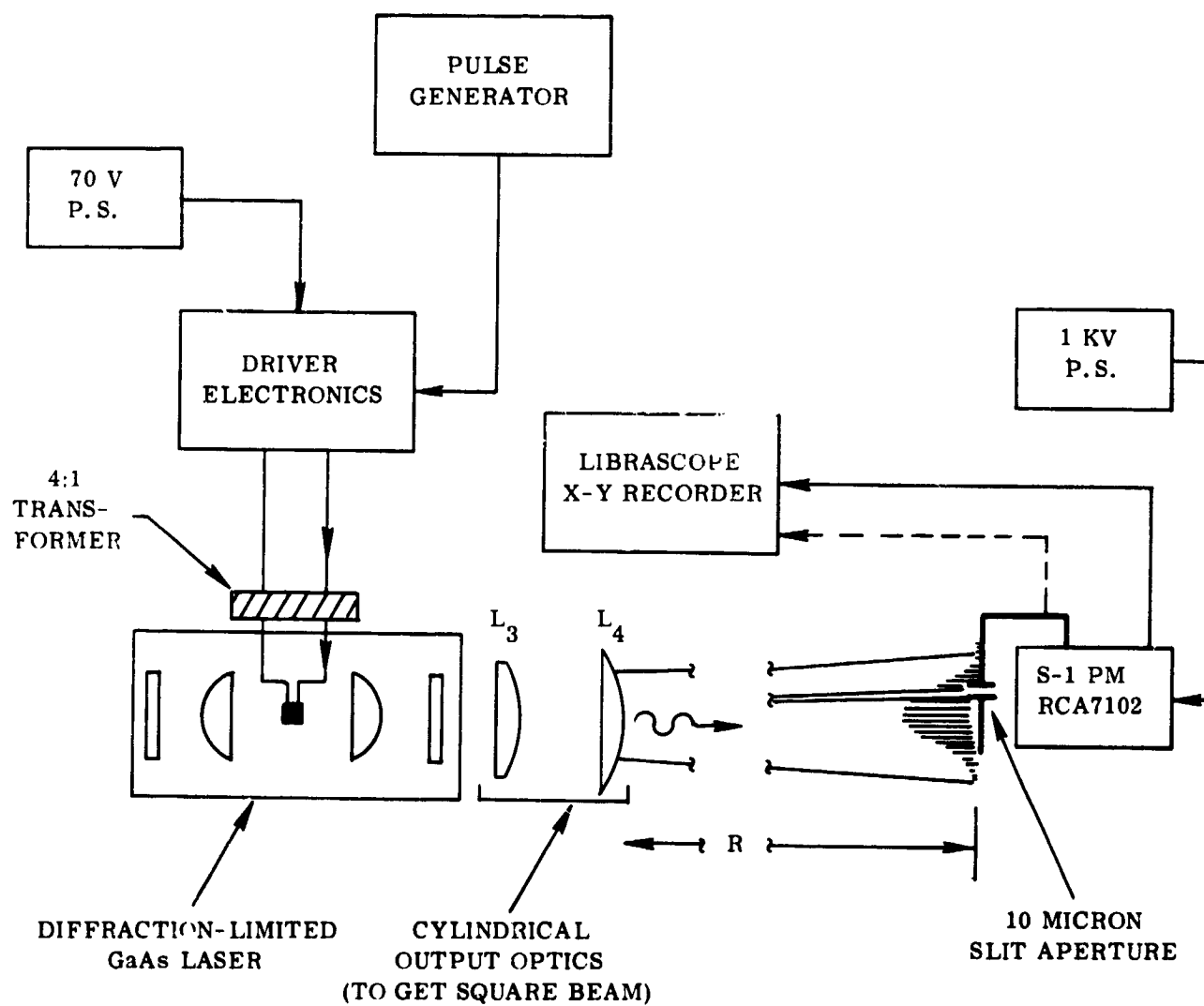


Figure F-5. Test Set-Up For Measuring Far-Field Radiation Pattern

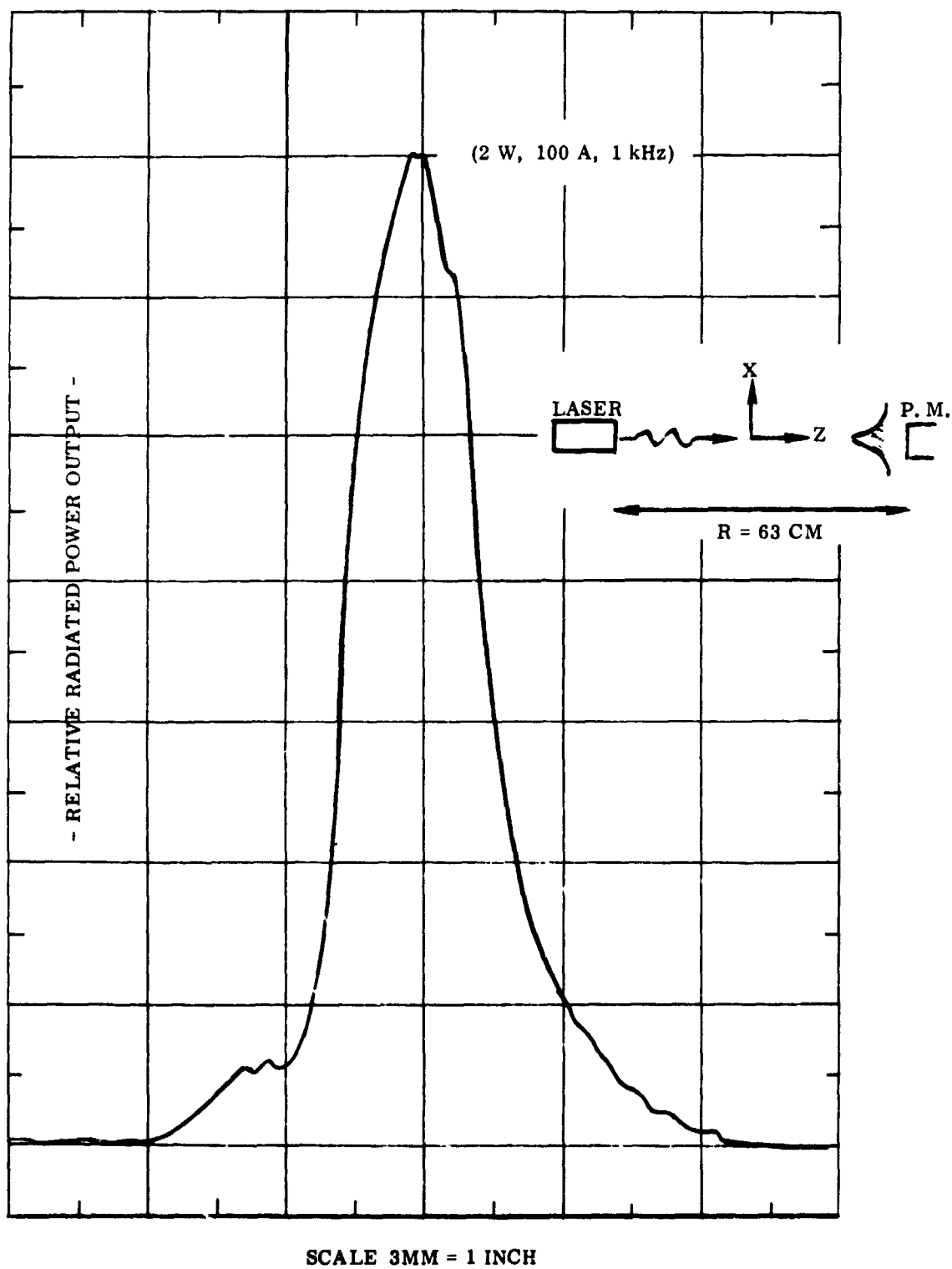


Figure F-6. Laser Far-Field Radiation Pattern (x z plane)

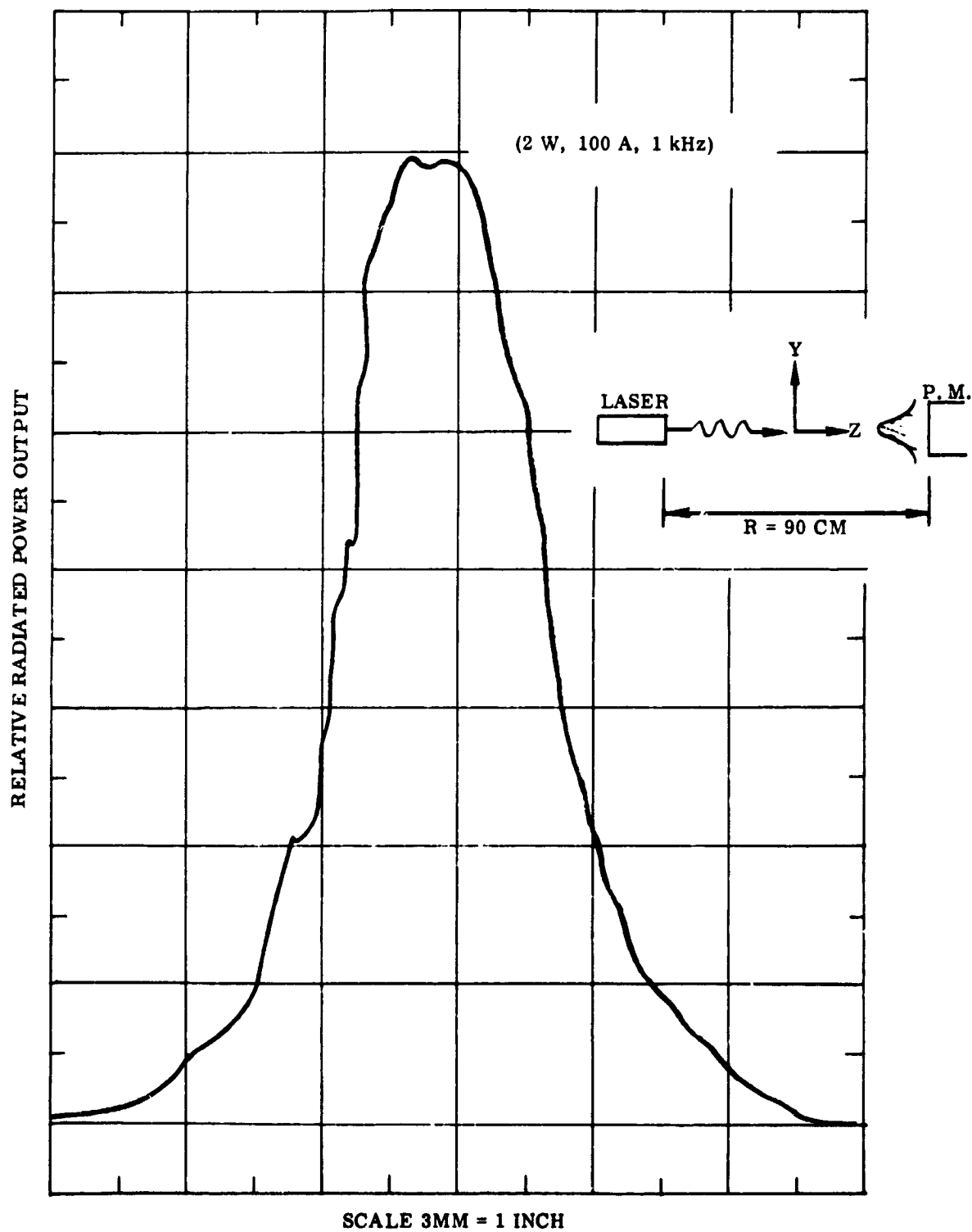


Figure F-7. Laser Far-Field Radiation Pattern (y z plane)

.035 degrees instead of the .3 degrees obtained from the far-field radiation plots. On the surface, this result indicates that the laser was not radiating in the diffraction-limited mode, however, the cylindrical lenses ( $L_3$  and  $L_4$ ) were last-minute additions to the laser and it is believed that they were the main cause of the discrepancy. Improper design and/or alignment with respect to the laser resonator could be an explanation. Due to lack of time, this could not be investigated on this contract. Extensive far-field radiation pattern tests on this same laser will be performed at ITT on another Contract (NAS8-20833).

### 1.3 WAVELENGTH DISTRIBUTION OF THE FAR-FIELD RADIATION

The wavelength distribution of the laser far-field radiation was measured with a Bausch and Lomb monochromator. The test setup is shown in Figure F-8. The wavelength distribution is obtained by plotting the relative intensity versus the wavelength of the laser output. Figure F-9 shows the wavelength distribution of the far-field radiation for three different laser outputs. The plots show the envelope of the wavelength distribution rather than the wavelengths of the individual longitudinal modes.

When the peak radiating power is increased from threshold to maximum output and the duty cycle is increased (thereby increasing the average input power to the laser), the spectral bandwidth ( $\Delta\lambda$ ) increases and the wavelength at the peak intensity becomes longer. For the lasing threshold case (.1 w, 46 a, 1 kHz) the spectral bandwidth ( $\Delta\lambda$ ) at the 1/2 power point is approximately 30 Å compared to 80 Å for the case where the laser is operated at its maximum duty cycle at maximum peak output (2 w, 100 a, 4 kHz). The peak intensity wavelengths were 9040 Å and 9080 Å, respectively. An in-between case for maximum peak output not at maximum duty cycle (2 w, 100 a, 1 kHz) is also plotted.

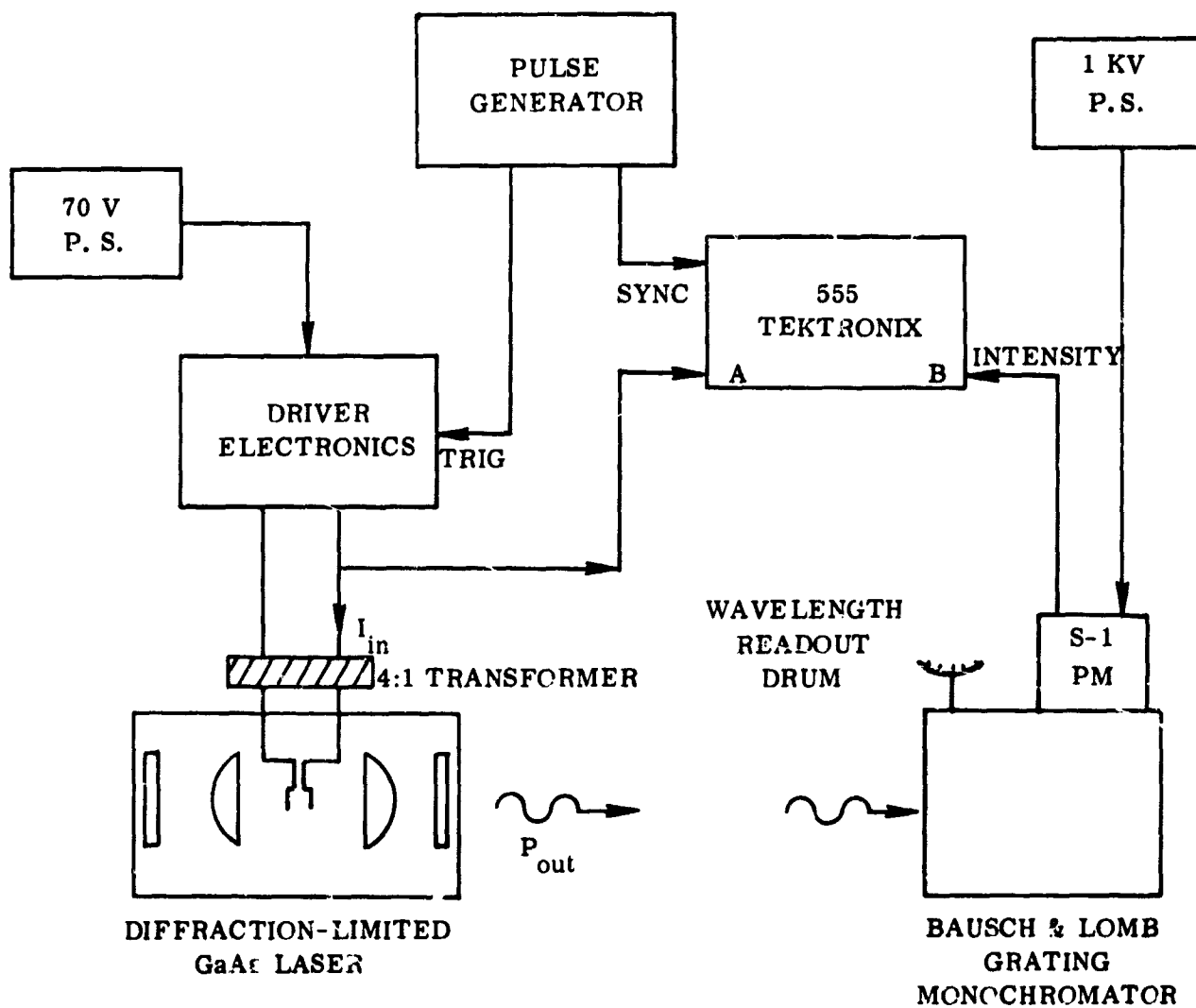


Figure F-8. Test Set-up for Measuring the Wavelength ( $\lambda$ ) Distribution of the Far-Field Radiation

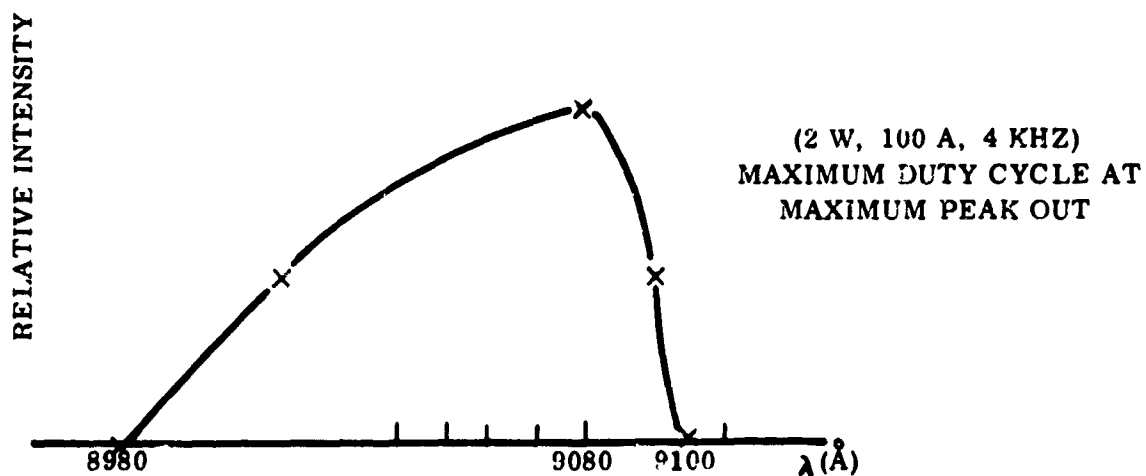
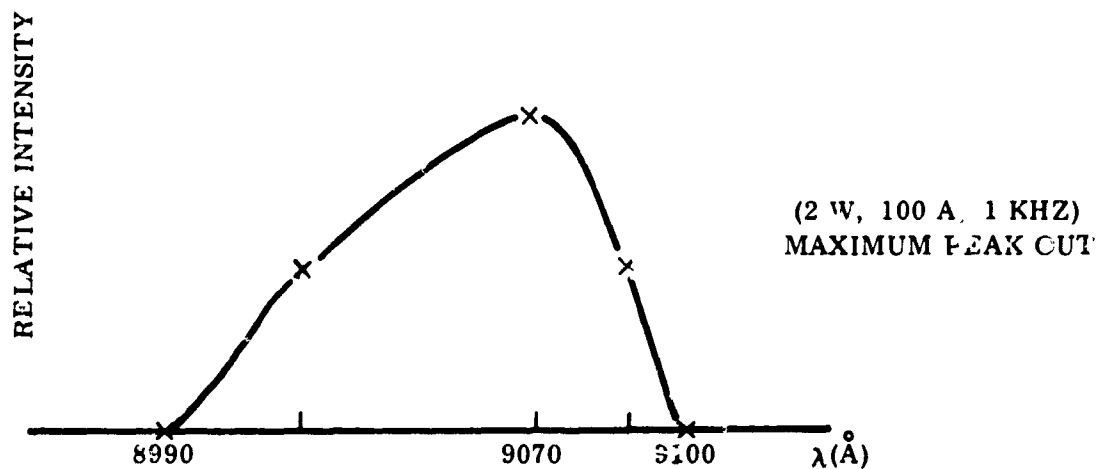
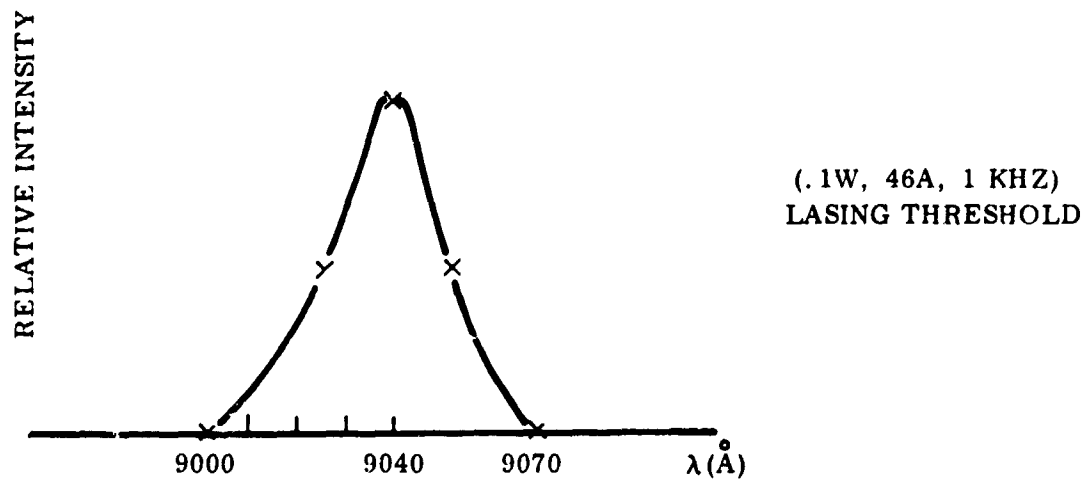


Figure F-9. Wavelength ( ) Distribution of Far-Field Radiation

#### 1.4 LASER DRIVER ELECTRONICS

Two different laser drivers have been built by ITTA to drive the low impedance laser diode ( $\approx 0.05\Omega$ ). Because of the desire for high peak current inputs to the laser and very fast rise time pulses, neither of the two laser drivers uses a transformer to step up the current to the laser. A current probe was placed in series with the laser diode and the following data was measured for the SCR and avalanche transistor driver (operated at its maximum capability).

Type Laser Driver	Peak Current Output (in. )	Rise Time $\tau_r$	Pulse Width
SCR	128 amps.	100 ns	200 ns
Avalanche Transistor (4 in parallel)	132 amps.	40 ns	90 ns

Extensive work will be performed on the "Advanced Laser Tracking Technique" contract (N 458-20833) to greatly improve the laser drivers that will be needed for the diffraction-limited GaAs laser.

#### 2.0 ANGLE TRACKER FUNCTIONAL VERIFICATION TESTS

##### 2.1 ACQUISITION SCAN

To provide a 30 degree by 30 degree acquisition scanning pattern, two 10-bit binary updown counters were constructed. Generated by the acquisition center's is a 1024 x 1024 step acquisition field. A 1000 x 1000 step field would be produced by replacing gates 8A and 8B (ITTA Drawing #5518187) with gates 8A2 and 8B2. A single field scan sequence is as follows. The yaw counter is driven one step with each successive C. P. a total of 1024 steps or "one line." A plus or minus line "end" is detected by gate 8A or 8B. At the line end - the yaw counter drive is inhibited while its up-down mode is changed. As the yaw drive is inhibited the pitch drive is enabled causing the pitch scan to deflect

one step. This - fast yaw slow pitch-scan continues to the end of the first field at which time coincident pitch and yaw "end" pulses will be detected. Coincident pitch and yaw end pulses define a field corner at which time the fast-slow pitch and yaw modes are interchanged. Fast scan is now developed by the pitch counter while slow scanning in the yaw. The four fields successively scanned are top to bottom, left to right, bottom to top, and right to left.

## 2.2 TRACK SCAN

The pitch and yaw track scan counters are each 5-bit binary up-down counters. The three MSB's generate the  $\pm 8$  step crusiciform type scan, while the two LSB's divide the return signal by four which provides the correct - return place to scan correct place - ratio. The track scan waveform, as observed by displaying the deflection coil current, has a rise time of 5 ns. The rise time is limited by the deflection coil impedance and distributed capacitance. If the track step level has stabilized, prior to receiving the return place, rise time prevents no problem. To provide accurate target position data, this is necessary. The transmit place is delayed relative to track step time ensuring correct stabilization. A second condition affecting the track step accuracy, is in the form of a transient generated by the D/A converter. The magnitude of the transient is determined by the number of acquisition and tracking counter bits which must change state to attain the next step position. From this, it can be seen that a worst case condition will exist when crossing zero. Each track and acquisition counter bit changes state when traversing the scan about boresight. In the D/A converter, the effect generated by a large bit change is a transient voltage generated by differential turn-on - turn-off response time of the buffer amplifiers. This in turn charges the distributed capacitance of the resistive ladder. Buffer amplifier differential  $t_{on} - t_{off}$  time can be optimized by trimming the +2.5V voltage supply to each unit. A lower impedance resistive ladder would reduce the capacitive discharge effects.



### 2.3 MINIAC SCAN

Two Miniac scan generators were constructed, Mod-1 and Mod-2.

Mod-1 utilizes three R. C. timing circuits. One circuit for each establishing line scan duration and one for establishing the desired number of fields. This circuit has potential flexibility for ease of changing field size and duration.

Mod-2 generator uses a digital approach eliminating the usual R. C. timing stability problems. It also economizes on circuitry, by utilizing the track control counter, as its digital source. Two four-bit counters of the track control counter provide the 16 x 16 step Miniac field. For both pitch and yaw line scan end place, a count of 8 is sensed to center the Miniac field about the last target position. Coincident pitch and yaw end place define a field "corner" (as in the acquisition scan generator) changing the state of the corner control mode flip-flop. Thus, the following field is scanned at right angles to the previous field. If at the end of the one shot timing cycle, the target has not been reacquired, the control counter is reset. The following end places are then generated by the full field acquisition counter.

### 2.4 MODE CHANGE - RETURN PULSE CORRELATION DETECTOR

The digital angle tracker may operate in any of three modes, Acquisition, Track or Miniac as determined by the presence or absence of target return signals. The Return Pulse Correlation Detector (ITTA Drawing #5518189) is the circuit primarily involved in mode switching. Circuits comprising the Correlation Detector are: Acquisition Stop, Return Signal Control and Track-Search Mode Control. Mode switching functions are performed as follows:

Acquisition to Track - Conditions necessary to create a mode switch from search to track involve:

1. A target return signal pulse
2. Stop acquisition scan

3. Differential true return signal from noise pulse
4. Switch from search to track mode
5. If signal proves to be noise, continue acquisition scan.

To prevent scanning past the target when in search, the acquisition scan is stopped upon receiving the first return signal pulse. The acquisition stop control flip-flop is reset as the return pulse triggers the timing one-shot (TOS-1). This discharges the acquisition stop delay timing capacitor (TC-1). Resetting the acquisition stop control prevents any further clock pulses from driving the acquisition scan generator. Next, a gate is formed to differentiate a true return pulse from noise signal. The gate width is sufficient to allow the return pulse to drive the return signal flip-flop. Its repetition period is established by the transmit clock pulse repetition period. (1 microsecond at 1 kHz or .1 microsecond at 10 kHz). The return pulse gate is applied to the "Set" inputs of the Return Flip-Flop and is formed by the combined action of timing one-shots TOS-1, 2 and 3. The Return Flip-Flop is "SET" by drive from the "SECOND" return pulse. In turn it "Enables" the track-search Flip-Flop which then switches to Track mode at the following clock pulse. If the second return pulse is not received (after a period determined by the charge time of the capacitor, (TC-1) the acquisition stop Flip-Flop will again be "set" allowing the acquisition scan to continue.

Track to Miniac - Should the target be lost while in track mode, the immediate area is searched by the Miniac (miniature acquisition scan) generator. The switch from track to Miniac is as follows: Loss of return signals allows the acquisition stop control to "Set" as aforementioned. This action resets the return signal Flip-Flop and enables the "K" input of the track search mode control. The track Flip-Flop then switches to search mode at the following transmit clock pulse. A "track-to-search" mode change, triggers the Miniac field one-shot whose duty cycle determines the number of fields to be scanned.

Miniac to Track or Acquisition - A switch from Miniac to track mode is accomplished in the same manner as from Acquisition to track. If the target lies outside the minifield, the miniscan continues till the end of the field timing one-shot cycle. The control counter at this time, resets, allowing the acquisition counters to scan the full 30 degrees by 30 degrees field.

## 2.5 LINEARITY COILS

A flux field uniformity test was run on a commercially available focus coil of the type used in the angle tracker. A new focus coil was wound from the detection of nonuniformities. In winding the coil, special attention was given to extending the linear portion of the field, such as to cover the greatest phototube area. Uniformity was extended toward the ends of the coil form by the addition of end coils consisting of a large number of turns of small conductor wire, placed as close to the ends of the coil form as practical. A plot of the resultant field distribution relative to the videsector is shown in Figure F-10.

## 2.6 POWER MEASUREMENTS

Power consumption of the angle tracker (critical components) under test has the following distribution. Setup: angle tracker tracking target at boresight.

<u>Supply Voltage</u>	<u>Power Consumption</u>
+5V DC	1.25 W
+15V DC	1.63 W
-15V DC	1.63 W
+18.5V DC	4.6 W
-2300V DC	2.0 W

Total = 11.14 W

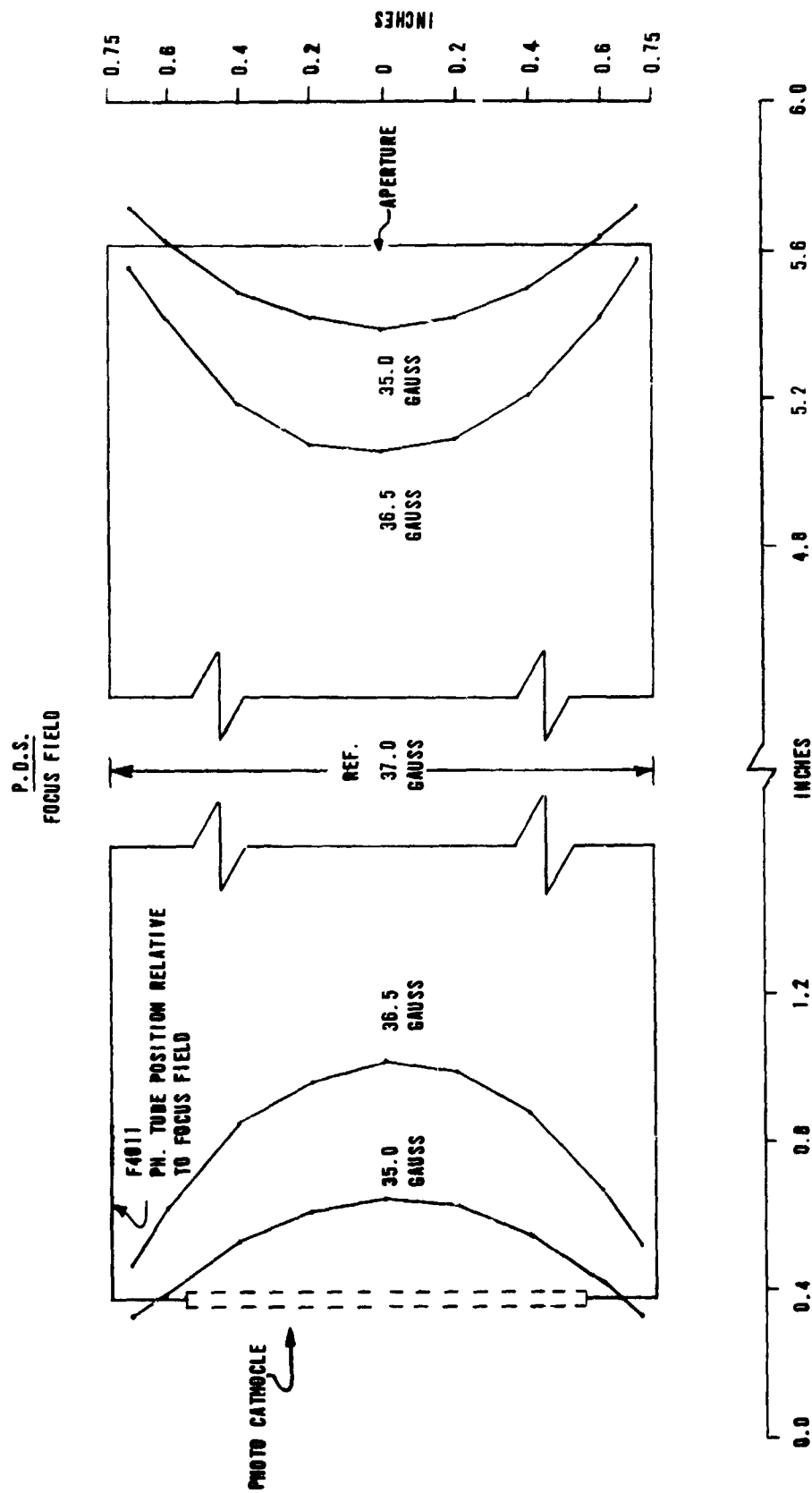
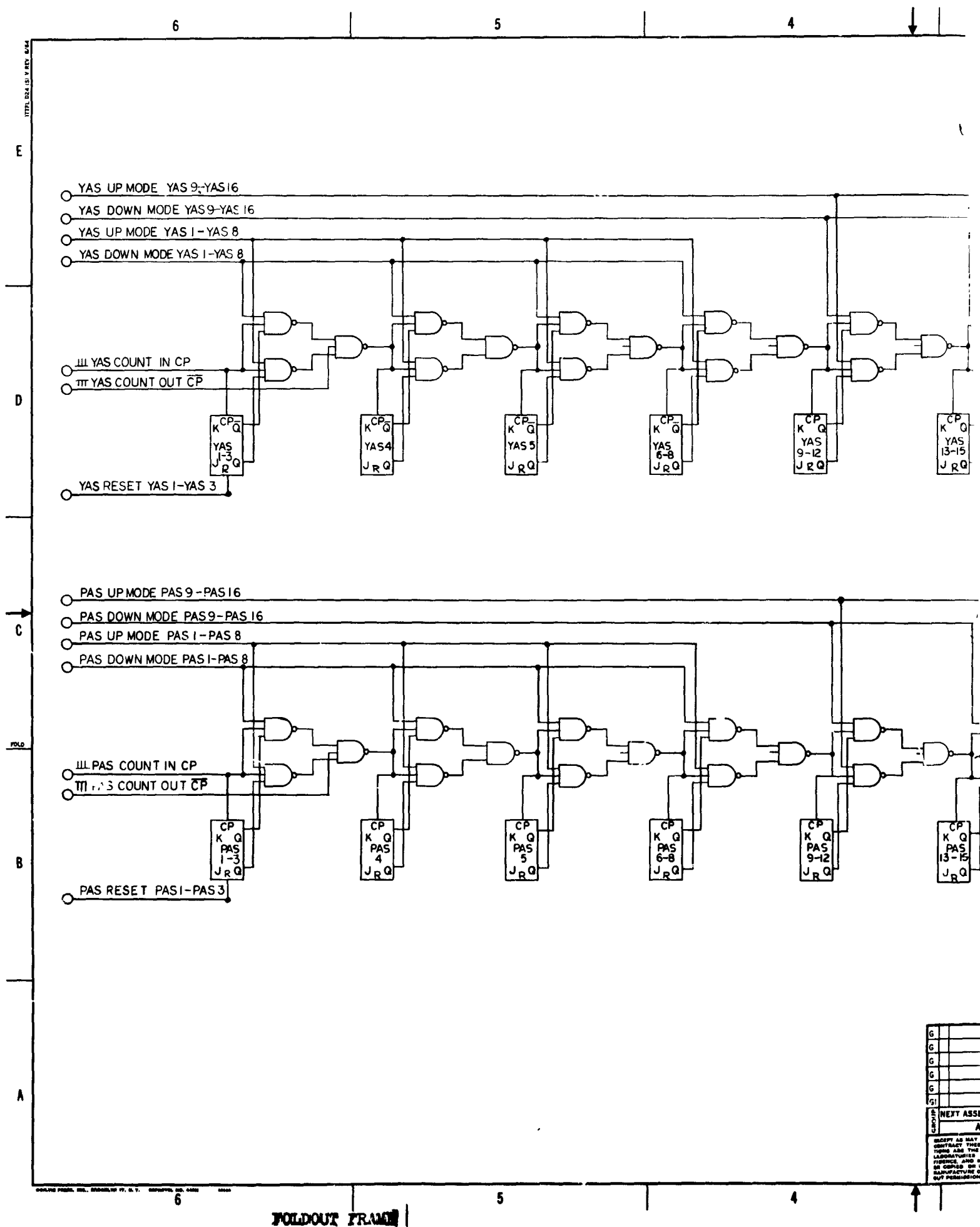


Figure F-10. Focus Field Plot



3

2

1

NOTE UNLESS OTHERWISE SPECIFIED

1 2 INPUT GATES = T I SN54L00R

2 3 INPUT GATES = T I SN54L10R

3 FLIP FLOPS T I SN54L73R

A ORIGINAL ISSUE

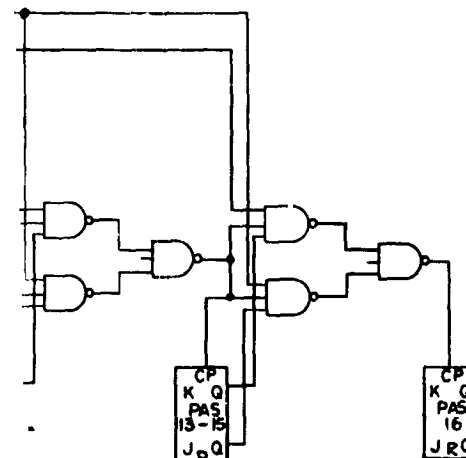
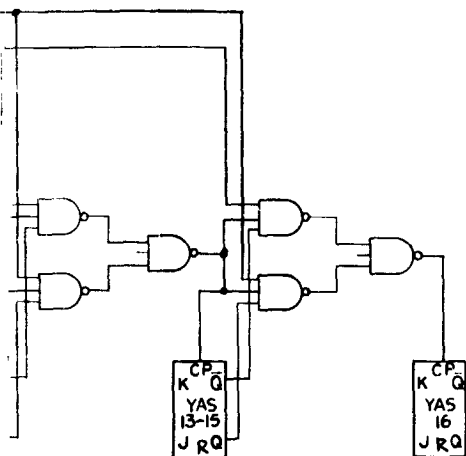
REVISIONS

ZONE LTR

DESCRIPTION

DATE

APPROVED



Q6	Q5	Q4	Q3	Q2	Q1	ITEM NO	CODE IDENT	PART OR IDENTIFYING NO	NOMENCLATURE OR DESCRIPTION	ITTL SOURCE
LIST OF MATERIALS										
MATERIAL						CONTRACT		APPROVALS SIGNATURE & DATE		
FINISH						DRAWN		CHECKED		
UNLESS OTHERWISE SPECIFIED DIMENSIONS ARE IN INCHES AND INCLUDE CHEMICALLY APPLIED OR PLATED FINISHES						ELECT		STDS		
TOLERANCES						E OF M		ITTL		
BASIC DIMENSION						MECH		OTHER		
2 PLACE						3 PLACE		FRACTIONS		
UNDER 8						± 02		± 008 ± 1/64		
8-24 INCL						± 03		± 010 ± 1/32		
OVER 24						± 04		± 015 ± 1/16		
ANGLES ± 1/2°						COML TOL APPLY TO STOCK SIZES		SHOP PRACTICE (ENGINEERING STD MANUAL SECT 38) APPLIES		
IN PART NO. COL DENOTT'S VENDOR ITEM; SEE SOURCE CONTROL OR SPECIFICATION CONTROL DRAWING.						SIZE		CODE IDENT NO.		
NEXT ASSEMBLY USED ON						D		90348		
APPLICATION						SCHEMATIC		PITCH AND YAW ANGLE SMOOTHING COUNTERS		
COPY AS MAY BE OTHERWISE PROVIDED BY CONTRACT, THESE DRAWINGS AND SPECIFICATIONS ARE THE PROPERTY OF ITT FEDERAL LABORATORIES AND SHALL NOT BE REPRODUCED, IN WHOLE OR IN PART, OR BY ANY MEANS, WITHOUT THE WRITTEN PERMISSION OF ITT FEDERAL LABORATORIES.						5518175		5518175		
U OF M						SCALF NONE		SHEET 1 OF 1		

3

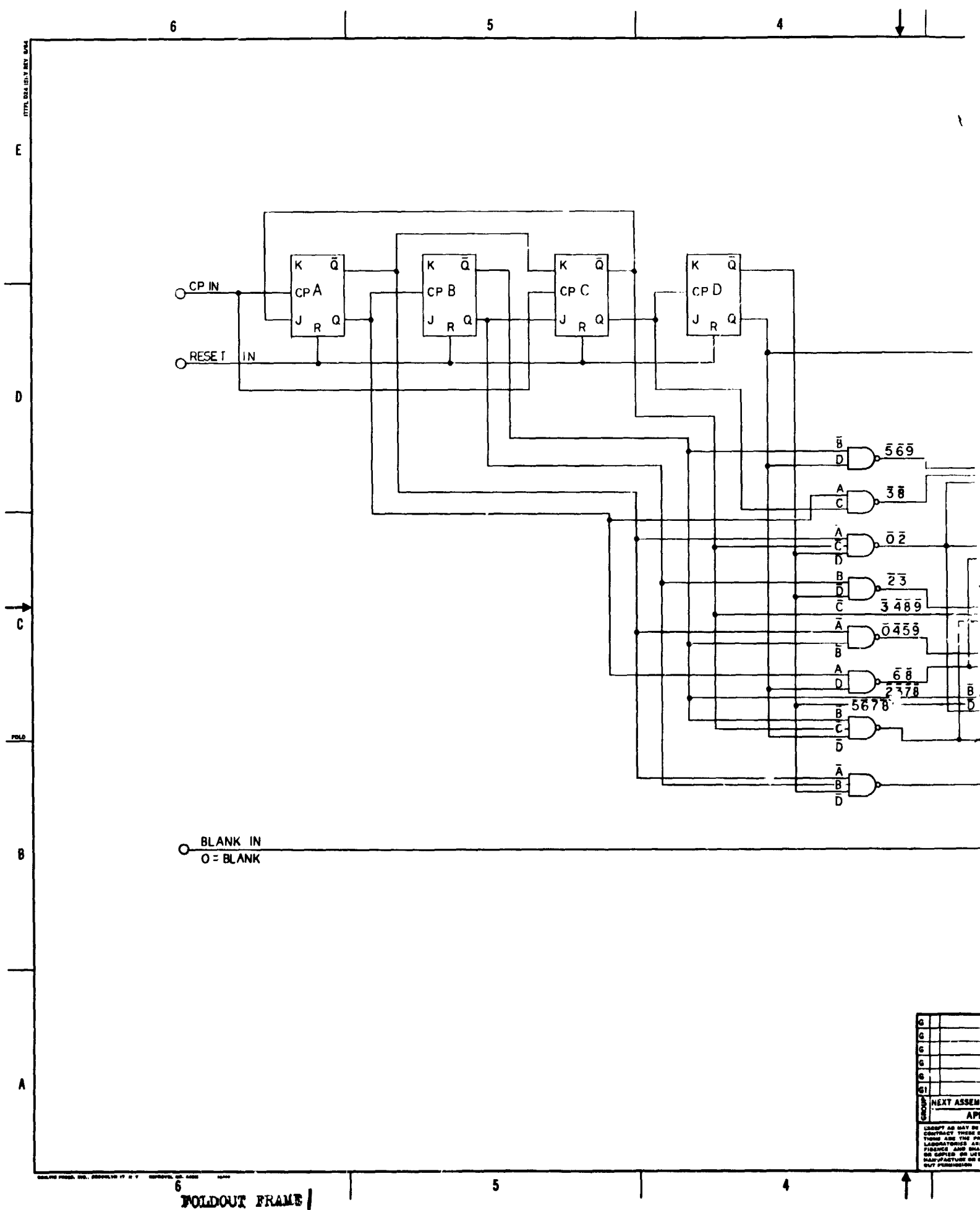
U OF M 1 PIECE 6 PAIR 32 FEET 2 32 U.S. FLUID OZ. 32 U.S. GAL 34 U.S. LIQUID QT. 66 LB. AVDP


2

FOLDOUT FRAME 2

FOLD

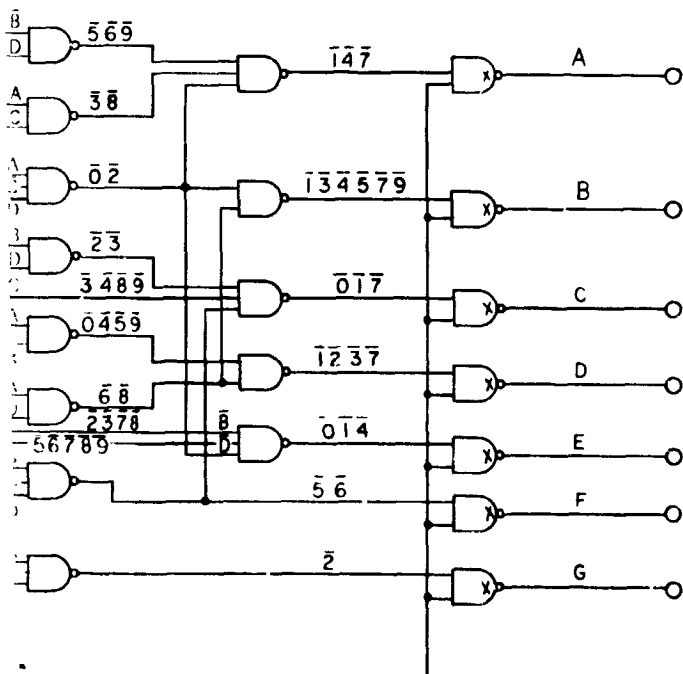
5518175



- NOTES: UNLESS OTHERWISE SPECIFIED,  
1. ALL FF'S - T1 SN54L73R  
2. 2 INPUT GATES - T1 SN54L00R  
3. 3 INPUT GATES - T1 SN54L10R  
4.  - OPEN COLLECTOR GATE T1 SN5401

A ORIGINAL ISSUE		REVISIONS		
ZONE	LTR	DESCRIPTION	DATE	APPROVED

TO MS DECADE DQ



64	65	64	63	62	61	U	ITEM	IN	CODE	PART OR	NOMENCLATURE OR		
QUANTITY PER GROUP						NO	IDENT	IDENTIFYING NO	DESCRIPTION			DESCRIPTION	
LIST OF MATERIALS												CONTRACT	
APPROVALS SIGNATURE & DATE												DRAWN	
CHECKED												MECH	
ELECT												STDS	
E OF M												ITTF	
OTHER												SCALE NONE	
SHEET 1 CFI												5518176	

UNLESS OTHERWISE SPECIFIED  
DIMENSIONS ARE IN INCHES AND  
INCLUDE CHEMICALLY APPLIED  
OR PLATED FINISHES

BASIC DIMENSION	DECIMALS	FRAC- TIONS
UNDER 6	± .02 ± .008 ± 1/64	
6-24 INCL	± .03 ± .010 ± 1/32	
OVER 24	± .06 ± .015 ± 1/16	

ANGLES ± 1/2°  
COML TOL APPLY TO STOCK SIZES  
SHOP PRACTICE (ENGINEERING  
STD. MANUAL SECT 38) APPLIES

IN PART NO COL DENOTES  
VENDOR ITEM, SEE SOURCE  
CONTROL OR SPECIFICATION  
CONTROL DRAWING.

SHOUP AS SHOWN - OTHERWISE PROVIDED BY  
CONTRACT. THE L. PROVISIONS AND SPECIFICATIONS  
ARE THE PROPERTY OF TTT FEDERAL  
LABORATORIES AND SHALL NOT BE REPRODUCED,  
COPIED, OR USED AS THE BASIS FOR THE  
MANUFACTURE OR SALE OF APPARATUS WITH-  
OUT PERMISSION.

TTT Federal LABORATORIES  
SAN PIERRE, CALIF., U.S.A.  
A DIVISION OF INTERNATIONAL TELEPHONE AND TELEGRAPH CORPORATION

SCHEMATIC  
DECADE READOUT REGISTER  
AND 7 SEGMENT DECODER

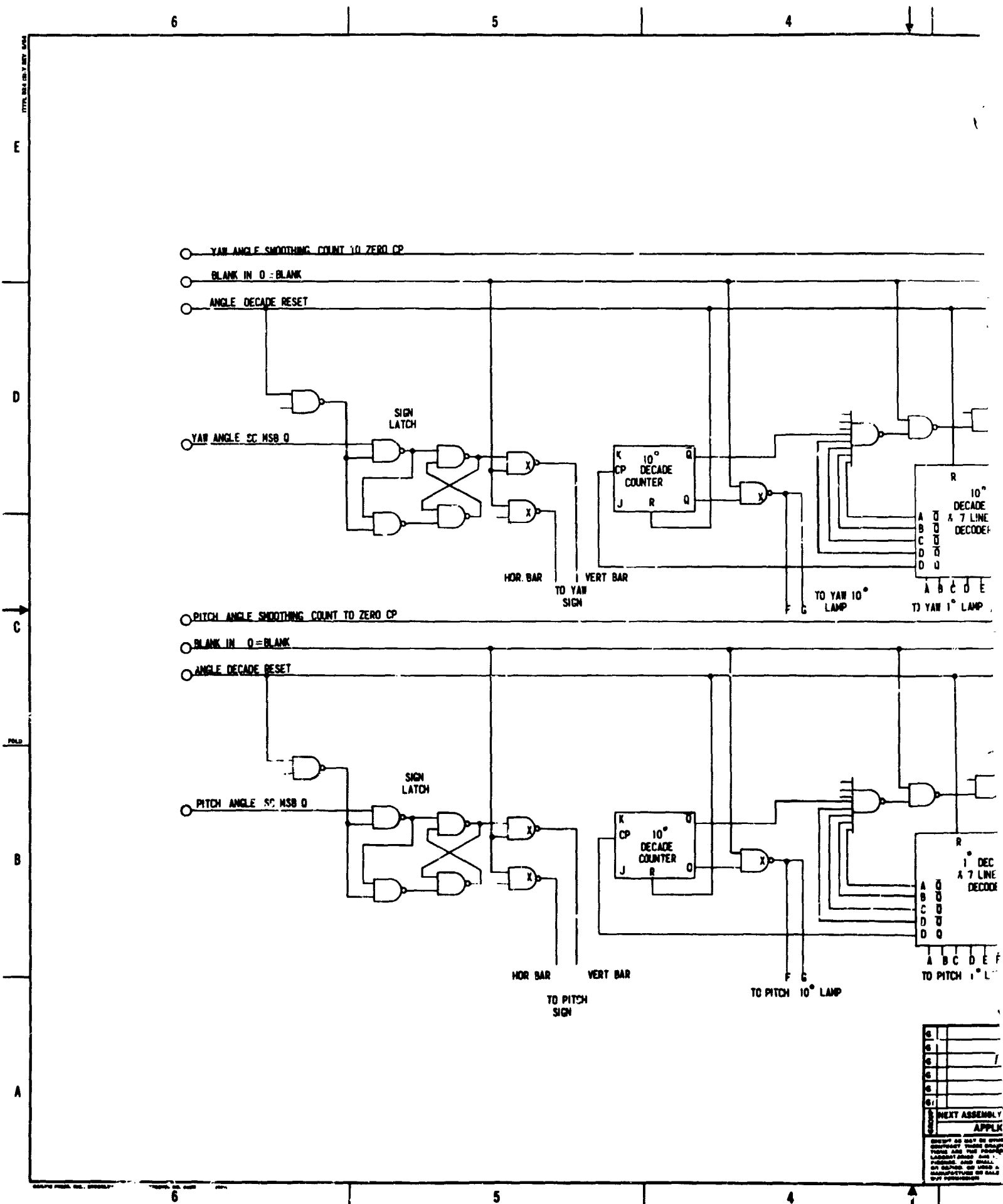
D 90348 5518176

SCALE NONE SHEET 1 CFI

3 U OF M 1 PIECE 8 PAIR 8 SET 32 FEET 2 82 U.S. FLUID OZ. 88 U.S. GAL. 84 U.S. LIQUID OT. 88 LB. AVDP 2

FOLDOUT FRAME 2





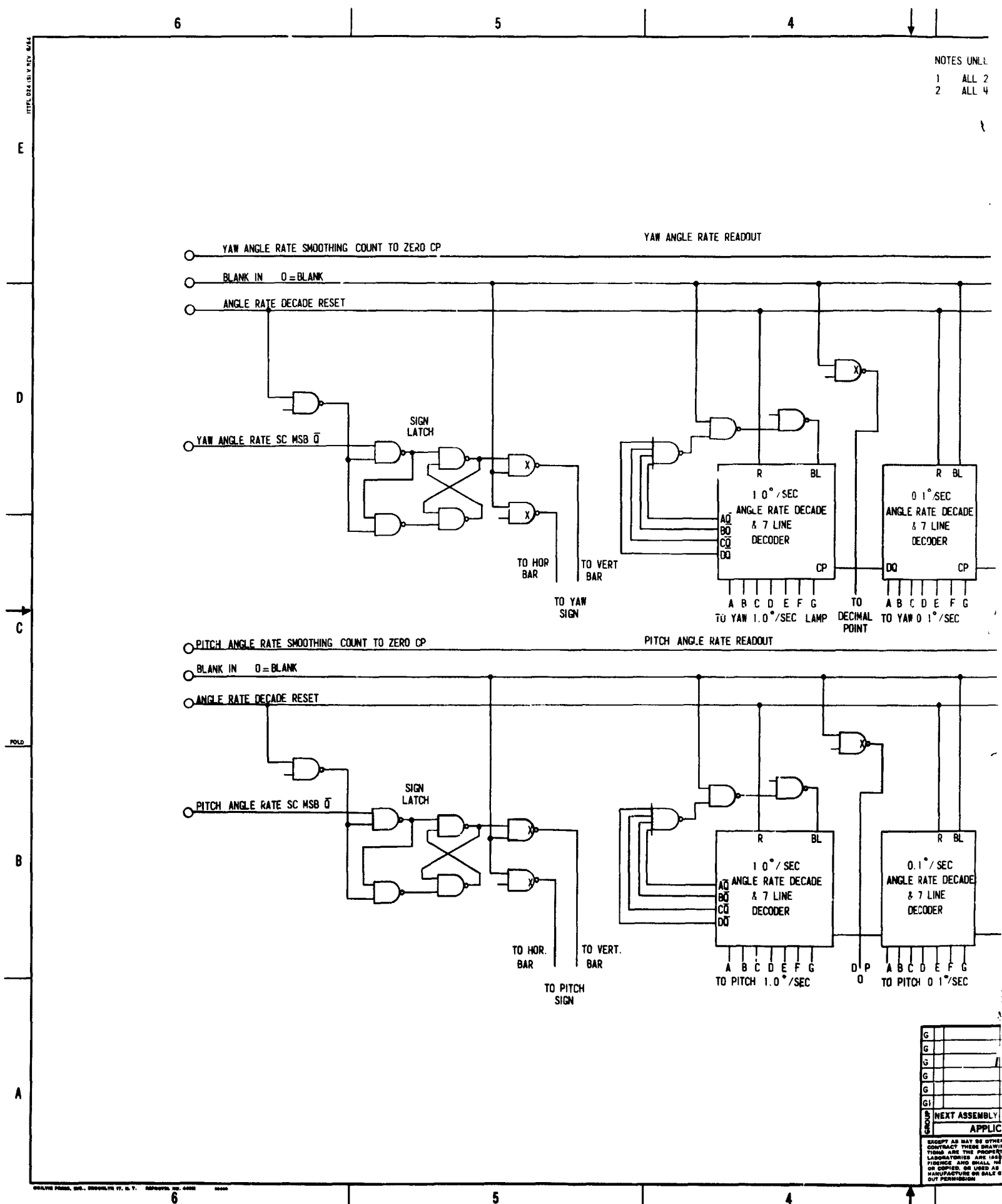
FOLDOUT FRAME

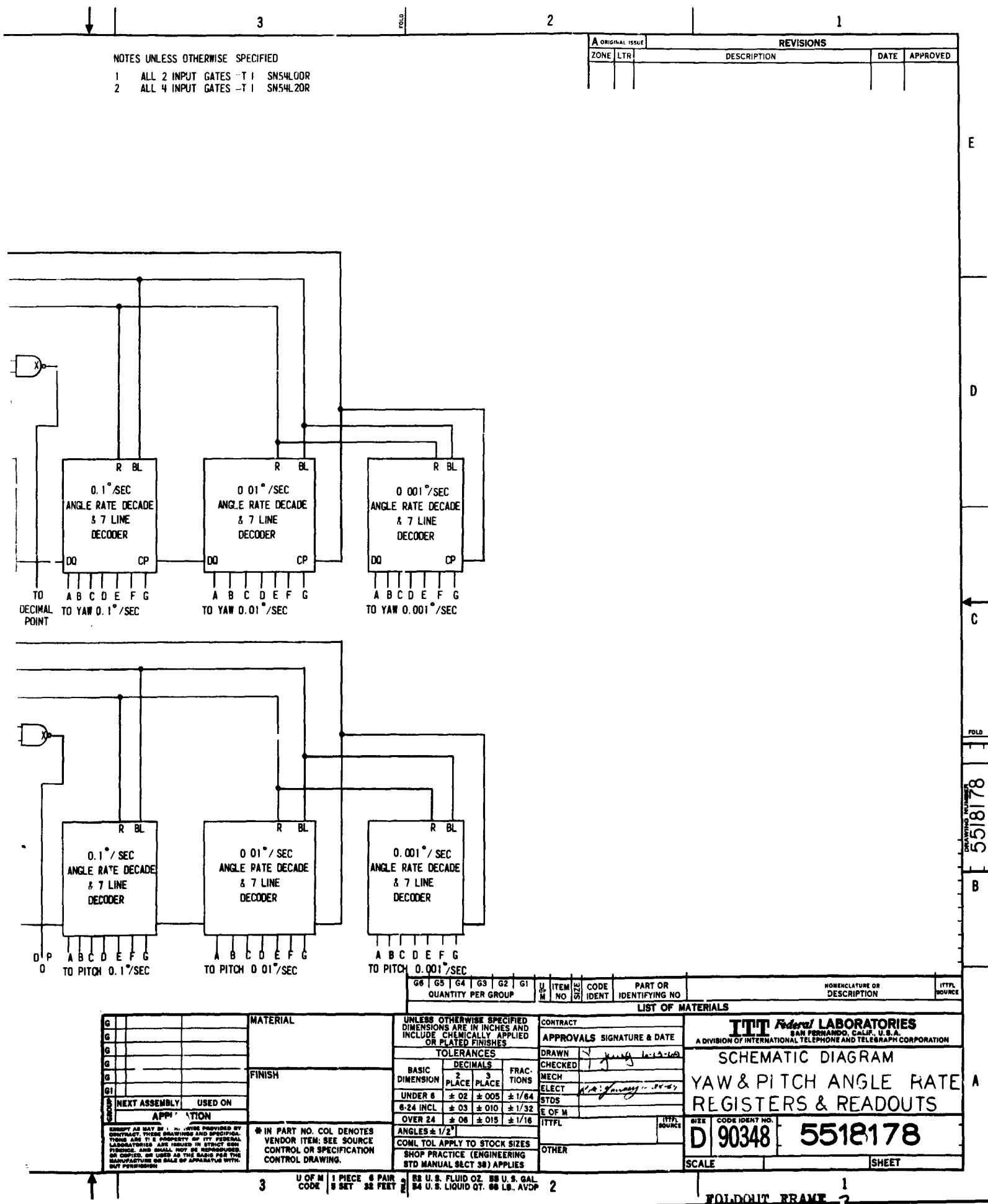
A ORIGINAL ISSUE		REVISIONS		
ZONE	LTR	DESCRIPTION	DATE	APPROVED

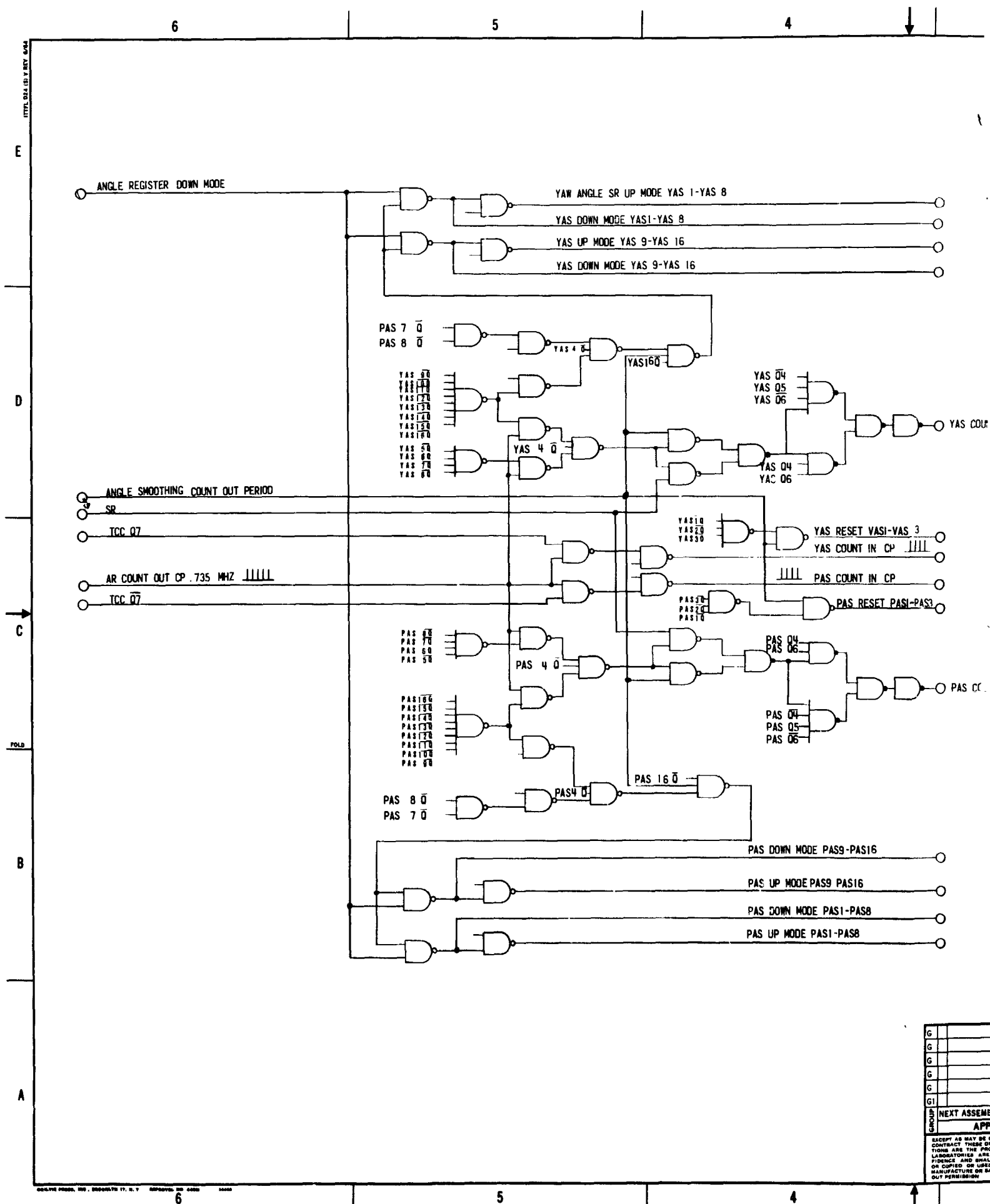


		LIST OF MATERIALS		ITT Federal Laboratories SAN FRANCISCO, CALIF., U.S.A. A DIVISION OF INTERNATIONAL TELEPHONE AND TELEGRAPH CORPORATION	
MATERIAL		JAWLESS DIMENSION SPECIFIED DIMENSIONS ARE IN INCHES AND INCLUDE CONTOURALLY APPLIED OR PLATED FINISHES		CONTRACT APPROVALS SIGNATURE & DATE	
FINISH		TOLERANCES		DRAWN CHECKED	
		BASIC DIMENSION		ELECT	
		DECIMALS		MECH	
		2 PLACE		BYDS	
		3 PLACE		BY M	
		FRACTIONAL		DATE	
		UNDER 8		DATE	
		8-24 INCL		DATE	
		OVER 24		DATE	
		± .02 ± .005 ± 1/64		DATE	
		± .03 ± .010 ± 1/32		DATE	
		± .06 ± .015 ± 1/16		DATE	
		ANGLES ± 1/2°		DATE	
		COMB. TOL. APPLY TO 5" STOCK SIZES		DATE	
		SHOP PRACTICE (ENGINEERING STD. MANUAL SECT. 36) APPLIES		DATE	
PART ASSEMBLY USED ON APPLICATION		B IN PART NO. COL. DENOTES VENDOR ITEM; SEE SOURCE CONTROL OR SPECIFICATION CONTROL DRAWING		OTHER	

1  
FOLDOUT FRAME 2



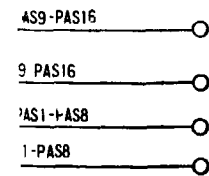
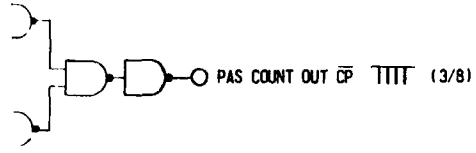
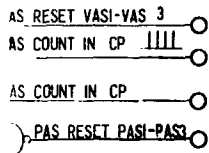
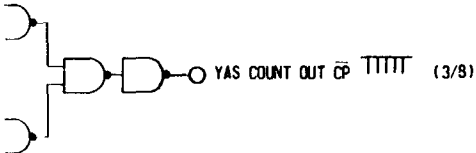
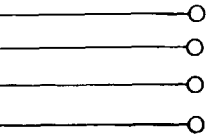




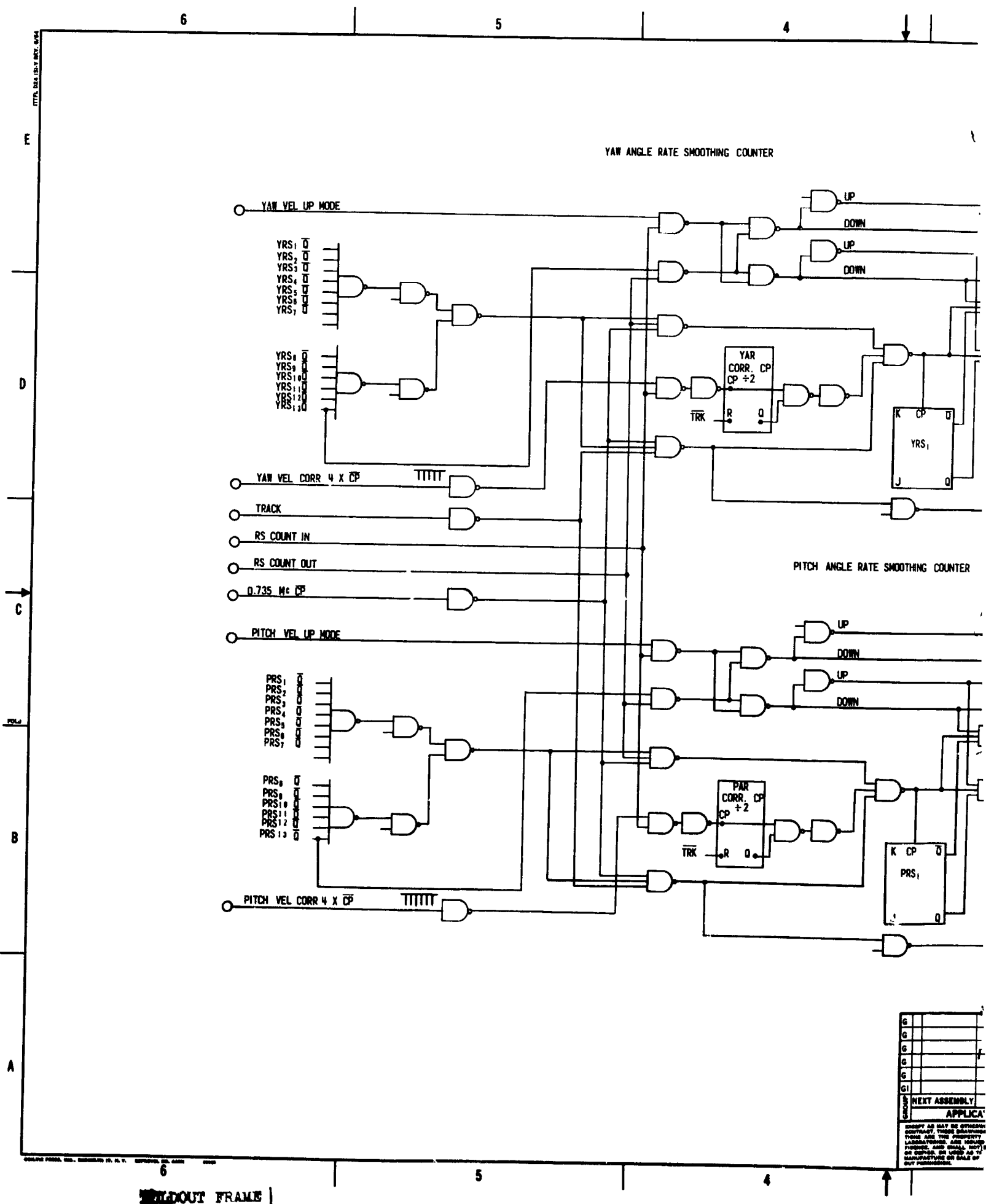
NOTES. UNLESS OTHERWISE SPECIFIED

- 1 2 INPUT GATES = T1 SN54L00R
- 3 INPUT GATES = T1 SN54L10R
- 4 INPUT GATES = T1 SN54L20R
- 8 INPUT GATES = T1 SN54L30R

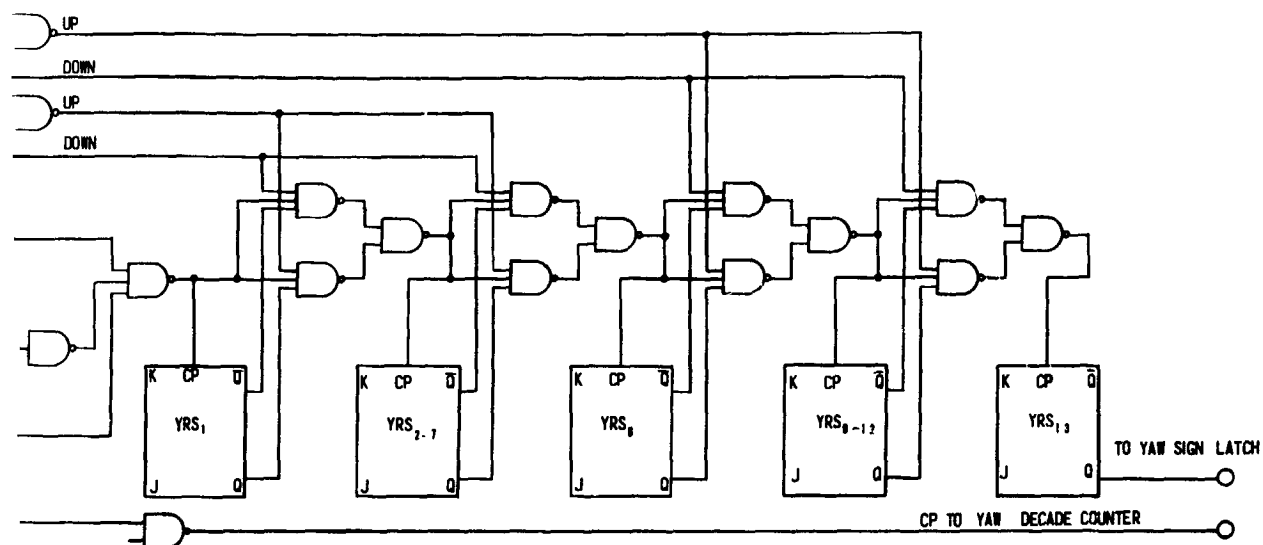
ORIGINAL ISSUE			REVISIONS		
ZONE	LTR		DESCRIPTION	DATE	APPROVED



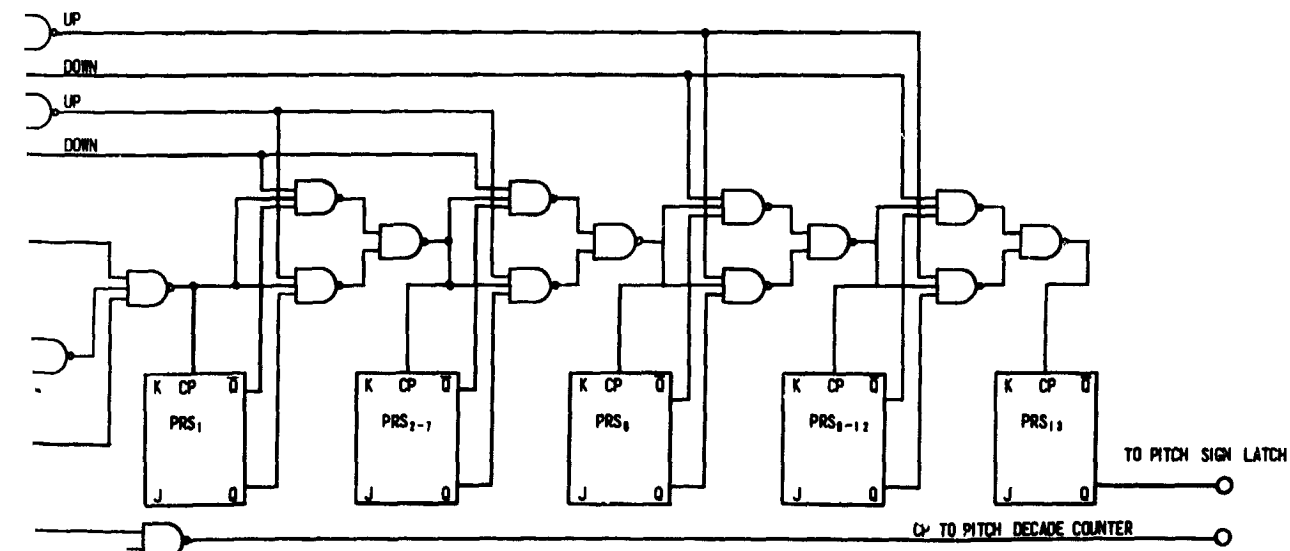
G6		G5	G4	G3	G2	G1	U	ITEM	CODE	PART OR	NOMENCLATURE OR		ITTL
QUANTITY PER GROUP							NO	IDENT	IDENTIFYING NO	DESCRIPTION		SOURCE	
LIST OF MATERIALS													
G6		G5		G4		G3		G2		G1		U	
MATERIAL		FINISH		TOLERANCES		BASIC DIMENSION		DECIMALS		FRACTIONS		CONTRACT	
UNLESS OTHERWISE SPECIFIED DIMENSIONS ARE IN INCHES AND INCLUDE CHEMICALLY APPLIED OR PLATED FINISHES												APPROVALS SIGNATURE & DATE	
DRAWN		CHECKED		MECH		ELECT		STDS		E OF M		ITTL	
NEXT ASSEMBLY USED ON		APPLICATION		* IN PART NO. COL DENOTES VENDOR ITEM; SEE SOURCE CONTROL OR SPECIFICATION CONTROL DRAWING.		ANGLES ± 1/2"		COML TOL APPLY TO STOCK SIZES		SHOP PRACTICE (ENGINEERING STD MANUAL SECT 38) APPLIES		OTHER	
SCALE		SHEET 1 OF 1		5518179		90348		D		CODE IDENT NO.		5518179	



3	2	1												
<table border="1" style="float: right; border-collapse: collapse;"> <tr> <th colspan="2">A ORIGINAL ISSUE</th> <th colspan="2">REVISIONS</th> </tr> <tr> <th>ZONE</th> <th>LTR</th> <th>DESCRIPTION</th> <th>DATE</th> </tr> <tr> <td> </td> <td> </td> <td> </td> <td> </td> </tr> </table>			A ORIGINAL ISSUE		REVISIONS		ZONE	LTR	DESCRIPTION	DATE				
A ORIGINAL ISSUE		REVISIONS												
ZONE	LTR	DESCRIPTION	DATE											



H ANGLE RATE SMOOTHING COUNTER



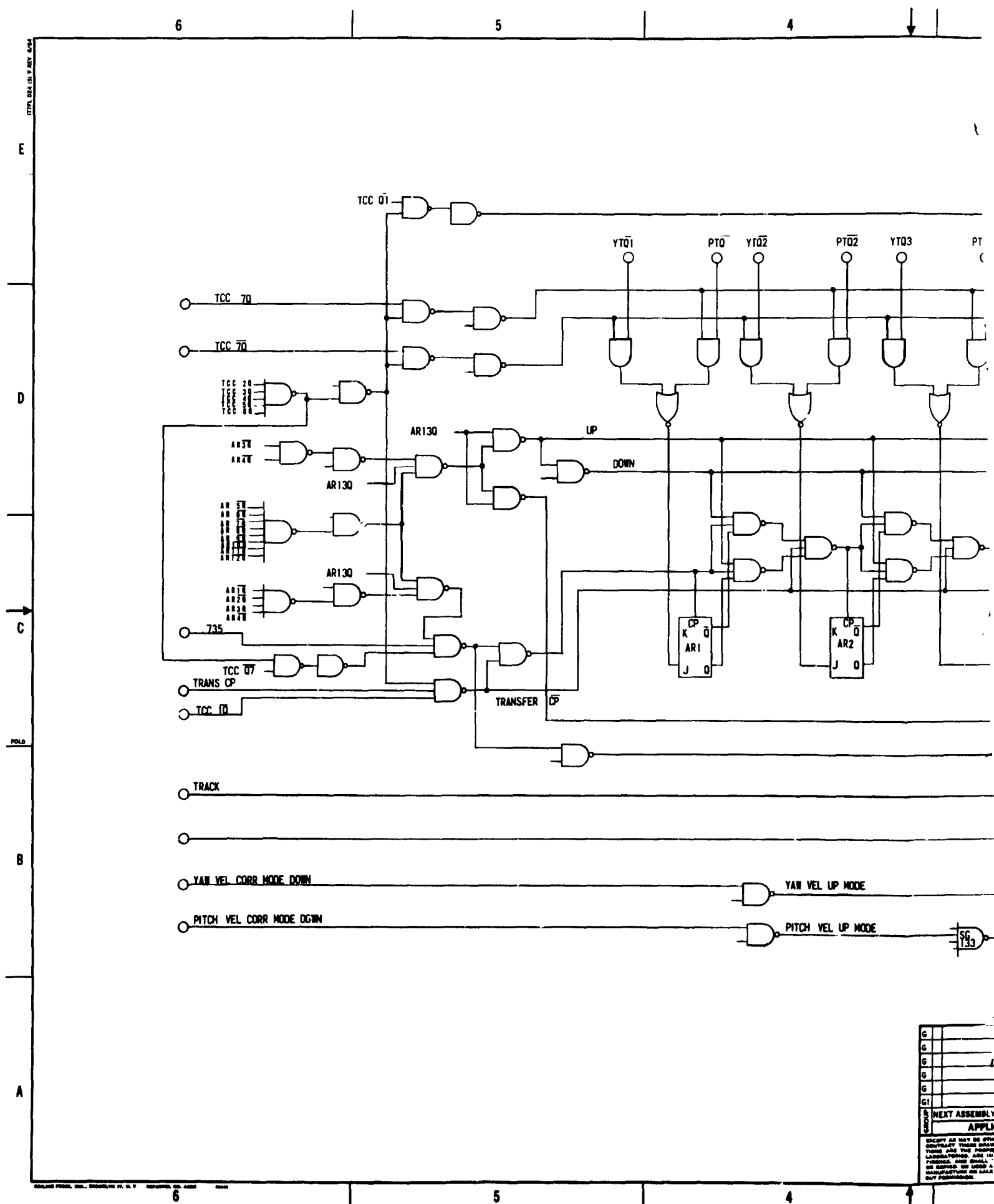
5518180

B

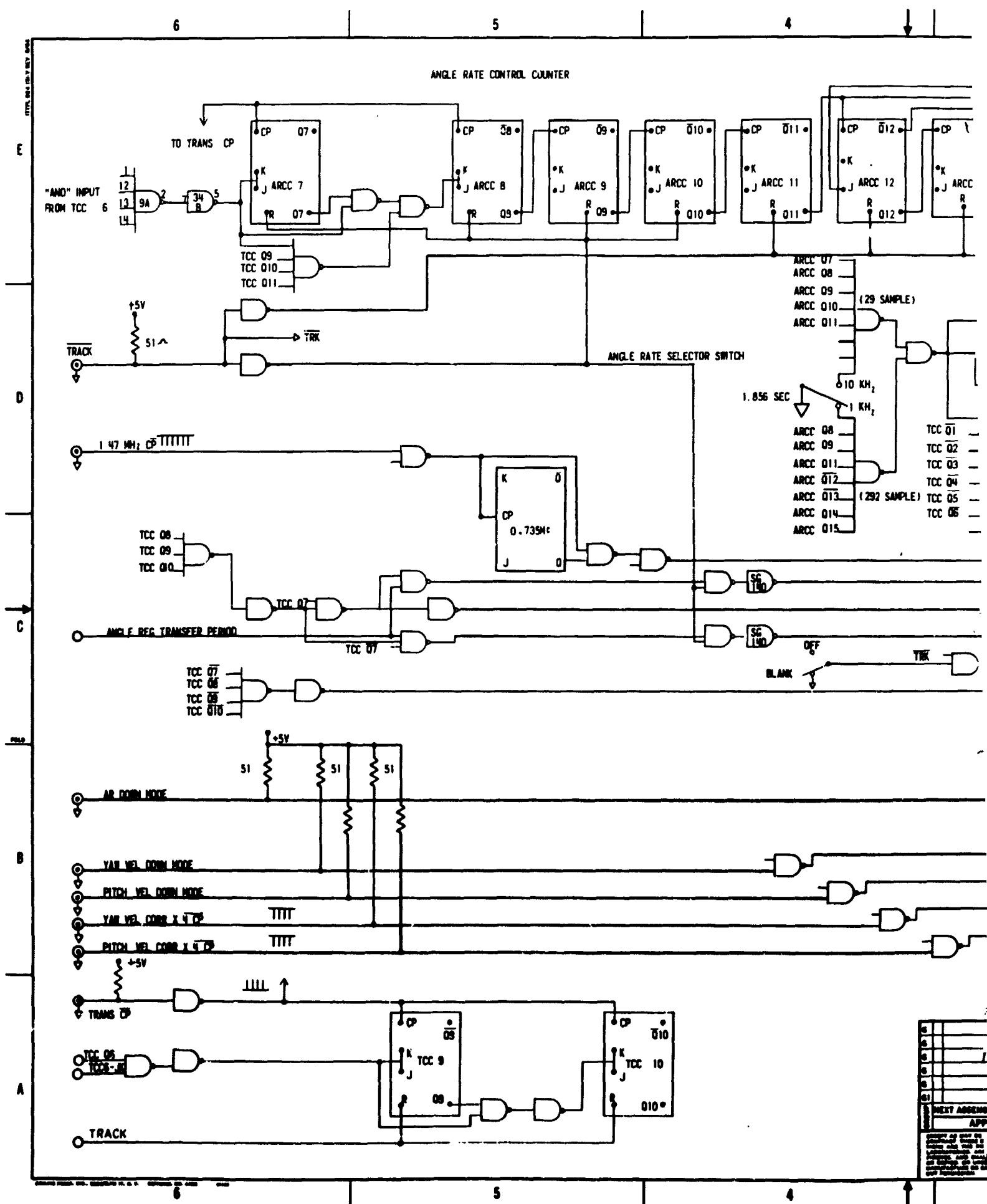
A

64	65	64	63	62	61	U	ITEM	CODE	PART OR	NOMENCLATURE OR	ITVL
QUANTITY PER GROUP						NO.	NO.	IDENT	IDENTIFYING NO.	DESCRIPTION	SOURCE
LIST OF MATERIALS											
MATERIAL						CONTRACT					
FINISH						APPROVALS SIGNATURE & DATE					
NEXT ASSEMBLY USED ON APPLICATION						DRAWN <i>[Signature]</i>					
IN PART NO. COL DENOTES VENDOR ITEM; SEE SOURCE CONTROL OR SPECIFICATION CONTROL DRAWING.						CHECKED <i>[Signature]</i>					
UNLESS OTHERWISE SPECIFIED DIMENSIONS ARE IN INCHES AND INCLUDE CHEMICALLY APPLIED OR PLATED FINISHES						ELECT <i>[Signature]</i>					
TOLERANCES						STDS					
BASIC DIMENSION						E OF M					
UNDER 6						ITVL					
6-24 INCL						OTHER					
OVER 24						SCALE					
ANGLES ± 1/2°						SHEET 1 OF 1					
COML TO APPLY TO STOCK SIZES						D 90348 5518180					
SHOP PRACTICE (ENGINEERING STD MANUAL SECT 38) APPLIES						5518180					

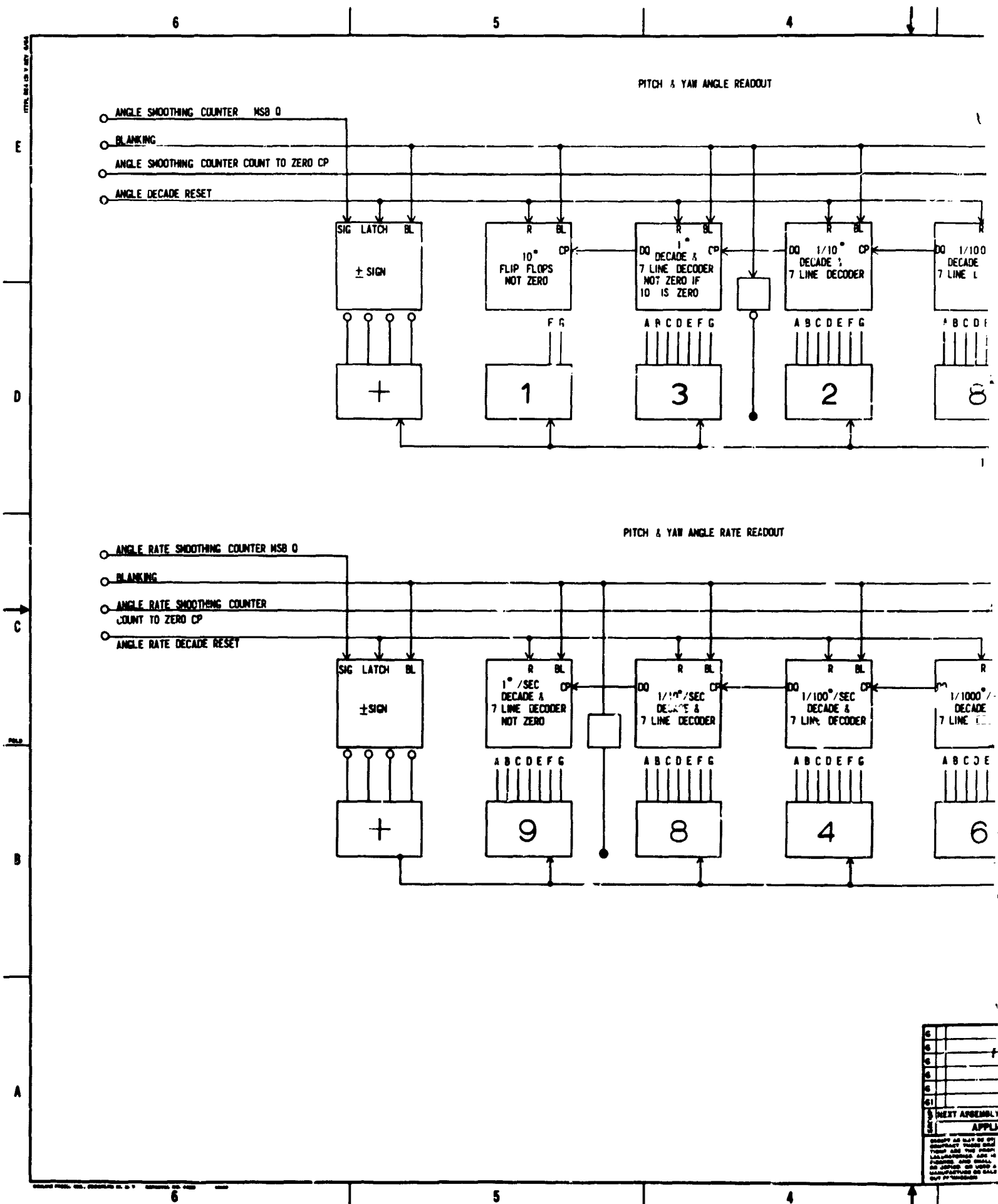


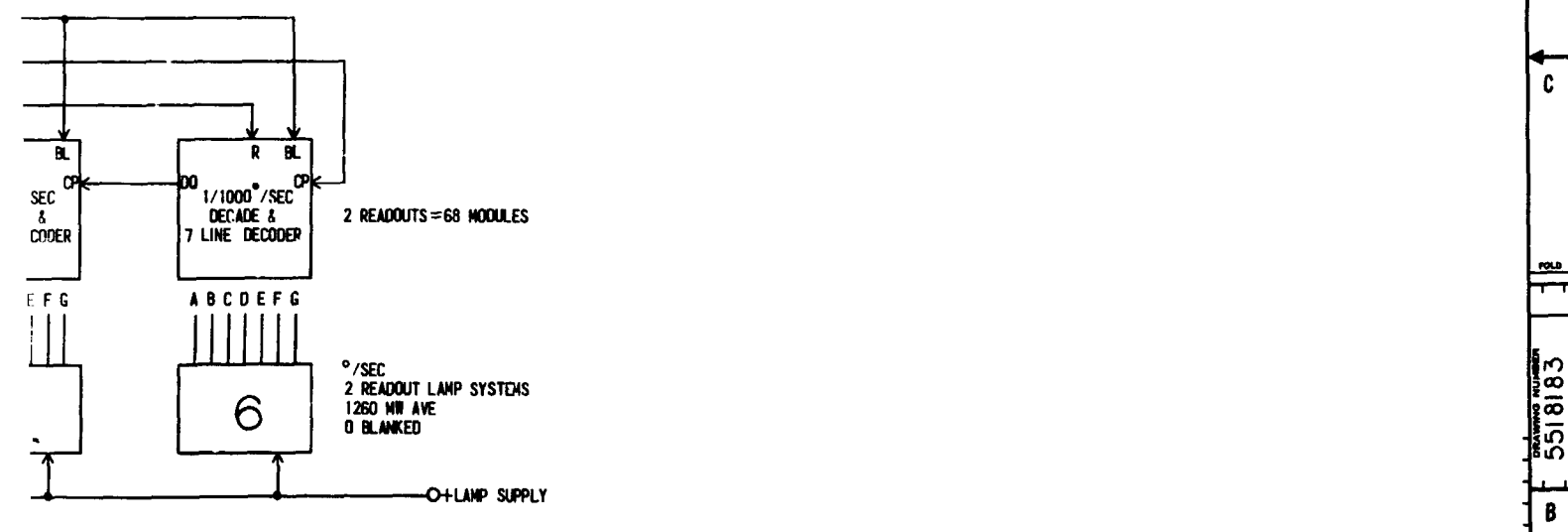
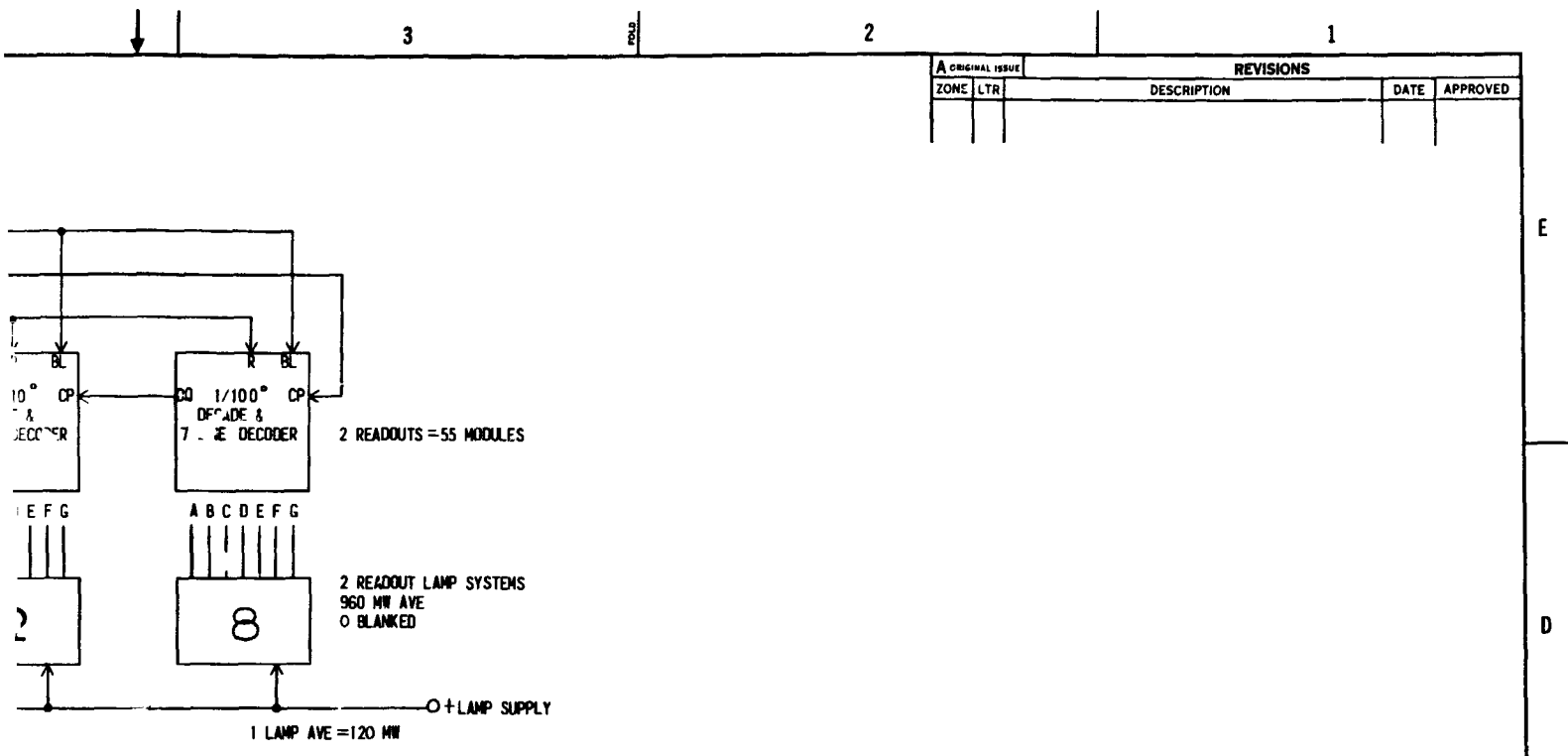












G6		G5		G4		G3		G2		G1		U		ITEM		CODE		PART OR		NOMENCLATURE OR		ITTL	
QUANTITY		PER GROUP										NO		SIZE		IDENT		IDENTIFYING NO.		DESCRIPTION		SOURCE	
LIST OF MATERIALS																							
MATERIAL												CONTRACT											
FINISH												APPROVALS SIGNATURE & DATE											
NEXT ASSEMBLY USED ON APPLICATION												DRAWN <i>[Signature]</i> 4-23-68											
UNLESS OTHERWISE SPECIFIED DIMENSIONS ARE IN INCHES AND INCLUDE CHEMICALLY APPLIED OR PLATED FINISHES												CHECKED <i>[Signature]</i>											
TOLERANCES												MECH											
BASIC DIMENSION												ELECT											
UNDER 6												STDS											
6-24 INCL												E OF N											
OVER 24												ITTL											
ANGLES ± 1/2°												OTHER											
COML TOL APPLY TO STOCK SIZES												SCALE											
SHOP PRACTICE (ENGINEERING STD MANUAL SECT 38) APPLIES												SHEET 1 OF 1											

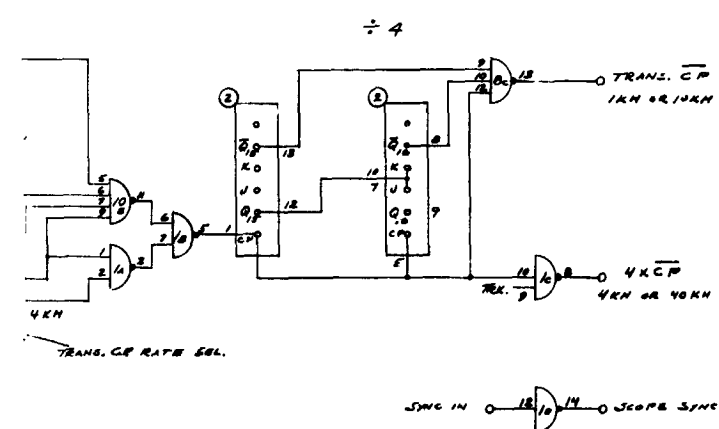
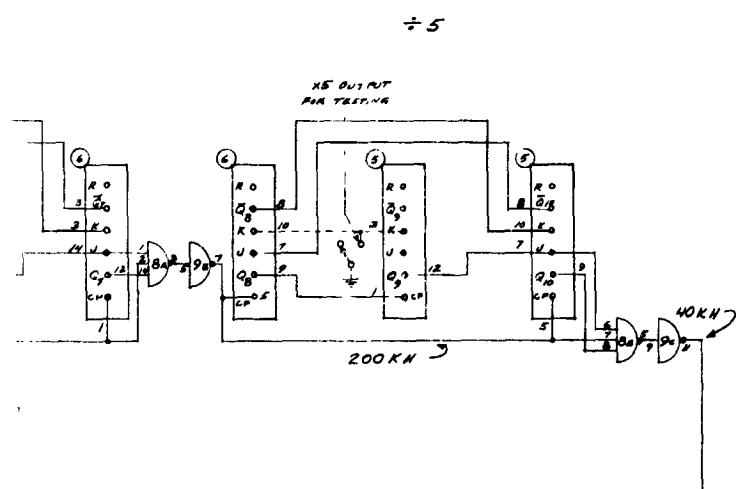
**ITT Federal Laboratories**  
SAN FERNANDO, CALIF., U.S.A.  
A DIVISION OF INTERNATIONAL TELEPHONE AND TELEGRAPH CORPORATION

**DIAGRAM SCHEMATIC  
ANGLE AND ANGLE  
RATE READOUTS**

**D 90348 5518183**



3	2	1												
<table border="1" style="width: 100%; border-collapse: collapse;"> <tr> <th colspan="2">ORIGINAL ISSUE</th> <th colspan="2">REVISIONS</th> </tr> <tr> <th>ZONE</th> <th>LTR</th> <th>DESCRIPTION</th> <th>DATE</th> </tr> <tr> <td> </td> <td> </td> <td> </td> <td> </td> </tr> </table>			ORIGINAL ISSUE		REVISIONS		ZONE	LTR	DESCRIPTION	DATE				
ORIGINAL ISSUE		REVISIONS												
ZONE	LTR	DESCRIPTION	DATE											



E  
D  
C  
B  
A

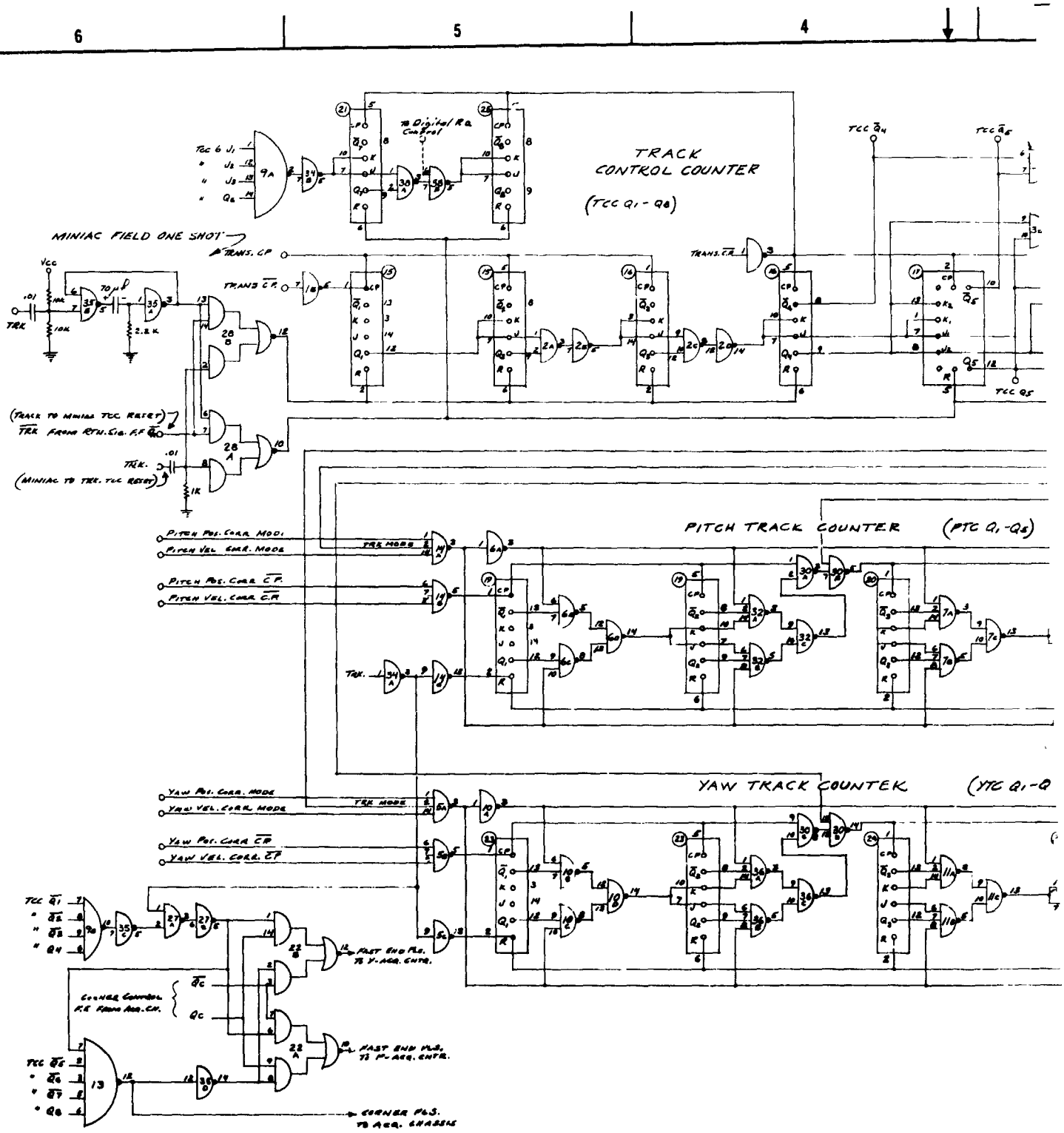
FOLD  
5518184  
1

G6	G5	G4	G3	G2	G1	U	ITEM NO	CODE IDENT	PART OR IDENTIFYING NO	NOMENCLATURE OR DESCRIPTION	ITTL SOURCE																																
LIST OF MATERIALS																																											
<table border="1" style="width: 100%; border-collapse: collapse;"> <tr> <th colspan="2">MATERIAL</th> <th colspan="2">FINISH</th> </tr> <tr> <td> </td> <td> </td> <td> </td> <td> </td> </tr> </table>						MATERIAL		FINISH						<table border="1" style="width: 100%; border-collapse: collapse;"> <tr> <th colspan="2">TOLERANCES</th> </tr> <tr> <td>BASIC DIMENSION</td> <td>DECIMALS</td> </tr> <tr> <td>UNDER 8</td> <td>± .02 ± .005 ± 1/64</td> </tr> <tr> <td>8-24 INCL</td> <td>± .03 ± .010 ± 1/32</td> </tr> <tr> <td>C/EN 24</td> <td>± .06 ± .015 ± 1/16</td> </tr> <tr> <td colspan="2">ANGLES ± 1/2°</td> </tr> </table>		TOLERANCES		BASIC DIMENSION	DECIMALS	UNDER 8	± .02 ± .005 ± 1/64	8-24 INCL	± .03 ± .010 ± 1/32	C/EN 24	± .06 ± .015 ± 1/16	ANGLES ± 1/2°		<table border="1" style="width: 100%; border-collapse: collapse;"> <tr> <td colspan="2">CONTRACT</td> </tr> <tr> <td colspan="2">APPROVALS SIGNATURE &amp; DATE</td> </tr> <tr> <td>DRAWN</td> <td>CHECKED</td> </tr> <tr> <td>MECH</td> <td>ELECT</td> </tr> <tr> <td>STDS</td> <td>E OF M</td> </tr> <tr> <td colspan="2">OTHER</td> </tr> </table>				CONTRACT		APPROVALS SIGNATURE & DATE		DRAWN	CHECKED	MECH	ELECT	STDS	E OF M	OTHER	
						MATERIAL		FINISH																																			
TOLERANCES																																											
BASIC DIMENSION	DECIMALS																																										
UNDER 8	± .02 ± .005 ± 1/64																																										
8-24 INCL	± .03 ± .010 ± 1/32																																										
C/EN 24	± .06 ± .015 ± 1/16																																										
ANGLES ± 1/2°																																											
CONTRACT																																											
APPROVALS SIGNATURE & DATE																																											
DRAWN	CHECKED																																										
MECH	ELECT																																										
STDS	E OF M																																										
OTHER																																											
<table border="1" style="width: 100%; border-collapse: collapse;"> <tr> <td colspan="2">NEXT ASSEMBLY USED ON APPLICATION</td> </tr> <tr> <td colspan="2"> </td> </tr> </table>						NEXT ASSEMBLY USED ON APPLICATION				<table border="1" style="width: 100%; border-collapse: collapse;"> <tr> <td colspan="2">ITTL SOURCE</td> </tr> <tr> <td colspan="2"> </td> </tr> </table>		ITTL SOURCE				<table border="1" style="width: 100%; border-collapse: collapse;"> <tr> <td colspan="2"> <b>ITT Federal LABORATORIES</b>            SAN FERNANDO, CALIF., U.S.A.            A DIVISION OF INTERNATIONAL TELEPHONE AND TELEGRAPH CORPORATION         </td> </tr> <tr> <td colspan="2" style="text-align: center;"> <b>DIAGRAM SCHEMATIC, CLOCK PULSE GENERATOR</b> </td> </tr> <tr> <td>           SIZE  <b>D 90348</b> </td> <td>           CODE IDENT NO.  <b>5518184</b> </td> </tr> <tr> <td colspan="2">           SCALE            SHEET         </td> </tr> </table>				<b>ITT Federal LABORATORIES</b> SAN FERNANDO, CALIF., U.S.A. A DIVISION OF INTERNATIONAL TELEPHONE AND TELEGRAPH CORPORATION		<b>DIAGRAM SCHEMATIC, CLOCK PULSE GENERATOR</b>		SIZE <b>D 90348</b>	CODE IDENT NO. <b>5518184</b>	SCALE SHEET																	
NEXT ASSEMBLY USED ON APPLICATION																																											
ITTL SOURCE																																											
<b>ITT Federal LABORATORIES</b> SAN FERNANDO, CALIF., U.S.A. A DIVISION OF INTERNATIONAL TELEPHONE AND TELEGRAPH CORPORATION																																											
<b>DIAGRAM SCHEMATIC, CLOCK PULSE GENERATOR</b>																																											
SIZE <b>D 90348</b>	CODE IDENT NO. <b>5518184</b>																																										
SCALE SHEET																																											

3 U OF M 1 PIECE 8 PAIR 32 U.S. FLUID OZ. 88 U.S. GAL  
CODE 8 SET 32 FEET 84 U.S. LIQUID QT. 66 LB. AVDP 2

FOLDOUT FRAME 2<sup>1</sup>





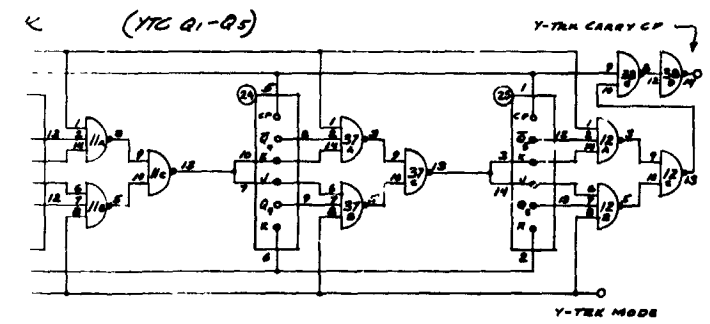
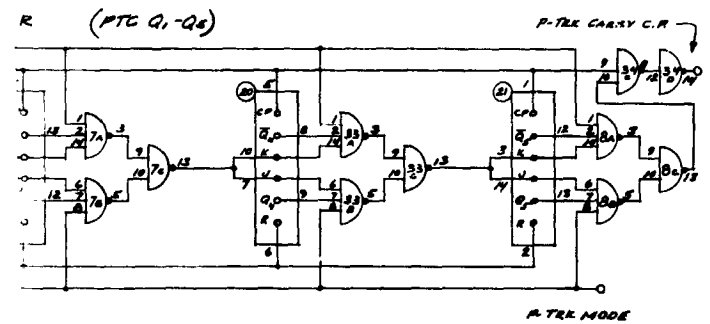
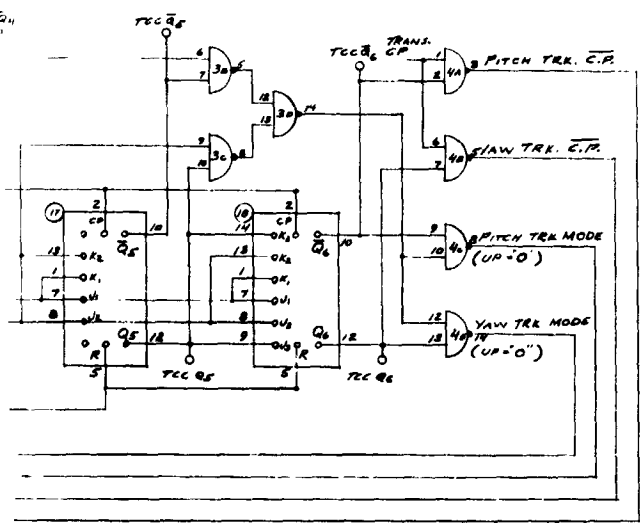
DIGITAL MINIAc GEN. - MOD. II.

6	
5	
4	
3	
2	
1	
0	
61	
60	
59	
58	
57	
56	
55	
54	
53	
52	
51	
50	
49	
48	
47	
46	
45	
44	
43	
42	
41	
40	
39	
38	
37	
36	
35	
34	
33	
32	
31	
30	
29	
28	
27	
26	
25	
24	
23	
22	
21	
20	
19	
18	
17	
16	
15	
14	
13	
12	
11	
10	
9	
8	
7	
6	
5	
4	
3	
2	
1	
0	

NEXT ASSEMBLY  
APPLIC

EXCEPT AS MAY BE OTHERWISE SPECIFIED, THESE DRAWINGS ARE THE PROPERTY OF THE UNITED STATES GOVERNMENT AND ARE NOT TO BE REPRODUCED OR USED IN ANY MANNER WITHOUT PERMISSION.

3	2	1
<div style="display: flex; justify-content: space-between;"> <div style="width: 20%;"> <b>A ORIGINAL ISSUE</b>          ZONE LTR       </div> <div style="width: 50%; text-align: center;"> <b>REVISIONS</b>          DESCRIPTION DATE APPROVED       </div> <div style="width: 30%;"></div> </div>		



G6	G5	G4	G3	G2	G1	U	ITEM	N	CODE	PART OR	NONENCLATURE OR	ITTL															
						QTY	NO	IDENT	IDENTIFYING NO	DESCRIPTION			SOURCE														
LIST OF MATERIALS																											
MATERIAL						CONTRACT						APPROVALS SIGNATURE & DATE															
UNLESS OTHERWISE SPECIFIED DIMENSIONS ARE IN INCHES AND INCLUDE CHEMICALLY APPLIED OR PLATED FINISHES <b>TOLERANCES</b> <table border="1" style="width:100%; border-collapse: collapse;"> <tr> <th>BASIC</th> <th>DECIMALS</th> <th>FRACTIONS</th> </tr> <tr> <th>DIMENSION</th> <th>2 PLACE</th> <th>3 PLACE</th> </tr> <tr> <td>UNDER 8</td> <td>± 02 ± 005 ± 1/64</td> <td></td> </tr> <tr> <td>8-24 INCL</td> <td>± 03 ± 010 ± 1/32</td> <td></td> </tr> <tr> <td>OVER 24</td> <td>± 06 ± 015 ± 1/16</td> <td></td> </tr> </table> ANGLES ± 1/2° COM. TOL APPLY TO STOCK SIZES SHOP PRACTICE (ENGINEERING STD MANUAL SEC 38) APPLIES						BASIC	DECIMALS	FRACTIONS	DIMENSION	2 PLACE	3 PLACE	UNDER 8	± 02 ± 005 ± 1/64		8-24 INCL	± 03 ± 010 ± 1/32		OVER 24	± 06 ± 015 ± 1/16		DRAWN <i>Gie Hays C-11 69</i> CHECKED MECH ELECT STDS E O' M ITTL						DATE SOURCE
						BASIC	DECIMALS	FRACTIONS																			
						DIMENSION	2 PLACE	3 PLACE																			
						UNDER 8	± 02 ± 005 ± 1/64																				
8-24 INCL	± 03 ± 010 ± 1/32																										
OVER 24	± 06 ± 015 ± 1/16																										
FINISH						<b>ITT Laboratories</b> SAN FERNANDO, CALIF. U.S.A. A DIVISION OF INTERNATIONAL TELEPHONE AND TELEGRAPH CORPORATION																					
NEXT ASSEMBLY USED ON <b>APPLICATION</b>						<b>DIAGRAM SCHEMATIC,</b> <b>TRACK &amp; CONTROL COUNTERS</b> <b>DIGITAL MINIC GENERATOR</b>																					
* IN PART NO. COL DENOTES VENDOR ITEM: SEE SOURCE CONTROL OR SPECIFICATION CONTROL DRAWING.						SIZE CODE IDENT NO. <b>D 90348 5518185</b>																					
SCALE						SHEET																					

6

5

4

E

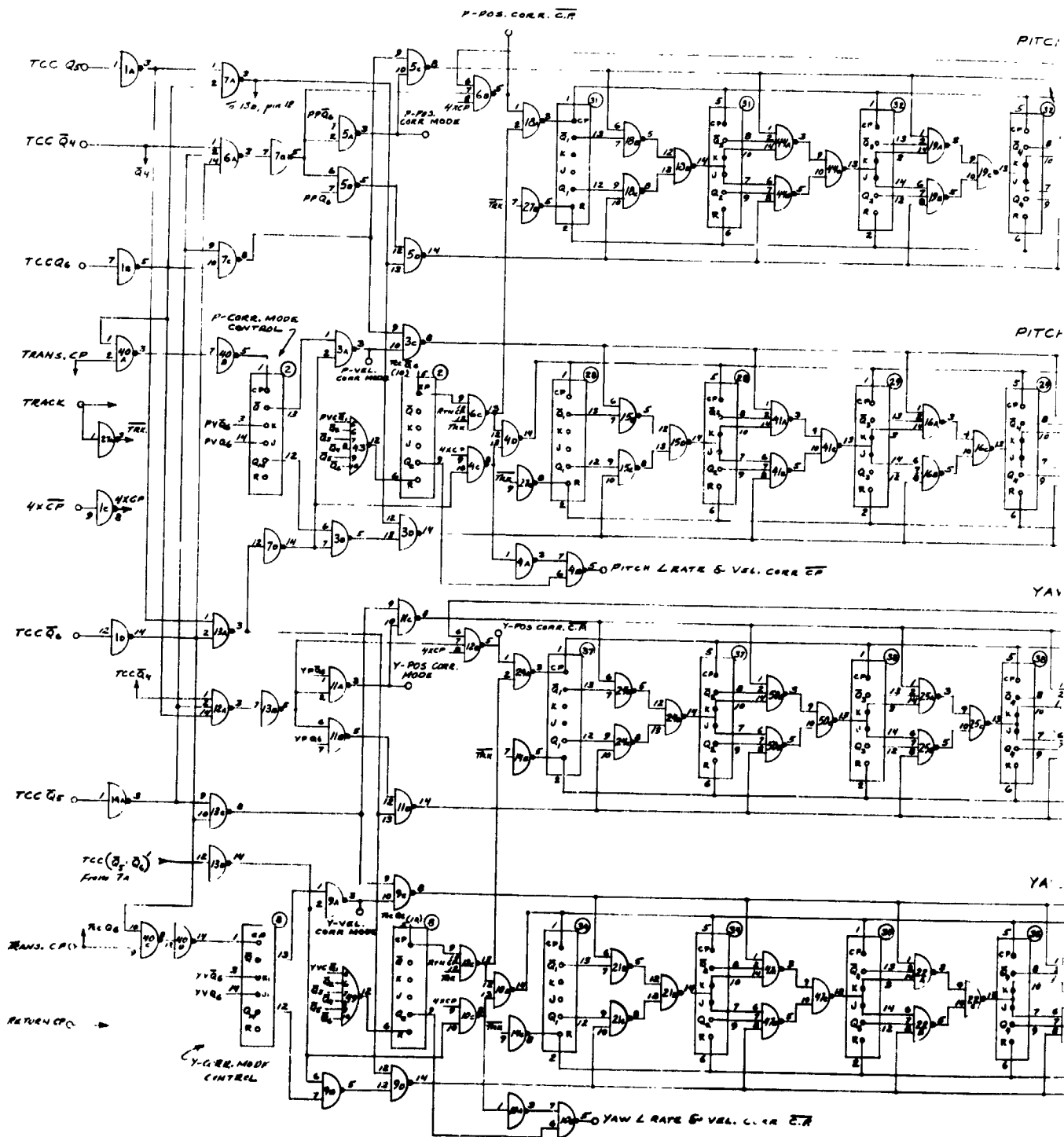
D

C

FOLD

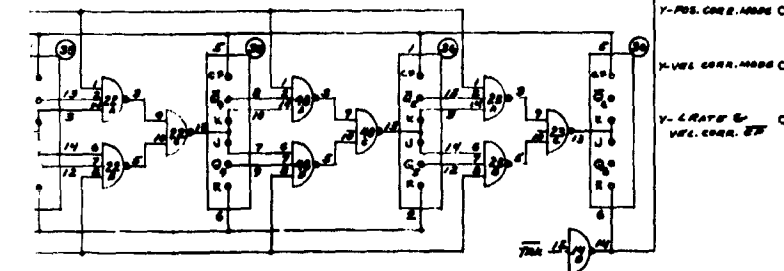
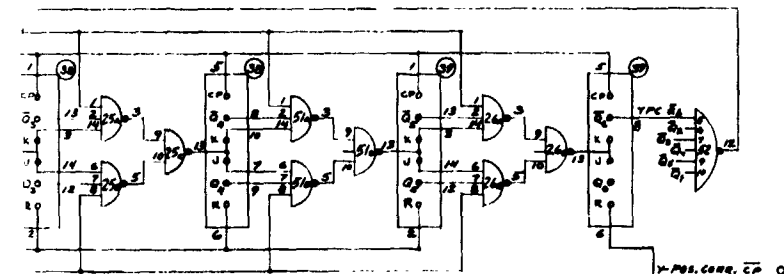
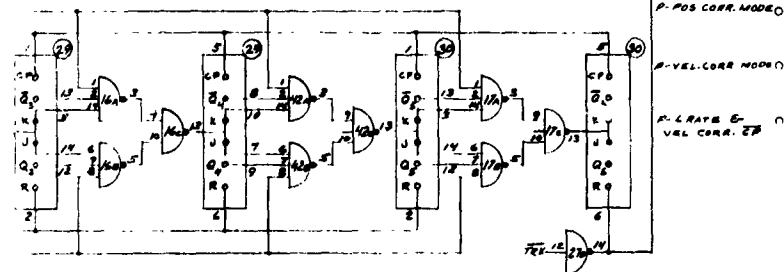
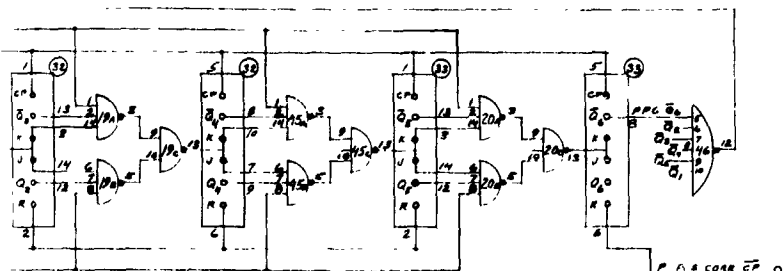
B

A



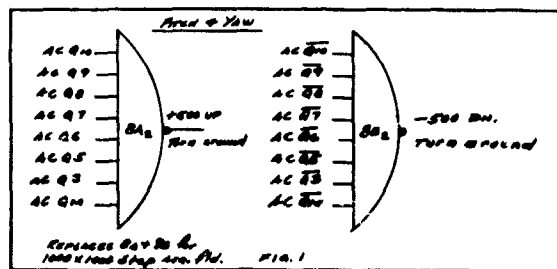
6	
5	
4	
3	
2	
1	
0	
61	
62	
63	
64	
65	
66	
67	
68	
69	
70	
71	
72	
73	
74	
75	
76	
77	
78	
79	
80	
81	
82	
83	
84	
85	
86	
87	
88	
89	
90	
91	
92	
93	
94	
95	
96	
97	
98	
99	
100	

NEXT ASSEMBLY  
APPL  
UNLESS SHOWN TO THE CONTRARY THIS DRAWING IS THE PROPERTY OF THE COMPANY AND IS NOT TO BE REPRODUCED OR USED IN ANY MANNER WITHOUT THE WRITTEN PERMISSION OF THE COMPANY



A ORIGINAL ISSUE		REVISIONS		
ZONE	LTR	DESCRIPTION	DATE	APPROVED

[illegible]

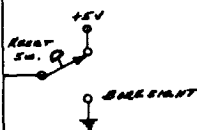
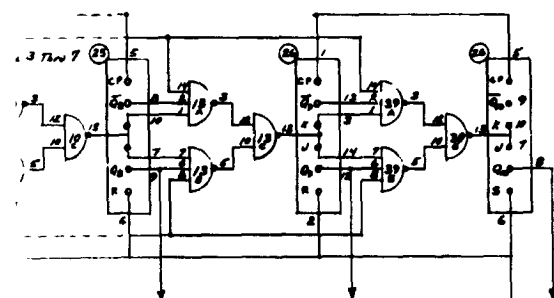


G	
G	
G	
G	
G	
G	
G1	
GROUP	NEXT ASSEMBLY
	APPLY

EXCEPT AS MAY BE OTHERWISE INDICATED THESE DRAWINGS ARE FOR INFORMATION ONLY AND SHALL NOT BE USED FOR CONSTRUCTION OF THE PROJECT.

3	2	1												
<table border="1" style="float: right; border-collapse: collapse;"> <tr> <th colspan="2">ORIGINAL ISSUE</th> <th colspan="2">REVISIONS</th> </tr> <tr> <th>ZONE</th> <th>LTR</th> <th>DESCRIPTION</th> <th>DATE</th> </tr> <tr> <td> </td> <td> </td> <td> </td> <td> </td> </tr> </table>			ORIGINAL ISSUE		REVISIONS		ZONE	LTR	DESCRIPTION	DATE				
ORIGINAL ISSUE		REVISIONS												
ZONE	LTR	DESCRIPTION	DATE											

YAW ACQUISITION COUNTER



YAW ACQUISITION COUNTER

(19)

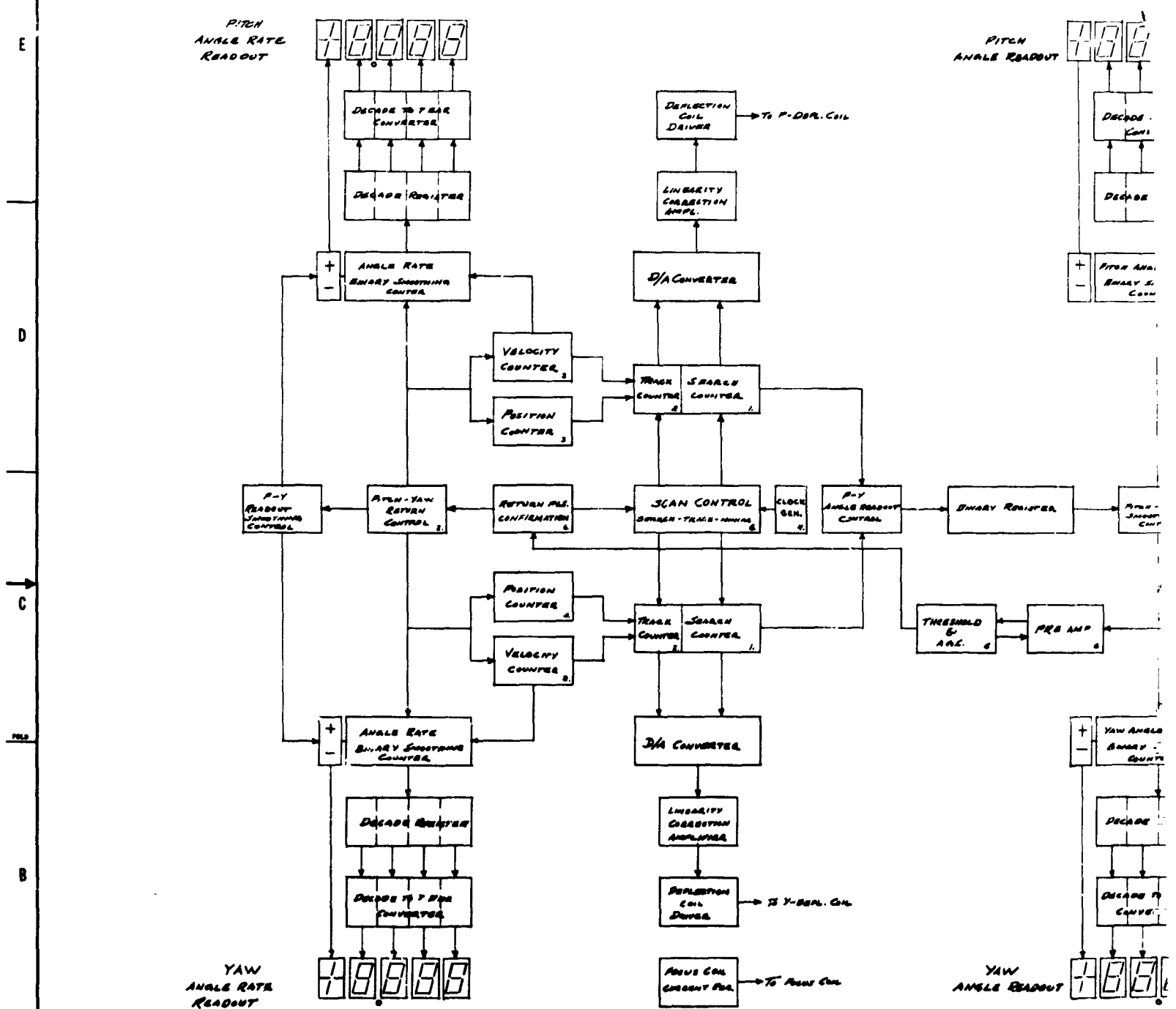
YAW COUNTER

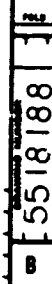
<table border="1" style="display: inline-table; border-collapse: collapse;"> <tr> <td>64</td><td>63</td><td>62</td><td>61</td> </tr> <tr> <td colspan="4" style="text-align: center;">QUANTITY PER GROUP</td> </tr> </table>		64	63	62	61	QUANTITY PER GROUP				<table border="1" style="display: inline-table; border-collapse: collapse;"> <tr> <td>U</td><td>ITEM</td><td>NO</td><td>CODE</td><td>PART OR IDENTIFYING NO</td> </tr> <tr> <td> </td><td> </td><td> </td><td> </td><td> </td> </tr> </table>		U	ITEM	NO	CODE	PART OR IDENTIFYING NO						<table border="1" style="display: inline-table; border-collapse: collapse;"> <tr> <td colspan="2">NOMENCLATURE OR DESCRIPTION</td> </tr> <tr> <td colspan="2"> </td> </tr> </table>		NOMENCLATURE OR DESCRIPTION				<table border="1" style="display: inline-table; border-collapse: collapse;"> <tr> <td>ITVL</td> </tr> <tr> <td> </td> </tr> </table>		ITVL																																																																						
64	63	62	61																																																																																																	
QUANTITY PER GROUP																																																																																																				
U	ITEM	NO	CODE	PART OR IDENTIFYING NO																																																																																																
NOMENCLATURE OR DESCRIPTION																																																																																																				
ITVL																																																																																																				
LIST OF MATERIALS																																																																																																				
<table border="1" style="width:100%; border-collapse: collapse;"> <tr> <td>60</td><td>59</td><td>58</td><td>57</td><td>56</td><td>55</td><td>54</td><td>53</td><td>52</td><td>51</td> </tr> <tr> <td colspan="10"> </td> </tr> </table>		60	59	58	57	56	55	54	53	52	51											<table border="1" style="width:100%; border-collapse: collapse;"> <tr> <td colspan="2">MATERIAL</td> </tr> <tr> <td colspan="2"> </td> </tr> <tr> <td colspan="2">FINISH</td> </tr> <tr> <td colspan="2"> </td> </tr> <tr> <td colspan="2">APPLICATION</td> </tr> <tr> <td colspan="2"> </td> </tr> </table>		MATERIAL				FINISH				APPLICATION				<table border="1" style="width:100%; border-collapse: collapse;"> <tr> <td colspan="3"> <small>UNLESS OTHERWISE SPECIFIED DIMENSIONS ARE IN INCHES AND INCLUDE CHEMICALLY APPLIED OR PLATED FINISHES</small> </td> </tr> <tr> <td colspan="3" style="text-align: center;">TOLERANCES</td> </tr> <tr> <td>BASIC DIMENSION</td> <td>DECIMALS</td> <td>FRACTIONS</td> </tr> <tr> <td>UNDER 6</td> <td>± .02</td> <td>± 1/64</td> </tr> <tr> <td>6-24 INCL</td> <td>± .03</td> <td>± 1/32</td> </tr> <tr> <td>OVER 24</td> <td>± .06</td> <td>± 1/16</td> </tr> <tr> <td colspan="3">ANGLES ± 1/2°</td> </tr> <tr> <td colspan="3">COMM. TOL. APPLY TO STOCK SIZES</td> </tr> <tr> <td colspan="3">SHOP PRACTICE (ENGINEERING STD MANUAL SECT 38) APPLIES</td> </tr> </table>		<small>UNLESS OTHERWISE SPECIFIED DIMENSIONS ARE IN INCHES AND INCLUDE CHEMICALLY APPLIED OR PLATED FINISHES</small>			TOLERANCES			BASIC DIMENSION	DECIMALS	FRACTIONS	UNDER 6	± .02	± 1/64	6-24 INCL	± .03	± 1/32	OVER 24	± .06	± 1/16	ANGLES ± 1/2°			COMM. TOL. APPLY TO STOCK SIZES			SHOP PRACTICE (ENGINEERING STD MANUAL SECT 38) APPLIES			<table border="1" style="width:100%; border-collapse: collapse;"> <tr> <td colspan="2">CONTRACT</td> </tr> <tr> <td colspan="2">APPROVALS SIGNATURE &amp; DATE</td> </tr> <tr> <td colspan="2">DRAWN</td> </tr> <tr> <td colspan="2">CHECKED</td> </tr> <tr> <td colspan="2">ELECT</td> </tr> <tr> <td colspan="2">STD</td> </tr> <tr> <td colspan="2">ITVL</td> </tr> <tr> <td colspan="2">OTHER</td> </tr> </table>		CONTRACT		APPROVALS SIGNATURE & DATE		DRAWN		CHECKED		ELECT		STD		ITVL		OTHER		<table border="1" style="width:100%; border-collapse: collapse;"> <tr> <td colspan="2" style="text-align: center;"> <b>ITT Advanced LABORATORIES</b>  <small>A DIVISION OF INTERNATIONAL TELEPHONE AND TELEGRAPH CORPORATION</small> </td> </tr> <tr> <td colspan="2" style="text-align: center;"> <b>DIAGRAM SCHEMATIC, ACQUISITION SCANNING GENERATOR</b> </td> </tr> <tr> <td> <table border="1" style="width:100%; border-collapse: collapse;"> <tr> <td>SIZE</td> <td>CODE</td> <td>ITEM NO.</td> </tr> <tr> <td>D</td> <td>90348</td> <td>5518187</td> </tr> </table> </td> <td> <table border="1" style="width:100%; border-collapse: collapse;"> <tr> <td>SCALE</td> <td>SHEET</td> </tr> <tr> <td> </td> <td> </td> </tr> </table> </td> </tr> </table>		<b>ITT Advanced LABORATORIES</b> <small>A DIVISION OF INTERNATIONAL TELEPHONE AND TELEGRAPH CORPORATION</small>		<b>DIAGRAM SCHEMATIC, ACQUISITION SCANNING GENERATOR</b>		<table border="1" style="width:100%; border-collapse: collapse;"> <tr> <td>SIZE</td> <td>CODE</td> <td>ITEM NO.</td> </tr> <tr> <td>D</td> <td>90348</td> <td>5518187</td> </tr> </table>	SIZE	CODE	ITEM NO.	D	90348	5518187	<table border="1" style="width:100%; border-collapse: collapse;"> <tr> <td>SCALE</td> <td>SHEET</td> </tr> <tr> <td> </td> <td> </td> </tr> </table>	SCALE	SHEET		
60	59	58	57	56	55	54	53	52	51																																																																																											
MATERIAL																																																																																																				
FINISH																																																																																																				
APPLICATION																																																																																																				
<small>UNLESS OTHERWISE SPECIFIED DIMENSIONS ARE IN INCHES AND INCLUDE CHEMICALLY APPLIED OR PLATED FINISHES</small>																																																																																																				
TOLERANCES																																																																																																				
BASIC DIMENSION	DECIMALS	FRACTIONS																																																																																																		
UNDER 6	± .02	± 1/64																																																																																																		
6-24 INCL	± .03	± 1/32																																																																																																		
OVER 24	± .06	± 1/16																																																																																																		
ANGLES ± 1/2°																																																																																																				
COMM. TOL. APPLY TO STOCK SIZES																																																																																																				
SHOP PRACTICE (ENGINEERING STD MANUAL SECT 38) APPLIES																																																																																																				
CONTRACT																																																																																																				
APPROVALS SIGNATURE & DATE																																																																																																				
DRAWN																																																																																																				
CHECKED																																																																																																				
ELECT																																																																																																				
STD																																																																																																				
ITVL																																																																																																				
OTHER																																																																																																				
<b>ITT Advanced LABORATORIES</b> <small>A DIVISION OF INTERNATIONAL TELEPHONE AND TELEGRAPH CORPORATION</small>																																																																																																				
<b>DIAGRAM SCHEMATIC, ACQUISITION SCANNING GENERATOR</b>																																																																																																				
<table border="1" style="width:100%; border-collapse: collapse;"> <tr> <td>SIZE</td> <td>CODE</td> <td>ITEM NO.</td> </tr> <tr> <td>D</td> <td>90348</td> <td>5518187</td> </tr> </table>	SIZE	CODE	ITEM NO.	D	90348	5518187	<table border="1" style="width:100%; border-collapse: collapse;"> <tr> <td>SCALE</td> <td>SHEET</td> </tr> <tr> <td> </td> <td> </td> </tr> </table>	SCALE	SHEET																																																																																											
SIZE	CODE	ITEM NO.																																																																																																		
D	90348	5518187																																																																																																		
SCALE	SHEET																																																																																																			

6

5

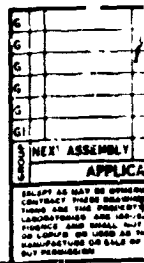
4





**FOLDOUT FRAME 2**





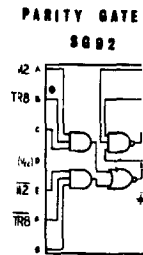
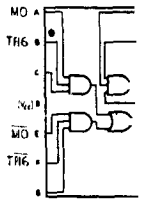
**FOLDOUT FRAME**



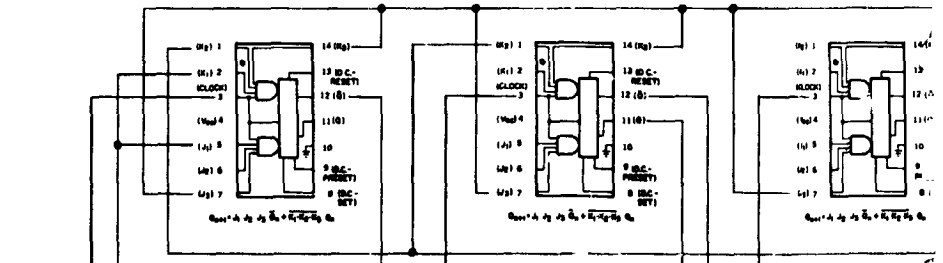
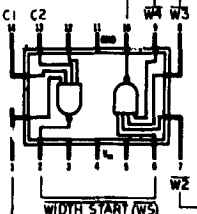
## FOLDOUT FRAME



PARITY 8  
8892



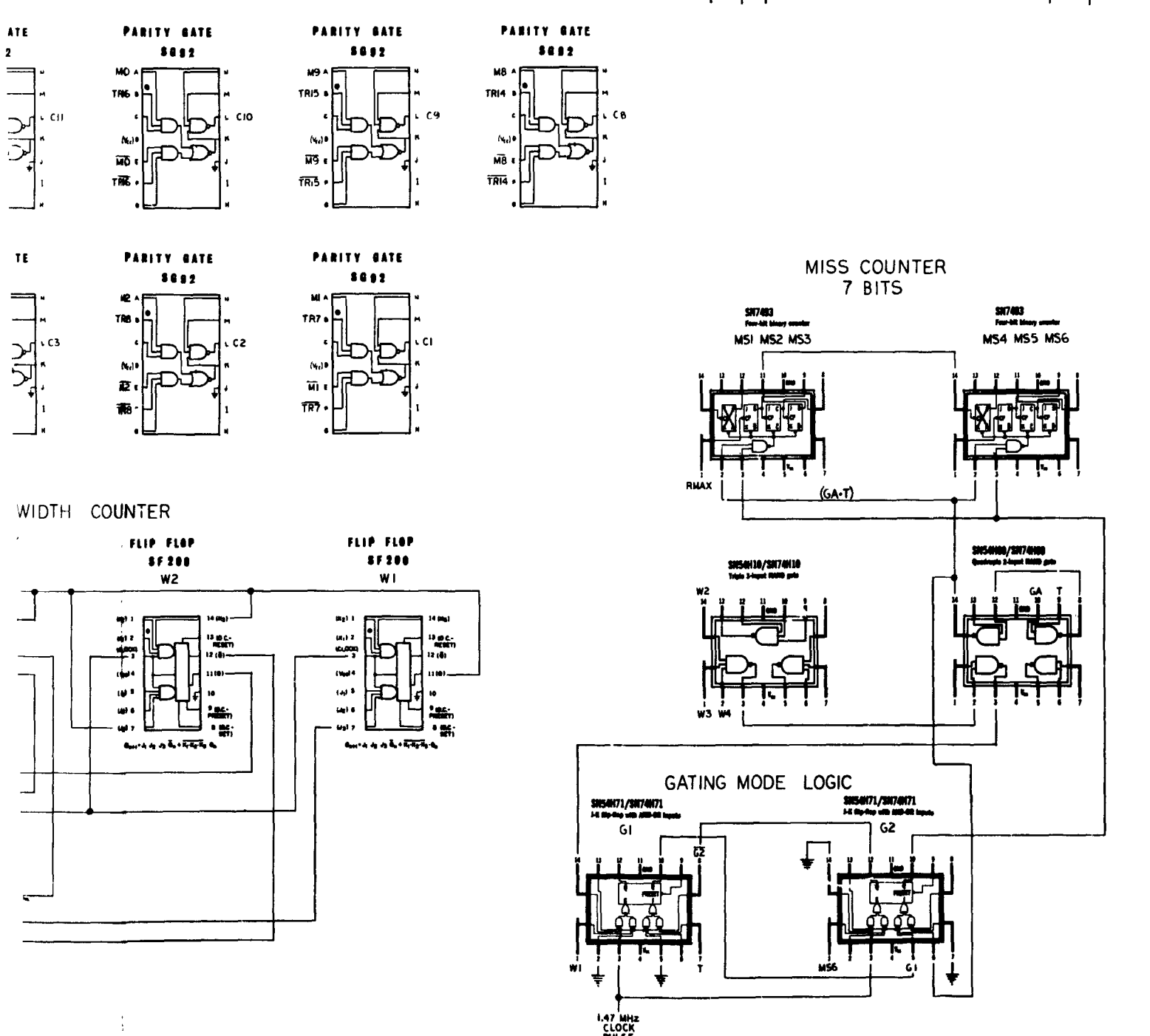
FLIP FLOP  
SF 200  
W2

S0154N120/S0174N120  
Dual 4-input NAND gate

WIDTH START (WS)

EXCEPT AS MAY BE OTHERWISE INDICATED, THESE DRAWINGS ARE THE PROPERTY OF THE FBI LABORATORIES AND ARE NOT TO BE REPRODUCED OR COPIED OR USED AS A BASIS FOR MANUFACTURE OR SALE OF ANY PRODUCT.

## FOLDOUT FRAME



QUANTITY PER GROUP		ITEM NO.	CODE IDENT	PART OR IDENTIFYING NO.	DESCRIPTION OR IDENTIFYING NO.	IT/FL SOURCE												
G8	G5	G4	G3	G2	G1													
<p align="center"><b>LIST OF MATERIALS</b></p>																		
<p><b>MATERIAL</b></p> <p> </p>		<p><b>FINISH</b></p> <p> </p>		<p><b>UNLESS OTHERWISE SPECIFIED DIMENSIONS ARE IN INCHES AND INCLUDE CHEMICALLY APPLIED OR PLATED FINISHES</b></p> <table border="1" style="width: 100%;"> <thead> <tr> <th>BASIC DIMENSION</th> <th>DECIMALS</th> <th>FRACTIONS</th> </tr> </thead> <tbody> <tr> <td>UNDER 8</td> <td>± .02</td> <td>± 1/64</td> </tr> <tr> <td>8-24 INCL</td> <td>± .03</td> <td>± 1/32</td> </tr> <tr> <td>OVER 24</td> <td>± .04</td> <td>± 1/16</td> </tr> </tbody> </table> <p>ANGLES ± 1/2°</p> <p>COUL TOL APPLY TO STOCK SIZES</p> <p>SHOP PRACTICE (ENGINEERING STD MANUAL SECT 38) APPLIES</p>			BASIC DIMENSION	DECIMALS	FRACTIONS	UNDER 8	± .02	± 1/64	8-24 INCL	± .03	± 1/32	OVER 24	± .04	± 1/16
BASIC DIMENSION	DECIMALS	FRACTIONS																
UNDER 8	± .02	± 1/64																
8-24 INCL	± .03	± 1/32																
OVER 24	± .04	± 1/16																
<p><b>CONTRACT</b></p> <p>APPROVALS SIGNATURE &amp; DATE</p> <p> </p>		<p><b>TTT Federal LABORATORIES</b></p> <p>SAN FERNANDO, CALIF., U.S.A.</p> <p>A DIVISION OF INTERNATIONAL TELEPHONE AND TELEGRAPH CORPORATION</p>																
<p><b>DIAGRAM SCHEMATIC</b></p> <p><b>RANGE GATING LOGIC</b></p>		<p><b>CODE IDENT NO.</b></p> <p><b>D 90348 5518194</b></p>																
<p><b>SCALE</b></p> <p> </p>		<p><b>SHEET</b></p> <p> </p>																

3 U OF N 1 PIECE 8 FAIR CODE 8 SET 88 FEET

88 U.S. FLUID OZ. 88 U.S. GAL 84 U.S. LIQUID QT. 88 LB. AVDP

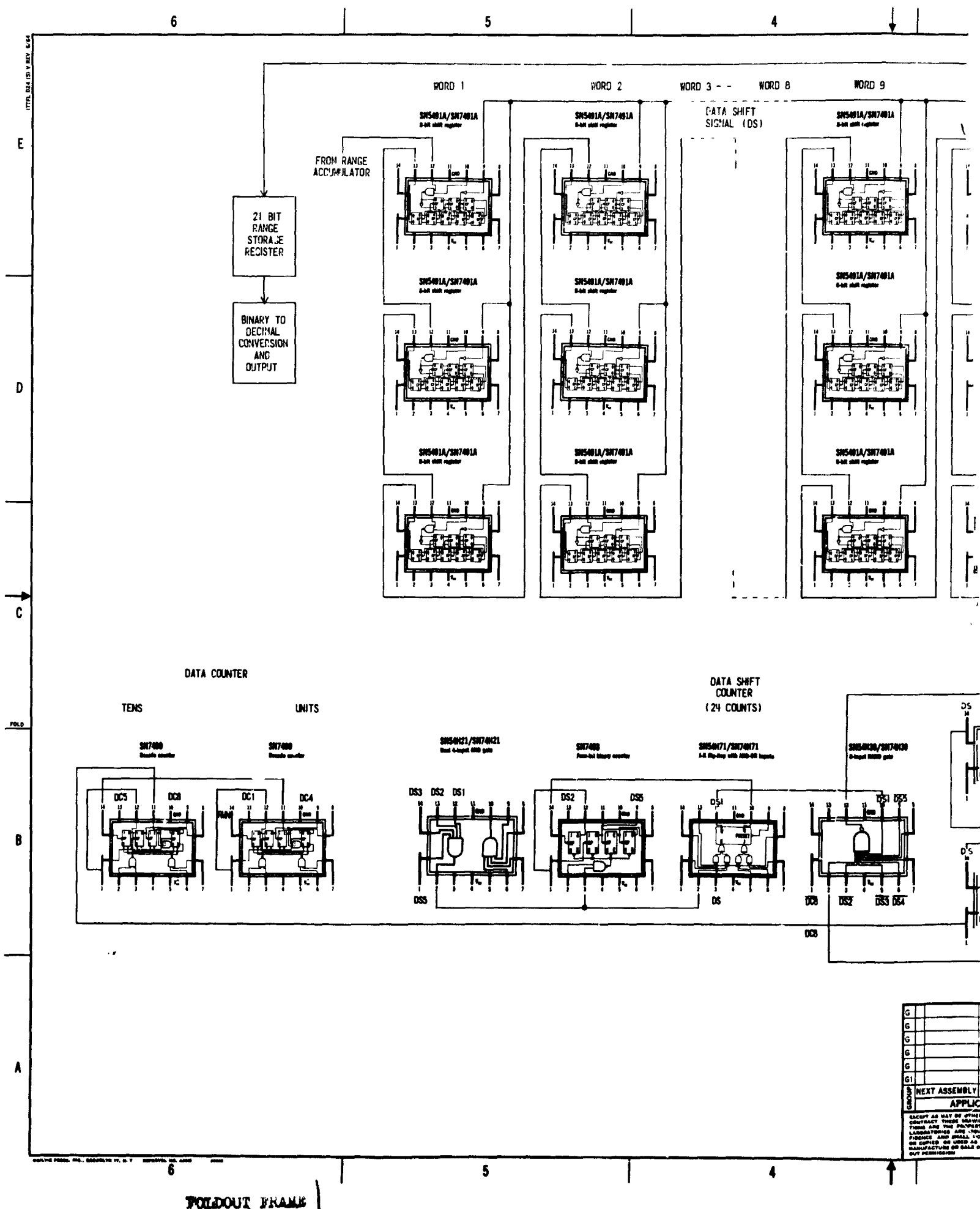
2

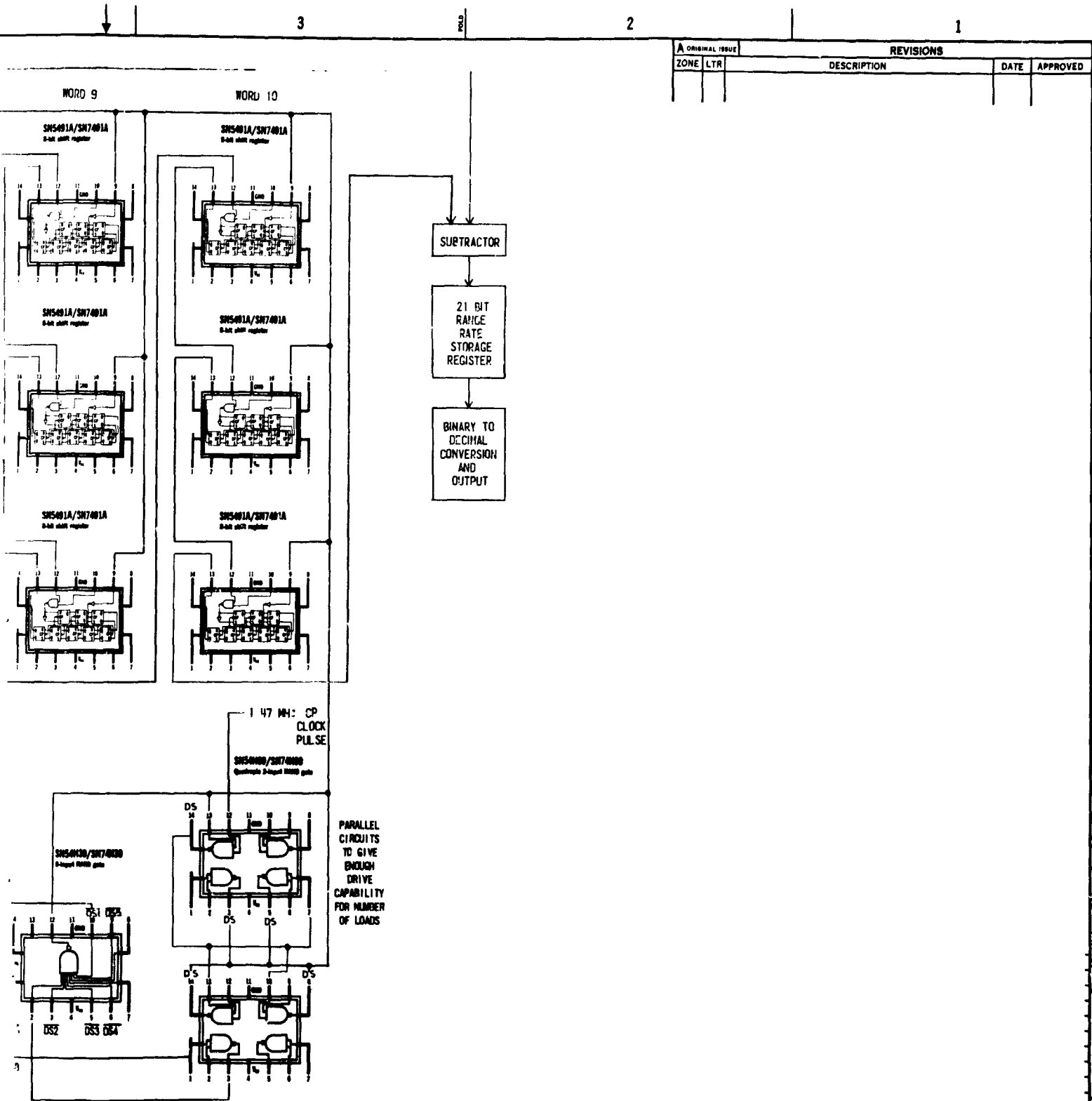
**FOLDOUT FRAME 2**











QUANTITY PER GROUP		U	M	ITEM NO	CODE IDENT	PART OR IDENTIFYING NO.	DESCRIPTION OF MATERIAL	ITTL SOURCE
LIST OF MATERIALS								
MATERIAL		FINISH		TOLERANCES		CONTRACT		
UNLESS OTHERWISE SPECIFIED DIMENSIONS ARE IN INCHES AND INCLUDE CHEMICALLY APPLIED OR PLATED FINISHES		BASIC DIMENSION		DECIMALS		APPROVALS SIGNATURE & DATE		
		PLACE		PLACE		DRAWN		
		UNDER 6		± .02 ± .008 ± 1/64		CHECKED		
		6-24 INCL		± .03 ± .010 ± 1/32		MECH		
		OVER 24		± .06 ± .015 ± 1/16		ELECT		
		ANGLES ± 1/2°				STDS		
		COML TOL APPLY TO STOCK SIZES				R OF M		
		SHOP PRACTICE (ENGINEERING STD MANUAL SECT 36) APPLIES				ITTL		
OTHER						ITTL		
SCALE						SHEET 1 OF 1		

DIAGRAM SCHEMATIC RANGE DATA STORAGE AND PROCESSING

90348 5518196

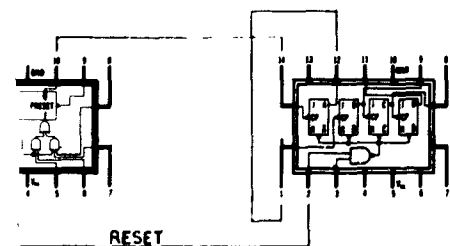


A ORIGINAL ISSUE		REVISIONS		
ZONE	LTR	DESCRIPTION	DATE	APPROVED

TIME ADDITION COUNTER  
29 COUNTS

SN74H71  
with 4000-series inputs  
A5

SN7403  
Four-bit binary inverter  
TA4 TA3 TA2 TA1



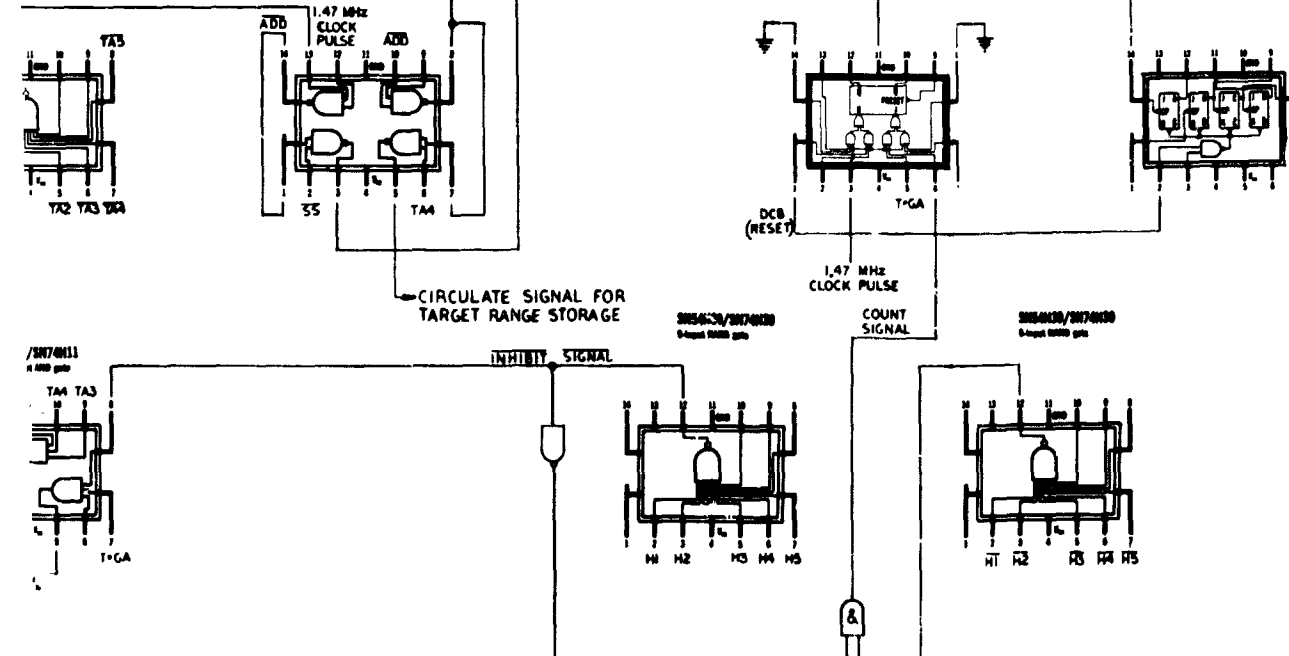
## HIT COUNTER

NO/SNT74030  
1999 gata

**325-4100/327-4100**  
**Quadruple 2-input NAND gate**

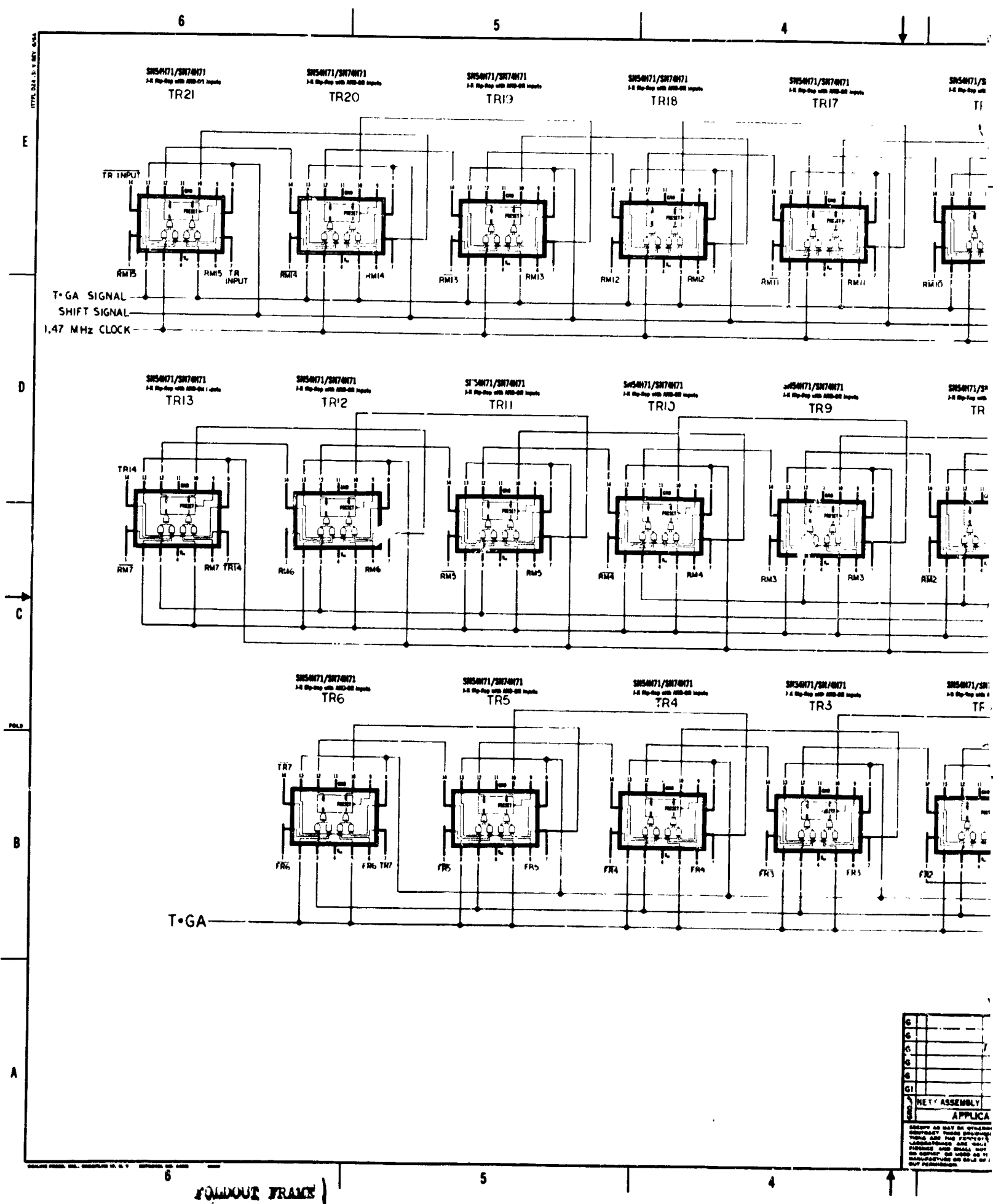
2025-01-17/2017-01-17  
I-1 Flip-flop with 2025-01-17 inputs  
H5

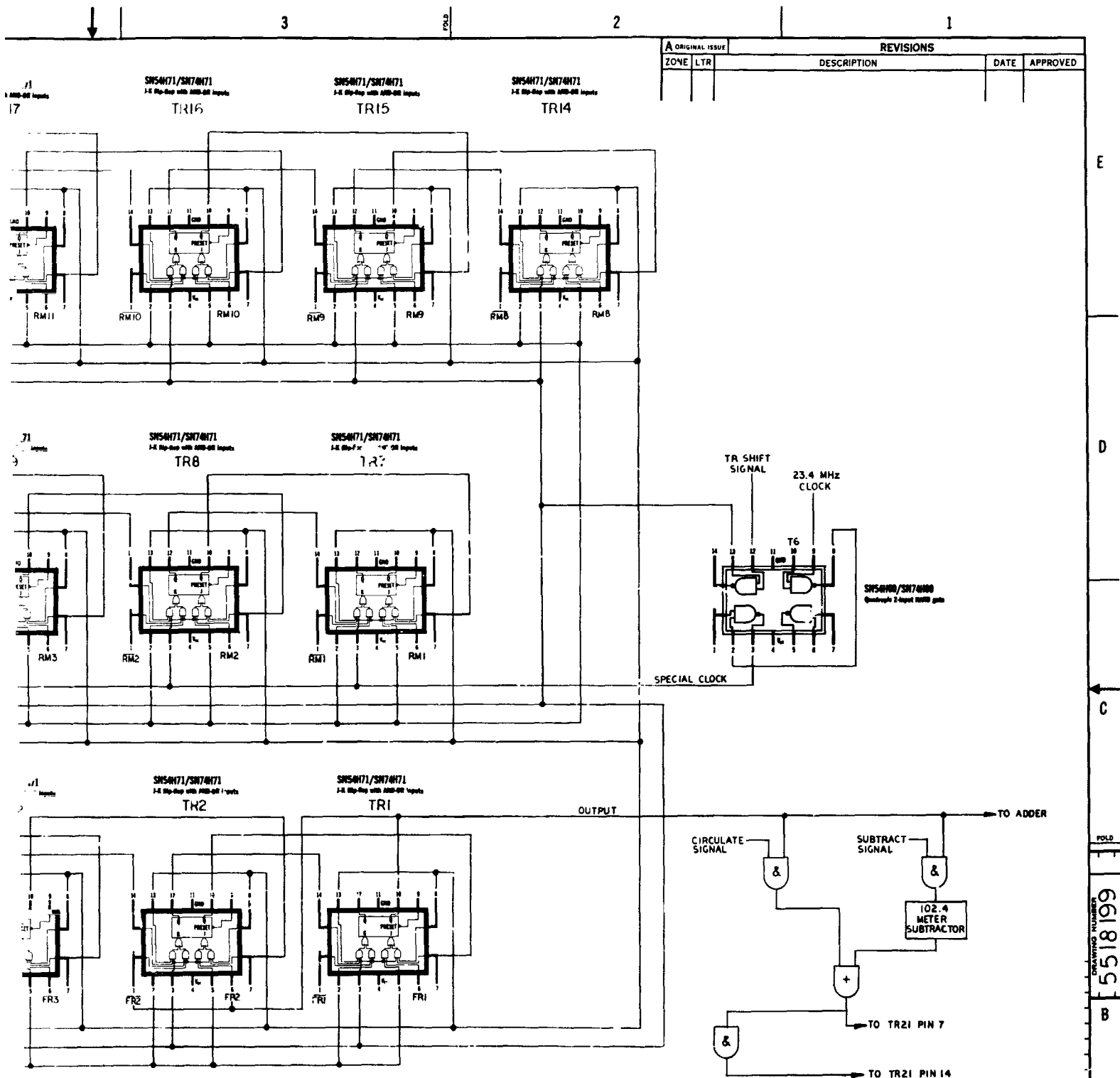
SN7403  
Four-bit binary counter  
H4 H3 H2 H1



		84		85	86	87	88	89	90	PART OR IDENTIFYING NO		NOMENCLATURE OR DESCRIPTION		HYPL SOURCE		
		QUANTITY PER GROUP		U	M	ITEM NO	ITEM	CODE								
LIST OF MATERIALS																
		MATERIAL		UNLESS OTHERWISE SPECIFIED DIMENSIONS ARE IN INCHES AND INCLUDE CHEMICALS APPLIED OR PLATED FINISHES				CONTRACT				<b>ITT Federal LABORATORIES</b> SAN FRANCISCO, CALIF., U.S.A. A DIVISION OF INTERNATIONAL T.E.L. PHONE AND TELEGRAPH CORPORATION				
				TOLERANCES				APPROVALS SIGNATURE & DATE				<b>DIAGRAM SCHEMATIC RANGE SMOOTHING LOGIC</b>				
								DRAWN <i>(Signature)</i> 6-21-63								
								CHECKED								
								MECH								
								ELECT								
												STDs				
												E OF M				
												HYPL SOURCE				
												SIZE CODE IDENT NO <b>D 90348 5518197</b>				
												SCALE				
												SHEET				

FOLDOUT FRAME 2





G6 G5 G4 G3 G2 G1		U	ITEM	CODE	PART OR	DESCRIPTION	ITFL
QUANTITY PER GROUP		OF	NO	IDENT	IDENTIFYING NO		SOURCE
LIST OF MATERIALS							
<b>TTT Federal Laboratories</b> SAN FERNANDO, CALIF. U.S.A. A DIVISION OF INTERNATIONAL TELEPHONE AND TELEGRAPH CORPORATION							
<b>DIAGRAM SCHEMATIC</b> <b>TARGET RANGE STORAGE</b>							
D		90348	5518199		SHEET		

FOLDOUT FRAME 2

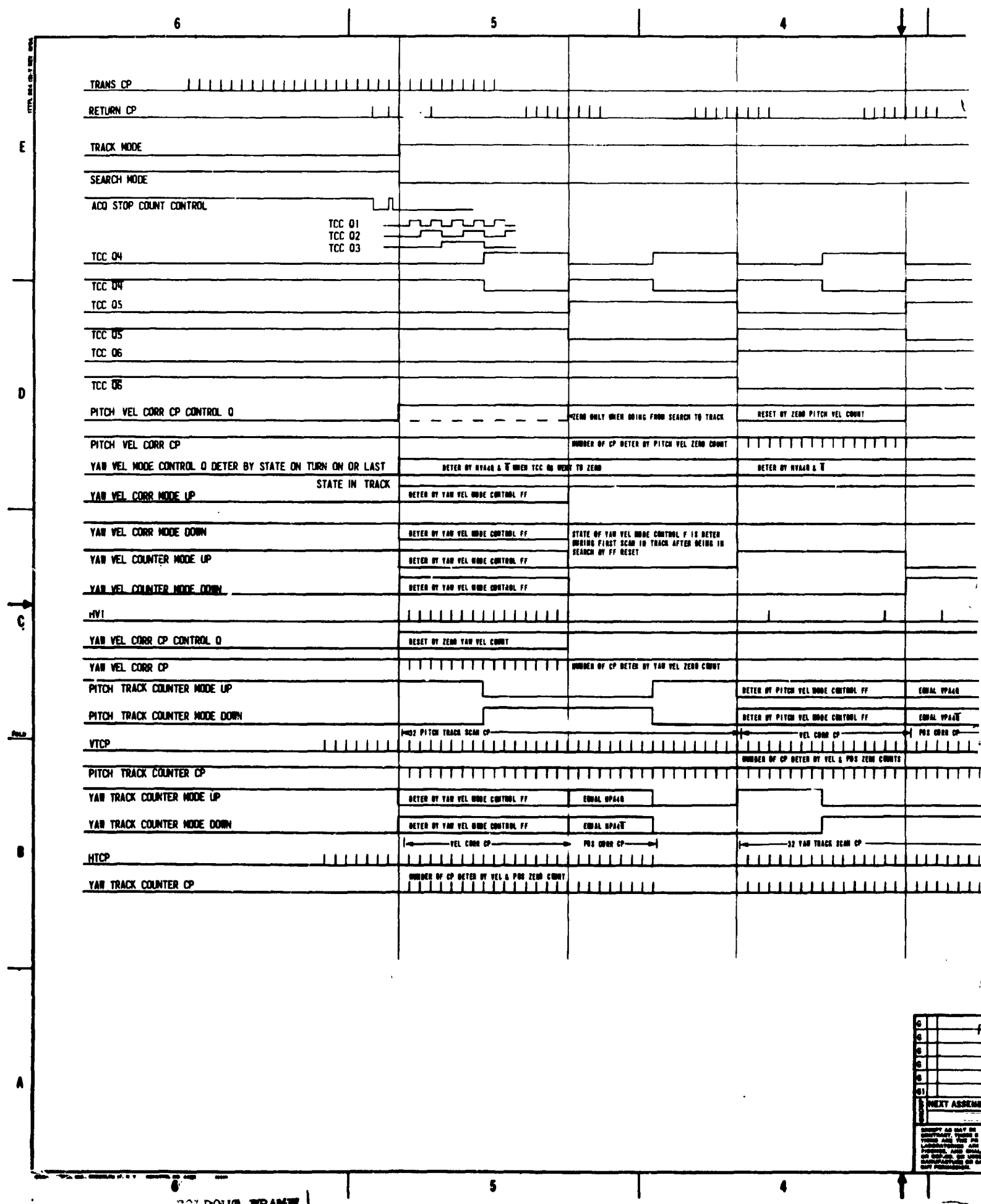


5518199  
DRAWING NUMBER  
POLY

3	U OF M CODE	1 PIECE 5 SET	6 PAIR 32 FEET	2	32 U.S. FLUID OZ. 64 U.S. LIQUID QT.	32 U.S. GAL. 60 LB. AVDP	2	1
---	----------------	------------------	-------------------	---	---	-----------------------------	---	---

NO 'DOUT TRAIN ?

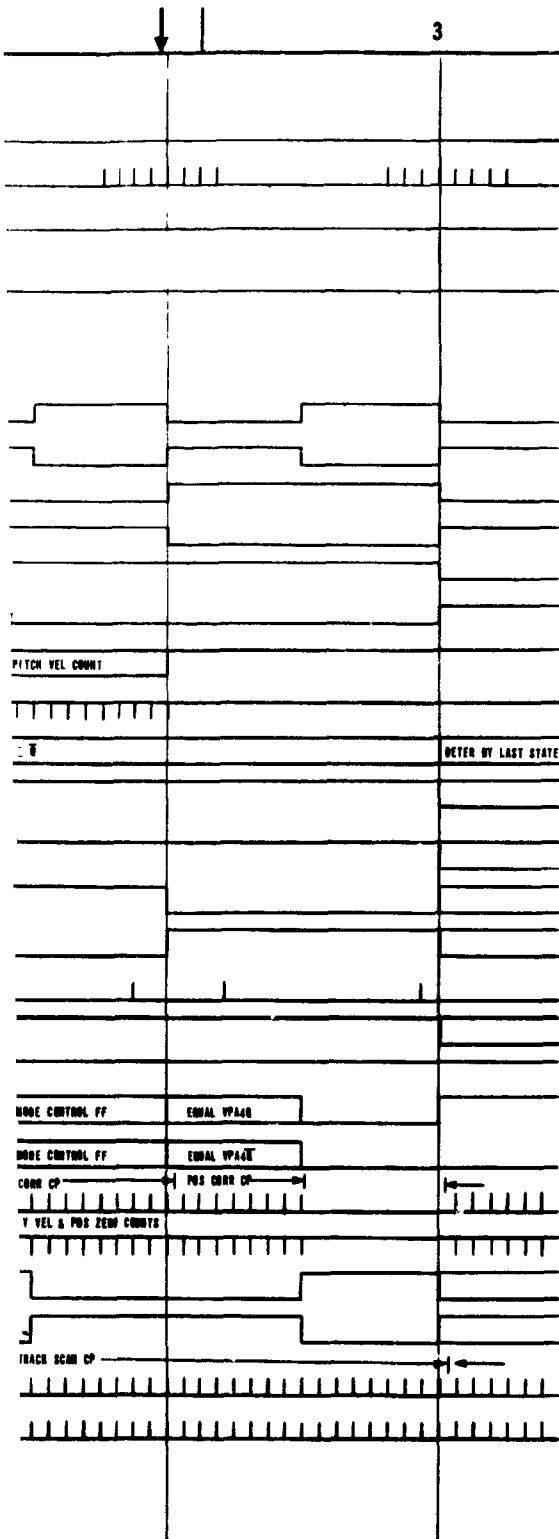




6	
6	
6	
6	
6	
61	

**NEXT ASSEMBLY**

**SHOOT AS MAY BE**  
**CONTRACT THREE**  
**THING ARE THE NO**  
**LABORERIES ARE**  
**PIPPERS AND SPALL**  
**OF THE AIR, THE**  
**MANUFACTURING OF**  
**OF THE**



ORIGINAL ISSUE		REVISIONS		
ZONE	LTR	DESCRIPTION	DATE	APPROVED

E  
D  
C  
5518199

60 61 62 63 64 65 66 67 68 69 70 71 72 73 74 75 76 77 78 79 80 81 82 83 84 85 86 87 88 89 90 91 92 93 94 95 96 97 98 99 100		QUANTITY PER GROUP		ITEM NO.	CODE IDENT	PART OR IDENTIFYING NO.	SIGNATURE OR DESCRIPTION	TYPE SOURCE
MATERIAL		UNLESS OTHERWISE SPECIFIED DIMENSIONS ARE IN INCHES AND INCLUDE DECIMALS APPLIED ON PLATED SURFACES		CONTRACT		TIT LABORATORIES SAN FRANCISCO, CALIF., U.S.A. A DIVISION OF INTERNATIONAL TELEPHONE AND TELEGRAPH CORPORATION		
FIN		TOLERANCES		APPROVALS SIGNATURE & DATE		P.D.S. CONTROL TIMING DIAGRAM		
NEXT ASSEMBLY USED ON APPLICATION		BASIC DIMENSION		DRAWN		D 90348 5518199		
IN PART NO. COL DET TES VENDOR ITEM; S.E. SOA CE CONTROL OR SPECIFICATION CONTROL DRAWING.		DECIMALS		CHECKED		SCALE		
		UNDER 6		ELECT		SHEET 3 of 3		
		6-24 INCL		TYPE				
		OVER 24		OTHER				
		ANGLES ± 1/2°						
		CONC. TOL. APPLY TO STOCK SIZES						
		SHOP PRACTICE (ENGINEERING STD MANUAL SECT 30) APPLIES						

## TABLE OF CONTENTS

<u>Section</u>	<u>Title</u>	<u>Page</u>
1.0	INTRODUCTION. . . . .	1-1
2.0	PROBLEM DEFINITION AND WORKING ASSUMPTION . . . . .	2-1
2.1	GENERAL RENDEZVOUS AND DOCKING PROBLEM . . . . .	2-1
2.2	VEHICLE ASSUMPTIONS . . . . .	2-2
3.0	BASELINE SYSTEM DESCRIPTION . . . . .	3-1
4.0	PERFORMANCE REQUIREMENTS AND SPECIFICATIONS. . . . .	4-1
5.0	TECHNICAL DISCUSSION OF THE BASELINE SYSTEM . . . . .	5-1
5.1	OPTICAL RADAR . . . . .	5-2
5.1.1	Laser and Driver Electronics . . . . .	5-2
5.1.2	Optics . . . . .	5-26
5.1.3	Range and Range Rate Subsystem (Timing and Data Processing). . . . .	5-30
5.1.4	Two-Axis Angle Tracker . . . . .	5-45
5.1.5	Mechanical . . . . .	5-53
5.2	BEACON/CORNER CUBE REFLECTOR/ ANGLE TRACKER . . . . .	5-57
5.2.1	Beacon . . . . .	5-57
5.2.2	Corner Cube Reflector . . . . .	5-58
5.2.3	Angle Tracker . . . . .	5-58
5.3	TWO AXIS GIMBAL AND SERVO CONTROL (TARGET AND CHASER). . . . .	5-60
5.3.1	Gimbal Specifications . . . . .	5-62
5.3.2	Servo Control System . . . . .	5-66
5.3.3	Angle, Angle Rate Sensing and Data Display. . . . .	5-80

## TABLE OF CONTENTS (Continued)

<u>Section</u>	<u>Title</u>	<u>Page</u>
5.4	THIRD AXIS ANGLE SENSOR (ROLL INDEXING FOR DOCKING) . . . . .	5-80
5.4.1	Performance Requirements . . . . .	5-80
5.4.2	Sensor Description . . . . .	5-82
5.4.3	Data Processing . . . . .	5-82
5.4.4	Mechanical Considerations . . . . .	5-85
5.5	COMMUNICATION SUBSYSTEM . . . . .	5-85
5.5.1	Performance Requirements . . . . .	5-85
5.5.2	Subsystem Description . . . . .	5-87
5.5.3	Data Processing . . . . .	5-89
5.5.4	Mechanical Considerations . . . . .	5-89
5.6	INTERFACE REQUIREMENTS . . . . .	5-89
5.6.1	Mechanical . . . . .	5-89
5.6.2	Electrical . . . . .	5-94
5.7	PARTS QUALIFICATION . . . . .	5-94
6.0	ALTERNATE CONFIGURATIONS . . . . .	6-1
7.0	CONCLUSIONS AND RECOMMENDATIONS . . . . .	7-1
APPENDIX A	RANGE AND RANGE RATE PERFORMANCE ANALYSIS . . . . .	A-1
APPENDIX B	ANGLE TRACKER ANALYSIS . . . . .	B-1
APPENDIX C	SENSOR PACKAGE THERMAL ANALYSIS . . . . .	C-1
APPENDIX D	LASER SAFETY ANALYSIS . . . . .	D-1
APPENDIX E	DETAILED GIMBAL CONSIDERATIONS . . . . .	E-1
APPENDIX F	LASER AND ANGLE TRACKER TESTS . . . . .	F-1

## LIST OF ILLUSTRATIONS

<u>Figure</u>	<u>Title</u>	<u>Page</u>
2-1	AAP Docking Cluster . . . . .	2-3
3-1	Baseline System Block Diagram . . . . .	3-2
3-2a	Block Diagram of Acquisition-Track Sequence . . . . .	3-5
3-2b	Block Diagram of Acquisition-Track Sequence . . . . .	3-6
5-1	Diffraction-Limited Gallium Arsenide Laser. . . . .	5-4
5-2	GaAs Laser Diode and Mounting . . . . .	5-6
5-3	Optical Resonator of the Diffraction-Limited GaAs Laser . . . . .	5-8
5-4	Contour of Dominant Mode in the Resonator Diffraction-Limited GaAs Laser. . . . .	5-18
5-5	Aberration in Unfolded Equivalent of Optical Resonator for Different Elevation Angles . . . . .	5-20
5-6	Transformation of Radiation from Diffraction Limited GaAs Laser in Y-Direction. . . . .	5-22
5-7	Laser Modulator Schematic . . . . .	5-25
5-8	Angenieux Lens MTF . . . . .	5-28
5-9	Range and Rate Unit Block Diagram . . . . .	5-31
5-10	Fine Range Stripline Logic . . . . .	5-34
5-11	Fine Range Timing Diagram . . . . .	5-35
5-12	Fine Range Logic. . . . .	5-36
5-13	Count Sequence . . . . .	5-38
5-14	Strip Delay Line Diagram . . . . .	5-39
5-15	Gate Feed Distribution Circuits . . . . .	5-41
5-16	Receiver Optics and Sensor . . . . .	5-47
5-17	Scan Pattern for Acquisition Mode (OGS Digital Tracker). . . . .	5-48
5-18	Scan Pattern for Track Mode (OGS Digital Tracker ). . . . .	5-48
5-19	Scan Pattern for Track Mode Detailed (OGS Digital Tracker). . . . .	5-50
5-20	Transmitter/Receiver Configuration . . . . .	5-54
5-21	Target Laser Beacon Schematic . . . . .	5-59
5-22	Limits for Performance, Rendezvous Radar Angular Coverage . . . . .	5-61
5-23	Two-Axis (X-Y) Gimbal. . . . .	5-63
5-24	Major Component Block Diagram . . . . .	5-69

## LIST OF ILLUSTRATIONS (Continued)

<u>Figure</u>	<u>Title</u>	<u>Page</u>
5-25	Tracker Block Diagram . . . . .	5-71
5-26	Tracker Servo Diagram . . . . .	5-74
5-27	Tracker Transfer Function and Bode Plot. . . . .	5-75
5-28	Total Loop Servo Diagram . . . . .	5-78
5-29	Nyquist Diagram of Open Loop Control System . . . . .	5-79
5-30	Hybrid Block Diagram of Control System . . . . .	5-81
5-31a	Roll Detector Outputs Versus Roll Position . . . . .	5-83
5-31b	Sum and Difference Channel Outputs Versus Roll Position . . . . .	5-83
5-32	Roll Detector Data Processing . . . . .	5-84
5-33	Typical Data Generated by Tracker for Transmission. . .	5-86
5-34	Schematic of Communication System Integrated with Tracker . . . . .	5-88
5-35	Data Processing System . . . . .	5-90
5-36	Sensor Package Mounted on X-Band Gimbals. . . . .	5-91
5-37	Sensor Package Mounted on OGS Gimbal. . . . .	5-93
6-1	Block Diagram of Alternate Configurations . . . . .	6-3

## LIST OF TABLES

<u>Table</u>	<u>Title</u>	<u>Page</u>
3-1	Baseline System Size-Weight-Power Estimates . . . . .	3-3
4-1	OGS System Requirements and Performance Characteristics . . . . .	4-2
4-2	OGS Subsystem Performance Specifications . . . . .	4-3
4-3	OGS Environmental Specifications . . . . .	4-4
5-1	Two-Axis Gimbal Performance Specifications . . . . .	5-64
5-2	Tracker Gain Units and Values . . . . .	5-73
5-3	Loop Gain Units and Values . . . . .	5-77
5-4	Decimal-Digital Representation of OGS Data . . . . .	5-95
6-1	Dynamic Range of OGS Data (at Chaser and Target for A, B, C and D Configurations) . . . . .	6-4

## 1.0 INTRODUCTION

A paper design of an Optical Guidance System (OGS) for rendezvous and docking, based on techniques and hardware components that are available now has been completed. The system was designed so that it could be used on any Apollo Applications Program mission with little or no modification. This paper design includes the design or technical specifications for all subsystems and a detailed performance analysis of the major system parameters. The OGS laboratory prototype (Contract NAS 8-11673, completed December, 1967 by ITT) was used as a design guideline. Due to significant hardware advances, since the completion of the OGS lab prototype, portions of two of the subsystems have been fabricated in order to assure that they could be incorporated in a near future flight system for AAP; the two are a digital angle tracker (including an image dissector) and a diffraction-limited GaAs laser transmitter.

Section 2.0 of this final report presents the general rendezvous and docking problem, and states problem definitions and working assumptions that are used for this design. Section 3.0 presents the various capabilities of the OGS, while outlining the baseline system. The baseline OGS includes all subsystems, thus providing the space vehicle with line-of-sight (LOS) range and range-rate, chaser pitch and yaw LOS angles and angle-rates, target pitch and yaw LOS angles and angle-rates, chaser-target relative roll angle (keying for docking), and also a low data rate two-way communications link. Section 4.0 presents the system performance requirements and specifications. Section 5.0 presents a detailed technical discussion of all the subsystems that make up the

baseline system. Included are detailed design parameters of the laser transmitter, receiver optics, receiver sensor, angle tracker electronics, range electronics, two-axis gimbals, etc. Requirements for interface with the space vehicles and a preliminary look at parts qualification are also presented in Section 5.0. Section 6.0 presents alternate system configurations and Section 7.0 presents ITT's conclusions and recommendations regarding a spaceborne system. Analysis of the expected system performance (i.e., maximum range, range accuracy, tracking rates, thermal, laser safety, etc.) is presented in the Appendix of the report.

One very significant subsystem that was not included in this OGS design was the newly developed piezoelectric beam steerers for scanning and pointing the laser transmitter. This has just recently been developed and tested on the Advanced OGS (Contract NAS 8-20833) and the use of this subsystem in future flight systems is discussed in the recommendations and conclusions section.



## 2.0 PROBLEM DEFINITION AND WORKING ASSUMPTIONS

### 2.1 GENERAL RENDEZVOUS AND DOCKING PROBLEM

Performance of rendezvous and docking requires knowledge of the relative positions and velocities of the spacecraft involved. Rendezvous and docking operations, manual or automatic, will be required in many of the future space missions. These missions will include assembly of large complexes in orbit, supply shuttles to large space stations, station-keeping of spacecraft in orbit, space rescue operations, orbital refueling, and a number of possible military operations.

Generally, a rendezvous and docking mission has a target vehicle in orbit with its orbital parameters known from ground tracking. The rendezvous vehicle (chaser) is launched into orbit, and when the relative range is short enough for the chaser vehicle on-board sensors to acquire target vehicle relative position and velocity data, thrusting is applied to cause the chaser vehicle to come within close proximity (1000 feet) of the target vehicle. A close proximity station-keeping mode can be used for final checkout prior to the docking stage. For docking, the target vehicle is maintained in a selected attitude and the chaser vehicle is piloted (manually or automatically) into the target docking adaptor at some small closing velocity.

The Optical Guidance System (OGS) addresses the problem of on-board sensors needed for in-flight acquisition and tracking from 120 km (75 miles) to final docking contact.

## 2.2 VEHICLE ASSUMPTIONS

The Optical Guidance System can generally be used on any two vehicles performing rendezvous and docking maneuvers, however, the application here is directed toward use on the Apollo Applications Program. The AAP Orbital Workshop (OWS) can be considered as the target vehicle and the Command Service Module (CSM) and the Lunar Module-Apollo Telescope Mount (LM-A) as the chaser vehicles. For convenience the LM-A has been chosen as the target vehicle, and docking port I of the Orbital Workshop's multiple docking adaptor (MDA) will be referenced as the docking port of the target vehicle. Figure 2-1 shows the AAP cluster of the Orbital Workshop, LM-A and CSM.

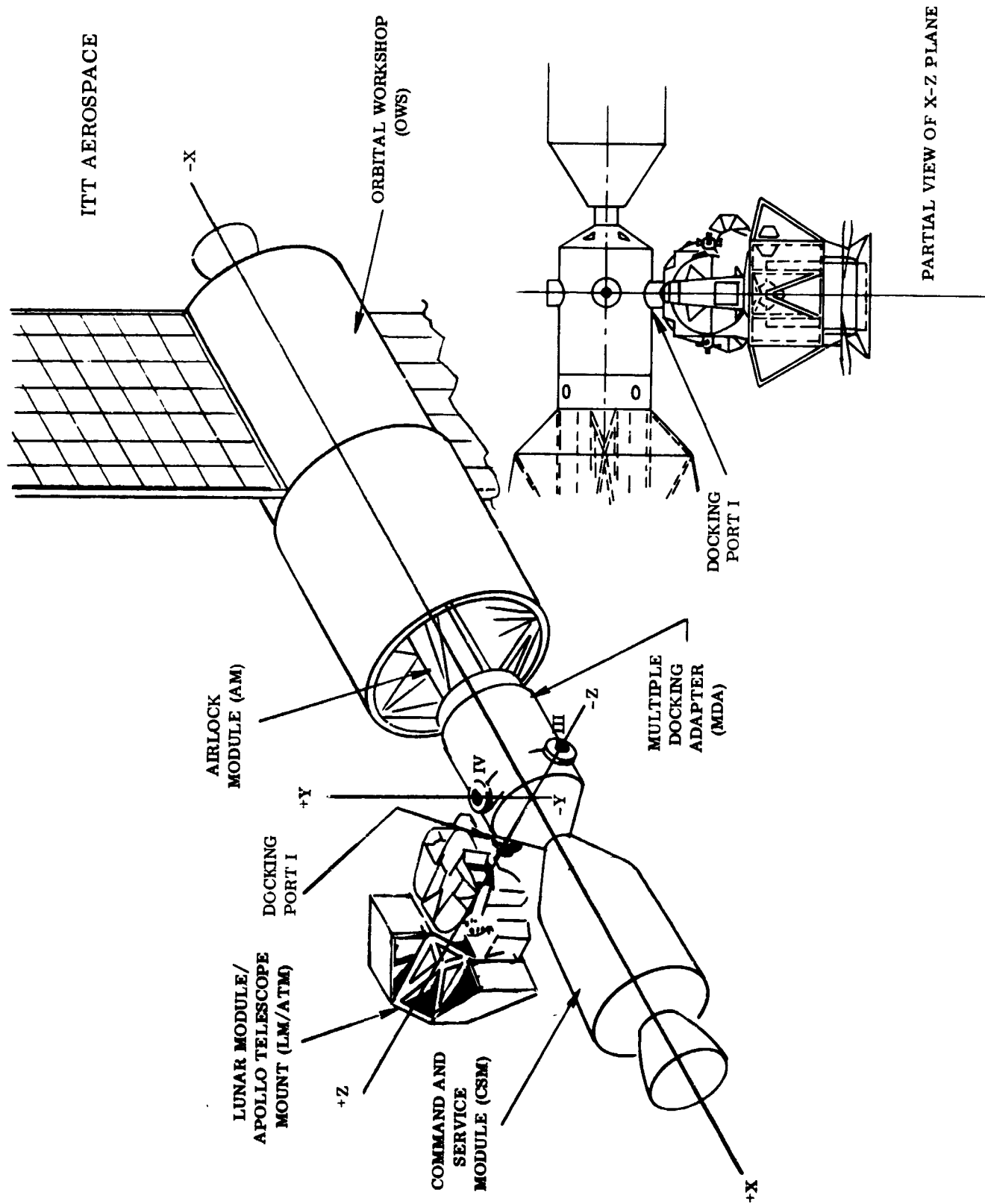


Figure 2-1. AAP Docking Cluster

### 3.0 BASELINE SYSTEM DESCRIPTION

The Optical Guidance System has the potential of performing many independent functions simultaneously (i. e., ranging, chaser and target angle tracking, relative roll index sensing, and two-way communications). This can be accomplished by integrating the various subsystems into one system. The "baseline system" referred to in this report will consist of all subsystems integrated together to form the full-blown Optical Guidance System.

The basic subsystems are:

- a. Optical Radar
- b. Beacon/Corner Reflector/Angle Tracker
- c. Two-Axis Gimbal and Servo Control
- d. Third-Axis Angle Sensor (Roll Indexing for Docking)
- e. Communications Subsystem
- f. Processing and Control Electronics Associated with the above.

The subsystems are shown in Baseline System Block Diagram in Figure 3-1. The integrated subsystems are arbitrarily located on the chaser and target vehicles as shown. The respective hardware for each vehicle could be interchanged, but for consistency it will not be interchanged for this report. Table 3-1 shows the size-weight-power estimates for the baseline system. System configurations other than the baseline system are presented and discussed in Section 6.0.

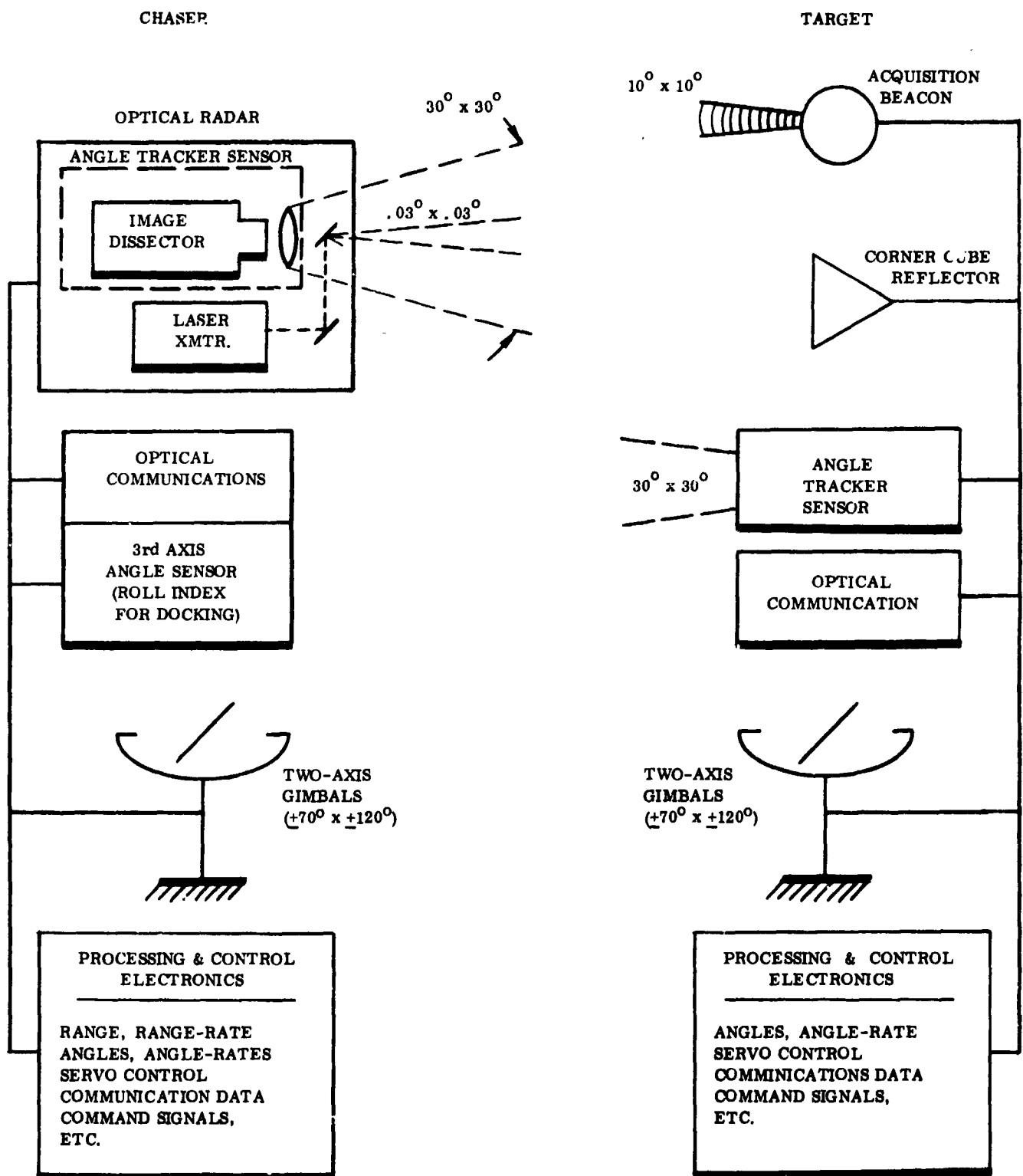


Figure 3-1. Baseline System Block Diagram

TABLE 3-1

## BASELINE SYSTEM SIZE-WEIGHT-POWER ESTIMATES

CHASER

	<u>Weight</u>	<u>Power</u>
Optical Radar	12#	12 W
Optical Communication	5#	5 W
Third-Axis Angle Sensor	2#	3 W
Payload Housing (Including misc. supports)	6#	-
Two-Axis Gimbal	20#	20 W
Electronics (Including display)	15#	17 W
	<hr/> 60#	<hr/> 47 W

TARGET

Beacon (On only during acquisition)	3#	50 W
Corner Cube	2#	-
Angle tracker	11#	11 W
Optical Communication	5#	5 W
Payload Housing (Including misc. supports)	6#	-
Two-Axis Gimbal	20#	20 W
Electronics (Including display)	12#	10 W
	<hr/> 59#	<hr/> 96 W

SIZE

Outline dimensions for the electro-optical payload mounted on the gimbals and for the electronics package external to the gimbals are approximately the same for both the chaser and target hardware. The size of the baseline OGS not including the gimbals, is approximately:

Electro-optical payload	7-1/2" dia. x 17" long (cylinder)
Electronics package	6" x 6" x 12"

A block diagram of the acquisition-track sequence is shown in Figures 3-2a and 3-2b. A sequence of operation for the baseline system is postulated as follows:

- When the chaser and target vehicles were within 120 km (75 miles) of each other the target acquisition beacon would be turned on and the chaser angle tracker sensor would start its "acquisition" scan. Initially, the target vehicle would have to point toward the chaser to within  $\pm 5^\circ$  (for  $10^\circ$  laser beacon) or it would have to tell the OGS where the chaser was to within  $\pm 5^\circ$  so the OGS could slew its two-axis gimbals toward the chaser to within  $\pm 5^\circ$ . Also, the chaser vehicle would have to point toward the target to within  $\pm 15^\circ$  initially ( $30^\circ \times 30^\circ$  electro-optical scan field) or it would have to tell the OGS where the target was to within  $\pm 15^\circ$  so the OGS could slew its two-axis gimbals toward the target to within  $\pm 15^\circ$ .
- The chaser angle tracker sensor scans a  $30^\circ \times 30^\circ$  field by looking at only a  $.03^\circ \times .03^\circ$  field-of-view (FOV) at one instant in time. The  $.03^\circ \times .03^\circ$  instantaneous FOV is stepped through the  $30^\circ \times 30^\circ$  field until the target acquisition beacon is located. For a 1 kHz scan rate it would take 1000 seconds (16.6 minutes) to completely scan the  $30^\circ \times 30^\circ$  field.
- After the chaser has located the target beacon to within a  $.03^\circ \times .03^\circ$  element in its acquisition an the chaser angle tracker sensor is switched to a "track" mode of operation. The track mode effectively dithers the  $.03^\circ \times .03^\circ$  instantaneous FOV around the position of target beacon thus enabling angle error signals to be generated so that the position and velocity information can be constantly updated for a moving target. The tracking is then performed via a closed-loop electro-optical-mechanical servo system.

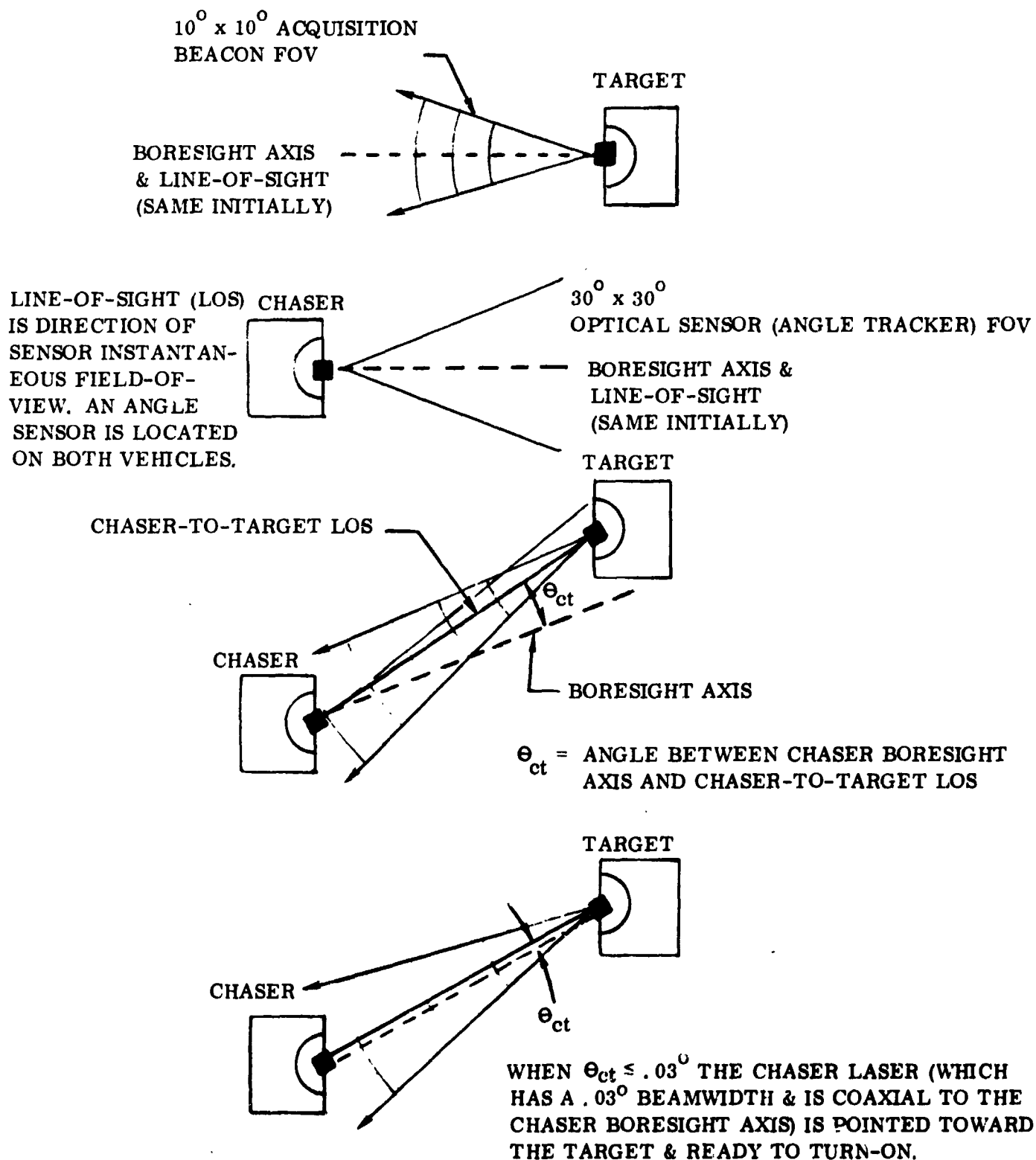


Figure 3-2a. Block Diagram of Acquisition-Track Sequence



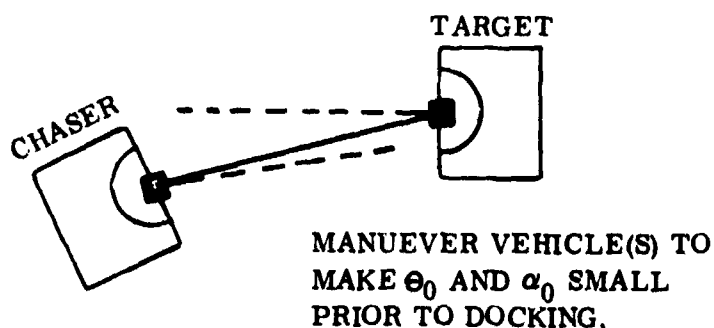
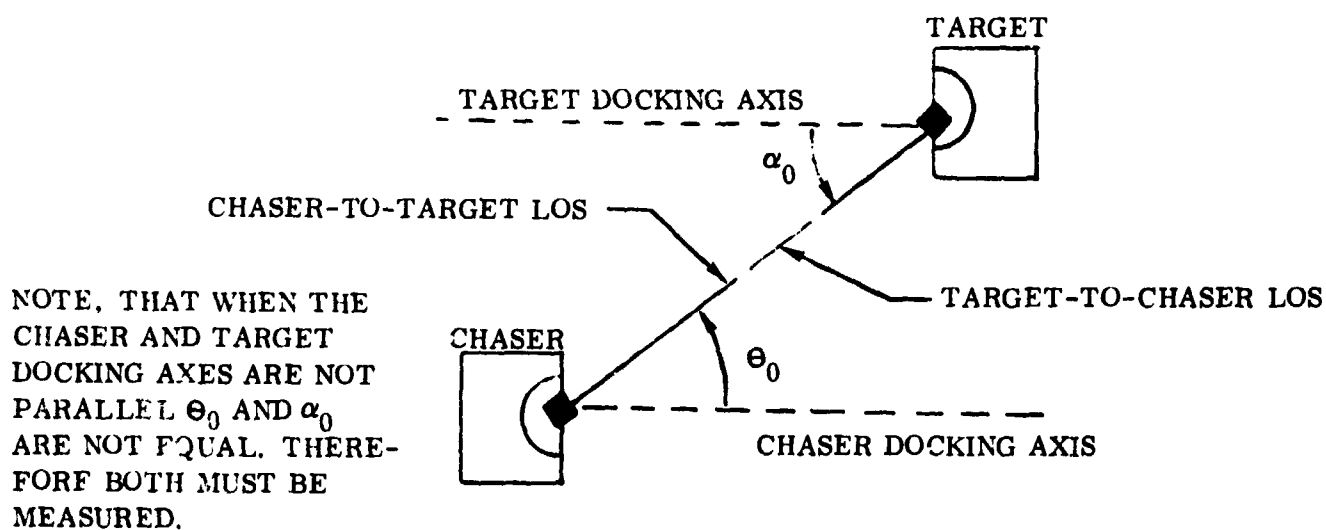
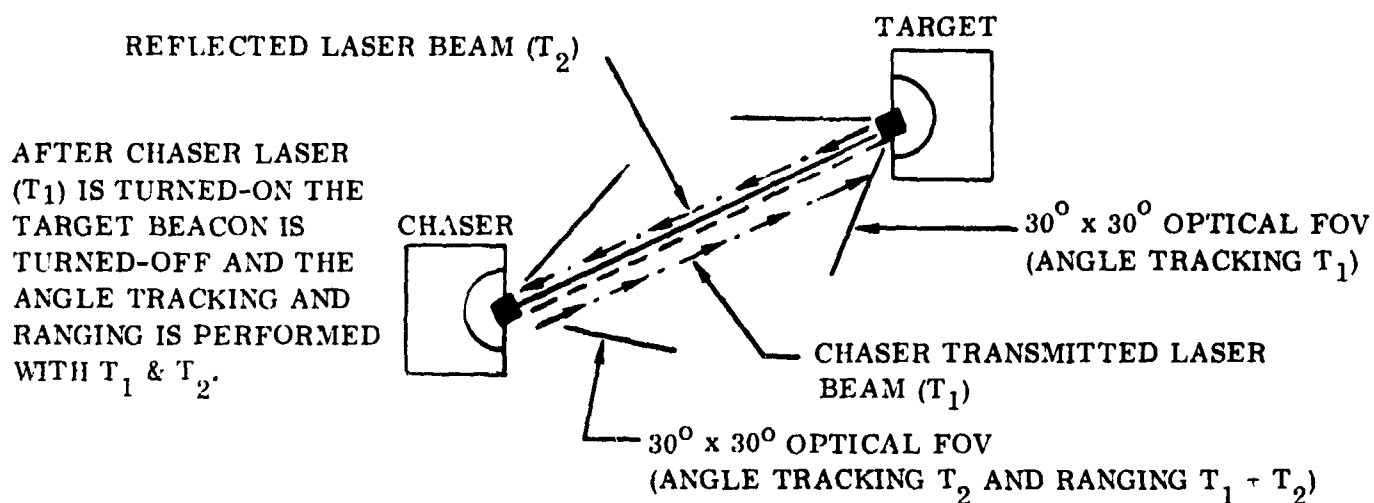


Figure 3-2b. Block Diagram of Acquisition-Track Sequence

- After the chaser angle tracker has been switched to the "track" mode, the chaser two-axis gimbals (on which the angle tracker is mounted) are slewed such that the angle tracker and gimbal bore-sight axes are nulled.
- After the chaser angle tracker and gimbals are nulled to within  $.03^\circ$ , the chaser laser transmitter is turned on. This laser has a  $.03^\circ \times .03^\circ$  beamwidth and will therefore be directed precisely at the target vehicle. The chaser laser beam will be reflected off the target vehicle by the corner cube reflectors and be returned to the chaser. The chaser now can track the target vehicle via its own two-way transmission beam and does not need the target laser beacon to maintain track. The target beacon is turned off automatically when the chaser laser beam is recognized by the angle tracker sensor mounted on the target vehicle.
- The target angle tracker and gimbal now senses and tracks the chaser vehicle similarly to the manner in which the chaser originally tracked the target beacon. Target and chaser line-of-sight (LOS) angles and angle-rates are now available on each respective vehicle.
- The chaser laser also uses its two-way transmission beam to measure the line-of-sight range between the two vehicles. Range rate is also obtained by differentiation of successive range readings.
- The third-axis angle which is essentially a roll-indexing angle is sensed at short ranges (<1000 feet). This roll-indexing angle is only needed for docking.
- The following relative position and velocity data is available at each respective vehicle:

<u>CHASER</u>	<u>TARGET</u>
Line-of-sight angles to target ( $\theta_x, \theta_y$ ).	Line-of-sight angle to chaser ( $\alpha_x, \alpha_y$ ).
LOS angle-rates wrt target ( $\dot{\theta}_x, \dot{\theta}_y$ )	LOS angle-rates wrt chaser ( $\dot{\alpha}_x, \dot{\alpha}_y$ )
LOS range (R) between chaser-target	
LOS range-rate ( $\dot{R}$ ) between chaser-target	
3rd axis angle ( $\phi$ )	
relative roll index between chaser-target	

- In order to have "all" the position and velocity data at one vehicle, it becomes necessary to telemeter the information from one vehicle to the other. A low data-rate (<9,000 bits/sec) telemetry link can be made available by using a PCM optical communication subsystem integrated into the Optical Guidance System. Only a small portion of this would be necessary to transmit the OGS data from chaser-to-target or vice versa. Commands and other information could also be transmitted on this communication link.

#### 4.0 PERFORMANCE REQUIREMENTS AND SPECIFICATIONS

A laboratory prototype of the "Optical Guidance System for Rendezvous and Docking" was designed, developed and tested by ITTA for NASA/MSFC from April 1964 to December 1967. This work was performed on Contract NAS8-11673. The performance specifications generated by NASA/MSFC for the laboratory prototype were used as guidelines for the generation of the performance requirements for the paper design of the OGS reported here (Contract NAS8-20717). A list of OGS system requirements for rendezvous and docking have been generated and are shown in Table 4-1. Also shown in Table 4-1 are the expected performance characteristics of the OGS. The basic performance specifications of the baseline subsystems are shown in Table 4-2.

A formalized set of environmental specifications for equipment to be used on AAP missions has not been generated. Therefore, ITTA has generated a set of environmental specifications for the Optical Guidance System based on various data collected from NASA, Martin-Marietta, Grumman, RCA, and McDonnell-Douglas. Table 4-3 shows the OGS environmental spec for all OGS equipment mounted outside the spacecraft. Electronics located inside the spacecraft should have a considerably easier environment especially with respect to temperature.

TABLE 4-1

## OGS SYSTEM REQUIREMENTS &amp; PERFORMANCE CHARACTERISTICS

<u>Parameter</u>	<u>Requirement</u>	<u>Performance Characteristic</u>
Maximum Range	120 km (75 mi)	120 km (75 mi)
Minimum Range	0 (dock)	0 (dock)
Range Accuracy		
(for $R > 3 \text{ km}$ )	$\pm .5\%$	$\pm .05\%$
(for $R < 3 \text{ km}$ )	$\pm 10 \text{ cm}$	$\pm 10 \text{ cm}$
Maximum Range-rate	150 m/sec	$\approx 10,000 \text{ m/sec}$
Minimum Range-rate	0	0
Range-rate Accuracy		
(for long range)	$\pm 1 \text{ m/sec}$	$\pm 1 \text{ m/sec}$
(for docking)	$\pm .03 \text{ m/sec}$	$\pm .03 \text{ m/sec}$
Total Angle Coverage		
(two-axis gimba's)	$\pm 70^\circ \times \pm 120^\circ$	$\pm 70^\circ \times \pm 120^\circ$
Line-of-Sight Angle Accuracy	$\pm .1^\circ$	$\pm .0^\circ$
LOS Angle-rate Accuracy	$\pm .003^\circ/\text{sec}$	$\pm .003^\circ/\text{sec}$

TABLE 4-2  
OGS SUBSYSTEM PERFORMANCE SPECIFICATIONS

1. OPTICAL RADAR (CHASER)

Ranging

Max Range	120 km (75 mi)
Min Range	0 (dock)
Range Accuracy (for $R > 3$ km)	$\pm .05\%$
(for $R < 3$ km)	$\pm 10$ cm
Max Range-rate	$\approx 10,000$ m/sec
Min Range-rate	0
Range-rate accuracy (long range)	$\pm 1$ m/sec
(docking)	$\pm .03$ m/sec

Angle Tracking

Sensor Total FOV	$30^\circ \times 30^\circ$
Sensor instantaneous FOV	$.03^\circ \times .03^\circ$
Laser transmitter beamwidth	$.03^\circ \times .03^\circ$
Max. Acquis. & Tracking range	120 km (75 mi)
LOS Angle accuracy	$< \pm .01^\circ$
LOS Angle-rate accuracy	$< \pm .003^\circ/\text{sec}$

2. BEACON/CORNER REFLECTOR/ANGLE TRACKER (TARGET)

Acquisition Beacon

Max. acquisition range	120 km (75 mi)
Transmitted beamwidth	$10^\circ \times 10^\circ$

Corner Cube Reflector

Retro-directiveness	$\pm 1$ arc sec.
---------------------	------------------

Angle Tracker

Same as for "Angle tracking" in Optical Radar listed above.

3. TWO AXIS GIMBAL AND SERVO CONTROL (CHASER & TARGET)

Total Angle coverage	$\pm 70^\circ \times \pm 120^\circ$
LOS Angle accuracy	$< \pm .01$
LOS Angle - rate accuracy	$< \pm .003^\circ/\text{sec}$

4. THIRD AXIS ANGLE SENSOR (ROLL INDEXING FOR DOCKING)

Angle coverage	$0 \pm 40^\circ$
Angle accuracy	$\pm 1^\circ$
Max. Range	1000 ft.

5. OPTICAL COMMUNICATIONS SUBSYSTEM

Data-rate	$\approx 9,000$ bits/sec.
-----------	---------------------------

TABLE 4-3

OGS ENVIRONMENTAL SPECIFICATIONS

LAUNCH AND ASCENT:

Temperature:	15.5°C to 21.5°C
Humidity:	0 to 95%
Pressure (mm.Hg):	1080.6 to 264 in 80 sec.
Acceleration (G):	7.0 Flight Axis 3.0 Lateral Axis
Vibration:	All axes - (20-2000 Hz at 1 octave/minute) 20 - 50 Hz @ 0.5 mm D.A. 50 - 2000 Hz @ 2.4 g's peak
Shock:	50G

STORAGE:

Temperature:	-40°C to +71°C
Humidity:	0 to 100%
Pressure (mm Hg):	86.9 to 1080.6
Acceleration (G):	4.0 fore and aft 3.0 lateral
Vibration:	12.7 mm. D.A. - 5-19 Hz 10G - 20-200 Hz Sine, all axes
Shock:	20G - MIL-STD-810 Method 516
Contaminants:	MSFC-SPEC-164, MSFC-PROC-151 and MSFC-PROC-166

OPERATIONAL:

Temperature:	-108°C to 126.6°C
Pressure (mm. Hg):	10 <sup>-8</sup>
Shock & Vibration:	Not Applicable

NOTE: This spec is for all OGS equipment mounted outside the spacecraft.

## 5.0 TECHNICAL DISCUSSION OF THE BASELINE SYSTEM

The technical discussion of the baseline Optical Guidance System is broken down into the following sub-sections:

- 5.1 Optical Radar
- 5.2 Beacon/Corner Cube Reflector/Angle Tracker
- 5.3 Two-Axis Gimbal and Servo Control
- 5.4 Third Axis Angle Sensor (Roll Indexing for Docking)
- 5.5 Communication Subsystem
- 5.6 Interface Requirements
- 5.7 Parts Qualification

At the request of NASA/MSFC, certain areas have been concentrated on more heavily than others. Some components of the various subsystems have had a technical specification generated while others have been actually designed. Two particular components of the Optical Radar subsystem were considered to be critical portions of a future flight prototype system. It was decided, therefore, to fabricate these units. These units are the diffraction-limited GaAs laser (including the driver electronics) and the angle tracker (including the image dissector). The design of these units is described in Section 5.1, and some of the test results obtained after they were built are reported in Appendix F.

A preliminary design of the Third Axis Sensor and the Communications Subsystem was performed to show their general feasibility and how they could be integrated into the Optical Guidance System.



## 5.1 OPTICAL RADAR

### 5.1.1 Laser and Driver Electronics

#### 5.1.1.1 Diffraction-Limited GaAs Laser

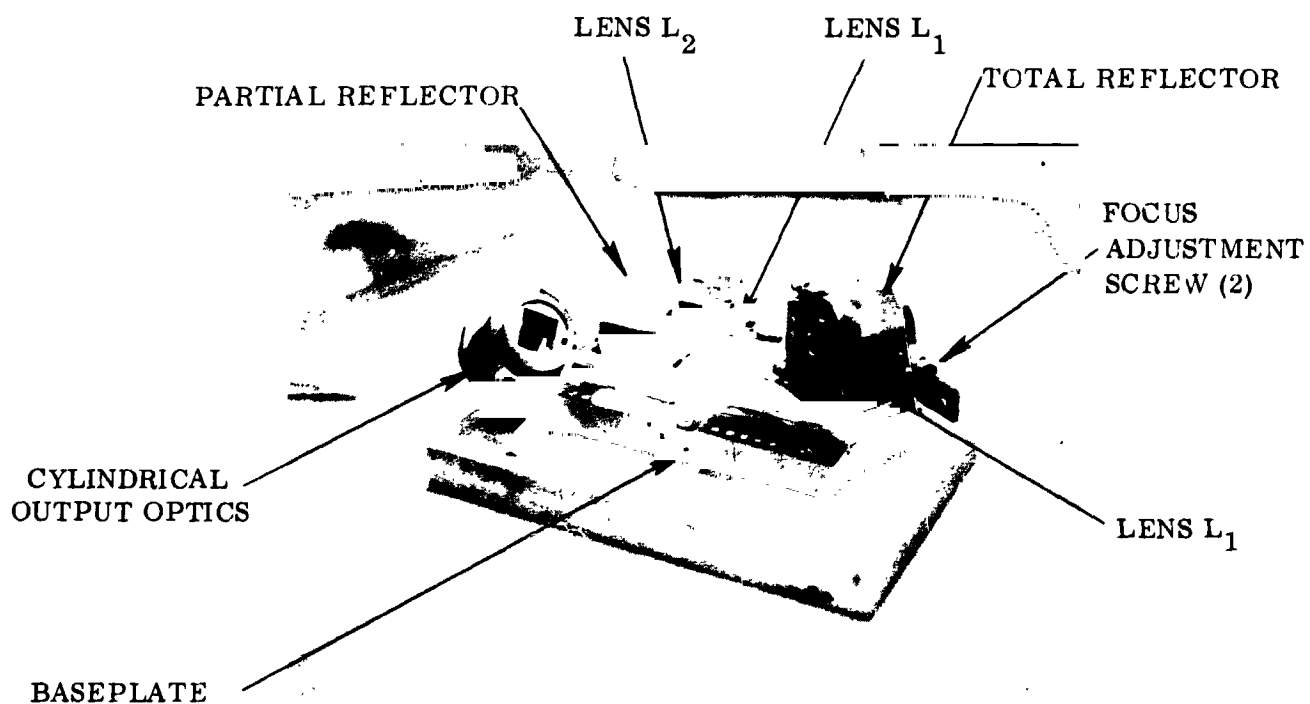
The narrow beam laser used in the chaser transmitter will be a diffraction-limited gallium arsenide (GaAs) laser. The particular laser used here by the OGS is referred to as a "diffraction-limited" GaAs laser because of its output beam characteristics. The smallest possible cone angle for a given beam diameter at its source is called the "diffraction-limited beam angle," which is proportional to the wavelength to source beam diameter ratio. The GaAs laser normally does not radiate with a diffraction-limited beam angle. It was only recently (1968) that IBM's Thomas Watson Research Center developed the first GaAs laser that radiated with a diffraction-limited beam angle. Until that time, all GaAs lasers radiated with a relatively large beam angle ( $\approx 20$  degree). The theoretical diffraction-limited beam angle of a GaAs laser can be as small as 0.2 degree for a typical size laser diode. The laser output will be pulsed, with the pulse repetition rate being 1-10 kHz. A 5-watt radiating peak output power is needed to obtain 120 km (75 mi) ranging. The transmitted wavelength ( $\lambda$ ) is approximately 9,000 Å.

The diffraction-limited GaAs laser consists mainly of a solid-state GaAs p-n junction diode and an optical resonator made of lenses and reflectors. The solid-state diode is placed inside the optical resonator in order to select the lowest order, or fundamental, traverse radiating mode (the diffraction-limited mode). The mechanism that induces lasing is the same as that used for a regular injection laser diode. Current is passed through the diode and light is emitted at the p-n junction. The amount and general characteristics of the light emitted are primarily a function of the input current, operating temperature, diode material, size of the diode, and the quality of the diode.

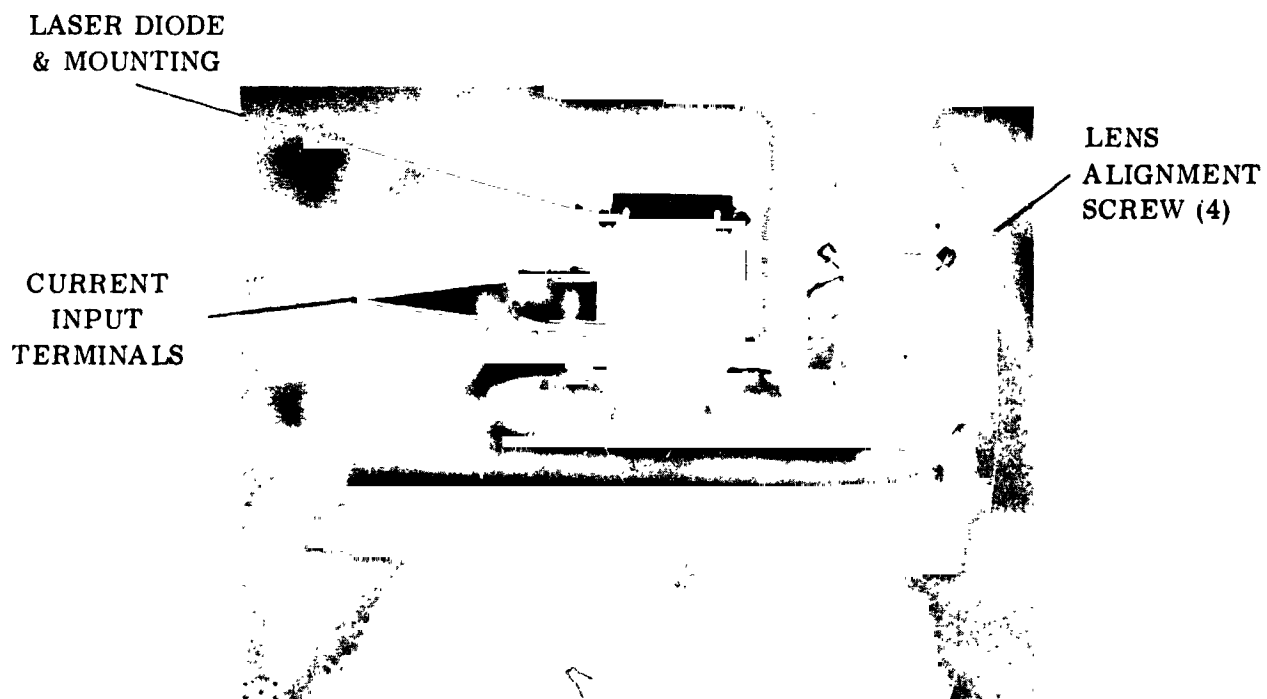
The laser diode is boresighted and aligned inside an optical resonator. A GaAs laser diode operated by itself (not in an external cavity) will radiate in many transverse modes. The beam divergence for multi-mode operation is relatively large ( $\approx 20$  degree for 60 percent of radiated power). Minimum beam divergence is of primary concern for the Optical Guidance System, therefore it is very beneficial to operate the GaAs laser in the single fundamental mode (the diffraction-limited mode). In laboratory tests, 50 percent of the radiated power in a .3 degree by .3 degree beamwidth was obtained from the output of the GaAs laser operated in the diffraction-limited mode. (Small cylindrical optics at the output of the diffraction-limited GaAs laser transformed the normal rectangular shaped beam to a square beam,)

A prototype diffraction-limited GaAs laser has been built and tested. Figure 5-1 shows two different pictures of the laser taken when the laser was partially disassembled. Detailed test results are reported in Appendix F. A summary of the performance characteristics of the prototype laser operated at room temperature are shown below:

- Peak radiated power ( $P_t$ )  
(at 100 A peak current input) 2 watts
- Max. duty cycle .001  
250 ns current pulse width  
4 kHz rep-rate
- Threshold peak current 50 amps
- Electrical-to-optical efficiency .5%
- Spectral output  $9050 \text{ \AA} \pm 30 \text{ \AA}$
- Output beamwidth at  $L_2^*$   $.3^\circ \times .3^\circ$
- Exit aperture at  $L_2^*$  1.5 mm x 1.5 mm  
 $^* L_2$  output lens of cylindrical output optics



NOTE: LASER WEIGHT INCLUDING BASEPLATE IS 0.89 KG (2.0 LBS)



ITT69/0392

Figure 5-1. Diffraction-Limited Gallium Arsenide Laser

Five watts peak radiated power is needed to obtain 120 km (75 miles) ranging. Five watts should be obtainable in the near future with the laser. The following sub-section is a technical discussion of the diffraction-limited GaAs laser developed for ITT's Optical Guidance System. This laser was developed by IBM's Thomas Watson Research Center by Dr. E. M. Rutz and H. D. Edmonds.

#### 5. 1. 1. 1. 1 Design Considerations

For diffraction limited radiation, a GaAs laser diode is placed in an external optical resonator. The GaAs laser diodes are diffused p-n junction diodes approximately  $15 \times 10^{-3}$  inches long and  $10 \times 10^{-3}$  inches wide. The two parallel faces of the diode which are cleaved, have anti-reflecting coatings in order to reduce losses in the laser cavity.

The IBM laser diodes are presently fabricated by a zinc diffusion process. Slices of {100} orientation are sawed from Bridgeman grown, n-type GaAs ingots and doped with tin in the range of  $1$  to  $3 \times 10^{18}$  atoms/cm<sup>3</sup>. Before diffusion, slices are chemically polished on one face and sealed with 5 to 10 mg of ZnAs<sub>2</sub> in a silica ampoule (hermetically sealed vessel) of about 7 cm<sup>3</sup> volume. The ampoule is then kept at 750 degree Centigrade for 16 hours followed by 850 degree Centigrade for 1.25 hours. The ampoule is then quickly cooled by placing it immediately on a transit bench top. When the diffusion is carried out at a single temperature (i. e. , 750 degree Centigrade) the resulting lasers have relatively long delay times at room temperature operation. After the diffusion, ohmic contacts are formed by plating thin layers of gold, tin, and indium on the slice. The slice is then cleaved into bars and sawed into the individual laser diodes. The laser diodes are mounted on a heat sink. Both the laser diode and the mount are plated with indium and the contact is made by cold-welding. The mount is flared at the ends in order to provide less obstruction to the light, and to provide more uniform pressure on the diode to minimize cracking problems. Figure 5-2 is a pictorial drawing of the laser diode and its heat sink mounting.

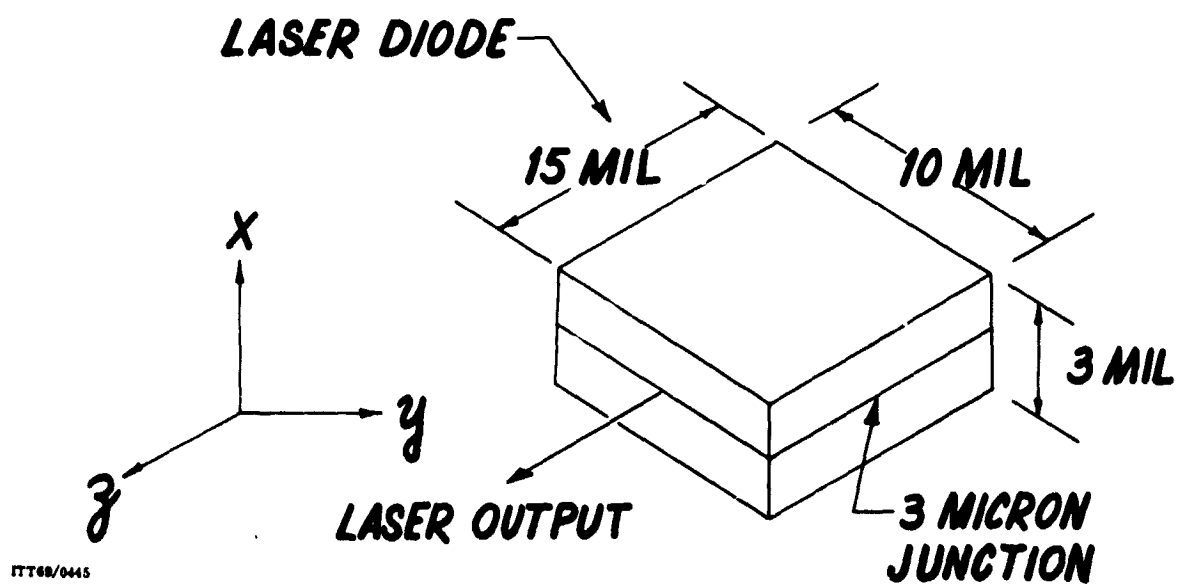
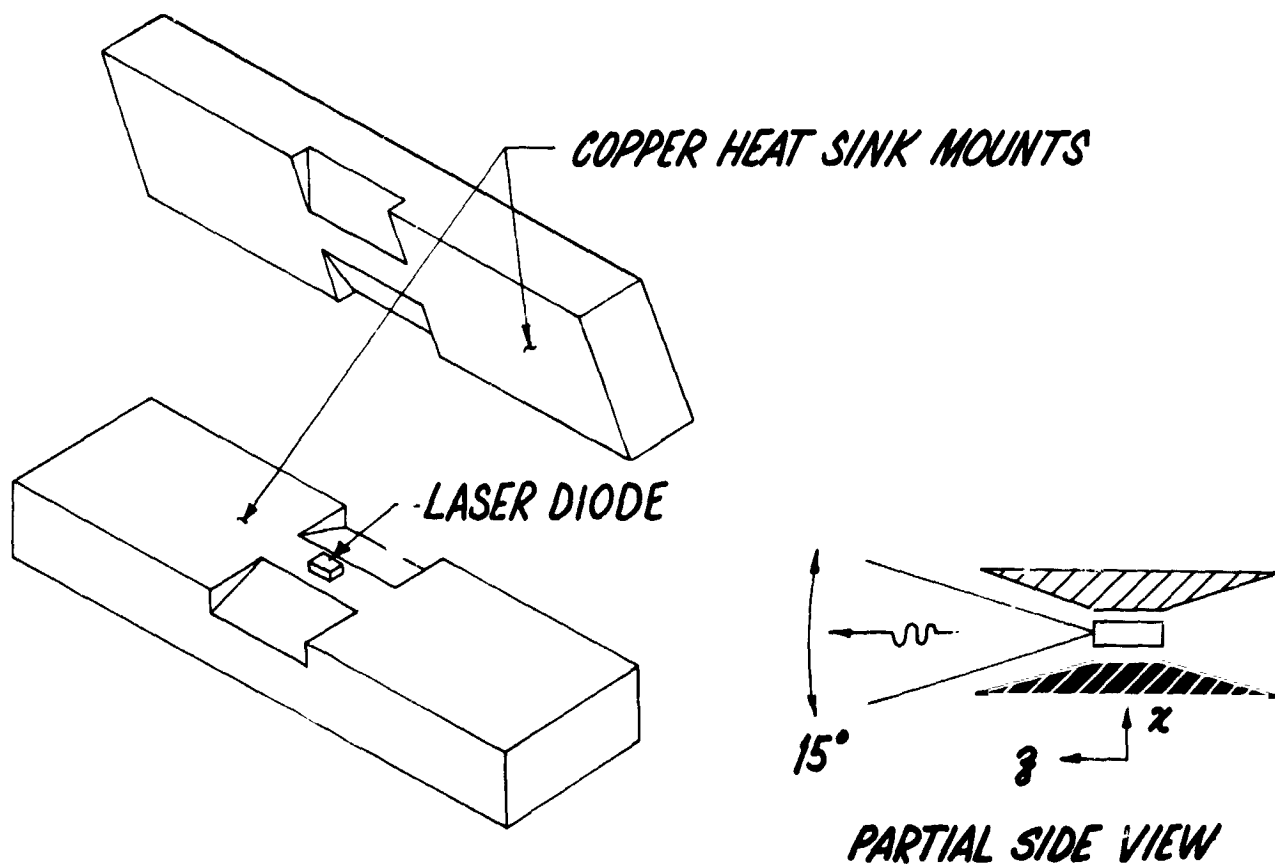


Figure 5-2. GaAs Laser Diode and Mounting

The external optical resonator, which can set up a self-reproducing field for the radiation from the asymmetrical GaAs laser diode, is built of spherical lenses and plane mirrors (Figure 5-3). To make the alignment of the optical resonator simple and to avoid critical dimensions, no mode-selecting aperture was included. Instead, the lowest order transverse mode is selected by properties of the GaAs laser diode and its optical resonator.

For the design of the spherical resonator for the GaAs laser, only the transformation of the radiation from the narrow dimension ( $2w_x$ ) of the laser diode through the internal focusing elements can be described in terms of Fraunhofer diffraction. The transformation of the waves from the wide dimension ( $2w_y$ ), must be described in terms of Fresnel diffraction. In effect, the transformation of a Gaussian beam through lenses is different in the Fraunhofer and Fresnel regions because of the approximations made in calculating Fraunhofer diffraction.

The design objective for the optical resonator is to set up a self-reproducing field pattern. To obtain the design parameters which meet this objective for the GaAs laser resonator, one can not make the assumption of uniformity of mode structure which is made in general resonator analysis. For the GaAs laser with external resonator, there is a change of mode configuration from a dielectric surface wave mode, guided by the p-region of the p-n junction in the GaAs diode, to the  $TEM_{0,0}$ -mode in the external resonator.

Instead, to derive the resonator parameters for the GaAs laser, IBM traced the transformation of the radiation from the laser diode through the unfolded equivalent of the optical resonator. For the x-direction, where the lasing junction is only a few wavelengths high, it is observed that the diverging phasefront is transformed by the first lens to a plane phasefront when the radiating aperture of the laser diode is at the focal point of the lens. In the second lens of the unfolded equivalent of the optical resonator the plane phasefront is transformed into a circular phasefront, which converges toward the focal point of

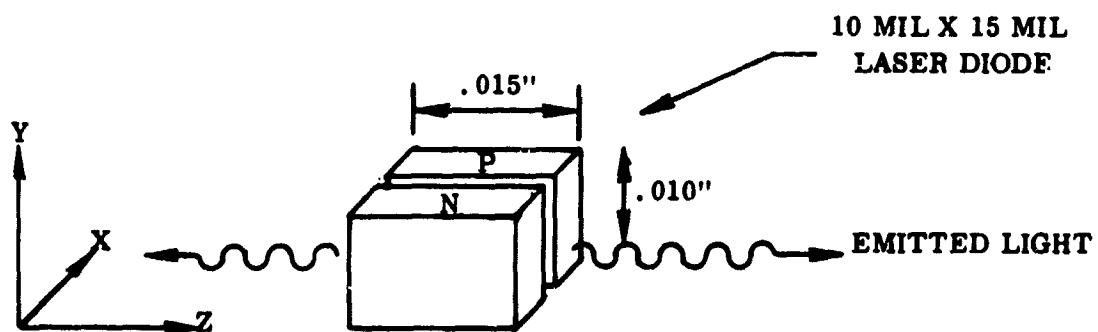
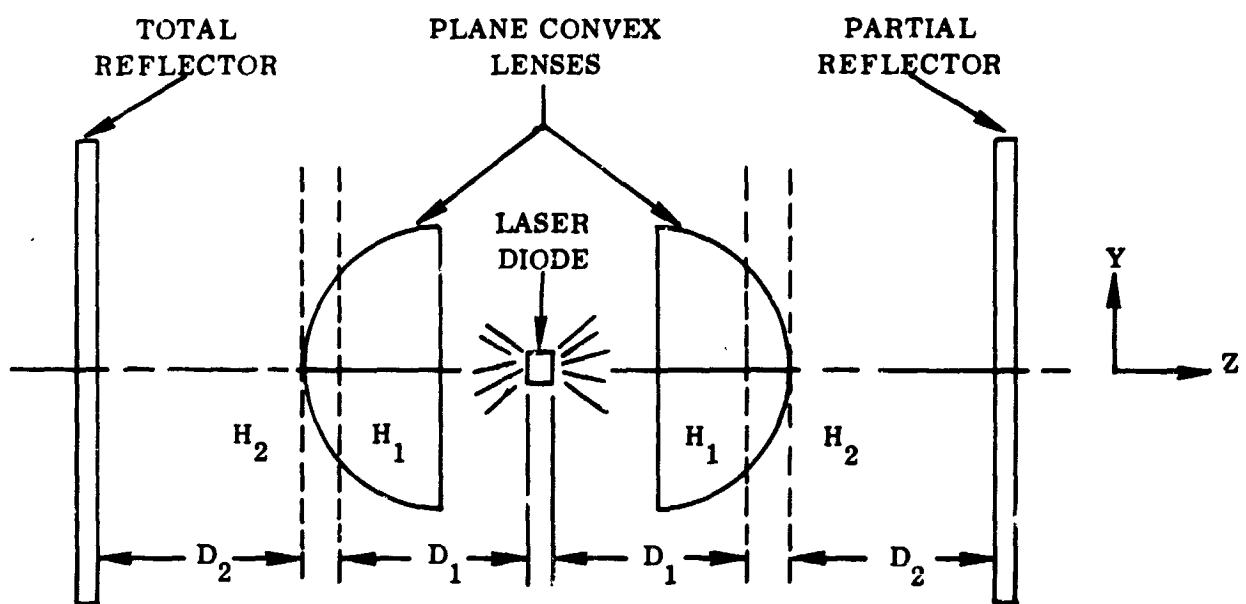


Figure 5-3. Optical Resonator of the Diffraction-limited GaAs Laser

this lens. A self-reproducing field, therefore, is set up in the x-direction when the distances  $d_1$  (see Figure 5-3) are equal to the focal length of the lenses ( $f$ ), that is  $d_1 = f$ .

For the wide dimension of the lasing junction (y-direction) the transformation of the radiation through the resonator must be described in terms of the Fresnel approximation. For this approximation there is complete symmetry of the mode parameters of the incident beam and of the beam transformed through the lenses in the resonator when  $d_1 = f$ . In the unfolded equivalent of the optical resonator, the symmetrical mode in the y-direction is iterated by the second lens when  $d_2 = f$ .

Because of this bifold symmetry in the y-direction, together with the unifold symmetry in the x-direction, it is concluded that a self-reproducing field is set up in the optical resonator of the GaAs laser when the radiating apertures of the GaAs diode, as well as the plane reflectors, are in the focal planes of the lenses; ( $d_1 = d_2 = f$ ).

There is no mode-selecting iris inside the GaAs laser resonator. For the wide dimension, the mode structure of the laser resonator together with the width of the junction discriminates against higher order transverse modes. From the Fresnel approximation for the transformation of coherent radiation through a lens,

$$\omega_0^2 = \frac{f\lambda}{\pi} \quad (5.1)$$

for

$$d_1 = d_2 = f$$

where  $2\omega_0$  is the minimum beam diameter of the coherent radiation.



From Equation 5.1, one can derive the focal length of the lenses in the resonator as a function of the minimum beam diameter for the lowest order transverse mode. When this minimum beam diameter is made equal to the width of the lasing junction, the gain of the GaAs laser becomes higher for the  $TEM_{00}$ -mode than for the higher order transverse modes.

The selection of the lowest order transverse mode in the GaAs laser is enhanced by gain saturation during the buildup of the stimulated emission. Because of the very high gain in the p-n junction, one can assume a spatially tapered distribution of the inverted population during the buildup of the stimulated emission which can result in phase-locking the oscillation over the entire lasing junction.

For the narrow dimension of the lasing junction, the field configuration of the dielectric surface wave mode in the laser diode, combined with the small junction height, inherently favors radiation in the lowest order transverse mode.

#### 5.1.1.1.2 Optical and Electrical Properties of the Diffraction-Limited GaAs Laser

##### 5.1.1.1.2.1 Threshold Current

The threshold current for self-sustaining oscillation in the diffraction-limited GaAs laser was measured and the experimental results are compared with values derived from theoretical considerations.

The threshold condition is obtained by setting the gain, due to stimulated emission, equal to the sum of all losses in the radiating device. For the GaAs laser without external resonator:

$$\text{Re}^{(g_t - \alpha)l} = 1 \quad (5.2)$$

where

$R = \sqrt{R_1 R_2}$ , is the geometric-mean reflectivity

$l$  = length of the active layer of the laser diode

$g_t$  = threshold gain per unit length of the active layer

$\alpha$  = sum of the losses in the GaAs laser.

The relationship between the gain in the active layer of the GaAs laser and the current density ( $j$ ) through the p-n junction was investigated experimentally as well as theoretically. This relationship was found to be linear ( $g \propto j$ ) at low temperature, the relationship holds up to room temperature.

The threshold current density is

$$j_{th} \text{ A/cm}^2 = \frac{8\pi n_0^2 \nu^2 \Delta\nu d}{\eta_c^2} \left[ \frac{1}{l} \ln(1/R) + \alpha \right] \quad (5.3)$$

$$= \frac{1}{\beta} \left[ \frac{1}{l} \ln(1/R) + \alpha \right]$$

where

$n_0$  = index of refraction

$\nu$  = frequency of the laser radiation

$\Delta\nu$  = line width of the spontaneous emission

$d$  = thickness of the active layer

$\eta$  = internal quantum efficiency, defined as the number of photons emitted internally (but not necessarily radiated externally) for each carrier crossing the p-n junction.

$c$  = velocity of light

The losses  $\alpha$  in a p-n junction laser without an external resonator, are caused primarily by penetration of the light from the active region into the p- and n-junction regions and by free carrier absorption.

Typical values for  $\alpha$  and  $\beta$  in Equation 5.3 are  $\alpha = 25 \text{ cm}^{-1}$  and  $\beta = 1.9 \times 10^{-3} \text{ cm}/\text{\AA}$ . (IBM's diffused GaAs injection laser for room temperature operation.) These values (for  $R = 0.3$ ) yield a threshold current density of  $j_{th} = 30,000 \text{ A/cm}^2$  and a threshold current  $i_{th} = 30 \text{ A}$  for a  $10 \times 10^{-3} \text{ in.}$  times  $15 \times 10^{-3} \text{ in.}$  diode (without external resonator).

In the GaAs laser with the external resonator in Figure 5-3 an additional loss mechanism is introduced. The power of the emitted radiation is comparatively low, because of the spherical aberration of the wide angle radiation from the narrow dimension of the GaAs diode inside the resonator. In the resonator in Figure 5-3, only radiation with small divergence angles can contribute actively to the feedback of the laser and a considerable amount of the wide angle radiation in the x-direction of the injection laser is lost. From the measured far-field radiation characteristics of the GaAs laser with the external resonator, it was concluded that approximately 3/4 of the radiation in the x-direction is lost because of the spherical aberration of the lenses in the external resonator.

The threshold condition for the GaAs laser with the external resonator is

$$(1 - P_\ell) R e^{(g_t - \alpha) \ell} = 1 \quad (5.4)$$

where  $P_\ell$  is the power lost because of spherical aberration in the resonator.

The threshold current density is

$$j_{th}^0 / \text{cm}^2 = \frac{1}{\beta} \left[ \frac{1}{l} \ln \frac{1}{(1-P_l) R} + \alpha \right] \quad (5.5)$$

$$j_{th} = 50,000 \text{ A/cm}^2$$

and the threshold current is  $i_{th}^0 = 50 \text{ A}$ , (this value was actually measured).

#### 5.1.1.1.2.2 Quantum Efficiency

The internal quantum efficiency ( $\eta_{in}$ ) of the injection laser is defined as the number of photons emitted internally (but not necessarily radiated externally) for each carrier crossing the p-n junction.

The external quantum efficiency ( $\eta_{ex}$ ) is defined by the number of photons radiated from the laser for each carrier crossing the p-n junction. The external quantum efficiency is related to the internal quantum efficiency by the probability (F) that an internally emitted photon escapes from the laser diode;

$$\eta_{ex} = F \eta_{in} \quad (5.6)$$

The escape probability for an injection laser without external resonator can be approximated by

$$F = T e^{-\alpha l} \quad (5.7)$$

Where T is the transmissivity of the output reflector,  $T = 1 - R$ .

For the GaAs laser with external resonator, the escape probability will be smaller because of the power losses in the resonator which are introduced by the spherical aberration of the lenses in the resonator. The escape probability can be approximated by

$$F = T (1-P_\ell) e^{-\alpha \ell} \quad (5.8)$$

For  $P_\ell = 3/4 P_0$ ,  $\alpha = 25 \text{ cm}^{-1}$ ,  $\ell = 15 \times 10^{-3} \text{ inch}$ , and  $R = 0.3$ , the escape probability is  $F = 0.07$ . For a typical value of internal quantum efficiency of a GaAs laser for room temperature operation,  $\eta_{\text{in.}} = 0.4$ ,  $\eta_{\text{ex}} = 0.028$ .

The peak radiated power in the  $\text{TEM}_{00}$ -mode and the corresponding input peak current was measured and from this the external quantum efficiency was determined experimentally. The highest measured peak power was 2.2 watts at a peak current of 102A. No saturation could be detected at this current level.

To evaluate the external quantum efficiency, it will be defined as the ratio of the rate of photon emission, that is, the peak radiated power ( $P$ ), to the difference between peak current ( $i$ ) and threshold current ( $i_{\text{th}}$ ) times the band gap voltage ( $V_g$ ).

$$\eta_{\text{ex}} = \frac{P}{(i - i_{\text{th}}) V_g} \quad (5.9)$$

where  $V_g$  is the band gap voltage, it is  $V_g = 1.38 \text{ volt}$  for a GaAs laser operated at room temperature.

The external quantum efficiency is  $\eta_{\text{ex}} = 0.031$  for  $i = 102 \text{ amperes}$ ,  $i_{\text{th}} = 50 \text{ amperes}$ , and  $P = 2.2 \text{ watts}$ . This value is in comparatively good agreement with the theoretical value of  $\eta_{\text{ex}} = 0.028$ .

#### 5.1.1.1.2.3 Equivalent Electrical Circuit of GaAs Laser

In the equivalent electrical circuit of the p-n junction laser the voltage-variable resistance of the depletion region is in series with the linear resistance of the p- and n-regions and the linear resistance of the contacts between doped semiconductor and metal. Without bias voltage, the voltage-variable resistance of the depletion region is considerably larger than resistance of the p- and n-regions and the contact resistance. With increasing forward bias, the

variable resistance of the depletion layer decreases and eventually becomes smaller than the linear series resistances in the equivalent circuit.

For the small signal analysis of general circuit theory, the effective resistance of a p-n junction is the variable slope resistance,  $de/di$ . This analysis, however, is valid only when the signal voltage is considerably smaller than the voltage range, where the current (i)-voltage (v) characteristic of the p-n junction can be defined by;

$$i = i_0 \left( e^{\frac{qv}{kT}} - 1 \right) \quad (5.10)$$

where  $q = 1.6 \times 10^{-19}$  amp sec

$k = 1.38 \times 10^{-23}$  watt sec/degree

and  $T = 300$  degrees kelvin

The voltage pulses required to invert the population in the GaAs laser, extend practically over the entire voltage range of the p-n junction characteristic.

The small signal analysis, therefore, is not valid any longer. For the GaAs laser diode, the instantaneous resistance of the depletion region is the ratio of voltage over current,

$$r_{inst} = \frac{v}{i} \quad (5.11)$$

To exceed the threshold for stimulated emission in the GaAs laser, the forward voltage ( $v$ ) across the depletion region must be approximately equal to the band gap voltage ( $v_g$ ):

$$V_g = \frac{h\nu}{q} \quad (5.12)$$

where

$$h\nu = 2.2 \times 10^{-19} \text{ watt-sec}$$

$$V_g = 1.38 \text{ volt for room temperature operation.}$$

Because of the exponential relationship between current and voltage in the depletion region, the instantaneous resistance ( $r_{inst}$ ) will decrease with increasing current.

The threshold current for IBM's diffraction-limited GaAs laser is 50 Amp, and the corresponding resistance is  $r_{inst} = 28 \times 10^{-3}$  ohms; for  $i = 100$  Amp, it is  $r_{inst} = 14 \times 10^{-3}$  ohm.

The linear resistance of the p- and n-regions and of the contacts between doped semiconductor and metal was measured to approximately  $25 \times 10^{-3}$  ohm. This linear resistance is in series with the variable resistance of the depletion region.

#### 5.1.1.1.2.4 Conversion Efficiency from Electrical Input to Optical Output Power

For a peak current of 102 Amp, the peak radiated power was measured to be 2.2 watts. The peak voltage across the depletion region is approximately equal to the band gap voltage of 1.38 volt. Then the electrical peak power required to generate 2.2 watt peak radiated power is 140 watts. The peak power dissipated in the linear series resistance of  $25 \times 10^{-3}$  ohm is 260 watts.

It follows that the conversion efficiency from peak electrical to peak optical power is 0.55 percent (2.2 watts output/400 watts input).

#### 5.1.1.1.3 Effective Radiating Aperture of the Diffraction-Limited GaAs Laser

In the diffraction-limited GaAs laser, where the GaAs diode is operated in an external resonator, the effective aperture is the transformation of the lasing junction through the spherical lens of the resonator rather than the lasing junction itself. Because of the asymmetry of the GaAs injection laser, its effective aperture is different in the x- and y-directions as shown schematically in Figure 5-4. The optical laws which describe the transformation of the radiation from the wide and from the narrow dimensions of the lasing junction through the spherical lens are not the same. The transformation of the radiation from the narrow dimension in terms of Fraunhofer diffraction because the difference between the width and length of the lasing junction is about two magnitudes.

Figure 5-4 shows the contour of the dominant mode in the resonator of a diffraction-limited GaAs laser in the x- and y-direction. In the y-direction, there is complete symmetry of the mode parameters in reference to the lenses in the resonator. The minimum beam diameter ( $2w_{0y}$ ) at the output reflector is the same as at the lasing junction. Thus, the effective aperture of IBM's diffraction-limited GaAs in the y-direction ( $2w_{0y}$ ) is approximately 150 wavelengths or 0.14 mm.

From the measured far-field pattern of the diffraction-limited GaAs laser in the y-direction, one can verify the dimension of its effective aperture in the y-direction. The far-field radiation pattern has a near-Gaussian spatial intensity distribution. The far-field angle ( $\theta$ ) for this intensity distribution is related to the effective aperture ( $2w_{\theta y}$ )

$$\theta = \tan^{-1} \frac{2\lambda}{\pi w_{0y}} \quad (5.13)$$



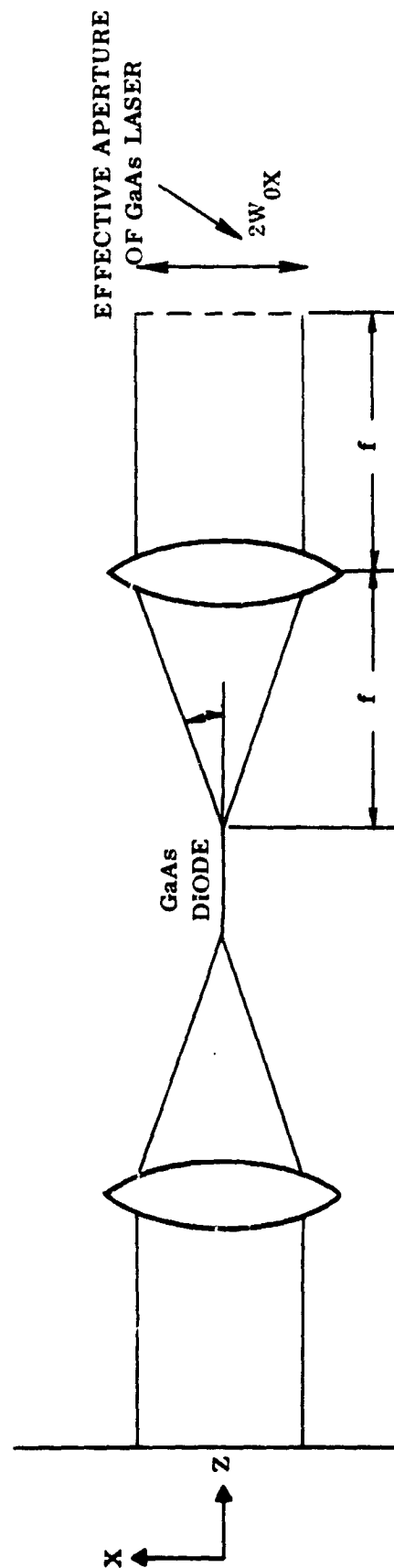
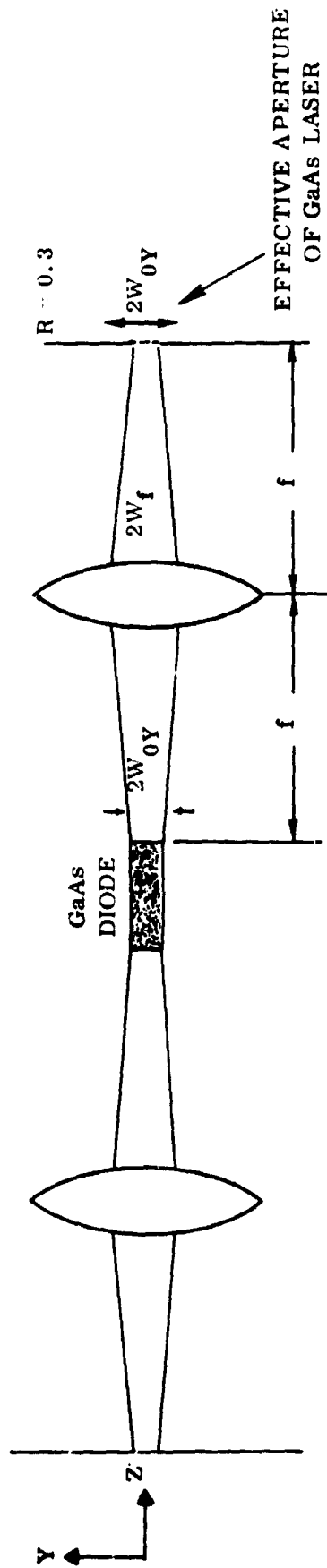


Figure 5-4. Contour of Dominant Mode in the Resonator Diffraction-Limited GaAs Laser

The angle  $\theta$  specifies the angle where the exponential factor in the field amplitude of the Gaussian beam falls to  $e^{-1}$ .

In the x-direction, where the lasing junction is a few wavelengths high, the phase front of its radiation is circular. This phase front becomes converted in the lenses of the resonator to a plane wavefront. The cross section of the dominant mode at the output reflector in the x-direction is approximately

$$2w_{\theta x} = 2f \tan \gamma,$$

where

$f$  = focal length of the lenses in the resonator

$\gamma$  = elevation angle of the mode in the x-direction.

The focal length of the lenses in the resonator is  $f = 1.0$  cm. The elevation angle ( $\gamma$ ) of the wide-angle mode in the x-direction is limited by the spherical aberration of the lenses in the resonator.

To evaluate the effect of the spherical aberration on the radiation characteristics of the GaAs laser, the optical path lengths through the resonator is computed. The results are shown in Figure 5-5. The wavefront of the radiation in the x-direction is given when transformed through the unfolded equivalent of the optical resonator.

For very small elevation angles ( $\gamma$ ) the radiation from the lasing junction is reflected back into the lasing junction. However, for larger elevation angles a caustic is formed by the transformed radiation which extends beyond the lasing junction. Furthermore, a quadratic phase error is introduced over the transformed wavefront. Because of these aberrations in the transformed wavefront, radiation with divergence angles of less than  $\gamma = 4$  degrees will contribute actively to the feedback of the laser.

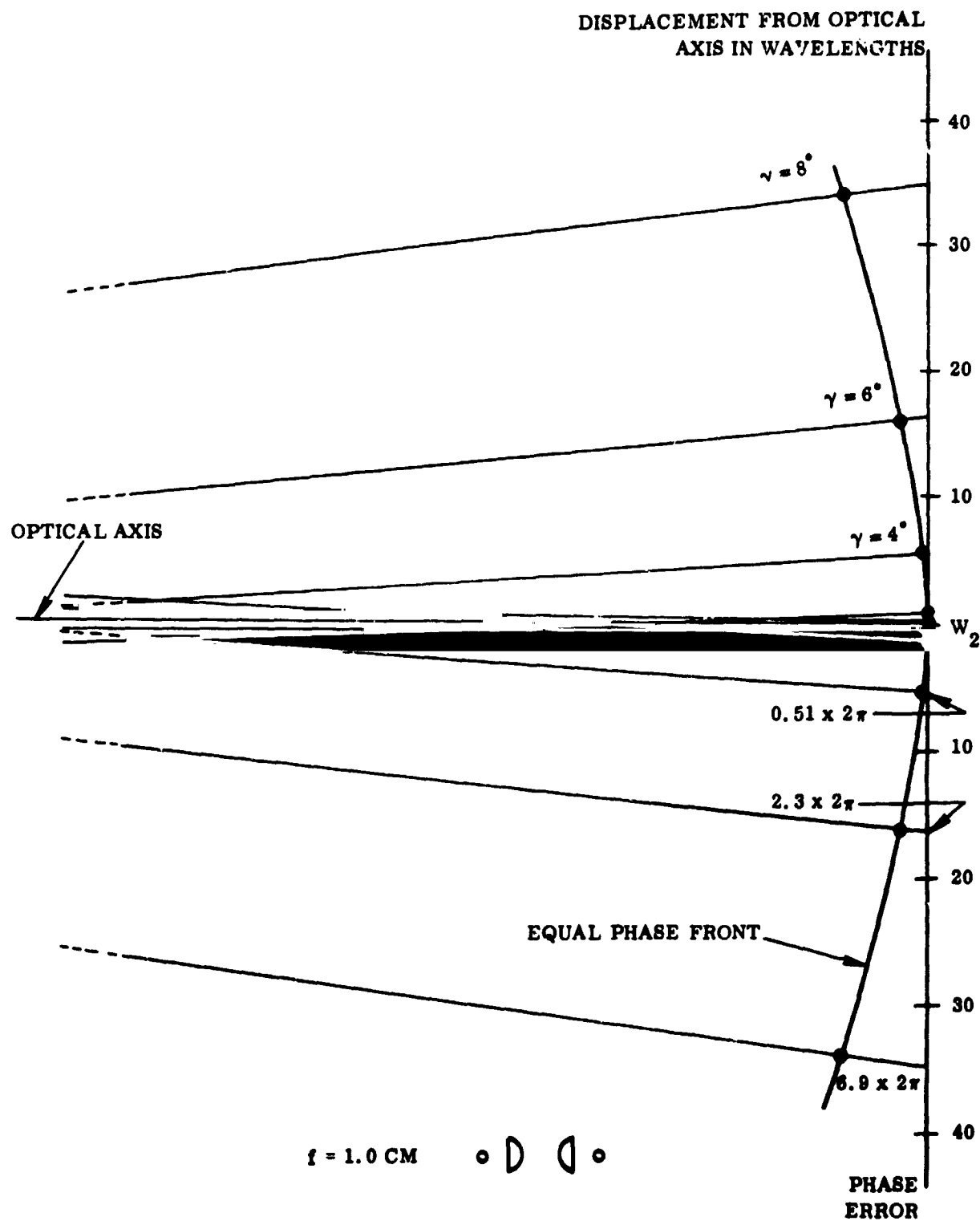


Figure 5-5. Aberration in Unfolded Equivalent of Optical Resonator for Different Elevation Angles

For  $f = 1.0$  cm and  $\gamma = 3$  degree-30 minutes, the effective aperture of the GaAs laser ( $2w_{0x}$ ) in the b-direction would be 1.2 mm. From the far-field radiation pattern of the diffraction-limited GaAs laser, the contour of the dominant mode in the x-direction is computed to be approximately  $2w_{0x} = 0.77$  mm. This corresponds to an elevation angle of  $\gamma = 2$  degree-30 minutes.

It follows that the angle range of radiation ( $2\gamma$ ) which actively contributes to the feedback of the laser with the external resonator is considerably smaller than the angle range of radiation from the GaAs diode in the x-direction, which is approximately  $2\gamma = 30$  degrees. This limitation in angle range in the x-direction of the laser with the external resonator to approximately 5 degrees, is primarily responsible for the power loss ( $P_l$ ).

It is desirable that the effective aperture of the diffraction-limited GaAs laser be symmetrical for use in the Optical Guidance System. To accomplish this the contour of the dominant mode at the output mirror was transformed in the y-direction to be equal to that in the x-direction. Two cylindrical lenses were used as shown in Figure 5-6, to accomplish this transformation without requiring too much space and without interfering physically with the structure of the optical resonator.

The beam transformation through the lenses  $L_1$  and  $L_2$  can be derived from the general equations for transformation of a Gaussian beam through a lens. Care must be taken to determine whether the transformation must be described in terms of Fresnel or Fraunhofer diffraction.

The lens  $L_1$  performs the function of reducing the minimum beam diameter ( $2w_0$ ) in Figure 5-5 to  $2w_1$ . Since lens  $L_1$  is a short focal length lens, the beam transformation must be described in terms of Fresnel diffraction. The relation for the transformation of a Gaussian beam through a lens with the focal length  $f_1$  in the Fresnel zone is

$$1/w_1^2 = 1/w_0^2 (1 - d_0/f)^2 + 1/f^2 (\pi w_0/\lambda)^2 \quad (5.14)$$

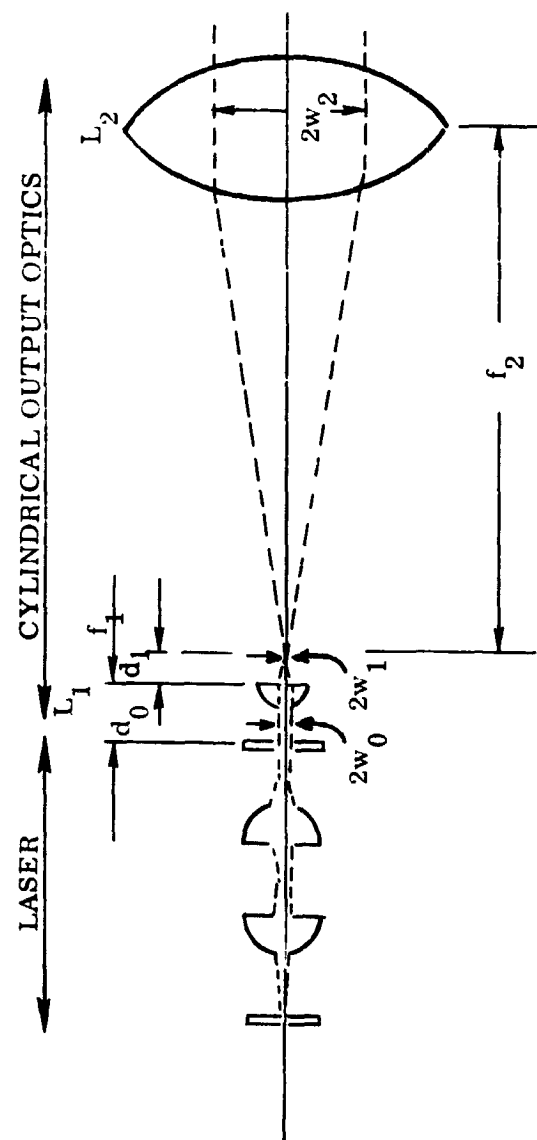


Figure 5-6. Transformation of Radiation from Diffraction Limited GaAs Laser in Y-direction.

and

$$d_1 - f_1 = (d_0 - f_1) \frac{f^2}{(d_0 - f)^2 + \frac{\pi w_0^2}{\lambda}} \quad (5.15)$$

where  $d_0$  is the spacing between the output reflector of the laser and lens and  $d_1$  is the spacing between the minimum beam diameter  $2w_1$ , and the lens.

Derived from Equation 5.14,  $f_1 = 1.9$  cm;  $d_0 = 5$  cm; and  $w_0 = 75\lambda$ ;  $w_1 = 41\lambda$ ; and from Equation 5.15,  $d_1 = 2.83$  cm.

The second lens ( $L_2$ ) is a long focal length lens ( $f_2 = 5$  cm). The transformation of the laser radiation through this lens must be described in terms of Fraunhofer diffraction. The light beam expands as it propagates from the position of the beam waist ( $2w_1$ ) to the second lens

$$w_2^2 = w_1^2 \left[ 1 + \frac{\lambda z}{\pi w_1^2} \right]^2 \quad (5.16)$$

When the beam waist ( $2w_1$ ) is in the focal plane of lens  $L_2$  ( $z = f_2$ ), then the beam waist ( $2w_1$ ) becomes transformed by lens  $L_2$  to the beam waist  $2w_2 = 0.77$  mm.

In effect, when the radiation from the diffraction-limited GaAs laser is transformed through the two lenses of focal lengths  $f_1 = 1.9$  cm and  $f_2 = 5$  cm, spaced at a distance  $d_1 + f_2 = 7.83$  cm, the effective aperture at the second lens becomes symmetrical and approximately 0.77 times 0.77 mm wide.

#### 5.1.1.2 Driver Electronics

In an effort to enhance the range resolution and minimize laser internal heating, ITTA/O designed, developed and tested fast rise-time and high peak current electronic circuitry to drive a very low impedance ( $\approx .050$  ohms) injection laser

diode. Operation of the diffraction-limited GaAs laser to the 10 kHz range without cooling has not been attempted to date because the high peak current laser drivers, which are at present available, have relatively slow rise-times and wide pulse widths. Minimization of the drive current rise-time and, therefore, pulsewidth will appreciably minimize heat dissipation within the diodes, thus allowing higher repetition rates to be obtained at room temperature.

The Modulator circuit consists basically of an energy storage device (capacitor or delay line), a switch (SCR or transistor), and a load (the laser diode). The switching component is most critical with respect to rise-time and energy transfer efficiency. A SCR is fairly versatile as the switching device and is capable of switching currents in the 100 amp range with rise-times of approximately 50 NS. However, an order of magnitude improvement is desired in the rise-time in order to improve the range measurement accuracy.

Several circuit configurations, utilizing transistors operated in the avalanche mode as switching devices, have been designed and tested by ITTA/O. Transistors are biased near the BV<sub>CES</sub> breakdown voltage. Application of a pulse at the transistor base causes base-to-collector and base-to-emitter junction breakdown producing a collector-to-emitter short. The transistor becomes a low resistance, fast electronic switch capable of providing short-duration, high current pulses.

Figure 5-7 shows the circuit designed. Note the use of four transistors as parallel switches. Normally, one transistor is capable of reliably switching 35 amps with a 15 NS rise-time to a maximum 10 kHz repetition rate. Parallel stages must be added in order to switch the higher currents required. Unfortunately, the addition of stages, especially more than two, requires exact switching synchronization of stages. In practice, exact addition of currents does not occur and pulse rise-time increases. Current pulses of 100 amps with 40 NS risetimes have been achieved with the circuit shown in Figure 5-7.

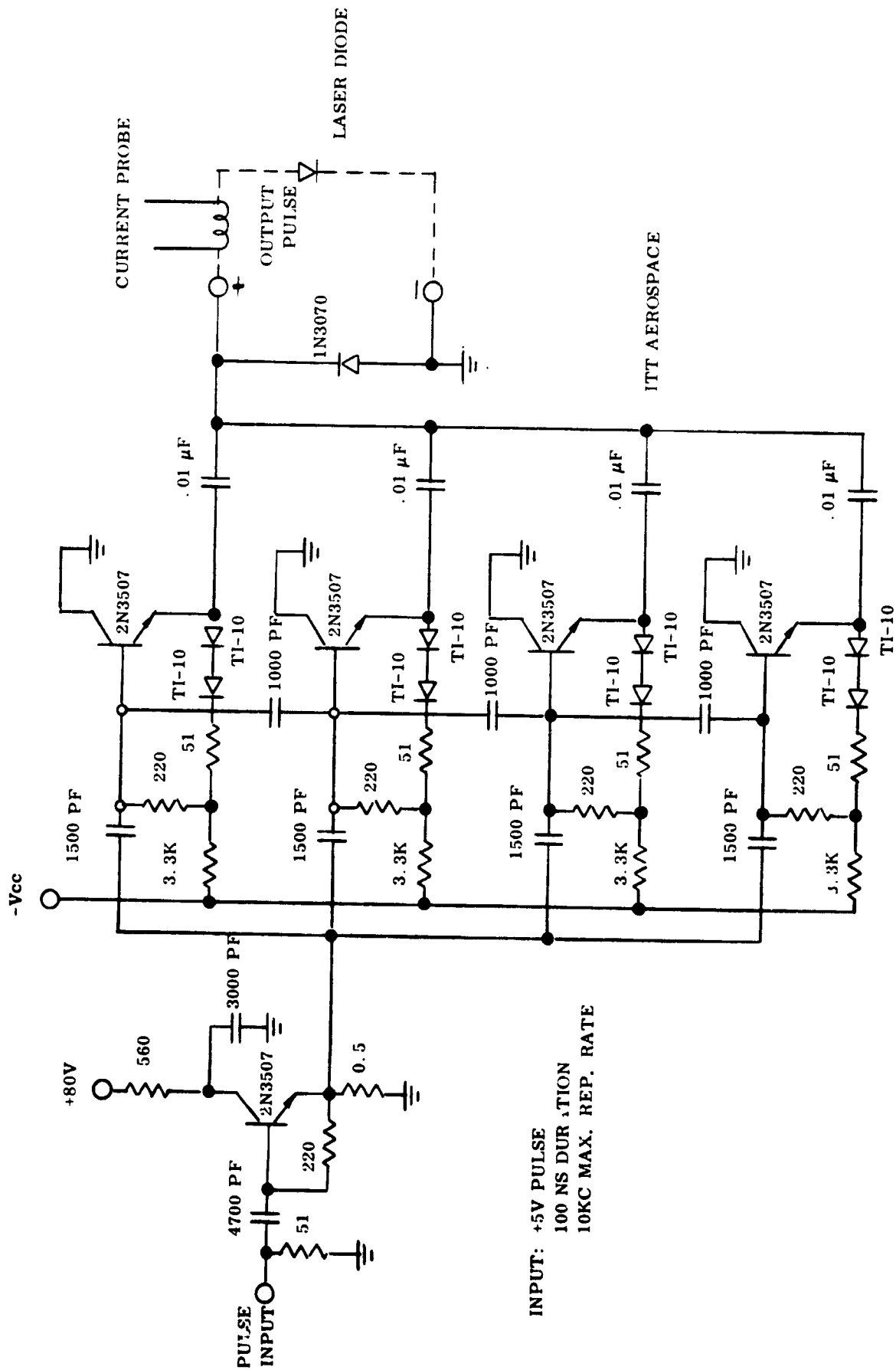


Figure 5-7. Laser Modulator Schematic



Thus far, the circuits have been built on brassboard type breadboards. Layout is extremely important and can add appreciably to current output if the switching circuit portion is minimized.

A model of the circuit was furnished for testing of the diffraction-limited GaAs laser. It did not provide a large enough current pulse to adequately test the laser and was used sparingly. Due to the faster rise-times, it is conceivable that larger current pulses will be required to provide the same laser outputs. The present ITTA/O goal is to increase the current pulse output above 100 amps while maintaining fast rise-times. The additional current is needed so that more meaningful data and the effect of faster rise-times can be seen.

An electron beam-semiconductor, linear switching device has been proposed by Watkins-Johnson Company of Palo Alto, California which appears to have some merit for use as very fast, high current switches.

The design of a pulse amplifier having 500 Amp capability into a half ohm load with 1 ns rise-time is quite straightforward. Peak current of 200 Amp with rise-time of 20 ns and a load impedance of  $0.05\Omega$ , the peak voltage would be 10 volts. Assuming  $L di/dt$  is less than 10 percent of output voltage, or 1 volt, the requirement would be that the total inductance be less than 0.1 nanohenry. To achieve such low inductances, it may be necessary to construct the pulse amplifier and the light emitting diode as an integral unit.

### 5.1.2 Optics

#### 5.1.2.1 Transmitter Optics

The radar transmitter optics will be self-contained within the laser assembly. The optics will collimate the laser output to a 0.03 degree beamwidth.

#### 5.1.2.2 Receiver Optics

The receiver utilizes a 50 mm f/0.95 lens manufactured by Angenieux. The 50 mm focal length has been selected to image a 30 degree field-of-view upon the F4011 Vidisector photocathode. The high speed of f/0.95 permits the largest collecting aperture possible, consistent with high resolution. The large aperture is necessary in order to facilitate a satisfactory signal-to-noise ratio at a range of 120 kilometers. The Angenieux lens has excellent resolution and has already been used in space on the Ranger and Mariner flights. An MTF plot of this lens, prepared at ITTA is shown in Figure 5-8. The plot was made in 7000 Å light, which is the longest wavelength available with the MTF machine. The off-axis curves show the tangential resolution on the surface of best tangential focus.

The following specification refers to a prototype, 2 inch, T/1.0 monochromatic objective lens, including spectral filter and threaded barrel mount, to be incorporated into a near IR electro optical sensor. The focal plane of the system is the plane inside surface of an image tube. The tube window (to be considered in all ray trackings) has a thickness of 0.08 inch and is made from Corning #7056 glass. The total length, weight and number of elements chosen by the design are not specified. The glasses chosen shall be of a common type and grade A quality.

Certain limitations apply to the first and last lens elements. The first lens element shall be a 3/16 inch thick, fused silica window with the spectral filter on its inner surface. The last element, at the designer's option, may be a field flattening lens. However this lens, if used, must have an uncoated plane rear surface and a diameter of 1.25 inches. The lens should be designed to be cemented to the sensor tube surface with no physical connection to the lens barrel mount.

- LENS PERFORMANCE (DESIGN)

The lens shall have a T number (ratio of relative aperture to the square root of the transmittance of 1.00 or less for 0.905 micron radiation).

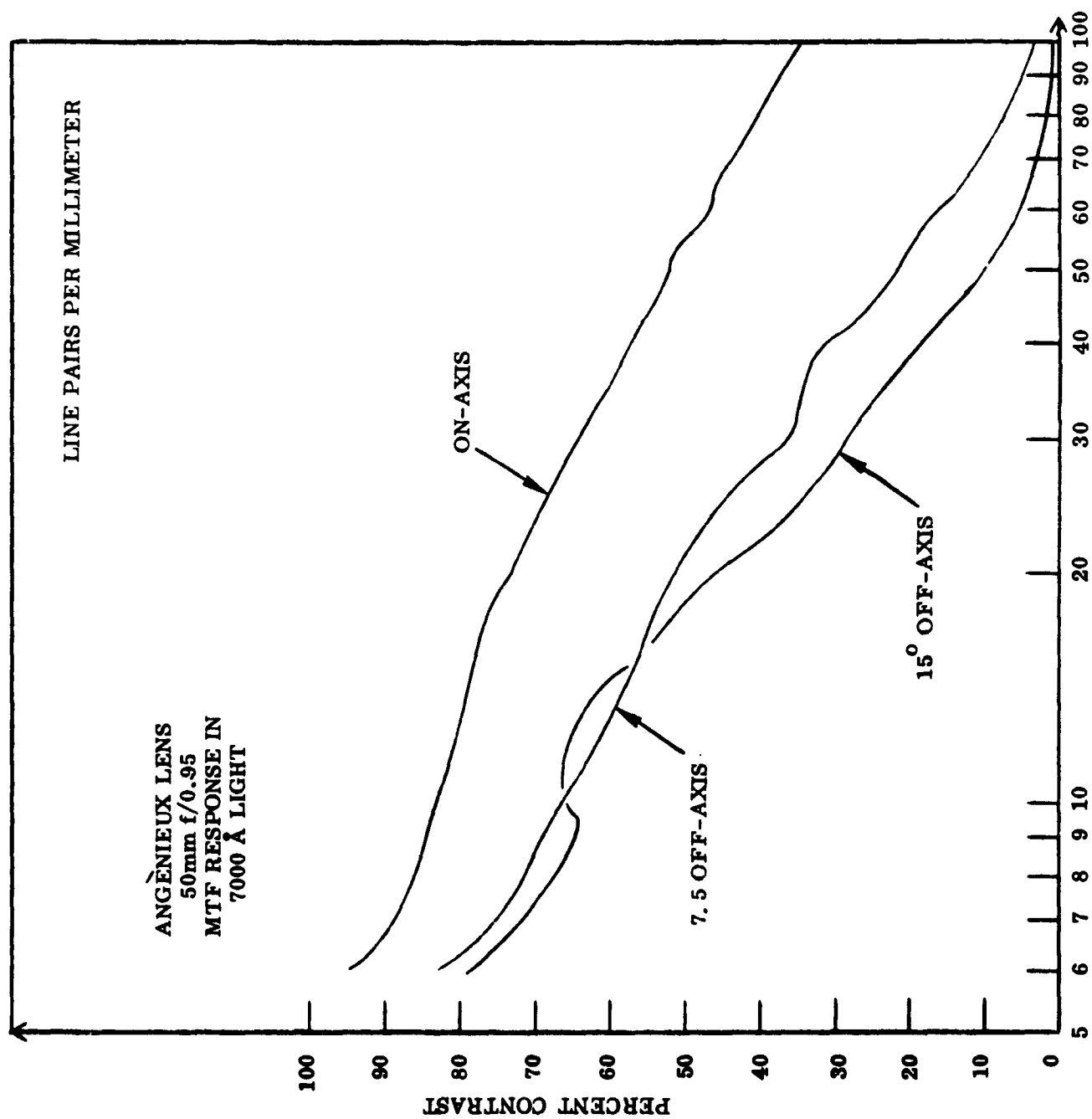


Figure 5-8. Angénieux Lens MTF

Vignetting over the field-of-view may not exceed 20 percent of on axis transmittance.

Anti-reflection coating may be used on all appropriate surfaces.

The field-of-view shall be 30 degrees ( $15^\circ$  half angle).

The effective focal length shall be  $2.00 \pm 0.10$  inches.

- RESOLUTION

The geometrical design shall be such that, across the entire field-of-view, 90 percent of the spectrally filtered radiation passing through the lens shall intercept the focal plane within a circle of  $0.005 (5 \times 10^{-4})$  inch diameter.

The Spectral filter shall have a 200 angstrom bandpass centered at 0.9050 microns. The optical transmittance between 0.895 and 0.915 microns shall be within 0.10 of the value at 0.905 microns. The transmittance at 0.88 and 0.92 microns shall be less than 0.10. Complete blocking for the S-1 spectrum.

The distortion shall be between 0 percent and -3 percent (barrel) to 0.5 inch off-axis.

- LENS BARREL MOUNT

The rear section of the lens barrel mount shall be finished and threaded.

Positioning and holding of the lens elements shall be such as to allow disassembly without damage to the lens elements.

The aluminum barrel design shall be such that the lens is assured of passing the appropriate tests described in MIL-0-13830, section 3.8.

- REQUIRED ITEMS (DESIGN)

A reproducible scale drawing of the designed lens (untoleranced).

Energy distribution data (either tables or plots as in Figure 8.2 of MIL-HDBK-141), for 0.9 microns radiation for on axis, 10.6 degrees off axis, and 15 degrees off axis beams in the same focal plane.

Reproducible complete design drawing of the lens barrel mount, spacers, rings, etc.

- **REQUIRED ITEMS (FABRICATION)**

All design specifications apply to the fabricated lens except 1.4, where 65 percent is substituted in place of 90 percent.

A reproducible toleranced drawing of the lens to be fabricated, based on melt sheets of the glasses to be used.

A measured transmittance curve of the spectral filter.

The assembled lens (and field flattening lens if applicable).

#### 5.1.3 Range and Range Rate Subsystem (Timing and Data Processing)

The range equipment measures the time interval between the laser transmission and the reflected target return. The time is basically measured by a conventional digital counter. In addition, a hybrid digital-analog system is used to attain a much finer granularity than would be possible with present digital techniques alone. Range rate is then determined by taking the range difference of two measurements and dividing by the time between the measurements. Time bin averaging is used to smooth the range data improving range rate accuracy. The range and range rate unit block diagram is shown in Figure 5-9. The major subunits and their functions are:

- Master range counter - the basic timing reference
- Fine range divider - divides each 6.4 meter range increment in 64 ten centimeter increments, stopping on a proper target return with the target fine range.
- Target range storage - holds the previous target return for accumulation and for range tracking.

# RANGE AND RANGE RATE MEASUREMENT UNIT

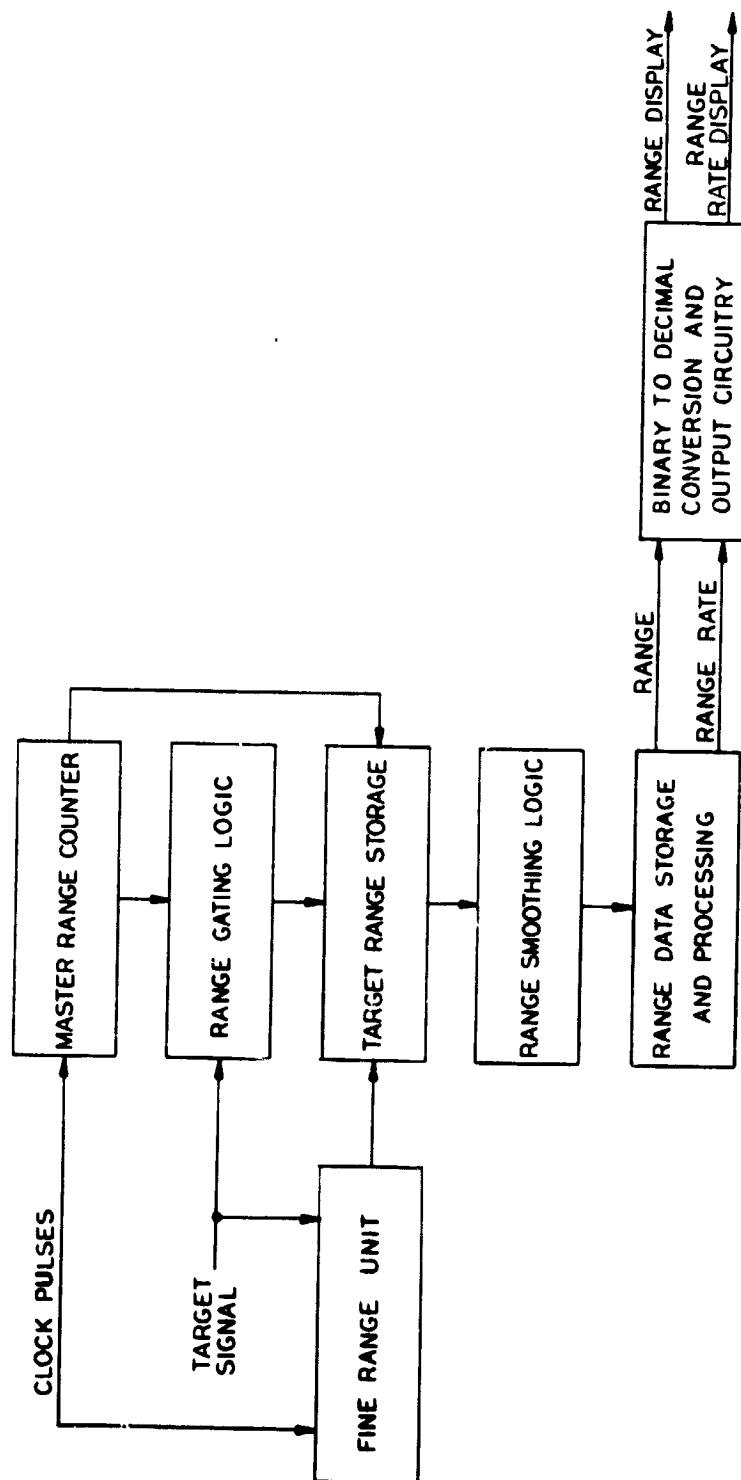


Figure 5-9. Range and Rate Unit Block Diagram

- Range gating logic - generates an acceptance gate about the target range, when adequate return data is available.
- Range smoothing logic - adds and averages target ranges for 0.1 second time bins providing smoothed values for determining range rate.
- Range data storage and processing - holds previous values of smoothed range and performs subtraction to get range rate.
- Binary to decimal output logic and circuitry - puts range and range rate into decimal output form.

#### 5.1.3.1 Master Range Counter

The master range counter is the timing reference for the range subsystem and the entire Optical Guidance System. The counter is 15 bits long, with the least significant bit representing 6.4 meters. It is free running up to the maximum range (R max) at which point it resets to zero. A selection can be made between a long range counting rate of 1 kHz, giving an unambiguous R max of 150 km (23, 421 counts, binary 101101101111101). A counting rate can be selected of 10 kHz, giving also an unambiguous R max of 15 km (12, 342 counts, binary 100100100110). The unambiguous R max is based on the elapsed time for a radar pulse to go out and come back before the next pulse starts. The logic of the master range counter is shown on ITT drawing #5518195 enclosed in Appendix G. The 4 least significant bits, (M4 through M1) are individual integrated circuits driven by a 23.4 MHz clock. For the other 11 bits (M 15-5), three more efficient integrated ripple counters are cascaded, and driven by a 1.47 MHz clock. The X1 flip-flop senses the M 15-M5 portion of the R max one count in advance so that the R max signal can be synchronized with the faster M4-M1.

#### 5.1.3.2 Fine Range

The Optical Guidance system requires a range measurement granularity of 10 cm. To attain this granularity to the required range maximum by a standard synchronous binary range counter would require a 21 bit counter counting a 1500 MHz clock, i.e., toggling at 750 MHz. Generation of the 1500 MHz clock is within the present state-of-the-art, but the counting at this rate is not. Thus the standard technique alone

is inadequate for the Optical Guidance System. For the Optical Guidance System, a hybrid digital analog technique is used. The master range counter described in 5.3.1.1 is driven by a 23.4 MHz clock, giving a basic range granularity of 0.4 meters. In addition there is a digital-analog fine range unit with 1/64 the granularity, or 10 cm.

The master range counter is sufficiently accurate for all system functions, other than range measurement, such as target range gating and R max resetting. The master range counter is synchronous which makes it useful for both real time range readings and range maximum timing, while a single ripple counter could perform only one of these functions.

In the fine range unit, a tapped stripline delay line and high speed logic circuits are used to give a special purpose counter at the required 1800 MHz rate.

**Fine Range Logic** - The fine range stripline logic is shown in Figure 5-10. A 42.7 nanosecond stripline delay line tapped at 64 equal 0.67 nanoseconds (equivalent to 10 centimeters of range) is the heart of the unit. The delay line acts as a clock pulse frequency multiplier and time shifter. At any tap the same basic clock wave form and frequency appears, but shifted in time by  $n \times 0.67$  nanoseconds. (See Figure 5-11). To get frequency multiplication, taps 1, 9, 17 . . . . 57 are "OR"ed together as Tap 1A; Taps 2, 20 . . . . 58 are Tap 2A; etc. The output at Tap nA is a pulse at a frequency 8 times the original frequency, and still displaced  $n \times 0.67$  nanoseconds from the basic clock.

**Frequency Multiplication** - Eightfold frequency multiplication is used because the resulting frequency of 187 MHz is the limit of the fastest integrated counters and flip-flops known, the Motorola MECL III Series. The signal from each combined tap is logically "AND"ed with the target signal, so its output will be cutoff when the target signal arrives. Inverted logic levels are used for "AND"ing since MECL III has only "OR"- "NOR" gates at present. In Figure 5-12, Tap 8A can be directly counted by an integrated counter which immediately gives the three most significant fine range bits; FR6, FR5, and FR4. For the least significant fine range bits, 4 flip-flops, FT1 - FT4, are sequentially turned ON by TAPS 1A - 4A and then OFF by TAPS 5A - 8A. Flip-flops FT1 - FT4 are decoded to give bits FR3, FR2 and FR1, as shown. This technique requires only a 187 MHz



# BASIC STRIPLINE

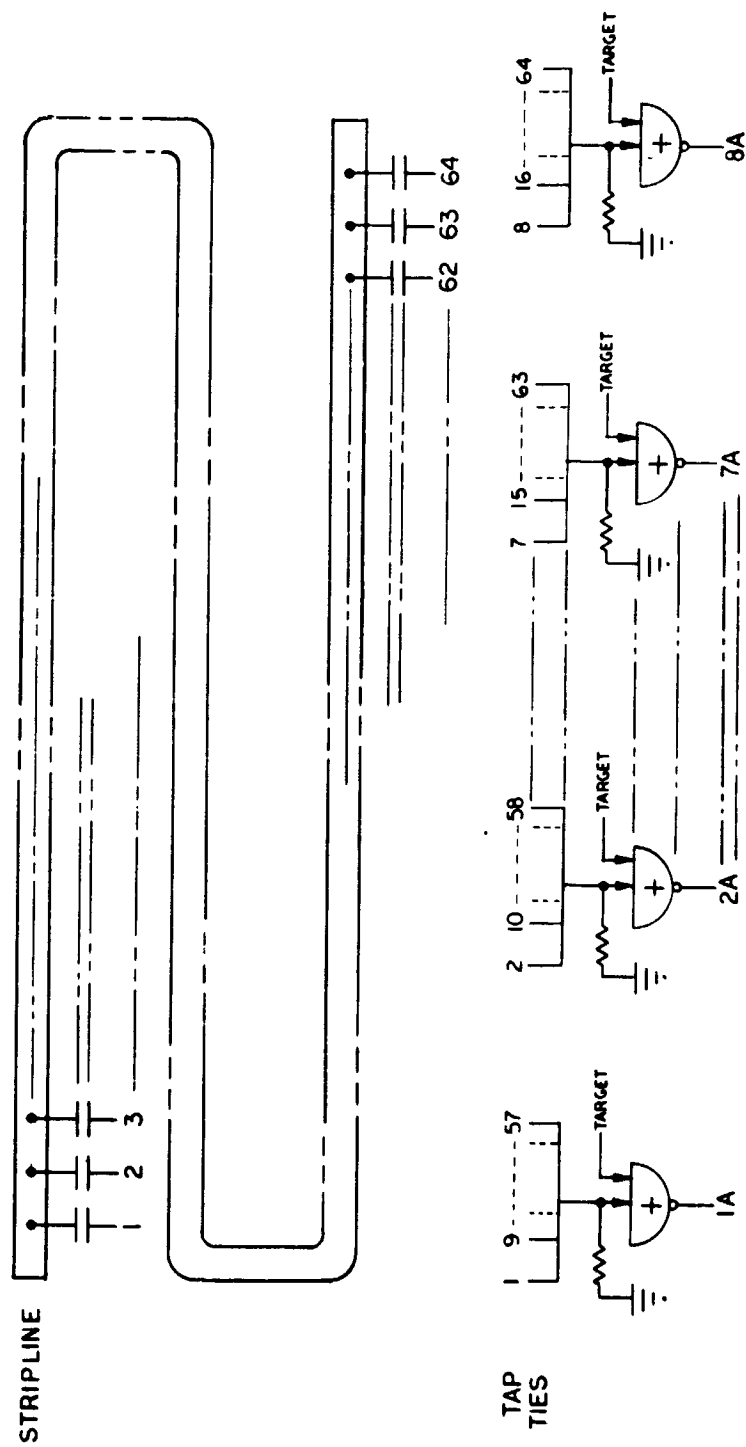


Figure 5-10. Fine Range Stripline Logic

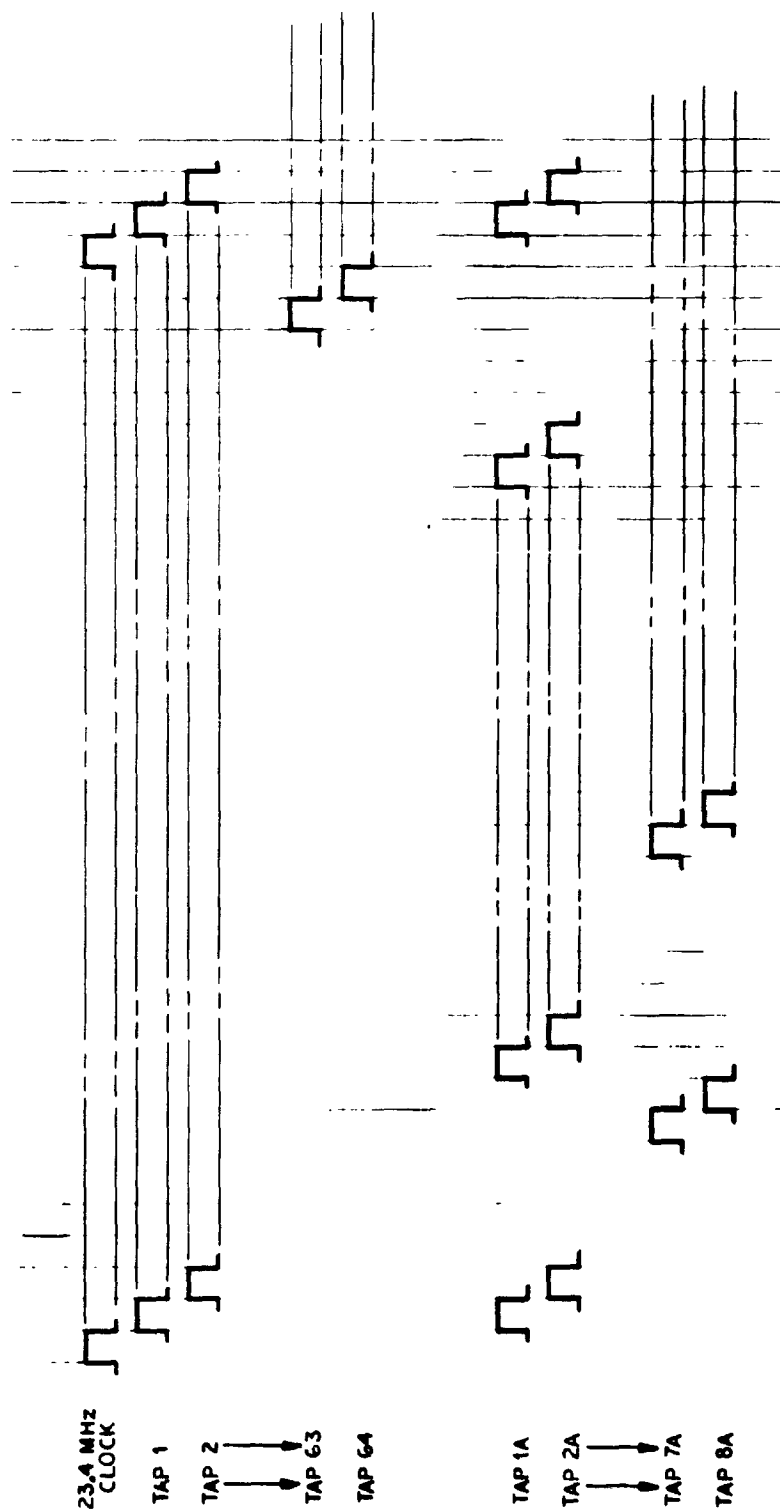


Figure 5-11. Fine Range Timing Diagram

TT4

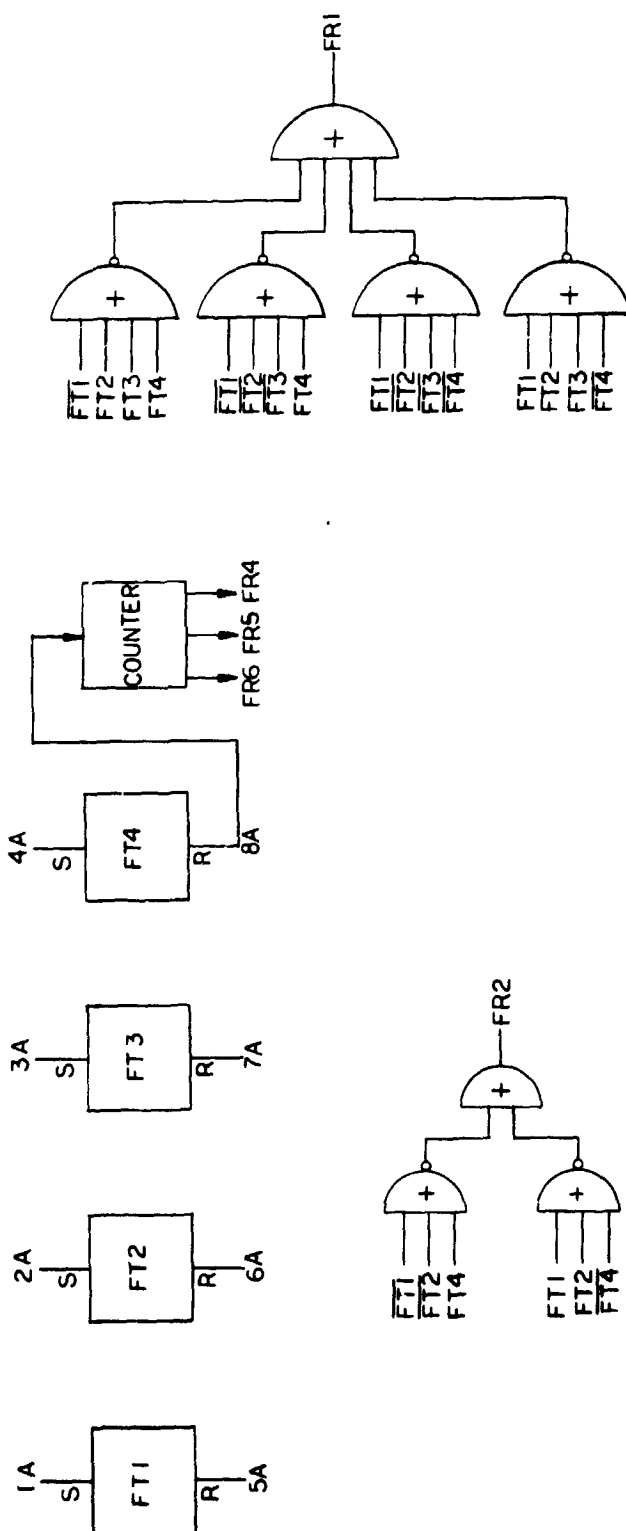


Figure 5-12. Fine Range Logic

toggle rate for the flip-flops, while the output value is toggling at the required 750 MHz rate. If no target pulse comes in the 42.7 nanosecond interval all flip-flops end up in their zero state just as the next main clock pulse reaches the stripline input. Thus the fine range unit operates modulo 6.4 meters. The count sequence and logic are shown in Figure 5-13.

**Stripline Delay Line** - The stripline sections handling the target and clock pulse within the range counter are, of necessity, microwave transmission lines. This is a consequence of the use of extremely short pulses. The requirements are to maintain a fairly good rectangular pulse shape at the inputs to the MECL III gates. Thus, the lines must propagate the first several Fourier components of the pulse with little relative attenuation and phase shift.

#### 5.1.3.3 Clock Pulse

For the one nanosecond rectangular clock pulse, the fundamental frequency on the line is 1 GHz. If we assume the first five Fourier components provide sufficient pulse fidelity, the line must operate satisfactorily up to at least 5 GHz. (Elimination of succeeding components introduces less than a 3 percent harmonic distortion into the pulse. These limits establish the maximum size of the transmission line and the minimum size of some of the components used to excite the gates.

The subsystem can then be considered to be a microwave delay line (serpentine in this case), coupling energy sequentially through each of the equal length microwave feed lines to the gates. Two basic stripline geometries are used to implement this circuitry:

A relatively low impedance (40 ohms) delay line section (Figure 5-14) which allows the use of wider strip dimensions with a consequent reduction of tolerance sensitivity. This is particularly important in the delay line where errors accumulate along the line and can contribute to increasing pulse distortion.

Relatively high impedance (100 ohms) lines used in feed lines to reduce the problems of impedance matching to the high input impedance of the MECL III gates. Here, error accumulation is less of a problem since these lines are essentially in parallel.

FT1	FT2	FT3	FT4	FR3	FR2	FR1
1	0	0	0	0	0	1
1	1	0	0	0	1	0
1	1	1	0	0	1	1
1	1	1	1	1	0	0
0	1	1	1	1	0	1
0	0	1	1	1	1	0
0	0	0	1	1	1	1
0	0	0	0	0	0	0

$$FR3 = FT4$$

$$FR2 = FT1 \overline{FT2} \overline{FT4} + \overline{FT1} \overline{FT2} FT4$$

$$FR1 = FT1 \overline{FT2} \overline{FT3} \overline{FT4} + FT1 FT2 FT3 \overline{FT4} \\ + \overline{FT1} FT2 FT3 FT4 + \overline{FT1} \overline{FT2} \overline{FT3} FT4$$

Figure 5-13. Count Sequence

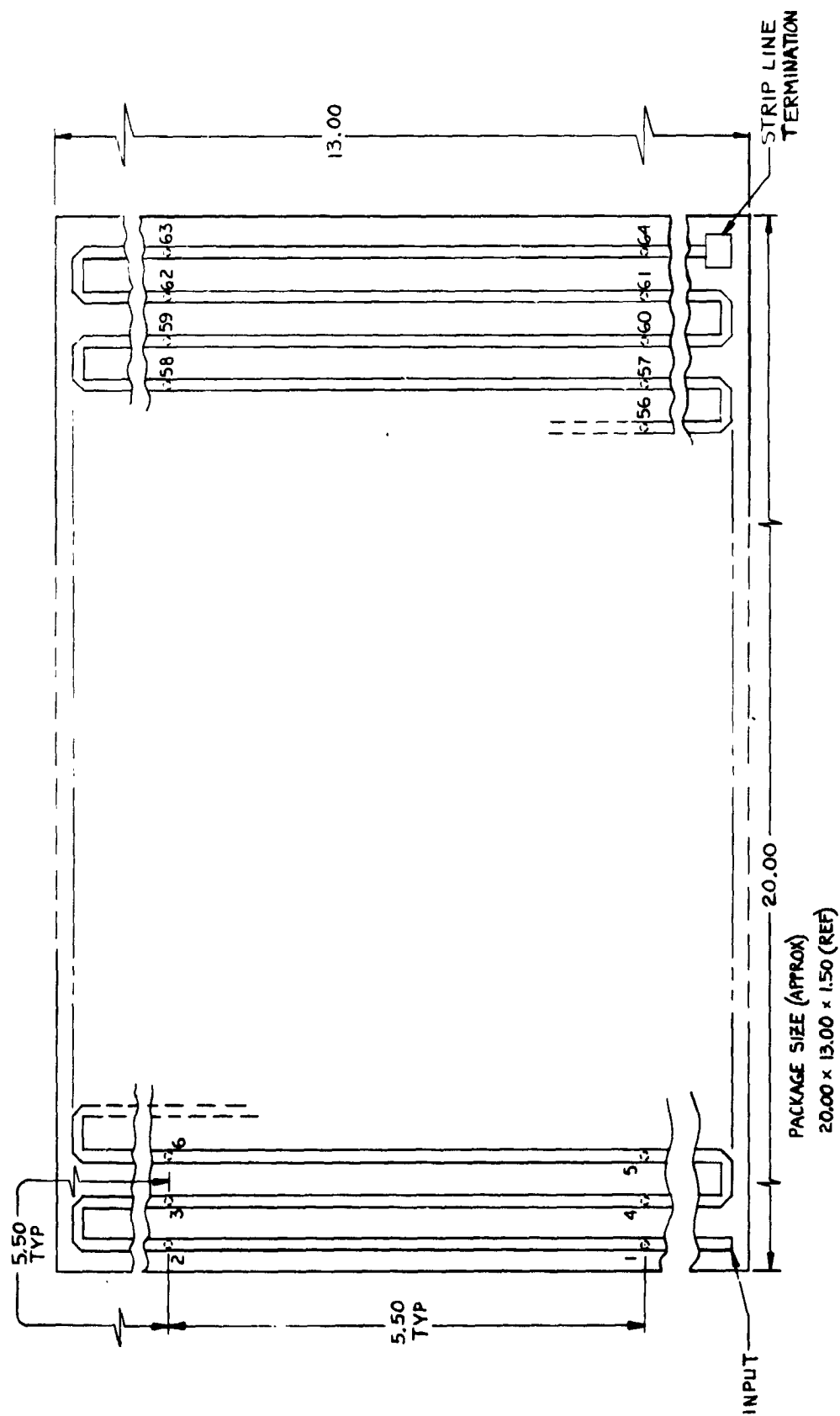


Figure 5-14. Strip Delay Line Diagram

#### 5.1.3.4 Microwave Delay Line Considerations

The microwave delay line is supported in a teflon dielectric sandwich. This dielectric serves to:

- Constrain the metallic strip line to the center between the upper and lower plates which further reduces error accumulations due to mechanical tolerances and,

- Provide dielectric loading of the line which reduces the length and width of the package by about 40 percent.

The microwave feed lines to the MECL III gates are essentially air dielectric lines since the metallic line support is provided by a dielectric sheet in the region between the two "center" conductors where, ideally, no RF field exists. This allows the realization of fairly high impedances with strip widths that are not uncomfortably small. A line drawing of this unit is shown in Figure 5-15.

Coupling to the feedlines is provided by small capacitive discs located at 0.67 nanosecond intervals along the delay line. These are connected through a short coaxial section to the multiple inputs of the "frequency multiplying", feed line distribution circuits. These coupling capacitors provide a coupling level 26 db below the delay line clock signal. Since this coupling level is so low, the power level seen in the delay line by the last capacitor is reduced by only about 0.6 db by the preceeding couplers. All the coupling discs are identical. However they result in a variation of gate currents by only 8 percent.

The clock signal power levels, required to provide triggering of the gates with these coupling levels, are about 860 milliwatts peak and -23 milliwatts average, assuming a gate signal of 0.9 volts and 300  $\mu$ amps, which is required for MECL III.

The final line section of the nA Tap is a short, high impedance (about 150 ohms) coaxial section, terminated in a resistive divider circuit functioning as a transformer into the high impedance MECL III gates.

#### 5.1.3.5 Target Range Processing, Range-Gating and Smoothing

The target range storage holds the data from a target return until the next target return come-in. Each target return is added to the accumulator for the range

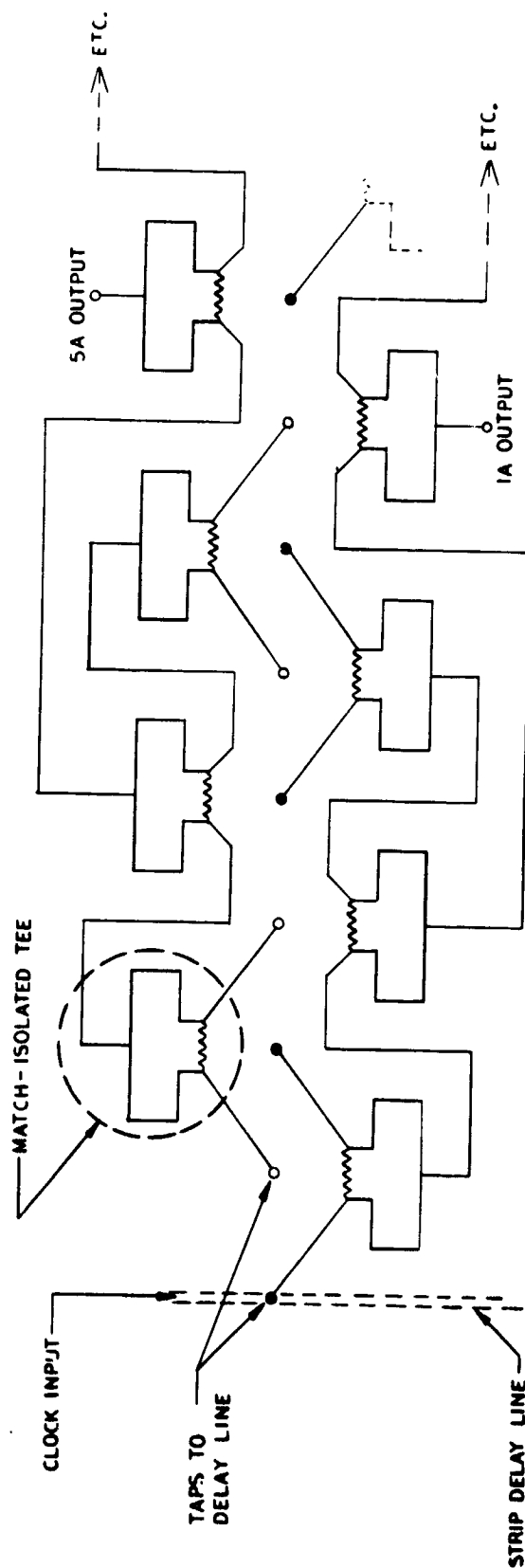


Figure 5-15. Gate Feed Distribution Circuits



smoothing. The target range stored also is used to center the range tracking gate. The target range storage subunit consists of a 21 bit register capable of storage and circulation (see ITT drawing #5518198 in Appendix G). Data is entered from the master range counter into flip-flops #TR21 through TR7 whenever a proper target return occurs. The fine range is entered into flip-flops #TR6 through TR1 at this time. The new range data is serially added to the range accumulator while the target range register circulates. A special clock is generated for flip-flops TR10 to TR7 to read data at high speed, and to shift at the same high speed on the other flip-flop. After the addition, the target range stored is reduced by 102.4 meters (not to a value less than zero) to simplify the range gate logic, as discussed below.

The range gating logic selects between two modes, ungated and gated. The ungated mode is used initially or whenever a target is lost. The gated mode is initiated whenever two successive returns occur within 51.2 meters of each other. Then a range gate of +51.2 meters is generated about the last observed target range. This gated mode is continued until 64 consecutive transmissions occur without one return within the gate, indicating the loss of target, and call for the ungated mode.

The range gate should start 51.2 meters before the target (or at zero for target range less than 51.2 meters). The method used to generate the starting time for the gate is to decrease the stored target range by one half the gate width, 51.2 meters, and to detect coincidence between the master range counter and the resulting stored target range. Synchronizing problems require an advance signal from most significant 11 bits, using an X2 flip-flop analogous to X1 in the R max logic. This advance technique requires another 51.2 meter decrease in the stored range (not to be less than zero). Thus the total requirement is a decrease in the stored target range of 102.4 meters as stated.

The range gating logic is shown in ITT drawing #5518194 in Appendix G. The 15 integrated coincident circuits compare the master range counter and the stored target range. The coincidence signal starts the gate width counter, which goes for 16 counts or 102.4 meters. Only a return during this 102.4 meters will be accepted. Any accepted return resets the miss counter to zero. Each R max signal advances the miss counter one count. If the miss counter reaches 64, the ungated mode is initiated. Flip-flop G1 senses one return in the ungated mode, initiating a trial gate. For the gated mode, flip-flop G2 turns ON if the next return is in gate. G1 otherwise goes OFF, continuing ungated mode.

The range smoothing logic accumulates the target ranges for the first 32 returns of each 0.1 second time bin. This sends the average value to the range data storage and processing unit. The number of target hits is fixed at 32, permitting division by simple shifting without requiring an arithmetic unit. The range smoothing logic is shown in ITT drawing #5518197 in Appendix G. Since the range accumulator sums 32 target ranges, it must be at least 5 bits longer than the 21 bit target storage register, or at least 26 bits total. Since the accumulator requires only circulating operations, it can be most efficiently designed using as many integrated shift registers as possible. In the transfer of smoothed range, accessibility is required to bit 6, which is the least significant bit, when the accumulator is divided by 32. Bits 1-5 for this reason are in individual integrated flip-flops. The highest 21 bits are in three 8 bit integrated shift registers. The highest 3 bits in the shift register are not used.

#### 5.1.3.6 Time Addition Counter

The time addition (TA) counter generates a 29 count "Add" signal for the serial addition of target range. The TA counter is normally zero. When the T-GA signal indicates a new value of target range, the TA starts counting (unless the hit counter has reached 32) and continues until 28, binary 11100, at which

point it resets to zero. Including the first pulse in state zero when TA turns ON, the desired 29 count signal is thus obtained. The Add signal is logically "OR"ed with the Data Shift signal to circulate the range accumulator. The circulation signal for the target range storage must be only 21 bits long to preserve the stored target range. The signal for this is obtained by logically "AND"ing the Add signal with TA4, eliminating the last 8 counts. The hit counter advances each time the T-GA signal indicates a new value of target range. When the counter reaches the 11111 state, which takes 32 hits, it holds its value, thus inhibiting additions, until the next DC8 signal resets it to zero and starts a new cycle.

#### 5.1.3.7 Range Data Storage and Processing

The range data storage and processing logic stores ten previous smoothed range values. Periodically determining range rate by taking the difference between a previous range and the most recent range. For longer ranges (1 kHz counting rate), the range data is stored and subtracted every 0.1 second giving range data is stored and subtracted every 0.1 second giving range rate on the basis of ranges 1 second apart. This gives the fastest response, at some sacrifice of accuracy. For shorter ranges (10 kHz counting rate), the data is stored and subtracted every 1 second, giving range rate on the basis of ranges 10 seconds apart. This improves accuracy at the expense of response time. A range determination is made every 100 transmissions as controlled by the data counter. The range data storage and processing logic is shown in ITT drawing #5518196. Each smoothed range is stored in three 8 bit shift registers. (Again 3 unused bits). Every time a new smoothed range is received, the new range rate is determined, and all data is shifted one word up by a 24 bit serial shift, timed by the data shift counter. The range rate subtraction is made serially at the same time as the shift, and the range rate is stored in a register.

The data counter is a two-stage decade ripple counter. It counts every transmission cycle using the R max signal as an indication of a cycle. The DC8 signal comes on each one-hundred transmissions, and initiates a range determination, resetting itself to zero.

The data shift (DS) counter generates the 24 count signal for the serial shift of stored smooth range data. The DS counter is normally at zero. At the time the DC8 signal comes ON, the counter starts counting to 23 (binary 10111). The shift signal (SS), DC8, or any bit of the DS counter, is thus on for 24 counts.

The binary to decimal output logic and circuitry will be of the same type as described in the 2 axis angle tracker. The logic will scale the range rate data to correspond to the 1 kHz and 10 kHz transmission frequencies.

The bulk of the logic uses standard Texas Instruments and Sylvania integrated circuits. Voltage levels will be: True,  $+4.5\text{V} \pm 0.5\text{V}$ ; False  $0\text{V} \pm 0.5\text{V}$ . Clock pulse frequencies of 1.47 MHz and 234 MHz will be used. For the fine range unit MECL III integrated circuits will be used. A 234 MHz clock with 1 nanosecond rise and fall time, and 1 nanosecond width will be used. Voltage levels will be: True,  $-0.85\text{V} \pm 0.05\text{V}$ ; False,  $-1.75 \pm 0.05\text{V}$ .

#### 5.1.4 Two-Axis Angle Tracker

##### 5.1.4.1 Performance Requirements

The two-axis angle tracker portion of the optical radar subsystem will be required to acquire and track the target over a  $\pm 15$  degree field-of-view. Having acquired the target, data must be generated to provide the gimbal servo control system with error signals as well as angle and rate data for the Read-out Display Subsystem. The digital tracker error accuracy must be sufficient to derive a system pointing accuracy of at least 0.1 degree. Inherent tracker accuracy in the neighborhood of null exceeds 0.1 degree by an order of magnitude.

#### 5.1.4.2 Tracker Description

The chaser angle tracker receiver collects the pulsed laser energy with a high-speed optical lens system, f/. 95, and then senses its direction and amplitude with an image dissecting photomultiplier. The receiver optics is a refractive lens system. The objective lens diameter is approximately 55 mm and the effective focal length is 50 mm. A narrowband interference filter is placed in the optical path to reduce the sunlit sky background. The optical sensor is an ITT F4011 vidisector. The F4011 vidisector is a magnetically focused and deflected image dissector tube that has a photocathode diameter of 1.1 inches. Coupled with the receiver optics, the sensor's maximum field-of-view is then 0.55 radians (27.5 mm/50 mm) or approximately 31 degree. Using the S-1 photoemissive surface, the radiant sensitivity will be approximately 0.002 amps/watt at 0.9100 microns. The photomultiplier gain will be at least  $5 \times 10^5$ . For an 0.03 degree instantaneous field-of-view and a receiver focal length of 5 mm, the scan aperture of the image dissector has to be 0.001 inches. Figure 5-16 is an electro-optical schematic of the receiver optics and sensor.

The following paragraphs are a discussion of the acquisition and track scan patterns for the angle tracker.

The angle tracker uses the dual-mode field-of-view (FOV) concept that has been proven extremely successful in the already space-qualified ITT DUAL-MODE STAR TRACKERS. The dual mode consists of an acquisition mode and track mode. A relatively large field-of-view ( $30^\circ \times 30^\circ$ ), is scanned as shown in Figure 5-17 when a target is initially acquired. The acquisition field-of-view through a square matrix pattern of approximately 1,000,000 elements. The stepping rate is the same as the pulsed laser repetition rate (1-10 kHz) insuring the dwell time (0.1-1.0 ms) on each element is sufficient to receive the transmitted pulse.

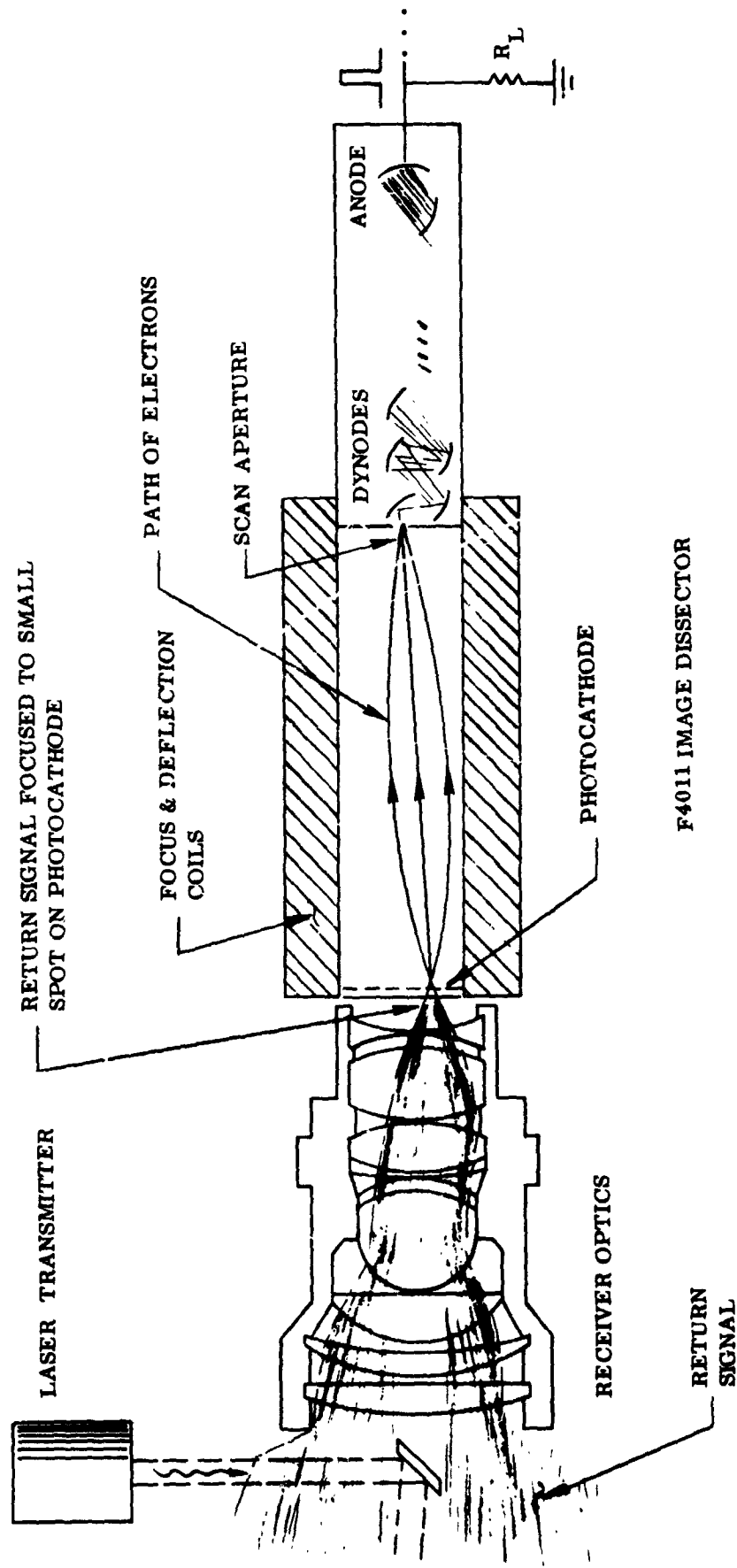
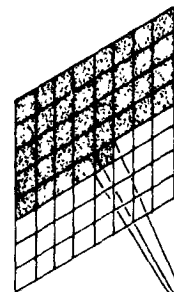


Figure 5-16. Receiver Optics and Sensor

# ACQUISITION MODE



- ACQUISITION FIELD-OF-VIEW  $30^{\circ} \times 30^{\circ}$
- INSTANTANEOUS F.O.V.  $0.02^{\circ} \times 0.03^{\circ}$
- # SCAN ELEMENTS 1,000,000
- $\Delta t$  PER ELEMENTS 1 MS (1 kHz)
- ACQUISITION SCAN TIME 1000 SECONDS (1 kHz)

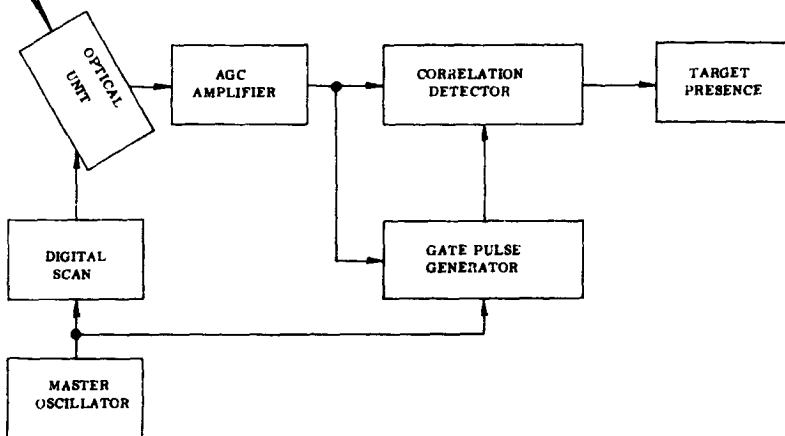
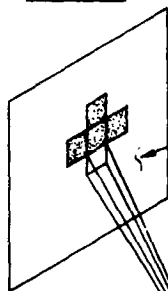


Figure 5-17. Scan Pattern for Acquisition Mode (OGS Digital Tracker)

# TRACK MODE



SEE BLOW-UP SKETCH FOR DETAILS OF SCAN

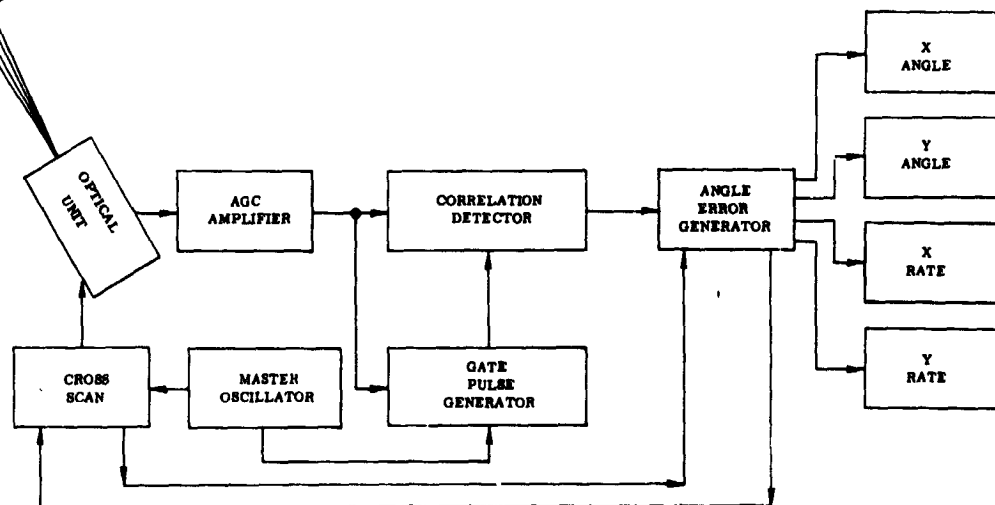


Figure 5-18. Scan Pattern for Track Mode (OGS Digital Tracker)

To optimize acquisition of the target relative to scan direction, target angle, and target angle rate, the acquisition and miniac scan generators utilize a quadrangular scan pattern. In successive fields, the pattern scanned travels from top to bottom, left to right, bottom to top, and right to left. Such a scan pattern tends to eliminate the effect of target angular motion during acquisition.

When the target is acquired, the angle tracker switches over to the track mode and a much smaller field-of-view around the target location is scanned. Figures 5-18 and 5-19 show the scan pattern for the track mode. The size of the scanned pattern is exaggerated for better visibility in the illustrations. The cruciform scan pattern of the track mode may be positioned at any point in the acquisition field, depending upon the location of the target at the time acquisition occurs. As the target moves across the tracking field, the cross scan pattern will move so as to stay centered around it.

The cross scan consists of stepping the instantaneous field-of-view ( $.03^{\circ} \times .03^{\circ}$ ) in 32 vertical increments and 32 horizontal increments. Each incremental movement of the scan element (one track step) corresponds to  $1/8$  ( $.03$ ) or  $0.06$  milliradians. See Figure 5-19 for the sequence of the scan pattern. The angular resolution is determined by the smallest track scan correction increment, equal to  $1/4$  track stop ( $.00375^{\circ}/4$ ) or  $0.016$  milliradians. The maximum angular rate capability is a function of acquisition field-of-view, instantaneous field-of-view, scan patterns, repetition and stepping rates, relative movement and position of target within the scan patterns, and velocity corrections introduced in the servo system. Certain aspects of this capability have been studied for a 1 kHz stepping-rate tracker. Details of the study are presented in Appendix B.

The pitch and yaw angle and angle rate data output from the Optical Guidance System will be made up from the angle tracker and the gimbal shaft angle encoder outputs. The angle tracker and gimbal subsystem will be boresighted and



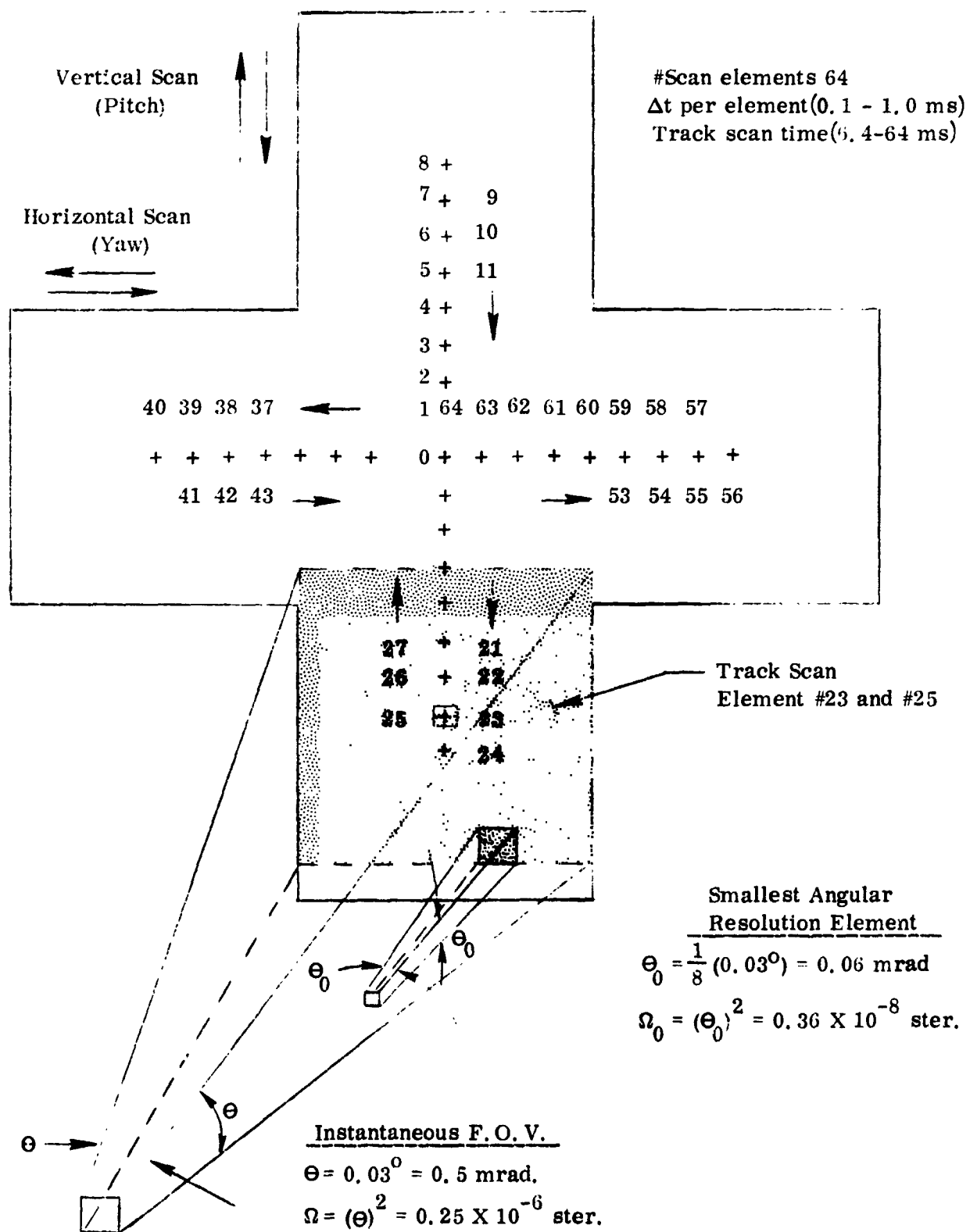


Figure 5-19. Scan Pattern for Track Mode Detailed (OGS Digital Tracker)

aligned to each other. Therefore, the OGS pitch and yaw angles will be the sum of the angles from the angle tracker and the gimbal encoders. During track, the angle tracker cannot be off the gimbal boresight by more than the halfwidth of the transmitter beam or no energy will be returned to the receiver. The maximum angular excursion of the angle tracker is therefore quite small in the track mode. In the acquisition mode when the beacon is ON, the difference between gimbal angle and tracker angle can be as large as  $\pm 15$  degrees.

#### 5.1.4.3 Angle Tracker Data Display Unit

##### Angle Readout Display:

To provide tracker angle data in a visual display, two conversions are required: binary to decade and decade decimal to 7 bar. The pitch and yaw angles are contained in binary form in the 3-bit track and 10-bit acquisition counters. The angle datum is parallel transferred into a  $\pm 12$  bit angle register at a time neither track or acquisition counters are being driven. During the yaw track scan, yaw angle and pitch scan, the pitch angle is transferred. The data is then read serially out of the angle register into a  $\pm 16$ -bit binary accumulator. The accumulator includes a three bit binary counter providing 8 sample smoothing per integration period (1.024 seconds). The angle represented by the LSB of the accumulator is equal to  $1/8$  acquisition step - or 0.00375 degree. The decade register LSP equals 0.01 degree therefore, for every 8 places in the accumulator (equal to 0.03 degree) three pulses must drive the angle decade register. This is accomplished by using count out pulses No. 2, 5 and 7 to drive the decade register per each 8 counts read out of the accumulator. This in a readout accuracy of  $\pm 0.0375$  degree  $\pm 0.005$  degree decade. A four decade angle register is used to store the  $\pm 15.00$  degree angle datum. Each decade consists of four flip-flops connected in a symmetrical divide by 10 configuration. The angle  $\pm$  sign bit is a nand gate "latch," driven by the MSB of the accumulator.

The angle is then converted to 7 bar form by a nand gate connected positive logic converter. Line drivers out of the converter provide the drive to the 7 segment, pen lite readout modules. The pitch and yaw, angle and angle rate display sub-systems dissipates 5.0 watts of power. During acquisition phase, the readouts are blanked and contain zero suppression. The serial-readin, readout-angle accumulation system was designed to minimize power dissipation and circuit complexity. A time-power trade-off could be achieved, if minimum time was the ultimate criteria, by use of adder-subtractors.

#### Angle Rate Readout Display:

Angle and angle rate readout systems use similar conversion techniques. Only the design necessary to achieve the required angle rate accuracy and accumulation timing is described. Angle rate data is that contained in the pitch and yaw velocity counters and is read serially into an up-down binary 13-bit accumulator coincident correction time. Factors influencing the angle rate accuracy are as follows: angle rate resolution = 1 vel return pulse which equals 1/4 track step or 0.0009375 degree. Resolution used for angle rate readout is 1/2 track step or 0.001875 degree. An angle rate of 0.001875 degree integrated for a period of 1.875 seconds yields an angle rate equivalent to 0.001 degree seconds. This is the least significant bit in the decimal readout display. One angle rate sample will be generated each 64 ms, taking into consideration a 1kHz transmit mode. This equals 15.625 samples/second or 29.296 samples/for integration period of 1.875 seconds. It is practical, for circuit considerations, to integrate an even number of samples, therefore, 29 samples are accumulated over a 1.856 second period. This results in a 29/29.29 sample ratio or an angle rate error of -1 percent integrated period. A maximum of  $\pm 464$  ( $\pm 16 \times 29$ ) angle rate increments can be accumulated, per integrated period giving a maximum angle rate readout of  $\pm 0.464$  degree/sec accurate to -1 percent or 0.00464 degree/sec. This is equal to an angle rate accuracy of -0.08 mrad/sec. Angle rate smoothing

occurs coincident with track scan angle rate correction time. Angle rate readout data is upgraded in the debase register each 29 samples as detected by the angle rate control counter. The control counter is a mod 30 counter; 29 smoothing samples and one readout. For the 10 kHz mode a mod 10 counter in tandem with the mod 30 is used to sense the 293 sample period. This yields an angle rate accuracy of  $\pm 0.034$  percent. At an angle rate of  $\pm 0.4688$  degree/sec, the angle accuracy equals  $\pm 0.0027$  mrad/sec. At the maximum angle rate of  $\pm 4.688$  degree/sec, the accuracy will equal  $\pm 0.027$  mrad/sec.

#### 5.1.5 Mechanical

##### 5.1.5.1 Transmitter/Receiver Configuration

The optical radar transmitter/receiver components are located in the sensor package mounted to the X-band antenna gimbals. The components are arranged as shown in Figure 5-20.

##### Receiver Components:

The collecting optics, phototube, phototube coils, and magnetic shield are precisely located with respect to each other. (See Figure 5-20). It is essential that the alignment of these items be exact and lasting. The lens assembly, phototube, coils and shield are aligned at assembly and potted solidly into the mount which is rigidly attached to the housing.

##### Transmitter Components:

The transmitter components consist of the laser itself, those optics required to properly shape the emitted beam, and the two diagonal flats utilized to transfer the laser beam to the optic axis of the receiver system. These components are mounted to the same base as the receiver components. Once the initial alignment and boresighting has been completed, the entire transmitter/receiver unit is solidly locked in position.

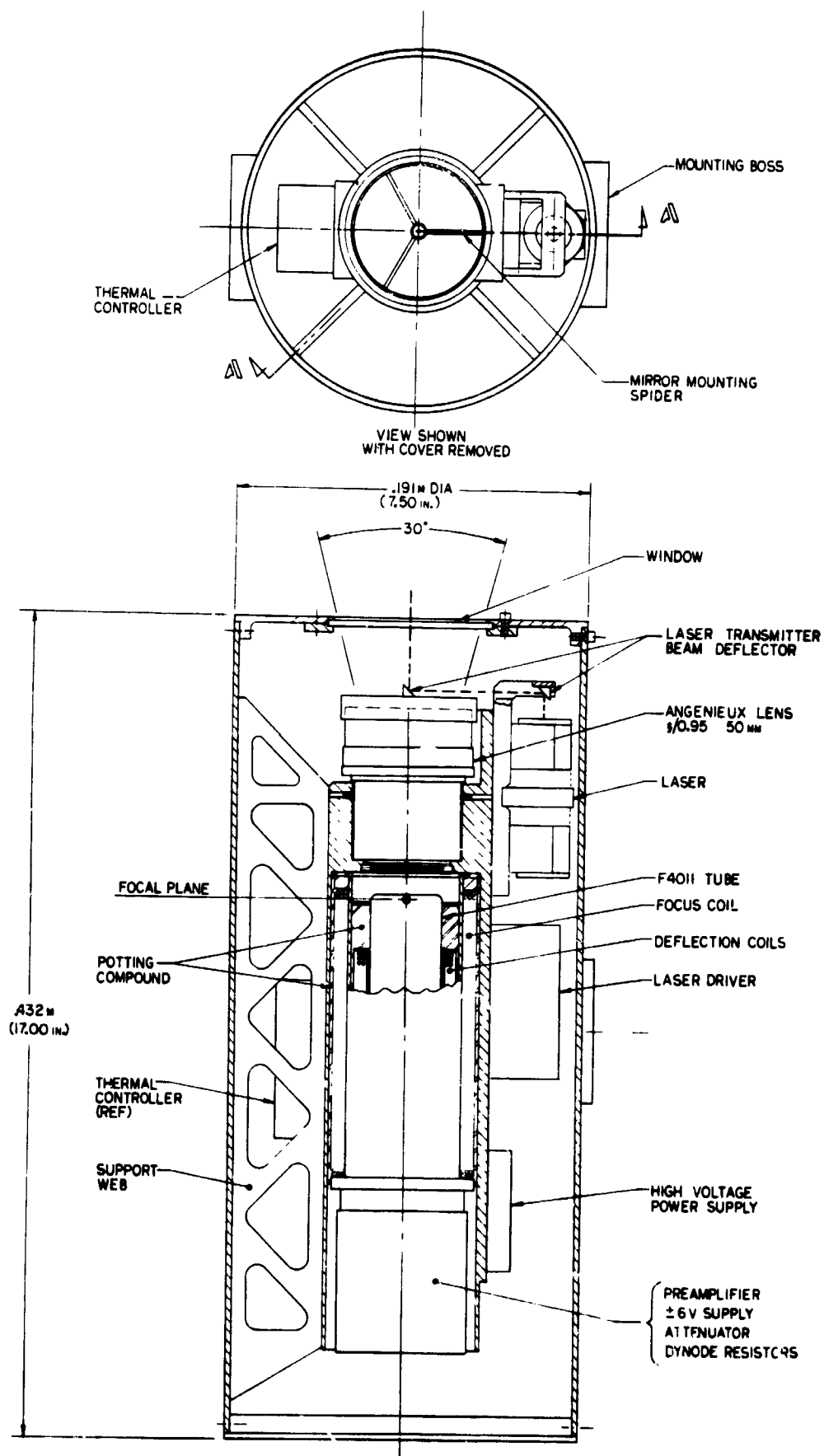


Figure 5-20. Transmitter/Receiver Configuration

The remaining components located in the sensor package are the laser driver electronics, the phototube preamplifier, dynode resistor string, high voltage power supply, attenuator and thermal sensing unit. The tentative material choice for the sensor package is 6061 aluminum. Since the sensor head is to be maintained at a near constant temperature while it is in use, thermal expansion/contraction does not appear to be a significant problem. The system does undergo fairly large temperature excursions when it is not in use; allowances must be made for these.

#### 5. 1. 5. 2 Electronic Packaging

With the exception of those few units located in the sensor package itself, all electronics are contained in a 0. 15 meter x 0. 15 meter x 0. 30 meter package (6 in. x 6 in. x 12 in. ) located in the spacecraft. This on-board unit is totally enclosed and is packaged utilizing normal, flight-proven techniques. The packaging techniques preclude the possibility of high voltage breakdown as well as the normal environmental restraints imposed upon any hardware purported to be spaceflight worthy.

#### 5. 1. 5. 3 Thermal Aspects

The on-board electronics and the sensor package are the two significant areas of concern thermally. Each of these is discussed below.

##### On-Board Electronics:

The on-board electronics dissipate approximately 15 watts of power as heat. The preferred thermal control mode is to conduct all internal heat to the mounting flanges and then to a cold rail. The cold rail then conducts the heat away.

#### Sensor Package:

The thermal restraints concerning the sensor package are more demanding than those of the on-board electronics. Since the laser undergoes a wavelength shift of  $2.5 \frac{\text{\AA}}{^\circ\text{C}}$ , and the operating optical bandwidth is to be held to  $100 \text{\AA}$ , it becomes necessary to hold the temperature excursions to  $\pm 20$  degrees Centigrade from an established value.

A thermal analysis of the sensor package is detailed in Appendix C of this report. The most significant points determined by the thermal evaluation are:

1. Operating at rated power input (20 watts), and under maximum solar impingement, the sensor package reaches thermal equilibrium at approximately 23.5 degrees Centigrade.
2. With internal power ON and no solar impingement, which occurs when the sensor package is shaded by the spacecraft, the package stabilizes at approximately -89 degrees Centigrade.
3. With all power OFF and no solar impingement, such as when the sensor package is not in use and is shaded, the temperature will stabilize at approximately -157 degrees Centigrade (the environmental low).

This data clearly indicates that the sensor package is capable of operating satisfactorily in its intended environment with only passive cooling techniques being utilized. The sensor package stabilizes at nearly room temperature under simulated worst case conditions, utilizing radiative cooling techniques. The data also indicates the need for heating to stabilize the sensor package when it is in use and is shaded from the sun. The maximum heater requirement is approximately 81 watts in order to maintain a constant temperature of 3.5 degree Centigrade when there is no solar impingement at all.

An alternate approach, which eliminates the heater requirement, is to thermally insulate the internal components using highly efficient insulation material. This approach utilizes the outer shell of the sensor package to eliminate only the solar heat input. The internal components then have a constant 20-watt thermal input which can be conducted, via the supporting structure, to the two ends of the sensor package. These two ends then act as radiators to dissipate the required portion of the 20 watts.

To test the theoretical values determined for the sensor package, a thermal model was constructed and tested in the ITTA space simulator. A close correlation was noted between the predicted temperature extremes and the actual values measured. A complete discussion of the thermal model is included in Appendix C.

## 5.2 BEACON/CORNER CUBE REFLECTOR/ANGLE TRACKER

This section describes the three major OGS equipment components associated with the target vehicle for the baseline system. The three components are: a beacon, a retro- or corner cube reflector, and an angle tracker. Functionally, the beacon serves as acquisition target for the chaser tracker, the corner cube reflector as the target during null tracking, and the angle tracker establishes the direction of the chase vehicle relative to the target vehicle.

### 5.2.1 Beacon

The beacon consists of a gallium arsenide diode array, timing/driver electronics, and suitable optics to provide a 10 degree by 10 degree radiation pattern at 9050 Å. The array is operated in a pulsed mode with pulse duration of approximately 50 nanoseconds. A peak power of two kilowatts occurs at a 10 kHz rate. One watt of average optical power results from this sequence. Given a conversion efficiency of 2 percent, the average electrical power required for the beacon during acquisition is 50 watts. While diode manufacturers



have indicated considerably higher conversion efficiencies will be available in the near term, the conservative value of 2 percent overall efficiency is being assumed at this point.

Timing and drive electronics complete the beacon equipment compliment. The laser circuitry develops the driving current by discharging a Pulse Forming Network (PFN) through the laser array. The circuitry consists of a 200-400 V power converter to charge the PFN, the PFN, and a switch between the PFN and the laser. Figure 5-21, shows schematically the beacon equipment.

#### 5.2.2 Corner Cube Reflector

The corner cube reflector has a clear aperture diameter of 10 centimeters on axis. For diffraction-limited performance, the entire prism is figured on all surfaces so as to produce a reflected wavefront distortion not to exceed the Rayleigh quarter-wave tolerance. The prism apex is truncated and polished flat to provide a 2.5 cm window through the glass for the communications receiver. A small corner reflector with a one centimeter diameter is cemented in the center of the flat rear surface in order to provide the required coaxial performance for the OGS at very short ranges.

#### 5.2.3 Angle Tracker

The target angle tracker is similar to the chaser angle tracker with the exception of providing one additional function, to turn OFF the target beacon. As the chaser acquires the target beacon, its position is slewed by gimbals until the chaser laser beam is returned by the target corner cube. The target angle tracker continues in acquisition mode until the chaser beam is acquired. When the target angle tracker acquires the chaser beam, the beacon is de-energized. Should the chaser laser beam leave the target corner cube reflector (and thus the target angle tracker also) the target beacon is automatically re-energized.

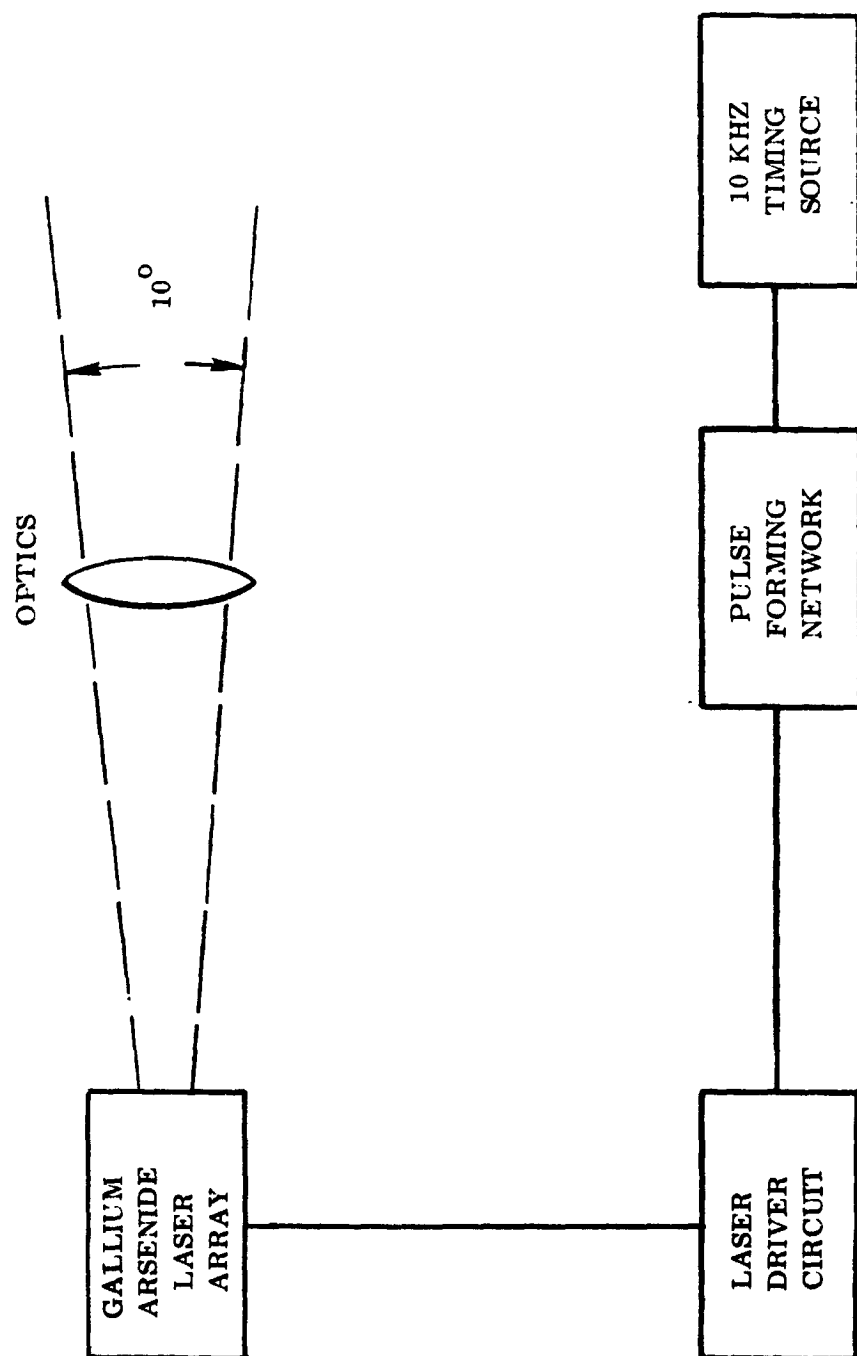


Figure 5-21. Target Laser Beacon Schematic

### 5.3 TWO AXIS GIMBAL AND SERVO CONTROL (TARGET AND CHASER)

As presented in the base-line system description, the two axis gimbaling mechanism and associated servo control has one primary purpose; to increase to a practicable maximum the solid angle in which the target/chaser line-of-sight (LOS) can be established and maintained during rendezvous and docking operations of subject spacecraft. While maintaining target/chaser line-of-sight, by responding to and nulling tracker errors, the gimbal/servo subsystem is naturally disposed to provide angle and angle rate measurements useful in rendezvous, docking or station keeping maneuvers. This being the case, the primary measureables of PITCH, YAW (or other appropriate angle) and their associated rates will generally be derived from the transducer within the gimbal/servo subsystem.

It has been ITTA intention and desire to utilize existing space-qualified gimbals supporting the RCA rendezvous radar dish on the LEM since they presently represent the most desirable existing hardware. The RCA gimbals provide 7.54 steradians of non-overlapping coverage in two modes of operation. The two-mode approach provides a suitable means of stretching angular coverage without suffering gimbal lock or operating at angles critically near the "Key Hole." One slightly awkward situation results from the two-mode operation in that different vehicle-related angles are measured in the two modes. This situation (and angular freedom in each mode) is clearly shown in Figure 5-22. In Mode I, the YAW and ROLL angles are sensed as against PITCH and YAW in Mode II. Suitability of the RCA gimbals for the ITTA OGS can only be determined by an intensive investigation of the gimbal details in light of performance requirements assigned to the proposed gimbal subsystem. These requirements are delineated in the next paragraph. Following the performance requirements is a technical discussion of the backup gimbal configuration being considered should the RCA gimbals prove unsuited to the application. This backup configuration will also

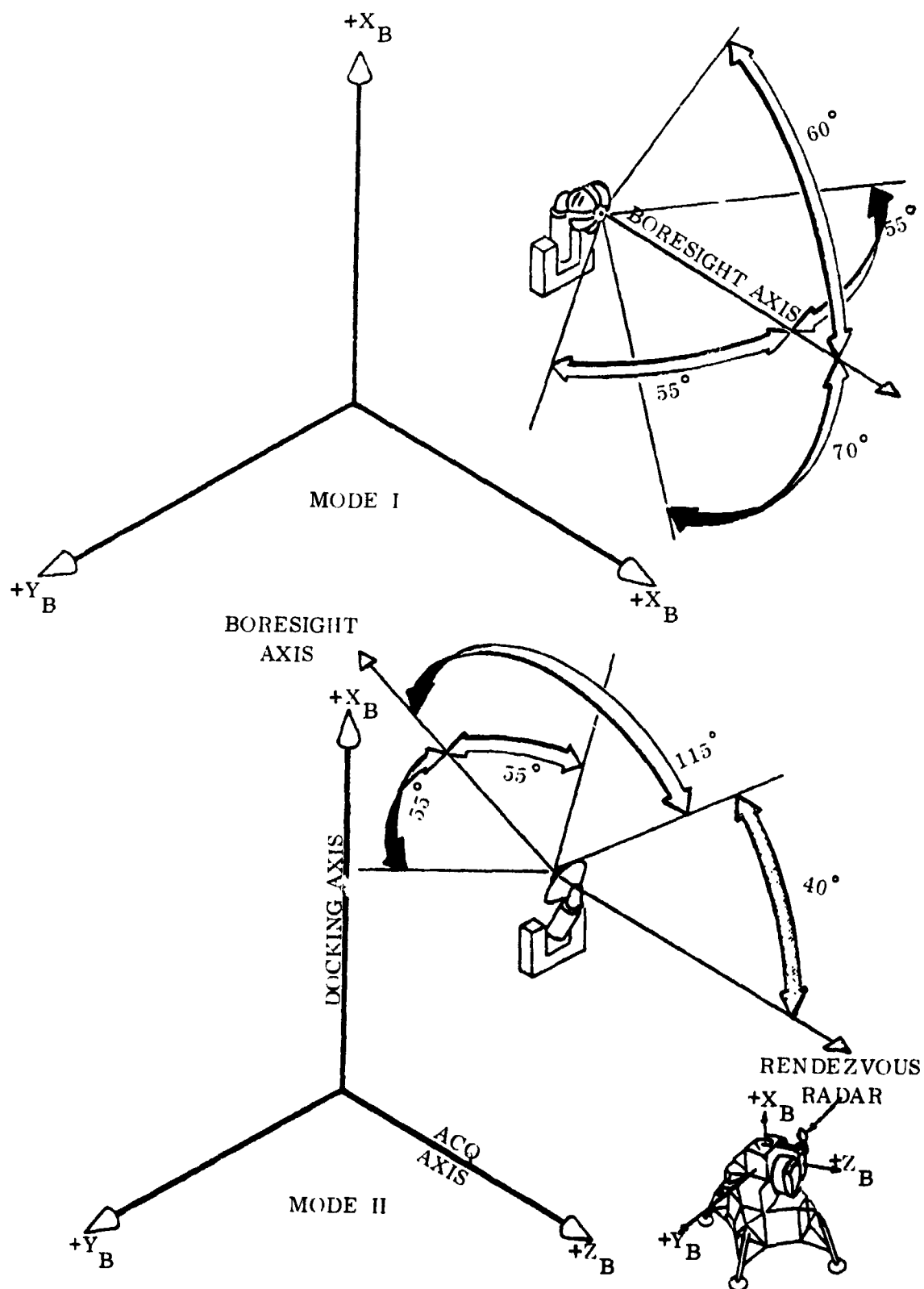


Figure 5-22. Limits for Performance, Rendezvous Radar Angular Coverage

serve as the basis of the servo design and analysis for two reasons. First, no design detail is available for the RCA gimbals. Second, little, if any, organic change to the servo would result should the RCA system prove suitable.

#### 5.3.1 Gimbal Specifications

The back-up two-axis gimbal is shown in Figure 5-23 and Table 5-1 is a list of the technical performance specifications.

##### Gimbal Type

The gimbals will be the so-called X-Y type. This configuration is chosen to avoid servo control ambiguities which can result with the azimuth over elevation gimbals for installation locations named previously.

##### Total Angular Coverage

The total angular coverage is determined by constraints which are discussed in a later paragraph. The actual angles provided are  $\pm 70$  degrees for the inner gimbal and  $\pm 120$  degrees for the outer gimbal. An additional  $\pm 15$  degrees is provided on each axis by the optical coverage of the tracker.

##### Tracking Rate

The tracking rate of 10 degrees/second should allow tracking all anticipated targets.

##### Acceleration

The acceleration rate is 20 degrees/second<sup>2</sup>. This value will provide adequate capability with acceptable torque requirements.

##### Slewing Rate

The slewing rate is 20 degrees/second which permits acquisition of any target within the angular coverage of the gimbals plus the angular coverage of the tracker, within 13.5 seconds maximum.

##### End of Travel Provisions

Limit stops will be provided at maximum gimbal travel of  $\pm 70$  degrees for the inner gimbal and  $\pm 120$  degrees for the outer gimbal. Limit switches will be

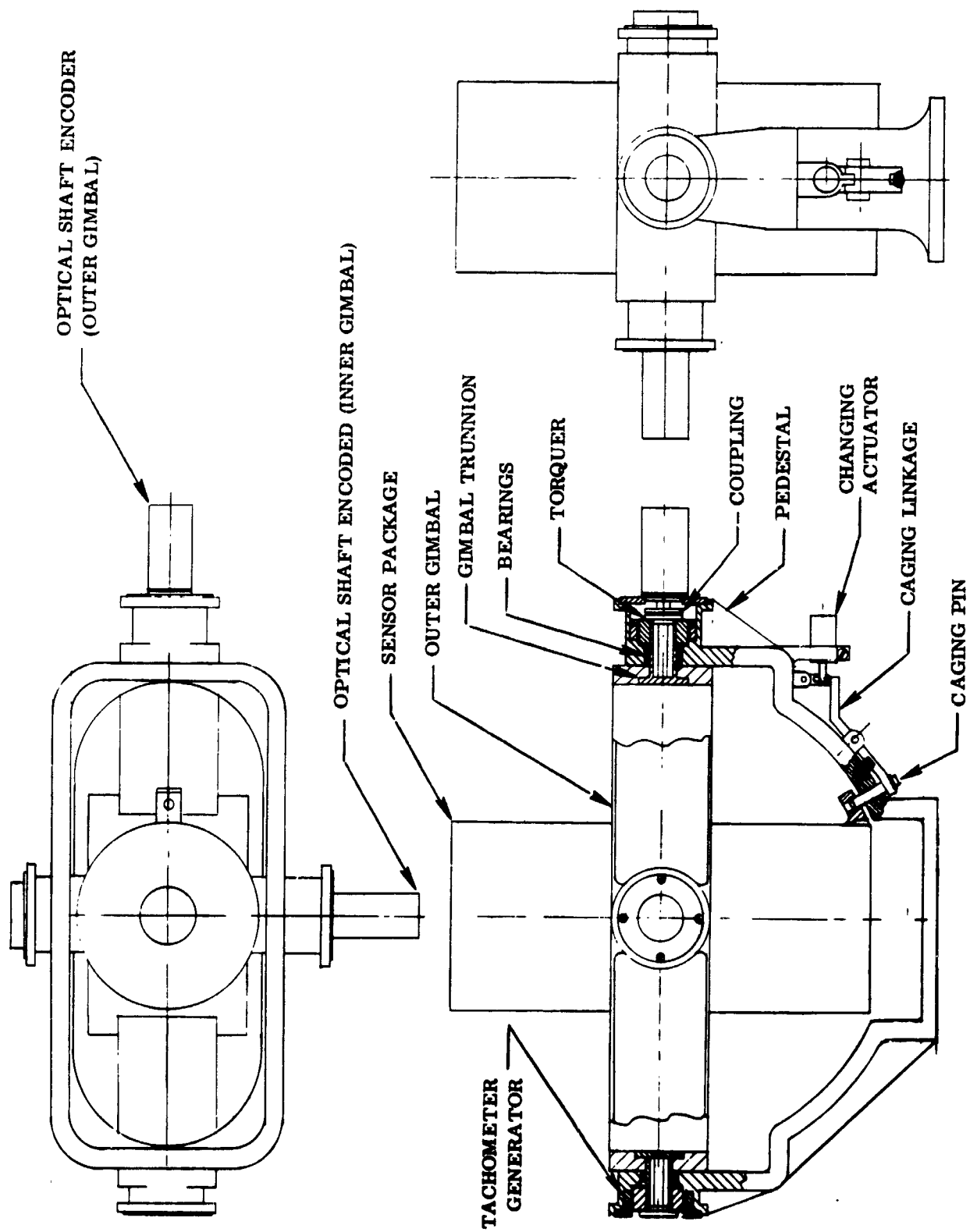


Figure 5-23. Two-Axis (X-Y) Gimbal

TABLE 5-1

TWO-AXIS GIMBAL PERFORMANCE SPECIFICATIONS

Gimbal type:	X - Y
Total angular coverage:	Outer gimbal $\pm 120^\circ$ Inner gimbal $\pm 70^\circ$
Maximum tracking rate:	$10^\circ/\text{second}$
Maximum acceleration:	$20^\circ/\text{second}^2$
Maximum slewing rate:	$20^\circ/\text{second}$
Gimbal and sensing head weight:	$\approx 40$ lbs.
Drive system:	D.C. torques and tachometers
Angle measuring devices:	Optical shaft encoders
Encoder resolution:	14 bits - 79.10 arc seconds
Encoder output:	Incremental or decoded binary
Input power:	$28 \pm 4$ V DC (30 watts peak, 12 watts average)
End of travel provisions:	Limit stops and reed switches
Alignment provisions:	Zero pins or adjustable zero plates
Caging provisions:	Solenoid actuated, nonresettable

provided in addition to the limit stops. The limit switches will consist of reed switches activated by permanent magnets mounted on the gimbals. The limit switches will be employed to limit the torque motor current when the gimbal is in the area of the limit stop.

#### Alignment Provisions

The basic alignment problem concerns the line-of-sight of the sensing head in reference to the readout of the optical shaft encoders. To facilitate this operation, the gimbals will be provided with zeroing devices which will establish a zero orientation and will be repeatable within  $\pm 2$  arc seconds. The zeroing devices will consist of flat ground plates bolted to ground surfaces on the gimbals. These will engage adjustable spring-loaded stops arranged to immobilize the gimbals in a precise and repeatable orientation. In addition to the zeroing provisions, mounting pads will be provided for optical alignment equipment. The optical shaft encoders will be mounted on adjustable mounts which will permit rotation in small angular increments.

#### Caging Provisions

The caging device will be a solenoid-actuated, non-resettable mechanism which immobilizes the gimbals with the sensing head in a vertical position and the outer gimbal level. A short voltage pulse will actuate the solenoid and withdraw a stop pin, freeing a spring-loaded lever. The spring-loaded lever will withdraw a pin which goes through the base into the inner gimbal. No provisions will be made for resetting the caging device while the vehicle is in flight. All bearings associated with the caging device will be "Rulon" manufactured by the Dixon Corporation, Bristol, Rhode Island or a similar low-friction material. Rulon bearings are a special teflon formulation with various inert materials providing support to the teflon, and minimize cold flow. Rulon bearings are capable of performing in hard vacuums, at temperatures from  $-400$  degrees to  $+500$  degrees F, and with no lubrication. The coefficient of friction of Rulon bearings which is approximately 0.10 when supporting small loads, decrease rapidly with increase in load. This characteristic makes it an ideal material where the prevention of sticking and galling is essential.



### Bearings and Lubrication

The bearings selected for the gimbals must be capable of operation in the space environment for the projected life of the system; without radical changes in friction and must provide precise positioning of the gimbal axes. The life of bearings used in spacecraft largely depend on two factors; resistance to shock loads and efficiency of the lubricant when exposed to temperature extremes, radioactivity, weightlessness and vacuum. To overcome the cumulative effects of the space environment, special radiation-resistant lubricants which do not depend on gravity flow must be used. In addition, for long-term use an efficient lubrication replenishment system must be provided.

The materials selected for the gimbals are those which will provide optimum performance under the environmental conditions noted in Section 4.0, and exhibit maximum stiffness to weight ratios. The physical properties of the candidate materials are shown in Table E-1, Appendix E.

The candidate materials are evaluated on the basis of achieving an optimized design in terms of minimum weight and maximum stability in the storage, launch and space environments.

Employing the criteria noted above, the alloys of magnesium were eliminated from contention. They do not provide a desirable weight to stiffness ratio. Appreciable sublimation of this material has been observed in high vacuums. (See JPL Technical Report No. 32-150.)

The balance of the materials are evaluated for use on the elevation gimbal since its weight and stiffness is critical. Appendix E contains detailed analysis showing deflections, stress, natural frequency and linear expansion for three of the candidate materials.

#### 5.3.2 Servo Control System

The OGS control system has two basic tasks:

- Maintain sensing head pointing, when locked onto its target source, within 0.015 degree for conditions defined in paragraph 5.3.1.

- Provide means for commanding or programming the sensing head in any direction within the range of gimbal freedom to effect target (or chaser) acquisition.

#### 5.3.2.1 Geometric Considerations

Three parameters of concern here are the angular freedom of the gimbals, the acquisition field of the sensor, and the near boresight or null tracking field of the sensor. These values are repeated here for convenience.

- Gimbal freedom:  
     Inner axis =  $\pm 70$   
     Inner axis maximum is based on outer gimbal constraints  
     Outer axis =  $\pm 120$   
     Outer axis maximum is based on estimated, unobstructed visibility for tentative installation locations.
- Acquisition Field of Sensor:  
     Full field - Circle inscribed in 30 degrees x 30 degrees square  
     Mini-scan - 0.48 degree x 0.48 degree square field.
- Null Tracking Field = 0.03 degree square field.

#### 5.3.2.2 Control Functions

To identify specifically what the control system shall supply in terms of functioning and mode control, the following is presented.

In region of free gimbals, closed-loop tracking will be that of a Type 2 system. That is, zero tracking error for steady-state rates [up to 0.1745 radians/second (10 degrees/second)].

In region of free gimbals, commands will be accepted to slew gimbals individually at rates of plus or minus 0.01745, 0.07725, 0.1745 and 0.349 radians/second, (1 degree, 5 degrees, 10 degrees and 20 degrees, respectively). Slew commands will always override closed-loop operation.

With no target present and no slew command, the gimbals will remain static by virtue of their own frictional forces and a grounded input signal.

Each gimbal will function independently. In certain cases one loop can be operated open, while the second is closed.

When a gimbal contacts a limit stop, open-loop operation for that loop is inaugurated. A programmed low-torque level is applied when this occurs to keep the gimbal against its stop. Two methods of reinstating closed-loop operation exist.

- a. Sensing an angular error sign change in the axis against its stop will reinitiate closed loop tracking.
- b. Command override by an appropriate slewing command will remove gimbal from stop and reconstitute system for subsequent target reacquisition.

Commands to enable and disable control loops will be received. Enabling or disabling can occur with or without tracker disabling.

Closed-loop operation will be initiated upon receipt of the enabling command and a target presence signal from the tracker in regions of free gimbals.

#### 5.3.2.3 Modeling of Control System

This section will define the control system in terms of components and performance models. Salient features of the components will be pointed out and transfer functions developed. Special attention will be given to the tracker in order to develop as accurate a model as practicable. Typical characteristics of performance will be presented such as a Nyquist diagram for the entire system.

##### 5.3.2.3.1 Component Block Diagram of Control System

The control system consists of the following major components: tracker, power amplifiers, gimbals containing torquers and tachometers, mode controlling logic, and suitable compensation networks for stabilizing closed-loop performance.

Figure 5-24 shows the basic relationships of these components for one axis of the control system. Generally, because of the nearly identical nature of the axes, the inner axis only will be discussed. Salient features and transfer functions of components will be discussed. Salient features and transfer functions of components will be discussed in the following paragraphs.

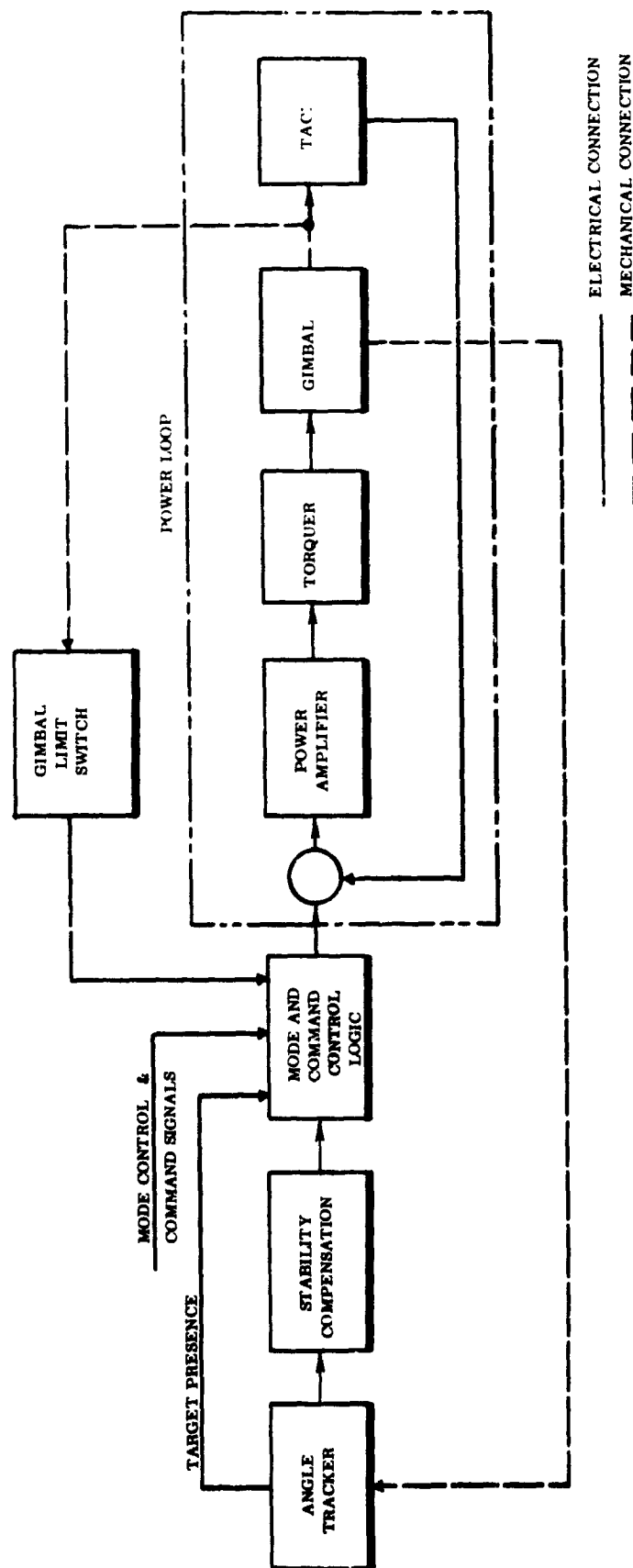


Figure 5-24. Major Component Block Diagram

### Angle Tracker

A considerable amount has already been said regarding the tracker; what it looks like, how it operates, how it develops error signals, and many other details. At this point, to develop a transfer function of the tracker, it is useful to consider it from a block diagram standpoint and to distinguish between the basic error sensor and the total closed loop tracker. Figure 5-25 will help in this regard. The Basic Error Sensor (BES) does the primary job of detecting the difference between the actual target location and the closed-loop estimate of the target location based upon previous measurements. The BES is essentially a position error detector, which develops an error signal after conducting a systematic scan of the target. Operating at a 10 kHz stepping rate for the scan, error information is available 3.2 milliseconds after scan is initiated. From a continuous system transfer function point of view the BES is a transport lag device of the form

$$KG(S)_T = K_1 e^{-\tau_1 S}, \text{ where } \tau = 3.2 \times 10^{-3}$$

seconds and  $K_1$  is a function of the units chosen. Consider now the other blocks. The proportional channel will be recognized as the range counter. The integral channel will be recognized as the velocity counter from earlier descriptions. Recalling the velocity measure (integral channel) is the first counter dumped into the track counter and D/A converter, (2nd integrator) and that its output represents an accumulation or integral of position change a nondelayed continuous transfer function can be assigned: viz,

$$KG(S)_I = \frac{K_z}{S}$$

The proportional channel or position counter is delayed 1.6 msec. Before being dumped into the track counter, hence another transport lag exists. The proportional channel transfer function is then

$$KG(S)_P = K_3 e^{-\tau_2 S}, \text{ where } \tau_2 \text{ is } 1.6 \times 10^{-3} \text{ sec.}$$

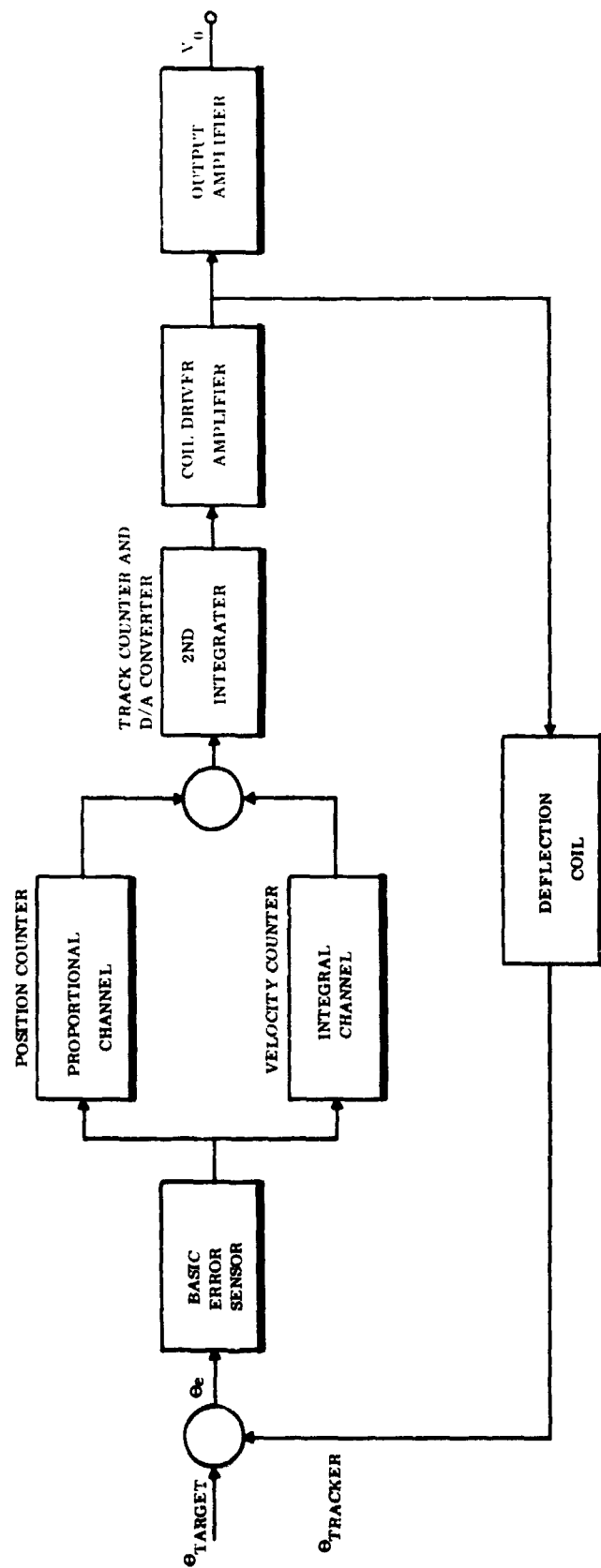


Figure 5-25. Tracker Block Diagram

No significant delays exist in the track counter and D/A converter so that its transfer function is simply  $\frac{K_4}{s}$ . This leaves the deflection coil driver, the deflection coil, and the output amplifier which to first approximations can be represented by non-frequency dependent gains  $K_5$ ,  $K_6$ , and  $K_7$ , respectively.

Units have been side-stepped purposely to this point. The reason is that the units  $K_1$ ,  $K_2$ ,  $K_3$ , and  $K_4$  are somewhat unusual, having been kept closely associated with tracker functioning and previous nomenclature. A few clarifying comments are in order.  $K_4$  is actually the combination of two gains, say  $K_a \cdot K_b$ .  $K_a$  is the second integrator gain of value equal to  $K_3$ , but with units "correction steps per correction pulse sec".  $K_b$  is the gain of the D/A converter with units "Volts Per Correction Step". Obviously,  $K_b$  is specified by the values of  $K_a$  and  $K_4$ . The unit "correction step" is equivalent to the angular displacement between the target and tracker netting one return during the scan sequence. The units of  $K_1$  are "Returns per Radian";  $K_2$  has units "correction pulses per return; and  $K_3$ , being an integrator has units "correction pulses per return seconds". Table 5-2 shows the units and value of gain for each of the tracker blocks. This completes the discussion of the salient features in block diagramming the tracker. Figure 5-26 shows the servo block diagram of the close loop tracker. Its transfer function from target angle input to volts output, and bode plot is presented in Figure 5-27.

#### Stability Compensation

Next in line of major components is compensation for realizing loop stability. This component takes the form of suitably isolated lead-lag circuits to supply the zeros necessary for stability. Synthesis of these circuits from required transfer functions is the final step in loop design since their characteristics are determined by the remainder of the system components.

#### Mode and Command Control Logic

This block, shown following compensations in Figure 5-24 has no servo transfer function as such. It is defined to indicate the point at which mode control will be exercised. The source of control for the power loop, be it external command or from the tracker, is decided by the logical state of this block. Note that its

TABLE 5-2

## TRACKER GAIN UNITS AND VALUES

<u>Component</u>	<u>Symbol</u>	<u>Units</u>	<u>Value</u>
Basic Sensor	$K_1$	$\frac{\text{Returns}}{\text{Radian}}$	$61.1 \times 10^3$
Proportional Channel	$K_2$	$\frac{\text{Correction Pulses}}{\text{Return}}$	1.0
Integral Channel	$K_3$	$\frac{\text{Correction Pulses}}{\text{Return sec.}}$	156.2
Track Counter & D/A Converter	$K_4$	$\frac{\text{Volts}}{\text{Correction Pulse Sec}}$	0.0488
Coil Driver	$K_5$	$\frac{\text{Amps}}{\text{Volt}}$	0.015
Deflection Coil	$K_6$	$\frac{\text{Radian}}{\text{Amp}}$	3.5
Output Amplifier	$K_7$	$\frac{\text{Volts}}{\text{Amp}}$	3,330

inputs come from three sources: 1. external commands, 1. angle tracker, and 3. gimbal limit switches. All the functional options specified will be programmed by this component.

#### Power Amplifier

The power amplifier is the first element of the power loop and has the task of converting the low-level signals from the tracker and tachometer feedback to signals of sufficient level to drive the torquer. Amplifier bandwidth is sufficient to allow a simple gain  $K_8 \frac{V}{V}$  to represent its transfer function.



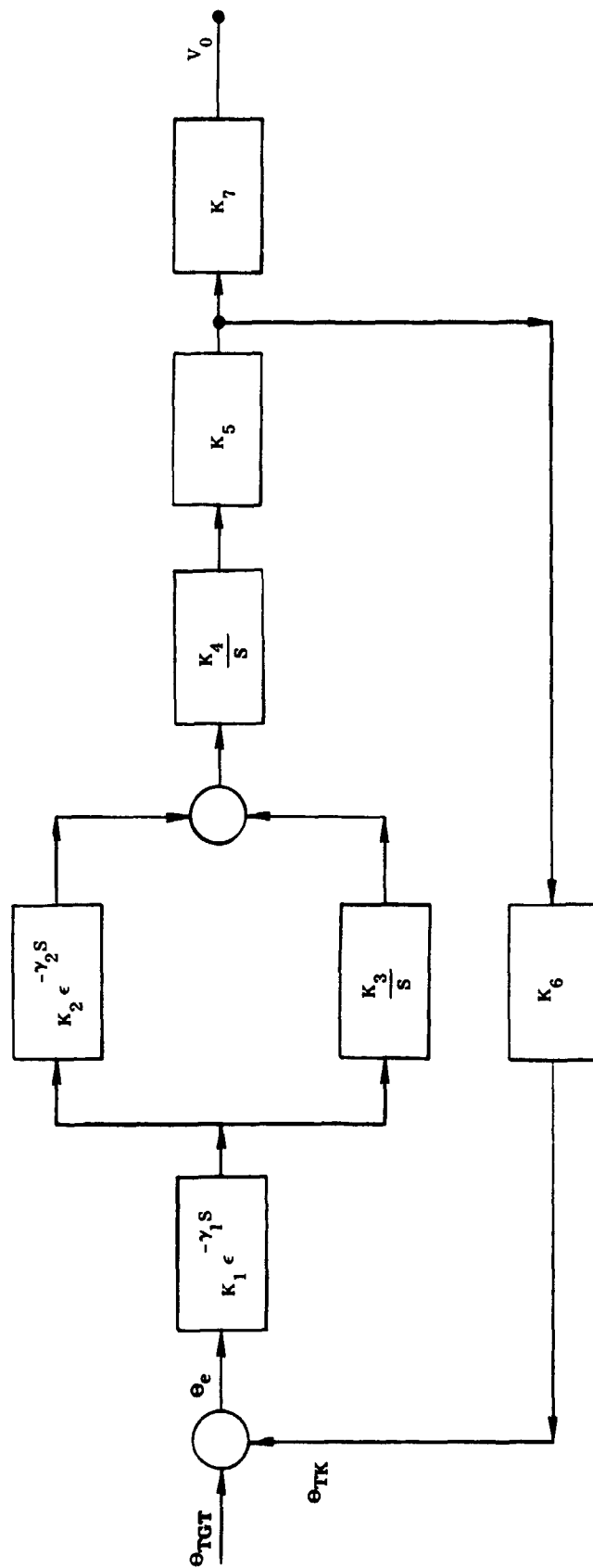


Figure 5-26. Tracker Servo Diagram

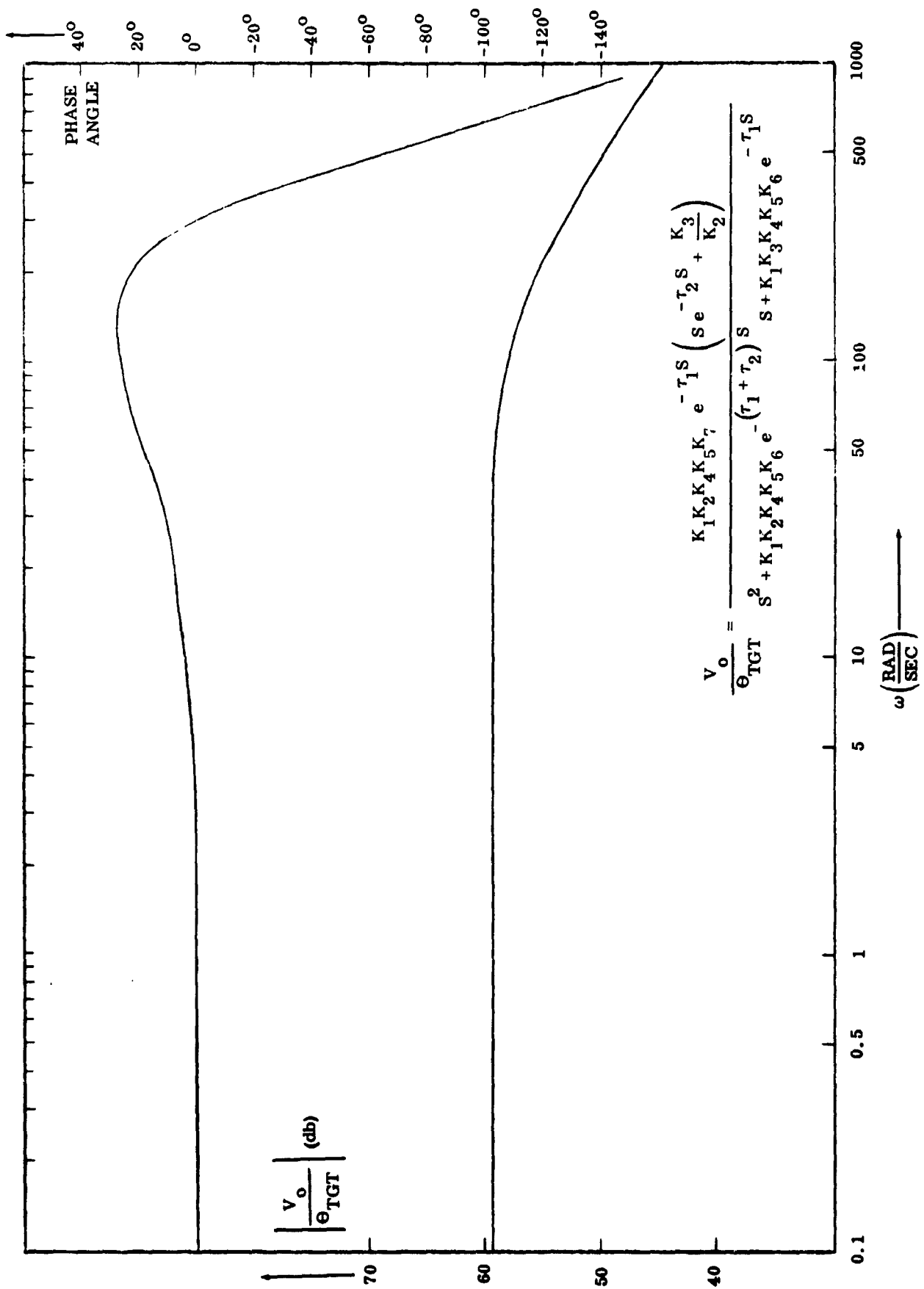


Figure 5-2.7. Tracker Transfer Function and Bode Plot

### Torquer

The general characteristics of the gimbal torquers have been adequately covered. Here the transfer function is defined. Considering the inland T-2170-D with low impedance power amplifier.

$$\frac{T}{V} = \frac{.0122}{S+1000} \frac{\text{ft lb}}{\text{volt}}$$

### Gimbal

Gimbal polar moment of inertia alone is of concern at this point.

$$J_G = .12 \text{ ft lb sec}^2,$$

since  $T = \alpha J = \frac{d\dot{\theta}}{dt} J$ , and  $T(s) = s \dot{\theta}(s) J$

then  $\frac{\dot{\theta}}{T}(s) = \frac{1}{Js}$

### Tachometer

Again, only the transfer function of the inland tachometer TG-2138A is of interest. Providing the tachometer drives a 70K load, the transfer function is simply:

$$\frac{V}{\dot{\theta}} = 2.20 \frac{\text{volts sec.}}{\text{radians}}$$

This completes detailing the loop component characteristic. Table 5-3 summarizes these results and Figure 5-28 provides the control block diagram of the complete loop, less logic operations. The loop compensation is set at unity for uncompensated conditions.

#### 5.3.2.3.2 Open-Loop Transfer

The open-loop transfer function  $[KG(S)]$  for the system shown in Figure 5-28 is presented below. Two simplifications are included:  $KG_T(S)$  is not expanded, and  $KG_C(S)$  is set equal to unity.

TABLE 5-3

## LOOP GAIN UNITS AND VALUES

<u>COMPONENT</u>	<u>SYMBOL</u>	<u>UNITS</u>	<u>VALUE</u>
Tracker	$KG_T(S)$	$\frac{\text{volts}}{\text{radian}}$	950 (D. C.)
Compensation	$KG_C(S)$	$\frac{\text{volts}}{\text{volt}}$	Unity (for uncompensated loop)
Power amplifier	$K_8$	$\frac{\text{volts}}{\text{volt}}$	Variable
Torquer	$\frac{K_T}{S + }$	$\frac{\text{ft lb}}{\text{volt}}$	$\frac{.0122}{S + 1000}$
Gimbal	$\frac{1}{JS}$	$\frac{\text{rad/sec.}}{\text{ft lb}}$	$\frac{1}{.012 S}$
Tachometer	$K_G$	$\frac{\text{volt sec.}}{\text{radian}}$	2.20

$$KG(S) = KG_T(S) \cdot \frac{\frac{K_8 K_T}{J}}{S \left( S^2 + \alpha S + \frac{K_8 K_T K_G}{J} \right)}$$

From this expression the Nyquist Diagram of Figure 5-29 is obtained. It is noted that for the first order approximation, the system is stable with rather good characteristics.

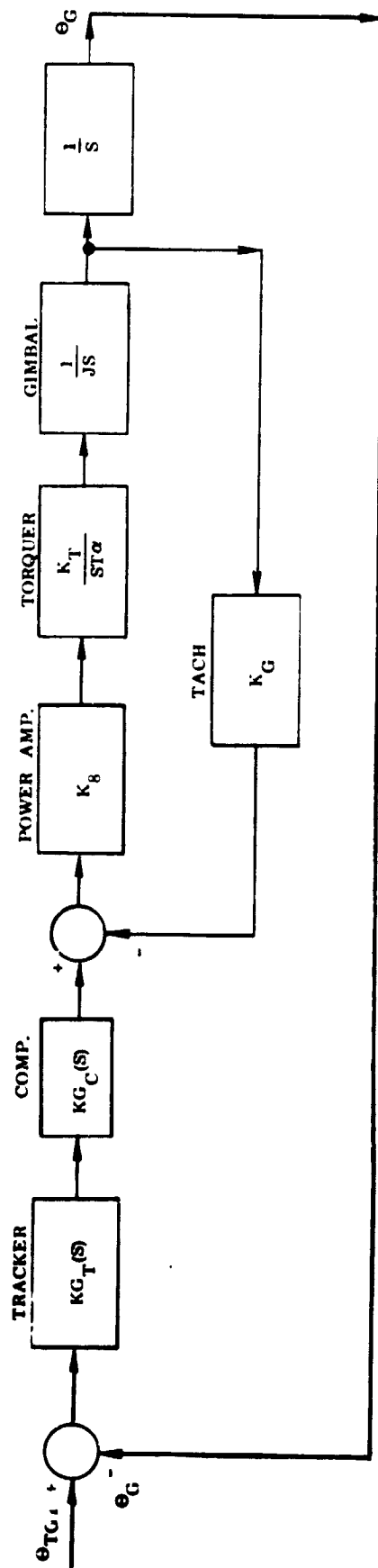


Figure 5-28. Total Loop Servo Diagram

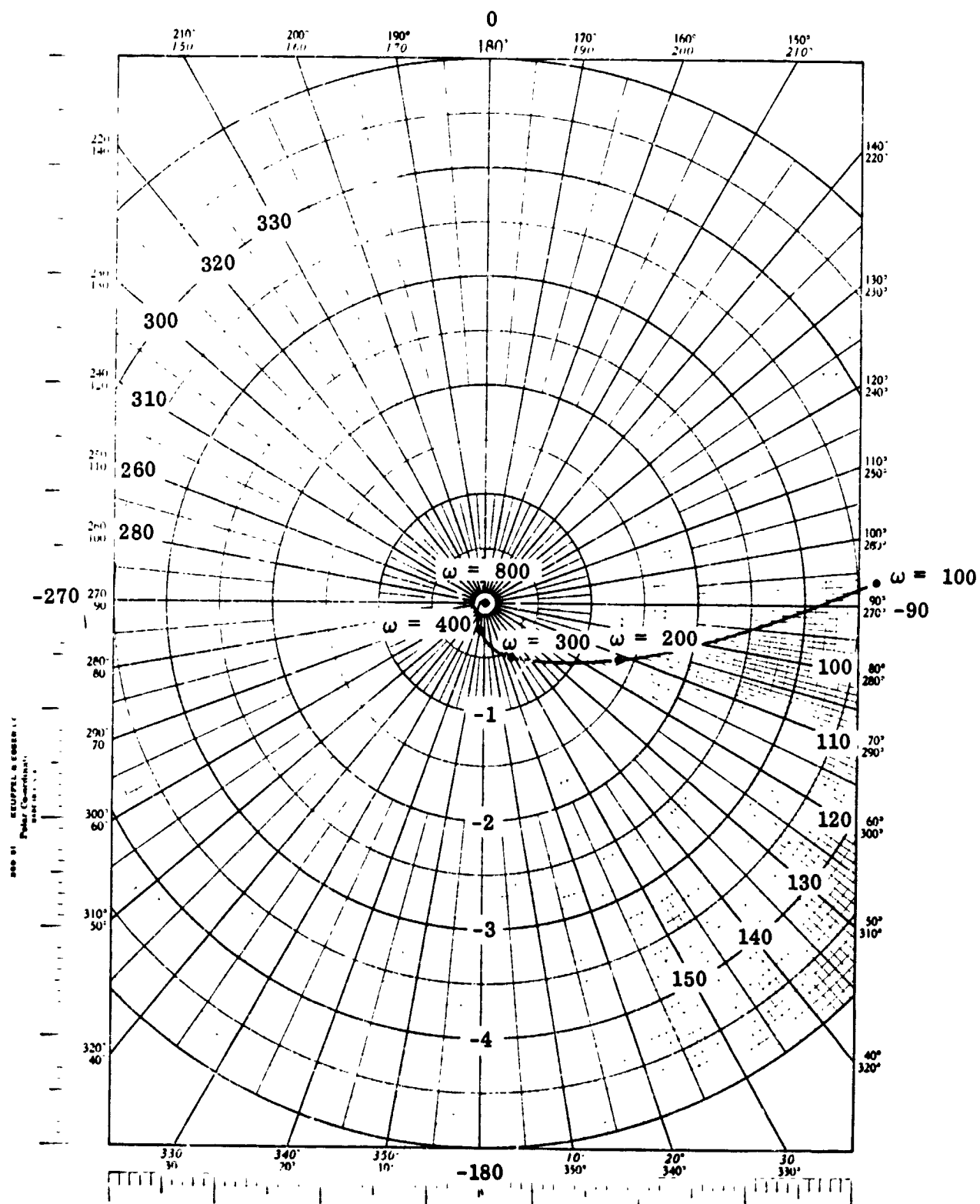


Figure 5-29. Nyquist Diagram of Open Loop Control System

#### 5.3.2.3.3 Hybrid Block Diagram of System

The hybrid block diagram, Figure 5-30, is presented to give a detailed overview of the complete control function including various modes of operation. The relay switching shown is for schematic purposes only and does not necessarily indicate that relays are actually used.

#### 5.3.3 Angle, Angle Rate Sensing and Data Display

Two sources of angle and angle rate measurements exist in the OGS; the angle tracker and the digital shaft encoders. Angle and rate data available from the tracker are, naturally, measured with respect to the null axis of the tracker, hence, in a gimballed system, where axis dynamics are likely, this data will not generally represent the total quantities involved. In fact, for the system configuration defined above, except in unusual cases, the tracker will function very near null. For the vast majority of operational situations, the angle and angle rate derived from the digital shaft encoders will supply the total set of angular information. The primary unusual case is where a gimbal stop is reached and the chaser tracker follows the target beacon off null to the 15 degree extreme possible in the off axis track mode. Since this can be a useful procedure, display of off axis angle would be desirable.

With respect to the type, quantity, and quality of display for angle and angle rate, ITT/A/OD is completely open because the method of display is closely correlated to the function it is to serve. As an example, should the data be used for information only, depending upon the precision desired, either a digital or an analog display is possible. On the other hand, if the data was for use in manual docking, a two-speed analog display would be most appropriate.

#### 5.4 THIRD AXIS ANGLE SENSOR (ROLL INDEXING FOR DOCKING)

##### 5.4.1 Performance Requirements

A null sensing device capable of indicating roll alignment between spacecraft to within 10 degrees is presently needed for the AAP missions. The device should be capable of operating at ranges from at least 1000 feet down to docking in order to facilitate proper docking orientation during the final stages of closure. Moreover the device should be capable of indicating the amount and direction of roll

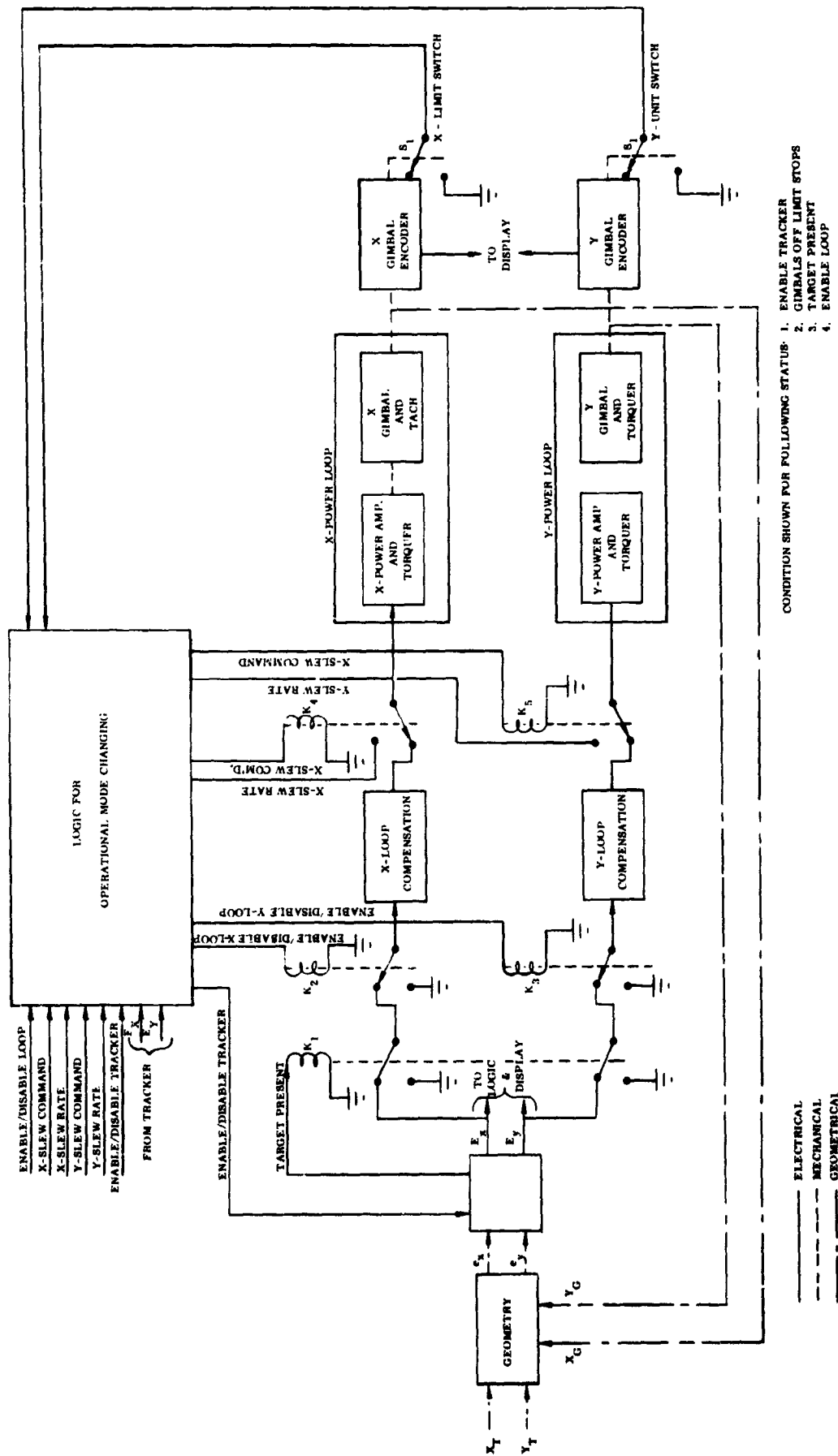


Figure 5-30. Hybrid Block Diagram of Control System



misalignment in a comparatively linear form at least over a limited range in order to provide satisfactory response characteristics to the overall roll-alignment servo loop.

#### 5.4.2 Sensor Description

The basic OGS roll sensing subsystem consists of three fundamental elements in addition to the data processing equipment as described in the following paragraphs.

A single GaAs laser diode emitting 10 watts of peak optical power into a beam approximately 20 degrees in diameter (no collecting optics are required). The prf and phasing are so selected as to circumvent any confusion with other optical sources.

A pair of small receivers located adjacent to the main receiver aboard the chaser vehicle, each utilizing a one-inch aperture f/3 lens imaging upon a 4 millimeter square silicon detector; thereby providing a field-of-view of approximately 50 milliradians square. In addition, both receivers have a polarizing filter situated in front of the lens. The plane of polarization of the two filters are mutually perpendicular. Thus, when one receiver senses a null, the other receiver detects a maximum.

A matrix for combining the video outputs of the two detectors to produce sum and difference channels. The utilization of these signals is discussed below.

#### 5.4.3 Data Processing

Figure 5-31(a) shows a plot of the outputs of the two receivers as a function of roll angle. Here, the levels indicated refer to the envelopes of the pulse train from the diode as seen by receivers A and B. In order to generate a satisfactory roll error voltage, it is necessary first to generate sum and difference signals. These are plotted in Figure 5-31(b). However, before this matrixing is accomplished, the A and B channel signals pass through sample and hold circuits which convert them to continuous DC signals (see Figure 5-32). It should be noted that AGC can be accomplished by use of the sum channel to provide a feedback reference to both channels. The signal levels can be completely normalized for variations due to range, alignment factors, etc. If a second order loop is employed for the AGC, an error voltage is generated by comparing the

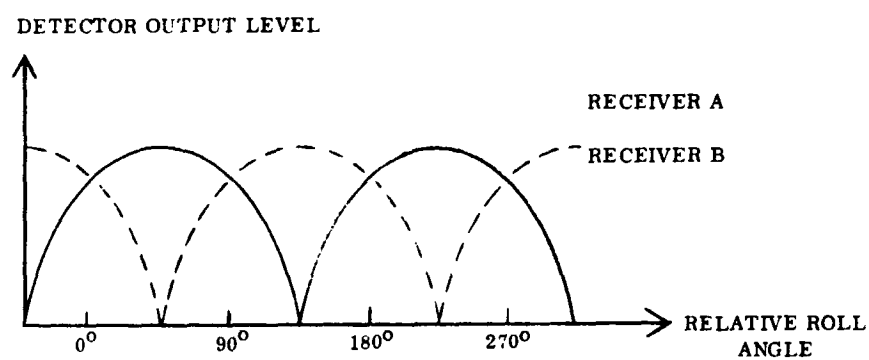


Figure 5-31(a). Roll Detector Outputs Versus Roll Position

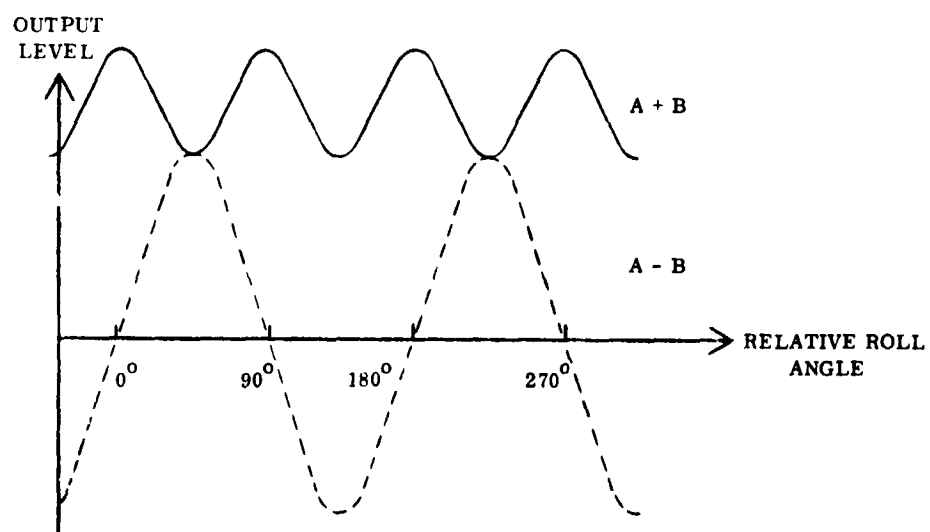


Figure 5-31(b). Sum and Difference Channel Outputs Versus Roll Position

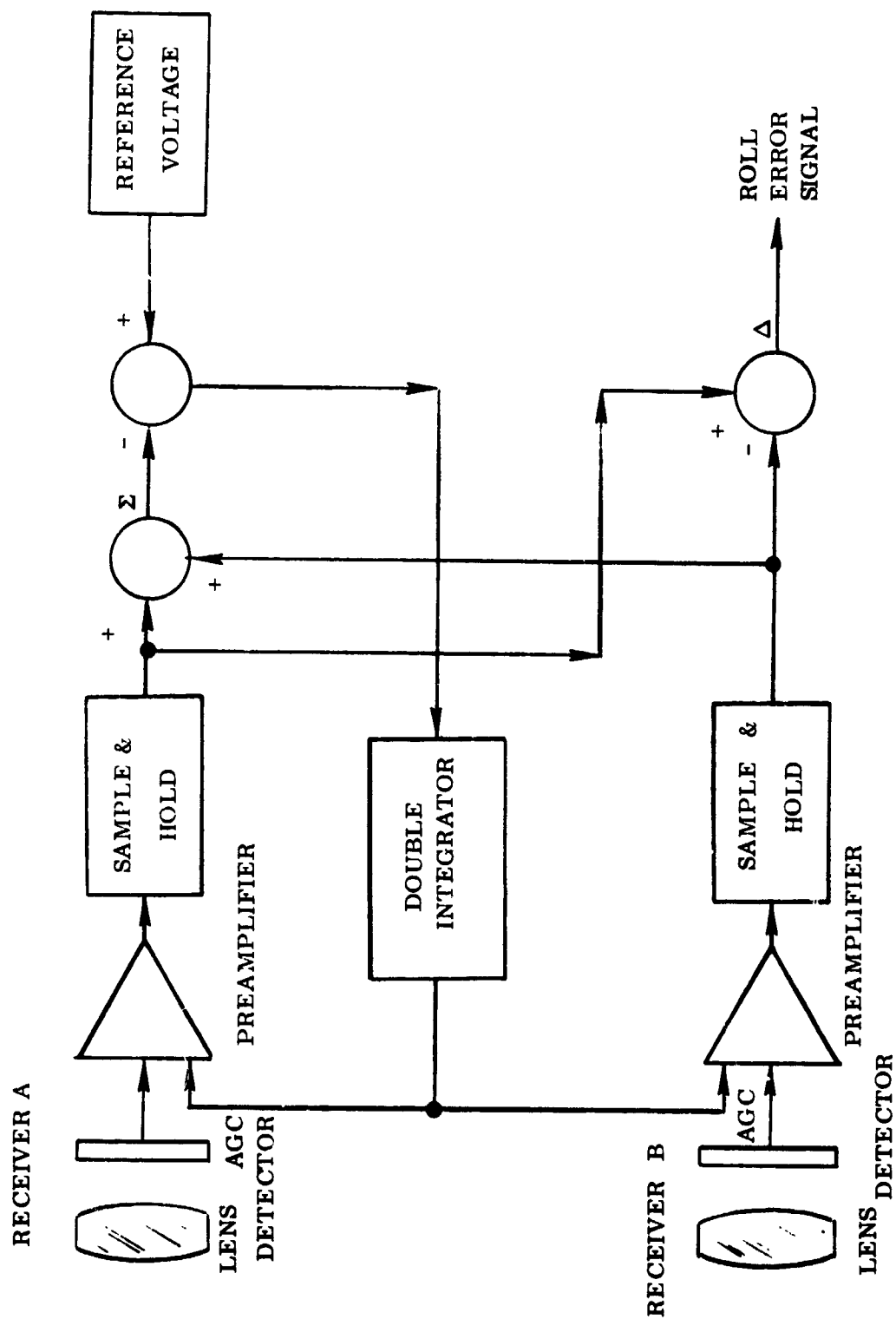


Figure 5-32. Roll Detector Data Processing

sum signal to a fixed reference voltage and feeding back the difference signal through a double integrator which makes the system a second order, servo loop. The output of the double integrator is used for an AGC signal by both receiver preamplifiers. The resultant difference signal is thus normalized and may be used as the final error signal. Not only does the AGC loop referenced to the sum channel normalize the signal level at the final output, but linearity is increased since the sum channel voltage is minimal when the difference channel voltage is at a maximum. Consequently the AGC "stretches out" the peaks of the difference channel and thereby makes the slopes more nearly linear. Of course this system is capable of operating only over a limited range, between approximately -40 degrees and +40 degrees. The fine roll alignment system just discussed should be capable of providing alignment of the roll axes on the order of 1 degree.

#### 5.4.4 Mechanical Considerations

Due to the comparatively large fields-of-view of the receivers, mechanical boresight alignment will not be as critical as in other portions of the OGS. However, alignment of the polarizing filters should be accomplished accurately, since this is the principal mechanical factor limiting the ultimate accuracy of the system. Due to the compact nature of the roll measurement components, excellent mechanical alignment and stability should be easily achieved.

### 5.5 COMMUNICATION SUBSYSTEM

#### 5.5.1 Performance Requirements

The communications subsystem gives reliable two-way transmission of data utilizing a digital format. Transmission is required only after the chaser's digital angle tracker is tracking the signal returned from the corner cube.

One configuration requires the transmission of data measured by the chaser radar to the target. A typical set of data and the number of digits for each is shown in Figure 5-33. Roughly 150 binary bits (including data, identification signal and parity bits) will suffice to communicate all seven measurements. If the information were to be used for display purposes where the data is changed once a second, then a data rate of 150 bits/second is sufficient. If instead the

IDENTIFICATION SIGNAL	DATA	NO. DIGITS
000	Range	8
001	Range Rate	5
010	Pitch Angle	4
011	Pitch Angle Rate	3
100	Yaw Angle	4
101	Yaw Angle Rate	3
110	Roll Angle	3

Figure 5-33. Typical Data Generated by Tracker for Transmission

data is to be used for automatic rendezvous and docking, then a set of data may be needed every tenth of a second which means a 1500 bits/second, data rate. In addition the communication subsystem can be used for turn ON - turn OFF commands, or any other function that can be transferred into a digital format.

The data rate is limited by the maximum pulse repetition frequency of the transmitter. If a 10 kHz transmission rate is used, then a data rate of 9000 bits/second is possible leaving the remaining 1000 pulses for ranging and angle tracking.

#### 5.5.2 Subsystem Description

The communications subsystem utilizes the two existing transmitters; the radar laser aboard the chaser and the beacon aboard the target vehicle. Very large advances are being made in Ga As laser technology which will permit substantial increases in frequencies of uncooled diodes (prf). For this reason, it will be possible to handle large data rates while these transmitters are also performing their normal functions.

The two main communications receivers are identical and employ 50 mm, f/2 collecting optics. The detectors are photomultiplier tubes with S-1 photocathodes. In addition, each photomultiplier has an electron aperture with a diameter of 25 microns. This provides each receiver with a 0.03 degree field-of-view. In addition, the receiver aboard the chaser vehicle is augmented with a small, wide-angle receiver for short range (less than 5 kilometer operation). This is necessary, since both the receiver aboard the chaser vehicle and the beacon which it observes are not coaxial with the main system. In most cases, this will cause the beacon to pass out of the field-of-view of the main receiver at short ranges. On the other hand, the 0.03 degree field of the main receiver is required at long ranges in order to see the beacon against a sunlit cloud background. The short range receiver utilizes a 2.5 cm aperture lens imaging upon a silicon detector subtending a 100 milliradian square field. A schematic diagram of the communications systems is given in Figure 5-34.

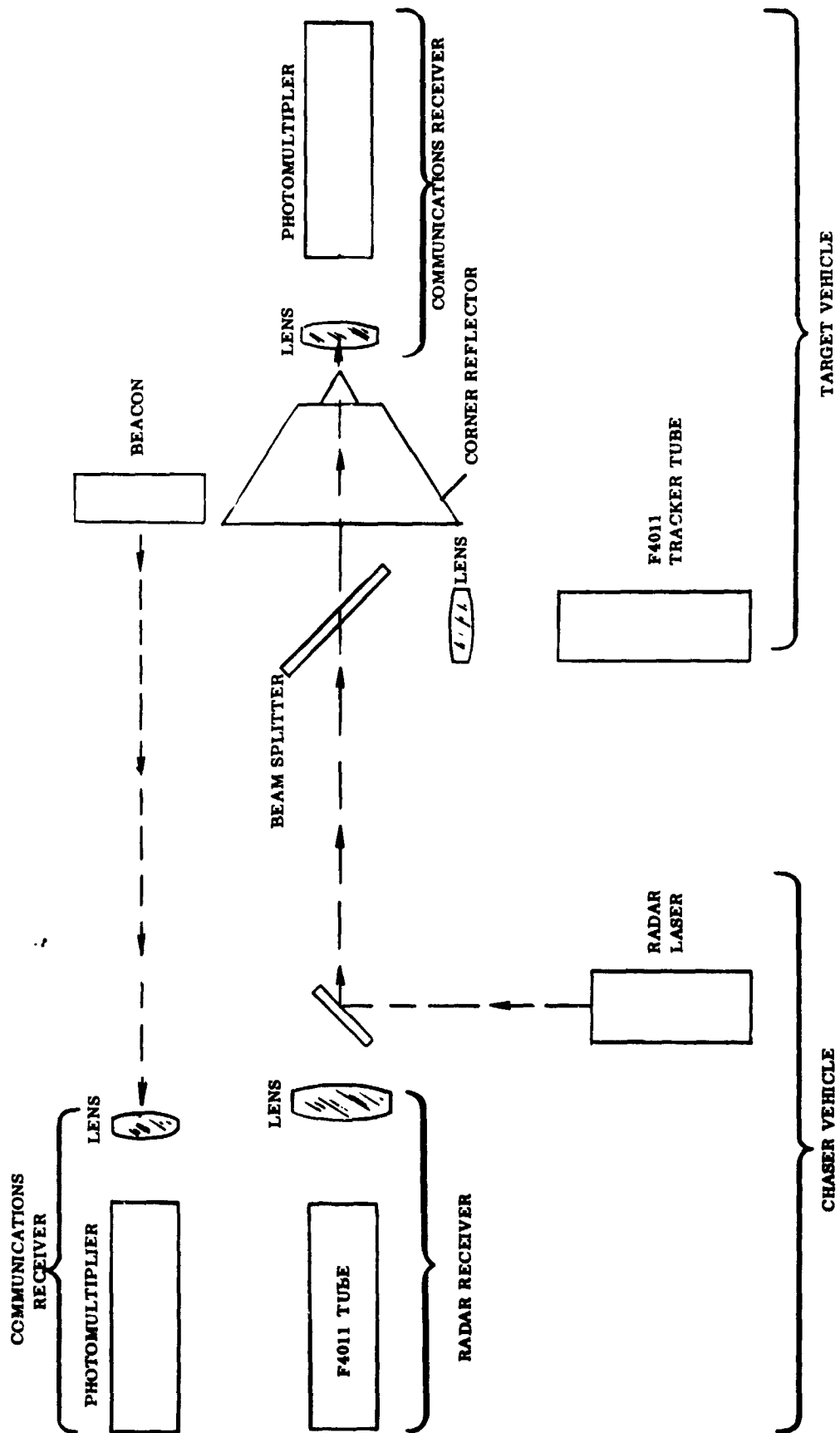


Figure 5-34. Schematic of Communication System Integrated With Tracker

### 5.5.3 Data Processing

OGS data to be transmitted is transferred in parallel into a storage register. Before the transmission of a given measurement, a signal is sent identifying the data. The last bit to be sent is a parity bit, this gives a check for errors (see Figure 5-35). At each communication receiver, a parity check network determines the validity of the incoming message. The message is then decoded according to the first few identification bits and stored in an output register. From the output register, the data is available for display or for processing by a computer.

### 5.5.4 Mechanical Considerations

Of paramount importance in fabricating the communications system hardware is the problem of accurately boresighting the two 0.03 degree field receivers so that their axes are accurately parallel (to within about 2 arc minutes) to the boresight axes of the associated radar assemblies. In addition, the hardware mountings must be sufficiently stable to maintain this alignment during launch and during the severe temperature changes which can occur in space.

## 5.6 INTERFACE REQUIREMENTS

### 5.6.1 Mechanical

#### 5.6.1.1 Mounting Conditions and Surface (Alignment Ref., Etc.).

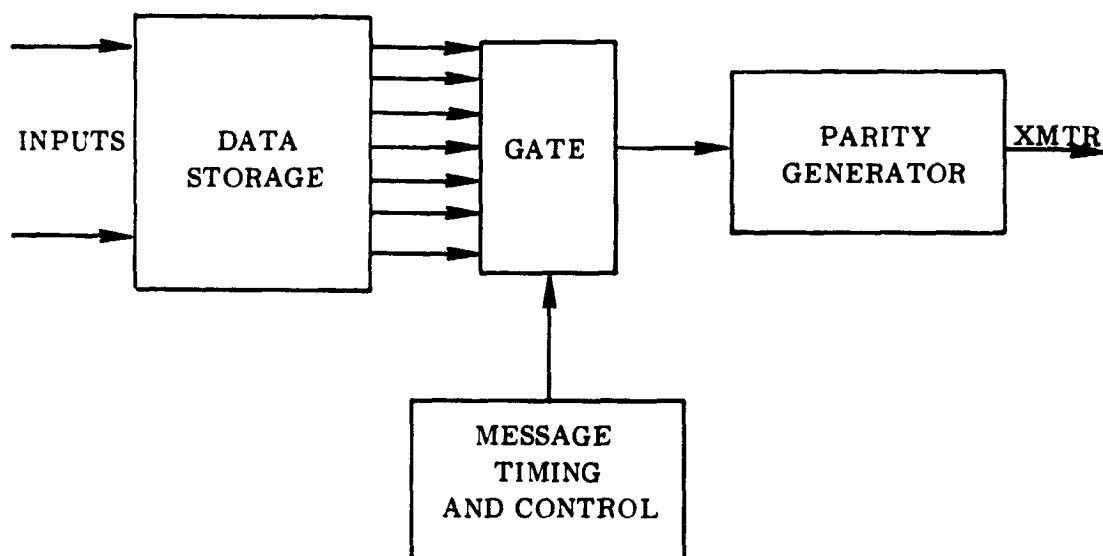
Present philosophy dictates the utilization of existing x-band radar antenna gimbals for mounting of the sensor package. An alternative approach is to design a new set of gimbals to best utilize the capabilities of the OGS. The two alternate approaches demand two different sensor package mountings:

Sensor package mounting utilizing x-band radar gimbals.

This approach requires that the sensor package be mounted as shown in Figure 5-36. The package is mounted in place of the x-band radar antenna, atop the cylinder that makes up the inner gimbal. The sensor package boresight then has the same viewing capabilities as the x-band radar. The weight of the sensor package is approximately one-half the weight of the x-band antenna. It is, therefore, well within the capabilities of the existing gimbals.



DATA TRANSMISSION:



DATA REDUCTION:

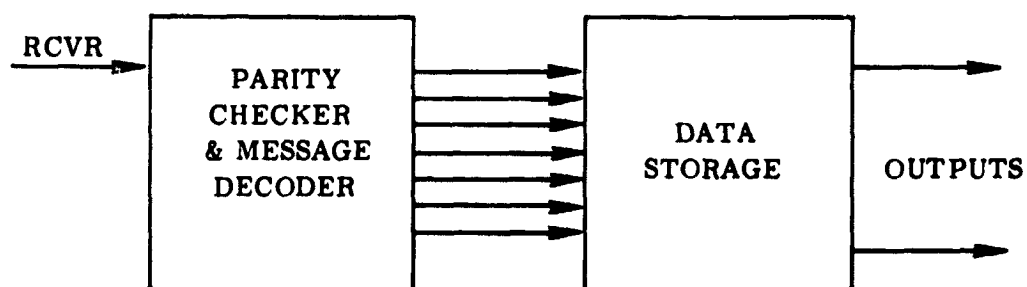


Figure 5-35. Data Processing System

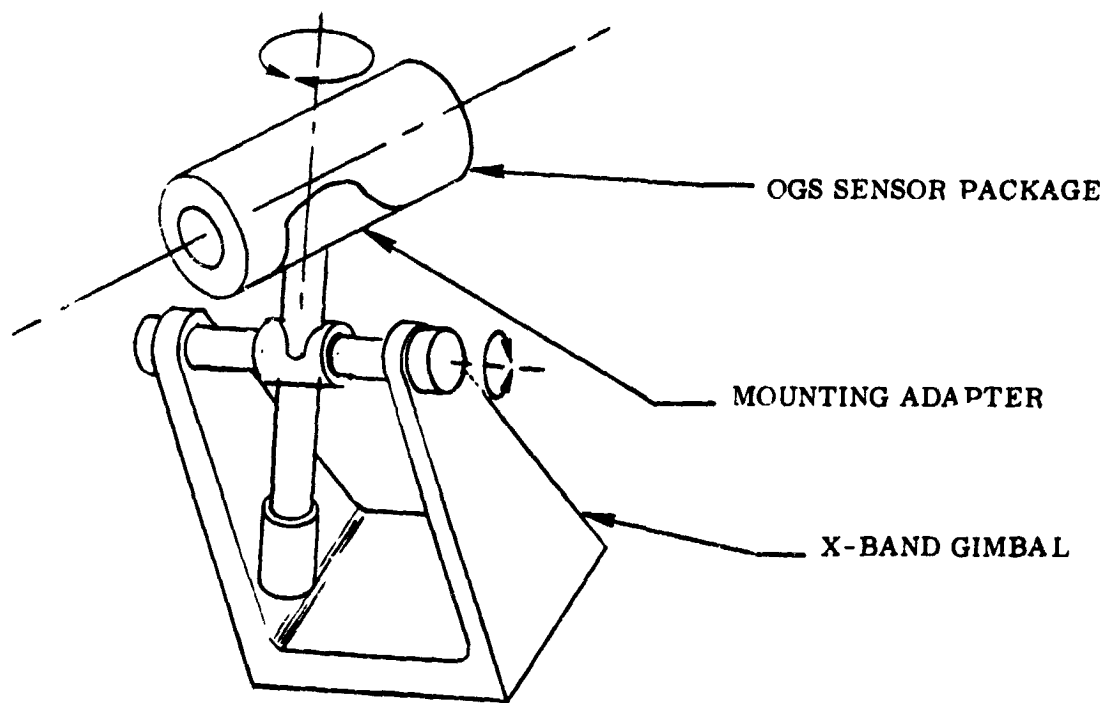


Figure 5-36. Sensor Package Mounted on X-Band Gimbals

Sensor package mounting utilizing OGS gimbals.

This approach utilizes a set of gimbals designed specifically for the OGS. In this proposed system, the sensor package is located at the intersection of the gimbal axes. This configuration allows for a more compact arrangement than does utilizing the existing x-band gimbal system (see Figure 5-37). This configuration also allows the sensor package to be mounted with its center of gravity at or near the intersection of the gimbal axes, which in turn permits a more symmetrical gimbal design.

#### 5.6.1.2 Thermal Conditions

The location of the sensor package external to the vehicle naturally results in some extreme thermal conditions. The sensor package may either be exposed to full sunlight, in which case it will have the radiant energy of the sun to contend with, or to deep, dark space, in which case it will have extreme cold to cope with. The sensor package is to be thermally isolated from the vehicle itself. The package must be capable of cooling and/or heating to provide the steady state temperature required to:

- Provide laser wavelength stability
- Provide mechanical-optical stability

#### 5.6.1.3 Preliminary Calculations

All preliminary calculations indicate that passive cooling is not difficult to obtain. The package equilibrium temperature, under worst case conditions, is near room temperature and is compatible with the laser requirements. It does seem clear, however, that some form of heating must be supplied to stabilize the package when direct solar impingement is lacking. Approximately 81 watts of heat are required for worst case "cold side" stabilization. This heat need not be supplied when the OGS is not active.

#### 5.6.1.4 Vibration and Shock

The OGS sensor package will be gimbal mounted. It must be capable of withstanding the same vibration and shock levels as the gimbal system itself.

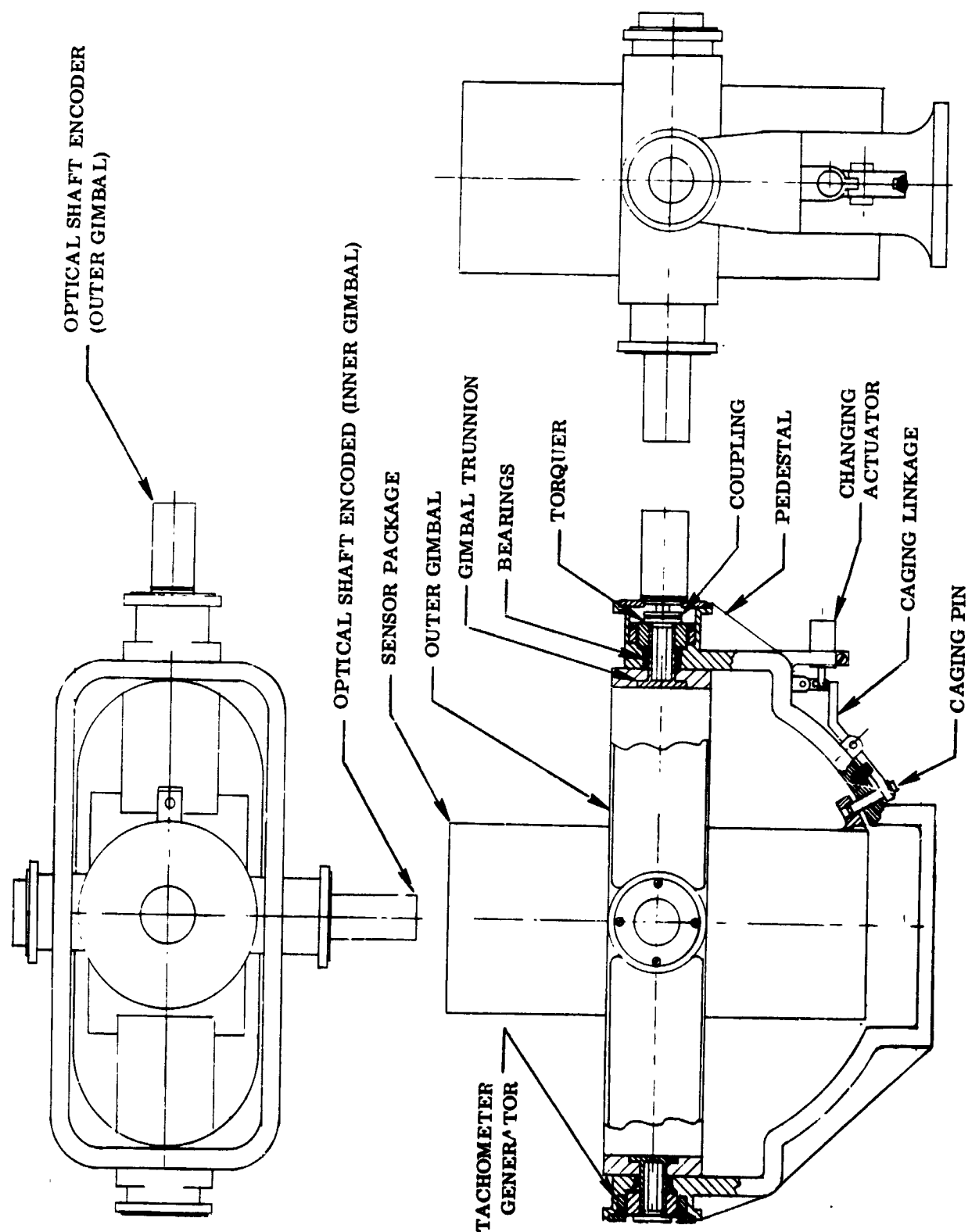


Figure 5-37. Sensor Package Mounted on OGS Gimbal

#### 5.6.2 Electrical

It is unlikely that the OGS will be activated prior to launch. Therefore, the system input power will have to be turned "ON" by the spacecraft. Command signals from the spacecraft navigation system should also be initially sent to the chaser and target gimbals prior to the start of the acquisition phase of rendezvous. These signals to the gimbal servo system should allow the OGS chaser and target two-axis gimbals to initially point the chaser sensor and the target acquisition beacon to within a field-of-view that makes the acquisition time as small as possible.

If initial pointing of  $\pm 5$  degrees is given to the target acquisition beacon and  $\pm 15$  degrees to the chaser sensor, then the maximum acquisition time would be approximately 15 minutes. It would be extremely time-consuming if no initial pointing information was provided and the gimbals were used to scan their entire  $\pm 70$  degree x  $\pm 120$  degree angular field of the gimbals.

The average input power needed for the OGS chaser hardware is approximately 46 watts. The OGS target hardware required 96 watts during acquisition and 46 watts for baseline system operation after acquisition. See Table 3-1 for size-weight-power estimates of the baseline system.

The OGS data output is presently in digital form but could be modified to analog if desired. Table 5-4 is a decimal-digital representation of basic data output from the Optical Guidance System.

#### 5.7 PARTS QUALIFICATION

ITTA used as many high-reliability type components in the OGS design as possible. The following NASA documents were used as guidelines:

85 MO 2716

#### PREFERRED ELECTRICAL PARTS LIST FOR APOLLO APPLICATIONS PROGRAM

85 MO 2715

#### PARTS SELECTION AND CONTROL REQUIREMENTS FOR APOLLO TELESCOPE MOUNT

TABLE 5-4  
DECIMAL-DIGITAL REPRESENTATION OF OGS DATA

PARAMETER	DECIMAL-DIGITS (Each Digit-One Word)								UNIT	NO. OF WORDS
	$10^5$	$10^4$	$10^3$	$10^2$	$10^1$	$10^0$	$10^{-1}$	$10^{-2}$		
Range (R)	X	X	X	X	X	X	.	X	meters	8
Range-rate ( $\dot{R}$ )			X	X	X	X	.	X	m/sec	5
Chaser-to-Target • LOS angle ( $\theta_x$ )				X	X	X	.	X	deg.	4
• LOS angle-rate ( $\dot{\theta}_x$ )					X	X	.	X	°/sec.	3
• LOS angle ( $\theta_y$ )				X	X	X	.	X	deg.	4
• LOS angle-rate ( $\dot{\theta}_y$ )					X	X	.	X	°/sec.	3
Third-Axis Angle Relative roll ( $\phi$ )				X	X	X	.		deg.	3
Target-to-Chaser • LOS angle ( $\alpha_x$ )				X	X	X	.	X	deg.	4
• LOS angle-rate ( $\dot{\alpha}_x$ )					X	X	.	X	°/sec.	3
• LOS angle ( $\alpha_y$ )				X	X	X	.	X	deg.	4
• LOS angle-rate ( $\dot{\alpha}_y$ )					X	X	.	X	°/sec.	3

40 Words

85 MO 2713

DISCRETE SEMICONDUCTOR DEVICES, QUALITY  
ASSURANCE AND SCREENING REQUIREMENTS FOR  
HIGH RELIABILITY

85 MO 2703

SEMICONDUCTOR DEVICES, SCREENED QUALIFIED  
PRODUCTS LIST

85 MO 2704

MICROCIRCUITS, QUALITY ASSURANCE AND SCREENING  
REQUIREMENTS FOR HIGH RELIABILITY

ITTA has sent the Optical Guidance System preliminary parts list to NASA/MSFC for review by the PARTS & COMPONENTS RELIABILITY ENGINEERING BRANCH (R-QUAL-RP). A MEETING BETWEEN ITTA and NASA/MSFC Reliability Engineering was held on 12 February 1969 to review and discuss ITT's parts list.

The following comments were made:

- Second source Texas Instruments in as many areas as possible.
- The SG 140 Microcircuit from Sylvania has a temperature range of 0 degree C to +75 degrees C.
- Cementing process of Sprague Electric's U LX-2102J Attenuator should be investigated.
- Sprague's U D-4024 Buffer Amplifier Design and Manufacturing processes should be researched.
- Amperex Electronics Corporation's 2N3640 Transistor, and the IN457 Diode manufactured by Sylvania, Dickson and Motorola are plastic devices, the use of such devices is prohibited by NASA.

## 6.0 ALTERNATE CONFIGURATIONS

System configurations other than the baseline system discussed in Section 3.0 are presented here. The main differences between these configurations are the maximum range capability, total angle coverage, acquisition time, and the line-of-sight angle data available. Combinations of separate subsystems that would comprise less complex system configuration can still form a functional rendezvous and docking system. Some examples of this are:

- If the OGS uses other vehicle telemetry equipment (i.e., VHF link) to transfer data from one vehicle to the other, it is not necessary to have an optical communications subsystem.
- The chaser can still acquire the target if the target acquisition beacon is not present (the acquisition time would be longer without the beacon).
- Two-Axis Gimbals that carry the transmitter-receiver can be eliminated if (a) vehicle navigation data regarding relative vehicle position is accurate to better than  $\pm 5$  degrees, and if (b) the respective vehicles can initially orient the OGS chaser-target equipment to within  $\pm 5$  degrees of each other, and then maintain  $\pm 15$  degrees pointing during the rest of the rendezvous and docking maneuvers. A small gimballed mirror internal to the OGS would be necessary to point the chaser laser beam if the beam-width was left at .03 degrees.



Figure 6-1 is a symbolic chart showing the hardware subsystems of four different system configurations. System configuration "A" is essentially the baseline system without the optical communication and third angle sensor. Configuration B, C, and D are successively less complex systems. Table 6-1 shows the dynamic range of the data available on the chaser and target for each of the four configurations.

As indicated in Table 6-1, the four basic system configurations differ considerably in their capability to provide LOS angles for both the chaser and target vehicles. Configuration "A" is the most versatile, providing large angle coverage for both vehicles. Configuration "D" is the most limited, providing only  $\pm 15$  degrees in x and y for the chaser vehicle and no angle data for the target vehicle which has only a passive corner cube reflector.

The maximum angle coverage of the Optical Guidance System is determined by the two-axis gimbals. For rendezvous and docking maneuvers there will be certain attitude constraints on the chaser and target vehicles while in orbit, however a two-axis gimbal, ( $\pm 110$  degree rotation in x and  $\pm 70$  degree rotation in y) should provide sufficient angle coverage. The minimum angle coverage of the Optical Guidance System is determined by the optical field-of-view (FOV) of the electro-optical angle tracker. If the Optical Guidance System is not placed on gimbals the effective angle coverage would then be  $\pm 15$  degrees in X and  $\pm 15$  degrees in Y.

Configurations "A" and "B" have a maximum range capability of 75 miles using a .03 degree by .03 degree chaser transmitter beamwidth. Configuration "C" and "D" do not have an acquisition beacon. The hardware needed to scan a narrow beam at higher scan rates coaxially with the receiver instantaneous field-of-view is not available. It is, therefore, necessary to increase the chaser transmitter beamwidth. ITT Aerospace/Optical Division (ITTA/OD) is presently developing, under a separate contract, and advanced Laser Guidance System for NASA/MSFC that incorporates a new beam steering technique that will have narrow beam, and high scan rate capabilities. However, this system

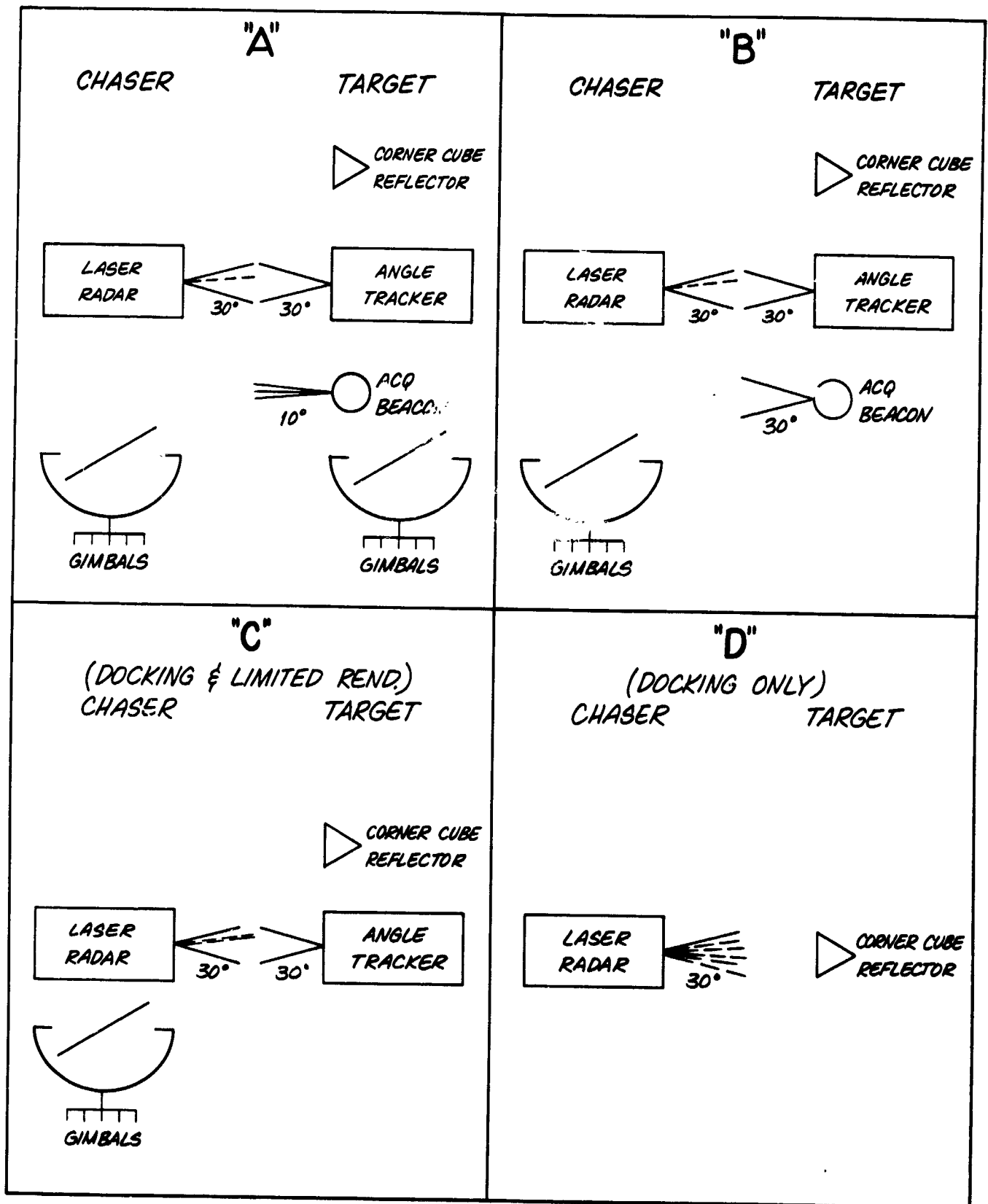


Figure 6-1. Block Diagram of Alternate Configurations

TABLE 6-1. Dynamic Range of OGS Data (at Chaser and Target for A, B, C and D Configurations)

Chaser									
Config.	R miles	$\dot{R}$ ft/sec	$\alpha_x$ (gimbals) degree	$\alpha_x$ (optics) degree	$\alpha_y$ (gimbals) degree	$\alpha_y$ (optics) degree	$\dot{\alpha}_x$ deg/sec	$\dot{\alpha}_y$ deg/sec	$\phi$ degree
A	0-75	0-120,000	0 $\pm$ 120	0 $\pm$ 15	0 $\pm$ 70	0 $\pm$ 15	*	*	0 $\pm$ 40
B	0-75	0-120,000	0 $\pm$ 120	0 $\pm$ 15	0 $\pm$ 70	0 $\pm$ 15	*	*	0 $\pm$ 40
C	0-5.0	0-120,000	0 $\pm$ 120	0 $\pm$ 15	0 $\pm$ 70	0 $\pm$ 15	*	*	0 $\pm$ 40
D	0-.2	0-120,000	-	0 $\pm$ 15	-	0 $\pm$ 15	*	*	0 $\pm$ 40

Target									
Config.			$\theta_x$ (gimbals) degree	$\theta_x$ (optics) degree	$\theta_y$ (gimbals)	$\theta_y$ (optics)	$\dot{\theta}_x$ deg/sec	$\dot{\theta}_y$ deg/sec	
A	-	-	0 $\pm$ 120	0 $\pm$ 15	0 $\pm$ 70	0 $\pm$ 15	*	*	-
B	-	-	-	0 $\pm$ 15	-	0 $\pm$ 15	*	*	-
C	-	-	-	0 $\pm$ 15	-	0 $\pm$ 15	*	*	-
D	-	-	-	-	-	-	*	*	-

R range (slant) between chaser and target vehicle  
 $\dot{R}$  range-rate  
 $\alpha_x, \alpha_y$  line-of-sight (LOS) angle from chaser  
 $\dot{\alpha}_x, \dot{\alpha}_y$  LOS angle-rate  
 $\phi$  relative roll angle between chaser and target  
 $\theta_x, \theta_y$  LOS angle from target  
 $\dot{\theta}_x, \dot{\theta}_y$  LOS angle-rate  
 \* see Appendix B

is not sufficiently developed to be utilized for spaceborne flight for the present AAP schedules. The maximum range for configuration "C" is 5 miles for a 6.75 degree by 6.75 degree transmitter beamwidth with all other range parameters (i.e., transmitted peak power, receiver instantaneous FOV, target area, receiver area, etc.) remaining the same as for configuration "A" and "B". Configuration "D" is a completely strapdown system (both vehicles) that has a maximum range of 1000 feet for a 30-degree by 30-degree transmitter beamwidth. LOS angle is available only for the chaser vehicle and not the target vehicle in this configuration.

## 7.0 CONCLUSIONS AND RECOMMENDATIONS

The OGS design presented here for performing future rendezvous and docking is recommended with the exception of one additional subsystem that should be added. Piezoelectric beam steerers have recently been developed and tested in an Advanced OGS (NAS8-20833) and will provide a significant advantage to the acquisition and tracking modes of operation. The beam deflectors can rapidly scan and point the laser beam very precisely in a  $30^{\circ} \times 30^{\circ}$  field-of-view (the present receiver sensor field-of-view). Since the receiver sensor already has the capability to electro-optically scan its field-of-view, the addition of the transmitter beam steerers will thus provide the capability for a scanning/pointing transmitter-receiver without mechanical gimbals. The only need for gimbals would be to extend the total angle coverage greater than  $30^{\circ} \times 30^{\circ}$ . The laser transmitter/receiver would provide the actual scanning, pointing, and precision tracking.

ITTA recommends that two areas be examined immediately to assure that an Optical Guidance System for rendezvous and docking can be ready for efficient use on near future spaceborne missions. The first general area is space qualification type testing of new components such as the diffraction-limited GaAs laser and the piezoelectric beam steerers. Also, environmental testing (thermal, shock, and vibration, etc.) and reliability testing (lifetime, MTBF, etc.) of the basic transmitter-receiver sensor is also recommended. A flight prototype could be built from the design presented here with little modification for such type testing.

The next general area that should be examined is the use of the OGS data by the space vehicles. The accuracy of the sensor data lends itself nicely to automatic rendezvous and docking maneuvers and therefore computer modeling of the problem could be very meaningful in obtaining minimum fuel requirements for various guidance laws. Computer modeling of automatic station-keeping between two vehicles with various orbits, orientations, attitude dead-bands, slant ranges, etc. could also be very beneficial in evaluating the efficiency of other guidance laws. Future station-keeping of experiment module, detached from a space station is one particular area that appears to lend itself to an automatic control study of this nature.